Tampere University

AMNA ABU KHAMIDAKH

Assessment of Ca^{2+} Dynamics in Human Retinal Pigment Epithelial Cell Cultures

Tampere University Dissertations 66

Tampere University Dissertations 66

AMNA ABU KHAMIDAKH

Assessment of Ca^{2+} Dynamics in Human Retinal Pigment Epithelial Cell Cultures

ACADEMIC DISSERTATION
To be presented, with the permission of
the Faculty Council of the Faculty of Medicine and Health Technology
of Tampere University,
for public discussion in the auditorium F115
of the Arvo Building, Arvo Ylpön katu 34, Tampere,
on 7 June 2019, at 12 o'clock.

ACADEMIC DISSERTATION
Tampere University, Faculty of Medicine and Health Technology
Finland

Responsible supervisor and Custos	Professor Jari Hyttinen Tampere University Finland	
Supervisor(s)	Professor Jari Hyttinen Tampere University Finland	Docent Kati Juuti-Uusitalo Tampere University Finland
Pre-examiner(s)	Associate professor Anna Herland Karolinska Institute Sweden	Professor Pasi Tavi University of Eastern Finland Finland
Opponent	Senior research fellow Sofija Andjelic Ljubljana University Medical Centre Slovenia	

Cover design: Roihu Inc.

ISBN 978-952-03-1099-8 (print)
ISBN 978-952-03-1100-1 (pdf)
ISSN 2489-9860 (print)
ISSN 2490-0028 (pdf)
http://urn.fi/URN:ISBN:978-952-03-1100-1

PunaMusta Oy – Yliopistopaino
Tampere 2019

"He created a human from a mere drop; and behold, this same human becomes an open disputer" 16:4 The Bee

ACKNOWLEDGEMENTS

The research has been conducted at Tampere University of Technology and BioMediTech (currently Tampere University). I would like to thank the Tampere University of Technology President's Doctoral Programme, the Center for International Mobility (CIMO), and the City of Tampere for providing financial support for this study.

I would like to warmly thank my supervisors Professor Jari Hyttinen and Docent Kati Juuti-Uusitalo. Jari, thank you for your support throughout my entire studies, for your trust and guidance. No matter how crazy (and costly) my ideas were, you always allowed me to give them a try. This immensely contributed to my independence as a researcher. Kati, I have learnt so much from you, thank you for teaching everything I needed to know about cells to perform high quality research. When times were tough, I always knew I could count on you not only as a supervisor, but also as a friend.

I would also like to express my gratitude to Professor Pasi Tavi and Associate Professor Anna Herland for the valuable comments that helped me improve this thesis.

My sincere thank you goes to Research Specialists PhD Kim Larsson and PhD Dmitry Fayuk for teaching me Ca^{2+} imaging techniques from ground zero to complete independence. Kim, you taught me to think critically and to pay attention to details. You invested months of your time in me and I am very grateful for your trust. Dmitry, thank you for sharing your tremendous scientific experience and insights. You were the one who casually asked whether my cells were blinking. Your question resulted in two years of research and half of my doctoral thesis.

I thank Professor Pavel Zak for opening the amazing world of science for me, for sharing your knowledge and enthusiasm. Thank you for your guidance during my first steps as a scientist.

I would also like to thank all the people who I had a pleasure working with during these years. Academy Fellow Soile Nymark and Associate Professor Heli Skottman, you are the most inspiring women I have ever met. You balance a mind-blowing career and a family life so effortlessly that sometimes I think you have more than 24 hours in your days. I am very lucky I had a chance to work with you. Iina Korkka,

out of all people you are the one who can relate to all the research struggles I have been through. Thank you for always being there for me, be it a discussion of a scientific paper or just a small talk in the coffee room. Brilliant laboratory technologists Hanna Pekkanen, Outi Heikkilä and Outi Melin, thank you for accuracy in everything you do. Without you this research would have lasted a couple of years longer. I would also like to thank PhD Florentino Caetano dos Santos, PhD Alejandra Rodriguez-Martinez, Professor Kai Kaarniranta, Professor Anne Kallioniemi, and Professor Hannu Uusitalo for their valuable discussions and contributions to this study.

And, finally, I would like to express my deepest gratitude to Docent Olli Lohi. I wish my family and I met you under different circumstances, nonetheless, I am happy I had a chance to learn from you. Our short cell biology discussions were the hardest conversations in my life, which had a huge impact on me as a scientist. You showed me what biomedical research is all about. It is about people. You know the people you do your research for. You know pain, and fear, and happiness, and hope behind every survival curve you plot. I cannot express in words how thankful I am to all the scientists who many years ago did not give up their research, despite the doubts and challenges they faced; to the scientists, whose names I do not even know; to the scientists, whose effort in the past saves people's lives today. And I truly wish that many years later someone will be grateful for the work we are doing here and now.

Esch-sur-Alzette, May 2019

ABSTRACT

Retinal pigment epithelium is a monolayer of cells located beneath photoreceptors of the retina maintaining their functionality. Malfunction of RPE leads to retinal degenerative diseases, such as age-related macular degeneration and Stargardt disease. Ca^{2+} is a ubiquitous ion that takes part in regulation of vital cellular processes. The knowledge of Ca^{2+} dynamics is essential for understanding RPE physiology. This is especially important for functionality assessment of cells intended for transplantation and for drug testing.

The aim of this thesis was to study spontaneous and mechanically induced Ca^{2+} activity in human RPE and to assess the effect of cellular maturation and wounding on the $[Ca^{2+}]_i$ dynamics. For this, various methods, such as fluorescent Ca^{2+} imaging, immunofluorescence staining, PCR, and mathematical modeling were applied. In addition, novel methods were developed to analyze large amounts of Ca^{2+} imaging data. ARPE-19 and human embryonic stem cell-derived RPE cells (hESC-RPE) were used as RPE cell models.

In this thesis, it was shown that both ARPE-19 and hESC-RPE exhibit intercellular Ca^{2+} waves upon mechanical stimulation. With live-cell Ca^{2+} imaging and mathematical modeling, it was demonstrated that in ARPE-19 cells, the mechanically induced Ca^{2+} waves propagate intracellularly through gap junctions and extracellularly involving diffusion of a paracrine factor. By applying in-house image analysis tools for the experimental fluorescence time-series, it was found that in hESC-RPE cells, spontaneous $[Ca^{2+}]_i$ transients and the ability to propagate intercellular Ca^{2+} waves upon mechanical stimulation strongly depend on the maturation status of the cells. Finally, it was demonstrated that wounding affects spontaneous Ca^{2+} activity close to the wound edges, and cells within the healed areas resemble Ca^{2+} dynamics of immature hESC-RPE.

To conclude, this thesis has provided important insights into human RPE Ca^{2+} dynamics, as well as into the events of single cell mechanical stimulation and large scale monolayer wounding. In addition, it was demonstrated that maturation drastically affects RPE Ca^{2+} dynamics. This knowledge and the developed image analysis algorithms contribute to understanding RPE physiology and can facilitate

establishment of novel tools for assessment of RPE functionality prior to transplantation and in drug testing assays.

CONTENTS

ABBREVIATIONS

18-α-GA	18-α-glycyrrhetinic acid
AM	Acetoxymethyl
AMD	Age-related macular degeneration
ATP	Adenosine triphosphate
BEST	Bestrophin
bFGF	Basic fibroblast growth factor
BSA	Bovine serum albumin
ColIV	Collagen IV
ColI	Collagen I
CRALBP	Cellular retinaldehyde-binding protein
Cx	Connexin
DAG	Diacylglycerol
DAPI	4', 6' diamidino-2-phenylidole
ECM	Extracellular matrix
ER	Endoplasmic reticulum
GAPDH	Glyceraldehyde 3-phosphate dehydrogenase
GJ	Gap junction
HBSS	Hanks balanced salt solution
hESC	Human embryonic stem cells
hESC-RPE	Human embryonic stem cell-derived retinal pigment epithelium
hiPSC	Human induced pluripotent stem cells
IF	Immunofluorescence
IP3	Inositol-1,4,5-trisphosphate
IP3R	Inositol-1,4,5-trisphosphate receptor
Ki67	Antigen Ki67
Lam	Laminin
LE-RPE	Long-Evans RPE
MERTK	Mer tyrosine kinase

MITF	Microphthalmia-associated transcription factor
MS	Mechanical stimulation
NB	Neighboring cell layer
NCX	Na^+/ Ca^{2+} exchanger
NF	Normalized fluorescence
OCT 3/4	Octamer-3/4, POU domain, class 5, transcription factor 1
PBS	Phosphate-buffered saline
PEDF	Pigment epithelium-derived factor
PFA	Paraformaldehyde
PIP2	Phosphatidylinositol-4,5-bisphosphate
PKC	Protein kinase C
PLC	Phospholipase C
PMCA	Plasma membrane Ca^{2+}-ATPase
qRT-PCR	Quantitative reverse transcription–polymerase chain reaction
RCS-RPE	Royal College of Surgeons RPE
RNA	Ribonucleic acid
ROCK	Rho-associated coiled-coil kinase
RPE65	Retinal pigment epithelium-specific 65 kDa protein
RPE	Retinal pigment epithelium
RT	Room temperature
RT-PCR	Reverse transcription–polymerase chain reaction
RyR	Ryanodine receptor
SERCA	Sarcoplasmic reticulum calcium transport ATPase
SSCC	Stretch-sensitive Ca^{2+} channel
TGF-β	Transforming growth factor β
TJ	Tight junction
TRP channel	Transient receptor potential channel
UTP	Uridine triphosphate
VEGF	Vascular endothelial growth factor
ZO-1	Zonula occludens protein 1
%RC	Percentage of responsive cells
%RCsp	Percentage of responsive cells with spontaneous $[Ca^{2+}]_i$ increases
%RCms	Percentage of responsive cells with mechanically induced $[Ca^{2+}]_i$ transients

ORIGINAL PUBLICATIONS

Publication I. Abu Khamidakh, A.E., Juuti-Uusitalo, K., Larsson, K., Skottman, H. & Hyttinen, J. (2013). Intercellular Ca^{2+} wave Propagation in Human Retinal Pigment Epithelium Cells Induced by Mechanical Stimulation, Experimental Eye Research, Vol. 108, pp. 129-139.

Publication II. Vainio I., Abu Khamidakh, A., Paci, M., Skottman, H., Juuti-Uusitalo, K., Hyttinen, J. & Nymark, S. (2015). Computational Model of Ca^{2+} Wave Propagation in Human Retinal Pigment Epithelial ARPE-19 Cells, PLoS One, Vol. 10(6), e0128434.

Publication III. Abu Khamidakh, A.E., Santos, F.C.D., Skottman, H., Juuti-Uusitalo, K. & Hyttinen, J. (2016). Semi-Automatic Method for Ca^{2+} Imaging Data Analysis of Maturing Human Embryonic Stem Cells-Derived Retinal Pigment Epithelium, Annals of Biomedical Engineering, Vol. 44(11), pp. 3408-3420.

Publication IV. Abu Khamidakh, A.E., Rodriguez-Martinez, A., Kaarniranta, K., Kallioniemi, A., Skottman, H., Hyttinen, J. & Juuti-Uusitalo, K. (2018). Wound Healing of Human Embryonic Stem Cell-Derived Retinal Pigment Epithelial Cells is Affected by Maturation Stage, Biomedical Engineering Online, Vol. 17(102), pp. 1-20.

Authors' contributions

Publication I: The author was responsible for defining the study aims, experiment design, experiment performance, data collection, data analysis, text writing and editing. Kati Juuti-Uusitalo and Kim Larsson took part in experiment design and helped with setting up the equipment and data analysis. Jari Hyttinen and Kati Juuti-Uusitalo supervised all stages of experimental work and paper writing. All co-authors contributed to results discussion and text improvement.

Publication II: The author was responsible for providing Ca^{2+} imaging experimental data (i.e., experiment design, experiment performance, data collection, data analysis) and text editing. Iina Vainio created the mathematical model based on the provided experimental data and wrote the text. All co-authors contributed to results discussion and text improvement.

Publication III: The author was responsible for defining the study aims, experiment design, experiment performance, data collection, data analysis, text writing and editing. Florentino Santos developed the method for semi-automatic cell segmentation. Jari Hyttinen and Kati Juuti-Uusitalo supervised all stages of experimental work and paper writing. All co-authors contributed to results discussion and text improvement.

Publication IV: The author was responsible for defining the study aims, experiment design, experiment performance, data collection, data analysis, text writing and editing. Kati Juuti-Uusitalo and Jari Hyttinen supervised all stages of experimental work and paper writing. Kati Juuti-Uusitalo handled the paper submission process. All co-authors contributed to results discussion and text improvement.

1 INTRODUCTION

Retinal pigment epithelium (RPE) is a single layer of cells beneath neurosensory retina, crucial for their survival. RPE forms a barrier between the blood vessels and retina controlling substances reaching the retina. RPE phagocytize shed photoreceptors allowing for their renewal. In addition, these cells secrete various growth factors and control visual cycle and water balance during dark and light adaptation. (Strauss, 2005) Dysfunction of RPE leads to retinal degenerative diseases, such as age-related macular degeneration (AMD), which is the major cause of blindness in elderly people living in developed countries. (Sparrow et al., 2010; Bonilha, 2008)

Because the single layer of cells is the key player in AMD, RPE is a very promising target for regenerative medicine approaches (Ramsden et al., 2013). Understanding the maturation and wound healing processes in RPE is essential for application of these cells in treating degenerative disorders (Sugino et al., 2003).

Ca^{2+} signaling plays a primary role in cell physiology. It controls major cellular processes from proliferation to apoptosis. In RPE, Ca^{2+} controls also transepithelial transport of substances, phagocytosis, growth factors secretion, differentiation, and other vital activities. (Wimmers et al., 2007)

Cells normally maintain low free cytoplasmic Ca^{2+} concentration ($[Ca^{2+}]_i$) and high concentration of Ca^{2+} in intracellular Ca^{2+} stores, such as endoplasmic reticulum (Berridge, 2003). When cells are stimulated, they can increase the $[Ca^{2+}]_i$ either using Ca^{2+} that comes either from extracellular space through plasma membrane Ca^{2+} channels, or recruiting Ca^{2+} from intracellular Ca^{2+} stores. These transient $[Ca^{2+}]_i$ spikes vary in temporal and spatial patterns (Bootman, 2012). The diverse $[Ca^{2+}]_i$ patterns arise from the vast variability of proteins that are responsible for allowing Ca^{2+} into the cytoplasm and removing Ca^{2+} from the cytoplasm (Bootman, 2012). The proteomes underlying Ca^{2+} signaling are tissue-specific and correspond to the cellular physiological needs. The transient $[Ca^{2+}]_i$ increases further interact with Ca^{2+} sensors (e.g., troponin, calmodulin) that result in various physiological responses. (Berridge, 2000)

Spontaneous $[Ca^{2+}]_i$ transients that occur without an externally applied stimulation have been demonstrated in many cell types. In some cell types (for example, in human cardiac progenitor cells, mesenchymal stem cells, carcinoma) these transients are known control cell growth and differentiation. (Ferreira-Martins et al., 2009; Resende et al., 2010) The $[Ca^{2+}]_i$ transients can be restricted to single cells or propagate to a small number of neighboring cells as spontaneous intercellular Ca^{2+} waves. (Rottingen and Iversen, 2000)

When a single cell in a monolayer is mechanically stimulated with, e.g., a glass micropipette, an intercellular Ca^{2+} wave occurs in various cell types, including RPE. (Rottingen and Iversen, 2000; Stalmans and Himpens, 1997) Such waves can propagate via two major pathways: intracellularly through gap junctions when the signaling molecules emerging in the cytoplasm of the stimulated cell pass directly to the cytoplasm of the neighboring cells, and extracellularly when the stimulated cell releases a signaling factor to the extracellular space stimulating neighboring cells. (Rottingen and Iversen, 2000; Charles et al., 1996; Gomes et al., 2005; Sanderson et al., 1994; Nezu et al., 2010)

When a large number of cells is being stimulated, as in the condition of scrape wounding of a monolayer, the Ca^{2+} waves spread from the wound edges to intact cells. This Ca^{2+} wave is the initial trigger of the wound healing process that allows undamaged cells to rearrange their intercellular junctions and enhance cell motility to seal the void. (Woolley and Martin, 2000) Wound healing of RPE has been studied in animal models (e.g., Oganesian et al., 1997; Verstraeten et al., 1990), as well as in hESC-RPE cells (Croze et al., 2016). However, Ca^{2+} signaling aspects of the wound healing in hESC-RPE have had less attention.

Ca^{2+} imaging experiments aiming at investigation of intercellular Ca^{2+} signals, such as experiments on Ca^{2+} wave spreading between cells or Ca^{2+}-related signaling during wounding, imply assessment of $[Ca^{2+}]_i$ from a large number of cells. Cell segmentation of the obtained fluorescence images is one of the most time-consuming steps in the analysis of Ca^{2+} imaging data. (Francis et al., 2014; Mukamel et al., 2009) The tools that allow for full or partial automatization of cell detection, as well as consequent fluorescence curves analysis, are highly beneficial for this process. To the best of our knowledge, no automatic tools for assessment of Ca^{2+} imaging data fine-tuned for RPE cells have been developed.

The aims of this thesis were to evaluate mechanically induced intercellular Ca^{2+} waves and spontaneous Ca^{2+} activity in human RPE, to investigate the mechanisms of Ca^{2+} waves propagation, and to assess the effect of maturation and wounding on human RPE Ca^{2+} dynamics. For this, the experimental techniques of live-cell Ca^{2+}

imaging, time-lapse phase-contrast microscopy, PCR, and immunofluorescence staining were combined with image analysis tools developed for fast and efficient assessment of cellular Ca^{2+} dynamics, as well as mathematical modeling.

With this research, we aimed at deeper understanding of Ca^{2+} signaling in RPE. This knowledge allows for better assessment of cellular functionality, which is essential for transplantations, drug discovery and toxicology tests. In addition, the knowledge of Ca^{2+} signaling can provide insights for a better control of wound healing processes and in-vitro cellular maturation.

2 LITERATURE REVIEW

Retina is a multicellular structure that allows for light perception (Ryan et al., 2012). Despite its complex architecture, many diseases of the retina are associated with a rather simple monolayer of RPE cells lying just beneath the retina. A lot of effort has been put into research and clinical trials to replace the damaged RPE monolayer in the eye with healthy autologous or donor cells (Carr et al., 2013). The recent success of deriving RPE from human pluripotent cells has provided a vast supply of material for transplantation and drug testing (Nommiste et al., 2017). Critical assessment of *in vitro* generated RPE physiology is essential for successful implementation of these cells into clinical practice.

2.1 RPE

2.1.1 Functions of RPE

RPE is the cellular monolayer located between neural retina and choroid (**Fig. 1**) (Strauss 2005, Sparrow 2010). RPE (**Fig. 1**) cells are crucial in maintaining photoreceptor viability. The RPE absorbs scattered light with their melanin granules. This allows for sharp vision and decreases photooxidative damage. Another major function is transportation of substances between blood and photoreceptor cells. (**Fig. 1**) From the subretinal space, the cells transport water, ions and photoreceptors waste products into the blood, while delivering nutrients (e.g., glucose, fatty acids) from blood to photoreceptors. (Ban and Rizzolo, 2000; Strauss, 2005) RPE cells are also responsible for renewal of rods and cones outer segments by phagocytizing shed photoreceptors membranes (Mazzoni et al., 2014). In addition, the RPE layer secretes different soluble factors essential for retinal and choriocapillaris (**Fig. 1**) integrity, such as vascular endothelial growth factor (VEGF) and pigment epithelium-derived factor (PEDF). (Bhutto et al., 2006)

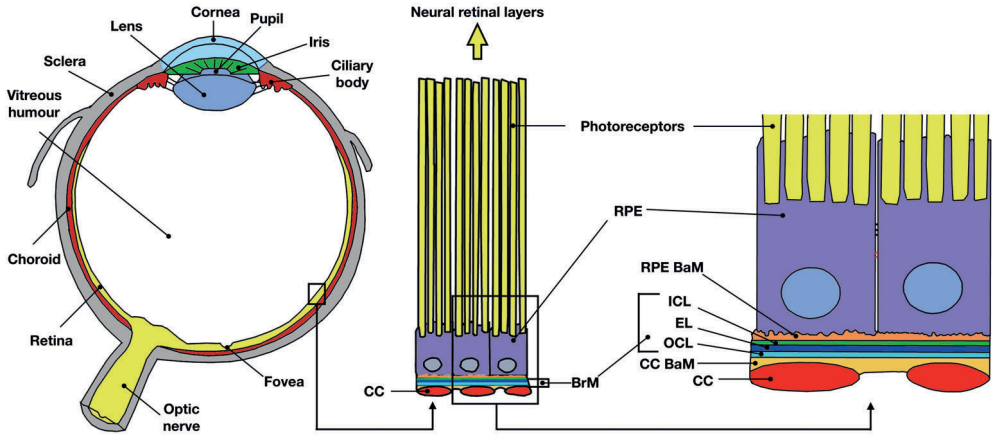

Figure 1. Schematic image of an eye (the image re-drawn with modifications from Shirinifard et al., 2012). CC – choriocapillaris; BrM – Bruch's membrane; RPE – retinal pigment epithelium; RPE BaM – RPE basement membrane; ICL – inner collagenous layer; EL – elastin layer; OCL – outer collagenous layer; CC BaM – choriocapillaris basement membrane;

Retinal photoreceptors detect light with a molecular complex that consists of an opsin protein attached to 11-cis-retinal. Upon the light absorption, 11-cis-retinal turns into all-trans-retinal activating opsin that further triggers phototransduction. The complex of opsin and all-trans-retinal is not photosensitive. To resume photosensitivity, all-trans-retinal is changed to 11-cis-retinal. The re-isomerization process takes place in RPE: the cells uptake all-trans-retinal that is formed in photoreceptors, re-isomerize it into 11-cis-retinal, and transport 11-cis-retinal to photoreceptors enabling their excitability. (Travis, 2007)

2.1.2 RPE morphology

The apical side of RPE cells (**Fig. 1**) faces photoreceptors and forms membrane extensions (microvilli) to envelope outer segments of rods and cones. (Sparrow 2010) The basal side lays on Bruch's membrane (**Fig. 1**) that separates RPE layer from choroid. The basal membrane of RPE has multiple complex folds that is typical for cells involved in transportation of ions and molecules. Lateral side of RPE cells has different types of cell-cell junctions: tight, adherence and gap junctions (**Fig. 2**). (Strauss, 2005)

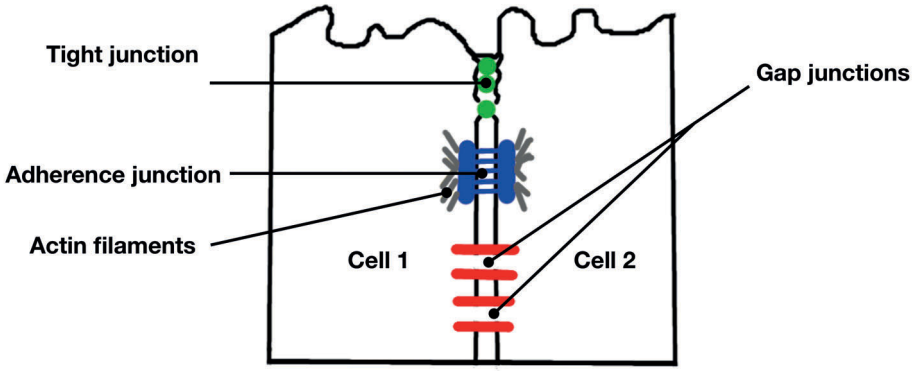

Figure 2. Overview of junctions between cells. The image re-drawn with modifications from Alberts et al., 2015.

2.1.2.1 Tight junctions

Tight junctions (TJs) locate in the apical part of RPE (**Fig. 1, 2**). They connect the membranes of neighboring cells creating a barrier which prevents free diffusion of substances between the apical and basolateral sides through paracellular space forming the blood-retinal barrier. (Rizzolo, 2007) However, the TJs exhibit leakiness (Sparrow et al., 2010; Hu and Bok 2007). In chick embryo's RPE, it has been demonstrated that the barrier properties of TJs depend on embryo's age and culture conditions (Peng et al., 2003).

Claudins and occludins are the major transmembrane proteins composing TJs. Claudins are the prime transmembrane proteins that form TJ strands. (Bauer et al., 2014) They are tissue-specific (Bauer et al., 2014) and are considered to determine TJ selectivity to different ions (Colegio et al., 2002; Van Itallie et al., 2001), while occludins have regulatory functions (Bauer et al., 2014). Another important group of TJs proteins are cytoplasmic plaque proteins, such as zonula occludens protein 1 (ZO-1), that connect transmembrane proteins with actin cytoskeleton and effector proteins (Rizzolo, 2007; Fanning et al., 1998). ZO-1 protein has been shown to interact with components of other junctions, including gap junctions (Giepmans and Moolenar, 1998; Palatinus et al., 2010).

2.1.2.2 Adherence junctions

Adherence junctions are cell-to-cell contacts in epithelial and endothelial tissue. Adherence junctions connect actin skeletons of adjacent cells. (**Fig. 2**) These junctions consist of transmembrane cadherin proteins that form homodimers with cadherin molecules on neighboring cells, and intracellular catenin proteins that link to actin filaments in the cytoplasm. (Hartsock and Nelson, 2008) Most epithelial cells express E-cadherin (Gama & Schmitt, 2012). In RPE cells, due to its neural origin, N-cadherin has been demonstrated as the most abundant cadherin of adherence junctions (Lagunowich & Grunwald, 1989; Kaida et al., 2000). This results in slower formation of cell-cell junctions between dissociated epithelioid RPE cells compared to other epithelia (Kaida et al., 2000).

2.1.2.3 Gap junctions

Gap junctions (GJs) consist of two hemi-channels, each of which is located on membranes of two adjacent cells. (**Fig. 2**) The connected hemi-channels form an intercellular "gap" that brings into contact cytoplasm of the two cells. Hemi-channels are formed by connexin (Cx) proteins that exist in different isoforms (**Fig. 3**). (Saez et al., 2003) A connexin protein consists of two extracellular loops, four transmembrane domains, and a cytoplasmic loop (Laird and Revel, 1990; Oshima, 2014).

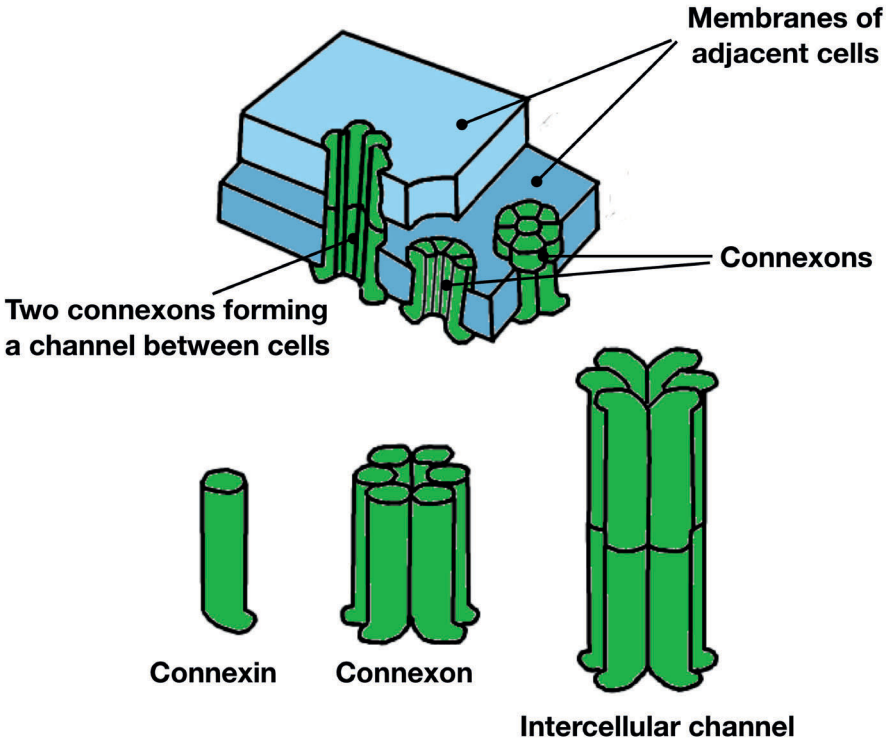

Figure 3. The structure of gap junctions. The image re-drawn with modifications from Alberts et al., 2015.

The type of Cx defines the pore size. Studies with uncharged tracers have shown the following order of the limiting pore sizes (from the smallest to the biggest):

Cx46 < Cx37 < Cx32/Cx26 = Cx26 < Cx32 < Cx43 (Harris, 2007).

Roughly, the maximum molecular weight of the substances that can pass through GJs is estimated to be 1500 (Saez et al., 1989). Recent studies show, however, that permeability of GJs is defined not only by the pore size and the size of the molecules passing through, but also by the charge of the permeants (Harris, 2007). For example, Cx32 GJs are slightly more selective for anions than cations (Suchyna et al., 1999), while Cx45 GJs are highly selective for cations (Veenstra et al., 1994).

IP3 and Ca^{2+} ions have been shown to permeate via different GJ channels. IP3 can pass through GJs composed of Cx26, Cx26/Cx30, (Zhang et al., 2005) Cx26/Cx32, Cx32, (Clair et al., 2001) and Cx43 (Romanello and D'Andrea, 2001), while Ca^{2+} can permeate through GJs comprised from Cx32 (Saez et al., 1989), Cx37, Cx37/Cx43, and Cx43 (Christ et al., 1992).

2.1.3 General biophysics of RPE membrane

RPE cells establish ion homeostasis in subretinal space as well as respond to fast changes in ionic concentration occurring due to excitation of photoreceptors by coordinating the movement of ions and water across the membrane.

Sodium gradient between subretinal space and RPE cytoplasm is maintained by Na^+/K^+-ATPase that is located in the apical membrane of RPE, unlike most other epithelia where it is located on the basal side. (Marmorstein, 2001) The main role of Na^+/K^+-ATPase is to support high Na^+ environment that is required to maintain the dark current (Marmorstein, 2001). Na^+/K^+-ATPase transports 3 Na^+ ions to the subretinal space in exchange for 2 K^+ ions into the cytoplasm against concentration gradient using the energy of ATP. The K^+ ions are then extruded via inward rectifier K^+ channels back into the subretinal space increasing the efficiency of the Na^+/K^+-ATPase. (Hughes et al., 1996; Kolb et al., 1995)

The established gradient of Na^+ drives Cl^- ions into the RPE via the $Na^+/K^+/2Cl^-$-co-transporter and results in accumulation of Cl^- in the RPE. The accumulated Cl^- leaves the RPE from the basolateral side through a large number of various Cl^- channels (Miller and Steinberg, 1977).

Light excitation of photoreceptors leads to fast changes in ionic concentrations in the subretinal space that are compensated by RPE cells. In the dark, c-GMP-gated cation channels are open in photoreceptors: Na^+ and Ca^{2+} ions leak into the cytoplasm of the outer segments, while K^+ ions leak out of the inner segments. When the outer segments of photoreceptors are excited with photons, c-GMP-gated cation channels close. This reduces the outflow of K^+ decreasing K^+ concentration in the subretinal space. The concentration is lowered even further due to activity of Na^+/K^+-ATPase in the inner photoreceptor segments (Steinberg, 1985). (Kolb et al., 1995) The decrease of subretinal K^+ concentration results in hyperpolarization of RPE apical membrane and subsequent activation of inward rectifier K^+ channels. The activation of these channels results in K^+ outflow from RPE to subretinal space compensating for light-induced changes (la Cour, 1985).

2.1.4 RPE-associated diseases

Dysfunction of the RPE layer ultimately leads to degeneration of photoreceptors and vision loss. The RPE cells can lose their functionality due to ageing or inherited diseases (e.g., retinitis pigmentosa, Stargardt disease). They undergo numerous daily stress conditions, such as heating caused by the absorption of light, phototoxicity and oxidative damage (Carr et al., 2013). While ageing, the RPE layer decreases its performance in supporting retina reducing the efficiency of phagocytosis and accumulating toxic products (Kinnunen et al., 2012). These alterations in functionality lead to numerous age-related structural modifications in RPE cells, such as accumulation of lipofuscin, decrease in the amount of melanin granules, basal deposits and thickening in Bruch's membrane (Bonilha, 2008). These structural and functional changes in RPE progress slowly during normal ageing and are more pronounced in the conditions of age-related macular degeneration disease (AMD) (Bonilha, 2008; Carr et al., 2013). Genetic predisposition as well as other factors, such as smoking and high blood pressure, have been linked to AMD (Kinnunen et al., 2011).

AMD is the primary reason of blindness in elderly people living in developed countries (Klein et al., 2004; Bonilha, 2008). Early AMD can emerge in two forms: neovascular ("wet") and atrophic ("dry"). In neovascular AMD, capillaries from choroid grow through Bruch's membrane and RPE effusing fluid into subretinal space. (Bonilha, 2008) The progression of "wet" AMD can be slowed down with intraocular injections of VEGF inhibitors (e.g., Lucentis, Avastin, and Eylea), or with surgical ablation of neovascular membranes (Carr et al., 2013; Leach and Clegg, 2015). Atrophic AMD is a more common form of the disease, constituting 80-90% of all patient cases (Clegg et al., 2013; Leach and Clegg, 2015). It is characterized by loss of RPE cells and photoreceptors in diseased regions. "Dry" AMD cannot be fully cured. (Leach and Clegg, 2015; Bonilha, 2008)

Stargardt disease is another form of macula dystrophy that, unlike AMD, affects children and young adults. The disease is inherited via autosomal recessive mode. Most often, the disease has an onset in early childhood. It is manifested as progressive vision loss in both eyes that occurs as a result of foveal degeneration (Tanna et al., 2017). It has been demonstrated that degeneration of photoreceptors in Stargardt disease is triggered by the failure of RPE cells (Cideciyan et al., 2004).

Because malfunction of a single layer of RPE cells results in the development of "dry" AMD and Stargardt disease, the regenerative medicine approaches are very promising for treating these disorders. Moreover, an eye itself is an excellent organ

for testing safety and efficacy of transplanted cells because it is the immune privileged site: an eye does not completely prevent the access of immune cells, but it can selectively allow them in to fine-tune reparation and healing processes (Benhar et al., 2012). In addition, it has a small size, so low number of cells would be sufficient for transplantation, and it allows for easy visual access to transplanted cells through cornea. (Leach and Clegg, 2015; Carr et al., 2013)

2.1.5 RPE cell models overview

2.1.5.1 Primary RPE

RPE tissue of living or sacrificed vertebrates was the only source of these cells available for research before cell lines were established. The main advantage of using the tissue as RPE source is that the cells are growing as a monolayer and maintain their pigmentation and cobblestone morphology. (Fronk and Vargis, 2016) However, the number of cells that can be obtained with this method is very limited. In addition, these cells have low viability, possess donor-dependent variability, and can only be passaged a limited number of times because aging cells cannot divide due to alterations in their gene expression. (Rawes et al., 1997; Kuznetsova et al., 2014) The RPE sheets have previously been collected from amphibians, birds, mammals, (Fronk and Vargis, 2016) as well as fetal (Maminishkis, 2006) and adult humans (Mannagh et al., 1973). The fetal (Algvere, 1997) and adult RPE from donors (Peyman, 1991) have been attempted for direct transplantation to AMD patients.

2.1.5.2 Immortalized human RPE cell lines

A cell line is a permanent cell culture that can proliferate for a long time when it is provided with fresh culture medium and enough space to grow. (Ulrich & Pour, 2001) Cell lines offer an alternative for using tissue RPE from living or deceased specimens. Some human RPE cell cultures (ARPE-19, D207) have been immortalized allowing for prolonged maintenance.

Macular degenerative disorders, such as AMD, implicate complex alterations in RPE physiology with various features specific to human eyes that cannot be modelled using animal tissues due to the cell functionality differences in species (Zeiss, 2010). *In vivo* observations in AMD patients are not enough to make

conclusions about the underlying cellular mechanisms of the disease. Therefore, *in vitro* human RPE cell cultures have become a valuable tool for studying disease-related changes. (Forest et al., 2015) In addition, conditions of cell growth in cell culture are relatively easy to control and manipulate, which make these models suitable for usage in drug testing studies.

ARPE-19 is a commercially available immortalized RPE cell line. It has been derived from a deceased 19-year-old human donor. (Dunn, 1996) ARPE-19 cell line provides a large supply of RPE cells and have been used in various studies (Morales et al., 2012; Qin and Rodrigues, 2012). The main disadvantage on ARPE-19 cells lies in their moderate morphological (e.g., low pigmentation, fusiform morphology) and functional differences from native RPE (Fronk and Vargis, 2016). Significant alterations in gene expression have been observed in ARPE-19 cells when compared to primary RPE (Samuel et al., 2017). Several studies have demonstrated that fine-tuning of cell culture conditions can improve ARPE-19 morphology to better resemble native RPE phenotype (Samuel et al., 2017; Ahmado et al., 2011).

2.1.5.3 Pluripotent stem cell-derived RPE lines

Human embryonic stem cells (hESC) offer an essentially unlimited supply of cells for transplantation therapies. Several studies have shown hESCs capacity to differentiate towards RPE (Klimanskaya et al., 2004; Carr et al., 2009; Vaajasaari et al., 2011).

The so-called embryoid body method is widely used to differentiate hESCs into RPE cells. In this method, hESCs are cultured in the media designed to induce differentiation for 1-3 weeks (Rowland et al., 2012). Then, the cells are plated on an adherent substrate, such as laminin, and the first signs of pigmentation are observed within 10 days (Vaajasaari et al., 2011).

In *in-vitro*, hESC-RPE express genes and proteins typical for primary RPE cells, form a highly polarized epithelial layer, secrete PEDF from the apical side and VEGF from the basal side, and possess barrier properties similar to cultured human RPE. HESC-RPEs are able to phagocytize photoreceptor outer segments through the same *MERTK*-specific mechanism as native RPE. (Carr et al., 2013; Liao et al., 2010)

With proteomics analysis, it has been demonstrated that hESC-RPE cells express the majority of proteins (more than 80%) at the same level as native human RPE, while only 7-8% of proteins are upregulated and 11% are downregulated. HESC-

RPEs have been found to have mitochondria dysfunction and decreased levels of oxidative phosphorylation. (Hongisto et al., 2017)

Somatic cells can be reprogrammed to become pluripotent. Initially, adult mouse fibroblasts have been genetically manipulated to enter the pluripotent state by transduction of four defined Yamanaka's factors (Takahashi and Yamanaka, 2006), and later similar procedures have been performed on human fibroblasts (Takahashi et al., 2007). This type of cells is called induced pluripotent stem cells (iPSCs). Various cell types (e.g., blood cells (Loh et al., 2009), exfoliated renal tubular epithelial cells (Zhou et al., 2011), keratinocytes (Aasen et al., 2008)) can be transformed into iPSCs. iPSCs resemble ESCs and can be differentiated to virtually any cell type. The technology of human iPSCs (hiPSCs) has introduced a new approach to studying cell functionality without the need of using human embryos. The hiPSC-derived cell cultures provide a new patient-specific approach for drug-testing and disease modeling (Malik and Rao, 2013). Differentiation of hiPSCs towards RPE has been reported in various studies (Buchholz et al., 2009; Carr et al., 2009). hiPSC-RPE grafts have been considered to have lower probability of rejection because such grafts are derived from patients' own cells. Recent studies, however, show that hiPSC-derived cells do exhibit immunogenicity that may affect graft transplantations (Taylor et al., 2011; Fu, 2014; Liu et al., 2017) Another safety concern of hiPSC-derived grafts is their genomic instability. (Liu et al., 2017)

2.1.5.4 Limitations of RPE cell models

The physiology of RPE layer is strongly interconnected with processes occurring in retina (Benedicto et al., 2017). Thus, observations made with RPE cell cultures should be confirmed *in vivo*.

To better mimic *in vivo* conditions, various methods of co-culturing RPE cells with photoreceptors (and its progenitors) and whole retinas have been used. (Deng et al., 2010; Kaempf et al., 2008; Simmons et al., 2011; Zhao et al., 2014; Amirpour et al., 2013)

2.1.6 Maturation markers of RPE

When pluripotent cells are differentiated towards RPE, the appearance of pigmentation and the expression of RPE-specific genes (such as *MERTK*, *RPE65,*

MITF, and *bestrophin*) are generally used to assess the maturation status of the produced cells (Bennis et al., 2017; Leach et al., 2016).

MERTK is a protein involved in the phagocytosis of shed photoreceptor outer segments. Genetically modified mice that do not express MERTK or its ligands, are not able to perform phagocytosis (Feng et al., 2002; Mazzoni et al., 2014).

RPE65 plays an important role in the visual cycle. It is an isomerohydrolase that converts all-trans-retinyl ester to 11-cis-retinol (Moiseyev et al., 2005). The expression of *RPE65* has been shown in hESC-RPE on day 28 of differentiation, but not on day 7 (Vaajasaari et al., 2011).

MITF is a protein that regulates differentiation of RPE and melanocytes. In addition, it is involved in melanogenesis. (Shibahara et al., 2001)

Bestrophin acts as an anion channel, as well as a regulator of intracellular Ca^{2+} signaling. Malfunctions of this protein lead to several retinal degenerative disorders – "bestrophinopathies". (Johnson et al., 2017) In hESC-RPE, the expression of *bestrophin* was observed after approximately 28 days of culture (Vaajasaari et al., 2011).

2.1.7 HESC and hiPSC-RPE transplants for treatment of macular degeneration

2.1.7.1 Recent clinical trials

Retina is considered the optimal site for cell-based therapies for several reasons. First, the subretinal space is the immune-privileged site, thus, the probability of graft rejection is lower than in other sites. Second, relatively small number of cells can comprise a successful transplant, and the transplanted cells can be visualized directly, without the need of biopsy. Third, a variety of non-invasive methods that are routinely used in ophthalmology can be used to assess the therapeutic effect. (Schwartz et al., 2016) Finally, in case of adverse effects, an eye can be dissected as it is a relatively isolated system.

The first human clinical trial involving hESC-RPE cells have been performed by Schwartz et al. (2012) The cells were delivered to the AMD patients' eyes via injections (Swartz et al., 2012). The 4-year follow-up showed absence of severe transplantation side effects and moderate functional improvements (Swartz et al., 2016).

Another clinical trial for hESC-RPE transplantation have been performed by da Cruz et al. (2018). In this trial, the fully differentiated hESC-RPE cells were placed

on a synthetic basement membrane. The authors reported successful delivery and survival of the grafts and improvement in patients' visual acuity over a period of 12 months. (da Cruz et al., 2018)

Mandai et al. have transplanted hiPSC-RPE into patients with AMD. The hiPSC were derived through reprograming patients' own fibroblasts. One year after the surgery, the transplants were intact, and the visual acuity was not changed. (Mandai et al., 2017)

2.1.7.2 Evaluation of RPE-specific features prior to transplantation

Before transplanting hESC-RPE cells into an eye to rescue photoreceptors, it is critically important to ensure hESC-RPE similarity to native RPE not only morphologically, but also functionally because manufacturing manipulations can result in epithelial to mesenchymal transition and senescence (Grisanti et al., 1995).

In RPE cells, Ca^{2+} ions play a major role in controlling such important physiological processes as differentiation, dark adaptation of photoreceptor activity, trans-epithelial transport of ions and water, phagocytosis, and secretion of growth factors (Wimmers et al., 2007). Hence, evaluation of Ca^{2+} signaling may serve to assess RPE functionality.

2.2 Ca^{2+} signaling

2.2.1 Ca^{2+} signaling general background

Calcium is a universal intracellular messenger that controls vital cellular functions (Berridge et al., 2012). It has been shown to trigger and modulate cell division (Pande et al., 1996; Humeau, 2018), migration (Wei, 2012), contraction (Cheng et al., 1993), exocytosis (Beutner et al., 2001), endocytosis (Sankaranarayanan and Ryan, 2001), necrosis (Kruman and Mattson, 1999), apoptosis (Pinton et al., 2008), and other physiological processes (Islam, 2012).

Concentration of free cytosolic Ca^{2+} inside cells ($[Ca^{2+}]_i$) is maintained as low as 100 nM with a 1:10,000 gradient between intra- and extracellular space. However, the total amount of Ca^{2+} inside cells is quite high because Ca^{2+} is stored in special compartments, such as endoplasmic reticulum (ER). Upon activation, $[Ca^{2+}]_i$ transiently increases up to 1000 nM. The $[Ca^{2+}]_i$ transients occur by means of various

"on" and "off" reactions that serve to increase and then decrease $[Ca^{2+}]_i$. Stimulation triggers the "on" reactions that result in Ca^{2+} entry into the cytoplasm either from extracellular space through the channels located on plasma membrane, or via indirect routes that recruit messengers to release Ca^{2+} from intracellular Ca^{2+} stores. Most of the entered Ca^{2+} ions bind to cytoplasmic buffer proteins. However, the non-buffered Ca^{2+} ions can directly bind to proteins changing their function. (Berridge, 2003; Bootman, 2012) Ca^{2+} responses vary greatly in temporal and spatial dynamics allowing for switching on a range of effectors, each of which is sensitive to a certain pattern of $[Ca^{2+}]_i$ dynamics. These effectors regulate a number of physiological processes from very fast ones (e.g. exocytosis, muscle contraction) to slow ones (e.g., transcription, cell proliferation). (Berridge, 2003; Wimmers et al., 2007) During the "off" reactions, Ca^{2+} dissociates from the effectors and buffer proteins and is actively eliminated from the cytoplasm via a number of exchangers and pumps to the extracellular space and to the intracellular Ca^{2+} stores. (Berridge, 2003)

2.2.2 Ca^{2+} homeostasis in RPE

The $[Ca^{2+}]_i$ level is regulated by the equilibrium between the efflux of Ca^{2+} from cytoplasm and the Ca^{2+} influx into cytoplasm. To maintain proper $[Ca^{2+}]_i$, RPE cells express various Ca^{2+} transporting proteins. The scheme of major Ca^{2+} fluxes in and out of cytoplasm are presented in **Fig. 4**.

RPE contains higher concentration of Ca^{2+} than most other cells because melanosomes are able to uptake and store large amounts of Ca^{2+}. The total amount of Ca^{2+} in the RPE cells directly correlates with the level of pigmentation. (Salceda and Riesgo-Escovar, 1990)

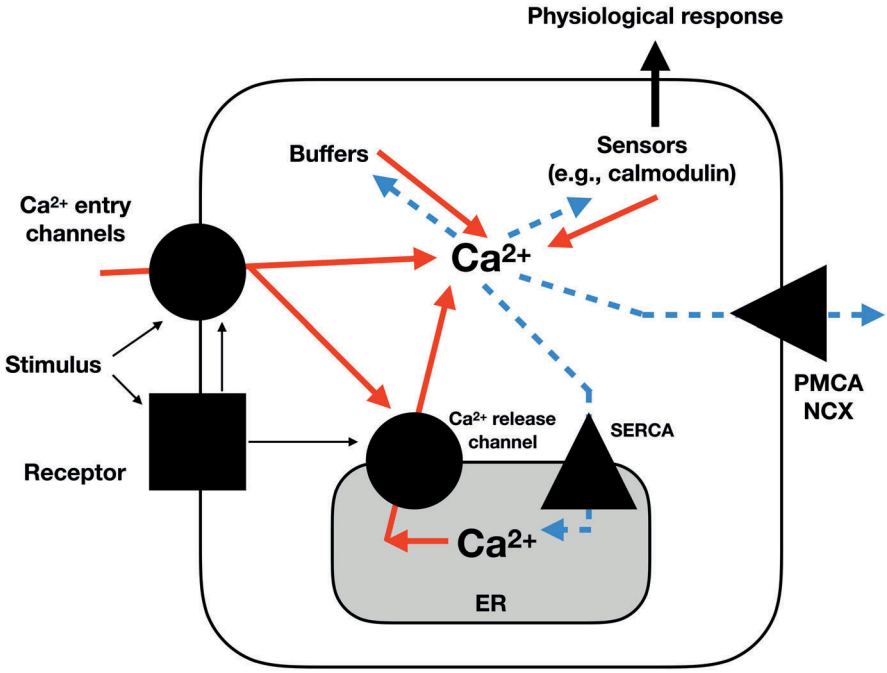

Figure 4. Major Ca^{2+} fluxes in and out of cytoplasm. The bold solid (red) arrows indicate the processes that increase $[Ca^{2+}]_i$. The bold dashed (blue) arrows indicate the processes that decrease $[Ca^{2+}]_i$. The image was re-drawn with modifications from Bootman, 2012.

2.2.2.1 Ca^{2+} efflux from the cytoplasm

The most studied transporter that eliminates free Ca^{2+} from the cytoplasm to maintain low $[Ca^{2+}]_i$ is the Na^+/ Ca^{2+} exchanger (NCX). It removes one Ca^{2+} ion from the cytoplasm in exchange for 3 Na^+ ions that enter the cell. NCX has been identified as a cardiac subtype in RPE. (Mangini, 1998) In case of strong depolarization, the exchanger can switch its working direction. (Wimmers et al., 2007)

The work of the NCX is supported with plasma membrane Ca^{2+}-ATPase (PMCA) that allows transportation of Ca^{2+} against the concentration gradient. PMCA has been found in human RPE (Kennedy and Mangini, 1996), and four isoforms of PMCA have been described in porcine RPE (Kennedy et al., 2007).

Ca^{2+} ions are removed actively from the cytoplasm not only to the extracellular space, but also to the intracellular Ca^{2+} stores. The sarcoendoplasmic reticulum

calcium transport ATPase (SERCA) transports Ca^{2+} from the cytoplasm to the ER (Periasamy, 2007). In RPE, the presence of SERCA has been shown indirectly by application of SERCA-specific blocker thapsigargin, which resulted in ER depletion (Stalmans and Himpens, 1998).

In addition to pumping Ca^{2+} out actively from the cytoplasm, Ca^{2+} ions can diffuse from the cytoplasm to neighboring cells via intercellular GJs. (**Fig. 3**) GJs act as gates for Ca^{2+}, as well as other small ions and molecules, efflux/influx between cells. (Rottingen and Iversen, 2000)

2.2.2.2 Ca^{2+} influx into the cytoplasm

There are two main routes of Ca^{2+} entry into the cytoplasm. First is the Ca^{2+} influx from extracellular space via special protein channels on plasma membrane that open in response to certain stimuli (e.g., ligand binding, depolarization) and allow for direct Ca^{2+} entry into the cytoplasm from extracellular space. Second is the release of Ca^{2+} from intracellular Ca^{2+} stores.

Many organelles, such as mitochondria (Contreras et al., 2010), Golgi apparatus (Micaroni, 2012), endosomes (Gerasimenko et al, 1998), and lysosomes (Lloyd-Evans et al., 2010) are involved in Ca^{2+} signaling as they act as intracellular Ca^{2+} stores. However, generally, ER is considered the main Ca^{2+} pool inside cells (Contreras et al., 2010).

Ca^{2+} release from ER is controlled by inositol-1,4,5-trisphosphate receptors (IP3R) and ryanodine receptors (RyR). (Berridge, 2003)

Three different ITPR genes encode IP3R family producing three subtypes of IP3R: IP3R1, IP3R2, and IP3R3 (Terry et al., 2018). These subtypes have similar basic properties, but differ in regulation (e.g., with small molecules, such as ATP). This allows for emergence of unique spatial and temporal $[Ca^{2+}]_i$ patterns. (Hattor et al., 2004) The opening of IP3R pore on ER requires the presence of both IP3 and Ca^{2+}. IP3 binds to IP3R and promotes binding of Ca^{2+} to a Ca^{2+}-binding site of the receptor. (Colin and Tovey, 2010) Ca^{2+} effect on IP3R is biphasic: low $[Ca^{2+}]_i$ increases the response of the receptor to IP3, while high $[Ca^{2+}]_i$ has inhibitory effect. IP3R has been identified in different epithelia, for example, intestinal (Maranto, 1994) and airway (Sugiyama, 1996).

RyR is activated and deactivated by Ca^{2+} in the same manner as IP3R: RyR is inactive at nanomolar and millimolar $[Ca^{2+}]_i$ levels, but active at micromolar $[Ca^{2+}]_i$. RyR has been shown to take part in Ca^{2+} signaling in rat RPE (Himpens et al., 1999) and ARPE-19 (Wimmers et al., 2008).

Activation of some receptors can stimulate a $[Ca^{2+}]_i$ transient. For example, purinergic P2X receptors act as ligand-gated ion channels and allow extracellular Ca^{2+} into the cytoplasm directly upon binding. Activation of other receptors, such as purinergic P2Y receptors, results in Ca^{2+} release from intracellular Ca^{2+} stores only, without recruiting extracellular Ca^{2+}. (Wimmers et al., 2007)

Below, the functionality of various receptors and channels that are implicated in increasing $[Ca^{2+}]_i$ is discussed.

Voltage-gated Ca^{2+} channels

Voltage-gated Ca^{2+} channels open in response to membrane depolarization. These channels are highly selective for Ca^{2+} conductance over other ions. L-type Ca^{2+} channels are activated by high voltage, have slow inactivation and high conductance, while T-type Ca^{2+} channels are activated by low voltage, have fast inactivation and low conductance. (Catterall, 2011) L-type voltage-gated Ca^{2+} channels have been characterized in primary cultures and freshly isolated RPE cells, as well as in RPE cell lines. (Wimmers et al., 2007) Vainio et al. have demonstrated both L- and T-type Ca^{2+} channels in hESC-RPE (Vainio et al., 2014; Korkka et al., 2018). The channels are considered to be involved in regulation of growth factor secretion (Rosenthal, 2005) and transportation of Cl^- and water (Wimmers et al., 2007). In addition, voltage-gated Ca^{2+} channels have been shown to take part in the generation of the light peak in the human electro-oculogram (Rosenthal, 2006).

Transient receptor potential (TRP) Ca^{2+} channels

TRP channels can be activated by various stimuli, for example, G protein subunits, depletion of Ca^{2+} stores, metabolites of IP3/Ca^{2+} second messenger pathway, temperature and pH change. In ARPE-19 cells, TRP channels define the resting $[Ca^{2+}]_i$. (Wimmers and Strauss, 2007) TRP channels have also been found in human fetal RPE. There, these channels act as Ca^{2+} sensors in the subretinal space. (Zhao, 2015)

Stretch-sensitive channels

Stretch-sensitive Ca^{2+} channels (SSCC) have been identified in a number of cell types. SSCC locate on cellular membranes and open in response to mechanical pressure. The channels close when mechanical stress is released or when cells adapt to the pressure by decreasing their sensitivity through reinforcing adhesion structures

or global repositioning of the stressed adhesions (Matthews et al., 2006). These channels control cell shape, volume and motility. (Hamil, 2006) Numerous articles have reported RPE to be sensitive to mechanical pressure (Sachs, 2010). In RPE cells, membrane stretch has been demonstrated to affect Ca^{2+}-activated potassium channels (Sheu et al., 2005), but to the best of our knowledge, no direct evidence of the presence of SSCCs in RPE has been presented to date.

Glutamate receptors

Glutamate can activate both ligand-gated ion channels and G protein coupled receptors (Kew and Kemp, 2005). The RPE express both types of the receptors (Feldman et al, 1991, Fragozo and Lopez-Colome, 1999). Glutamate has been proposed to regulate dark adaptation of photoreceptors and phagocytic activity of RPE (Wimmers et al., 2007).

P2X receptors

P2X receptors act as ion channels. They can be activated by ATP, and with much lower efficiency by ADP. P2X receptors cannot be activated by AMP, adenosine or other purines or pyrimidines. Ligand binding results in channel opening that selectively conducts small cations (Ca^{2+}, Na^{+}, K^{+}), but not anions. (North and Jarvis, 2013) The expression of P2X receptors has been demonstrated in primary RPE cells (Ryan et al., 1999; Yang, 2011), as well as ARPE-19 cell line (Dutot et al., 2008). P2X receptors have been shown to induce apoptosis in human RPE. In other cell types, P2X receptors are involved in oxidative stress and inflammation, which are also implications in AMD. Therefore, these receptors are potential key players in AMD pathogenesis. (Yang, 2011)

P2Y receptors

P2Y receptors act as G protein-coupled receptors activated by ATP and other extracellular nucleotides (von Kügelgen and Hoffmann, 2016). The ligand binding causes conformational change of a G protein. Next, α-subunit exchanges GDP for GTP, which results in G protein dissociation into a GTP-bound α-monomer and a βγ-dimer. In next step, GTP-bound α–monomer activates phospholipase C (PLC), which then hydrolyzes membrane-bound phosphatidylinositol-4,5-bisphosphate (PIP2) into inositol-1,4,5-trisphosphate (IP3) and diacylglycerol (DAG). The IP3 then activates receptors on endoplasmic reticulum releasing Ca^{2+} into the cytoplasm.

In addition, both Ca^{2+} and DAG activate protein kinase C (PKC). PKC is a major effector of cellular functional regulation. Receptor activation is terminated by G protein-coupled receptor kinases and arrestins. (Stone and Molliver, 2009) The RPE cells express P2Y receptors (Peterson et al., 1997, Tovell, 2008). Their activation has been reported to increase membrane conductance of Ca^{2+}, Cl^-, and K^+ and transport of ions and fluids across epithelia (Peterson et al., 1997; Ryan et al., 1999).

In chapter 2.2.3 the importance of Ca^{2+} signaling triggered by ATP is discussed.

2.2.3 The role of Ca^{2+} signaling triggered by ATP in RPE

ATP, that acts not only as an energy mediator, but also as a modulator of cell signals, can activate P2X and P2Y receptors in RPE, as described earlier. ATP acts as an intercellular messenger. RPE cells can be stimulated by ATP that comes from other cells through paracrine signaling or can release ATP themselves inducing autocrine signaling. (Wimmers et al., 2007)

It has been proposed that ATP signaling between RPE and developing retina is essential for retinal cell proliferation and differentiation. For example, application of extracellular ATP to neural retinal progenitor cells increased the speed of mitosis by activating P2Y receptors (Pearson, 2002). Pearson et al. have shown that ATP was released by RPE cells through spontaneous openings in GJ hemi-channels (Pearson et al., 2005).

In the mature RPE layers, ATP increases flows of ions and water from subretinal space towards choroid. It has been shown that application of ATP (or UTP) to bovine RPE resulted in cellular $[Ca^{2+}]_i$ transients and subsequent increase in fluid absorption. (Peterson et al., 1997)

In pathological conditions, RPE cells have been shown to release ATP during swelling (Mitchell, 2001). The RPE swelling is typical in retinal degeneration diseases. Thus, chronic swelling that accompanies these medical conditions could lead to continuous increased ATP release that contributes to the development of the diseases. (Guha et al., 2013) Moreover, Guha et al. have suggested that the concentration ratio of extracellular ATP and adenosine may affect lipofuscin production in AMD (Guha et al., 2014).

2.2.4 Spontaneous $[Ca^{2+}]_i$ transients

$[Ca^{2+}]_i$ can elevate in cells without application of an external stimulus. Spontaneous $[Ca^{2+}]_i$ transients have been observed in various tissues, such as developing retina (Catsicas et al., 1998), smooth muscle cells (Dabertrand et al., 2008), glia (Mathiesen et al., 2013), cardiomyocytes (Lukyanenko and Györke, 1999), mesenchymal stem cells (Kawano et al., 2002), capillary epithelia (Ying et al., 1996), and other (Leybaert and Sanderson, 2012).

In developing chick retina, the spontaneous $[Ca^{2+}]_i$ spikes have been observed from day 8 embryos onwards. The spikes reached their peaks within 2-3 seconds and then decayed back to initial $[Ca^{2+}]_i$ within 20-30 seconds. The spontaneous $[Ca^{2+}]_i$ transients propagated as Ca^{2+} waves towards neighboring cells to a 1 mm distance at a speed of 150 μm/s. It was determined that extracellular Ca^{2+} was the main source of the $[Ca^{2+}]_i$ increases. The Ca^{2+} waves could be blocked with the GJ blocker octanol. (Catsicas, 1998)

Pearson et al. have shown that RPE cells in chick embryos exhibited spontaneous $[Ca^{2+}]_i$ transients in individual cells, 5 to 10 per cent of which propagated as intercellular Ca^{2+} waves (Pearson et al., 2004). The waves spread with the speed of 9 ± 1 μm/s to 10-20 neighboring cells away from the trigger cells. The direct measurements of ATP with ATP-sensitive biosensors showed that RPE cells secreted ATP. Moreover, the authors provided evidence that ATP was spontaneously released by trigger cells through Cx43 uncoupled hemi-channels. The blockade of these ATP releases resulted in markedly reduced speed of cell division in the underlying progenitor retina. (Pearson et al., 2005)

Spontaneous $[Ca^{2+}]_i$ transients play a major role in cell proliferation and differentiation. For example, in Xenopus laevis Ca^{2+}spontaneously released from ER through activation of RyR have been shown to control differentiation of myocytes towards somites (Ferrari, 1998). In addition, spontaneous $[Ca^{2+}]_i$ transients have been demonstrated to occur in the G1 to S transition phase of the cell cycle in neural progenitor and undifferentiated cells. The transients depended on voltage-gated Ca^{2+} channels and IP3R. (Resende et al., 2010)

To our knowledge, spontaneous Ca^{2+} activity has not been previously studied in hESC-RPE cells.

2.2.5 Cellular mechanosensitivity and mechanically induced Ca^{2+} waves

Electrophysiological recordings obtained from vertebrate hair cells were pioneer experiments that proposed the presence of ion channels directly activated by mechanical stimuli (Corey and Hudspeth, 1979). Later, mechanosensitive ion channels have also been found in non-sensory tissues, for example, in skeletal muscle (Guharay and Sachs, 1984). Since then, a number of mechanosensitive channels have been discovered. Among them are mechanically activated sodium channels (Chalfie, 2009), transient receptor potential ion channels (AbouAlaiwi et al, 2009), potassium channels (Brohawn et al., 2014), and piezo ion channels (Coste et al., 2010) These channels are considered to be activated by the mechanical force that is transduced through the lipid bilayer with possible involvement of auxiliary force transmission proteins (e.g., extracellular matrix or cytoskeleton proteins). (Ranade et al., 2015)

Single cell mechanical stimulation (with, e.g., with a glass micropipette) evokes $[Ca^{2+}]_i$ transients in the stimulated cell that travel to neighboring cells in a wave-like manner. These mechanically induced Ca^{2+} waves have been observed in various cell types: epithelial cells (Churchill et al., 1996; Stalmans and Himpens, 1998), glial cells (Charles et al., 1991), hepatocytes (Schlosser et al., 1996), neurons (Charles et al., 1996), osteoblasts (Xia and Ferrier, 1992), endothelial cells (D'hondt et al., 2007).

There are two possible routes of transient $[Ca^{2+}]_i$ propagation between cells: gap junctional and paracrine.

2.2.5.1 Gap junctional propagation route

Mechanical stimulus results in membrane stress that triggers IP3 production in the stimulated cell. IP_3 then diffuses towards the ER and activates IP3R. This causes $[Ca^{2+}]_i$ increase that is further amplified through the activation of RyR. The remaining IP3 can diffuse together with Ca^{2+} ions through GJs to adjacent cells, initiating $[Ca^{2+}]_i$ transients. (Leybaert and Sanderson, 2012)

A number of studies have proved the ability of IP3 to diffuse via GJs (**Fig. 3**) and take part in the Ca^{2+} wave propagation (Leybaert and Sanderson, 2012). In one of the studies, cells with a mutant Cx26 that were impermeable to IP3 were not able to produce intercellular Ca^{2+} waves in response to IP3 injection (Beltramello et al., 2005).

Ca^{2+} ions can also pass through GJs. However, unlike IP3, Ca^{2+} ions are strongly buffered in the cytoplasm (Berridge, 2003). The buffering is one of the mechanisms to control the number of free cytosolic Ca^{2+} ions, when the ions are bound to or

released from special cytosolic molecules. It happens rapidly compared to Ca^{2+} sequestration to the intracellular stores. (Gilabert, 2012) The Ca^{2+} buffering restricts Ca^{2+} diffusion across the cytoplasm and, thus, chances to reach a neighboring cell via GJs. The effective diffusion coefficient for IP3 is 280 $\mu m^2/s$, while for Ca^{2+} it is only 13 $\mu m^2/s$ (Allbritton et al., 1992). Hence, it is more likely that IP3 has a greater impact than Ca^{2+} in propagating Ca^{2+} waves to the neighboring cells.

The involvement of GJs in mechanically induced Ca^{2+} waves spreading has been shown in a number of cell types (Sanderson et al., 1990; D'Andrea and Vittur, 1996; Boitano et al., 1992; Gomes et al., 2006; Churchill et al., 1996; Himpens et al., 1999). When glioma cells that lacked GJs were mechanically stimulated, the resulting $[Ca^{2+}]_i$ transient was restricted to the stimulated cell and did not propagate as a wave. However, when the cells were transfected with Cx43 and gained electrical coupling, the mechanical stimulation resulted in intercellular Ca^{2+} waves. Moreover, the distance of the Ca^{2+} wave propagation was directly proportional to the Cx43 expression level. Similar results were obtained after transfection of cells with Cx26. (Charles et al., 1992)

2.2.5.2 Paracrine propagation route

Cells can use a paracrine route as an alternative or together with gap junctional route of Ca^{2+} wave propagation. Upon stimulation, a cell can release ATP via unopposed Cx hemi-channels, anion channels, or vesicular release. ATP diffuses from the stimulated cell activating P2 receptors on neighboring cells, which triggers IP3 production and, subsequently, $[Ca^{2+}]_i$ increases. (Leybaert and Sanderson, 2012)

When an extracellular factor takes part in intercellular Ca^{2+} wave propagation, the waves are able to "jump" over cell-free lanes. In addition, perfusion flow usually affects the direction of the wave spreading. (Leybaert and Sanderson, 2012)

The mechanical stimulation has been reported to induce ATP-dependent signaling in different cell types including endothelial cells (Gomes et al., 2005), epithelial cells (Homolya et al., 2000), and hepatocytes (Schlosser et al., 1996).

In retinal astrocytes and Müller cells, mechanical stimulation has been shown to induce ATP release. ATP concentration at the stimulation site was at the level of 78 μM, while at a distance of about 100 μm from the stimulation site, the concentration decreased to 7 μM. (Newman, 2001) It has been demonstrated that $[Ca^{2+}]_i$ transients lagged behind ATP propagation (ATP diffusion speed was 41 $\mu m/s$, while Ca^{2+} wave propagation speed was 28 $\mu m/s$), which was also consistent with modeling results (Newman, 2001; Bennett et al., 2005).

2.2.5.3 Mechanically induced Ca^{2+} waves in RPE

Mechanically induced Ca^{2+} waves have been investigated in several rat RPE cell lines. Rat RPE has been shown to produce intercellular Ca^{2+} waves upon mechanical stimulation (Stalmans and Himpens, 1997; Gomes et al., 2003). The Ca^{2+} wave propagation depended on Cx43 GJ route of propagation and had no evidence of paracrine route of the wave spreading (Stalmans and Himpens, 1997; Stalmans and Himpens, 1999). The Ca^{2+} waves could be inhibited by high glucose concentrations (above 14 mM) and by activation of PKC (Stalmans and Himpens, 1997; Stalmans and Himpens, 1999; Gomes et al., 2003). Depletion of intracellular Ca^{2+} stores with thapsigargin significantly reduced the amplitudes of $[Ca^{2+}]_i$ transients but could not fully block the wave spreading.

2.2.6 $[Ca^{2+}]_i$ measurements with fluorescent dyes

Ca^{2+} concentrations are routinely measured in cellular cytoplasm with fluorescent indicators. In general, molecules of such indicators consist of a Ca^{2+}-biding part and a fluorescent part.

Fluorescent Ca^{2+} dyes are classified as ratiometric (dual wavelength) and non-ratiometric (single wavelength) dyes. (Vetter, 2012)

2.2.6.1 Ratiometric dyes

Ratiometric dyes shift their excitation or emission spectra upon binding of Ca^{2+}. These dyes contain electron-donating and electron-accepting groups within one molecule. Upon a photon absorption by a fluorophore, electrons move from the donor side to the acceptor side. When a metal interacts with an electron-donating group, the electron donating capacity of the group decreases. This leads to the blue-shift of the absorption spectrum. When a metal interacts with an electron-accepting group, the internal charge transfer increases resulting in the red-shift of the absorption spectrum. (Atwood, 2017) Fura-2 is a ratiometric dye. Its Ca^{2+}-free form has an excitation maximum at 362 nm, while the excitation maximum of a Ca^{2+}-bound form is at 335 nm. The binding of Ca^{2+} is also accompanied by a two-fold increase in fluorescence emission intensity. The emission maximum, however, virtually stays unchanged at about 510 nm. The measurements are performed by altering excitation wavelengths from 340 to 380 nm with a minimum time delay. The

ratio of emitted fluorescence intensities F340/F380 is used to follow the changes of $[Ca^{2+}]_i$. The value of the ratio does not depend on the absolute fluorescence intensities. This is beneficial because it eliminates several measurement artefacts that normally affect single-wavelength dyes, such as dye leakage, photobleaching, and other. (Dustin, 2000) Most ratiometric dyes have excitation maxima in the ultraviolet range. Therefore, the main disadvantages of these dyes include cellular photodamage and increased autofluorescence that occur due to exposure to the ultraviolet light. (Vetter, 2012)

2.2.6.2 Non-ratiometric dyes

Non-ratiometric dyes increase fluorescence emission intensity upon Ca^{2+} binding. In the ion-free form, the fluorescence of the fluorophore is quenched, for example, via electron transfer from the aniline donor. Upon binding of Ca^{2+}, the electron transfer becomes thermodynamically unfavorable, which results in the fluorescence increase. (Batat et al., 2012) Non-ratiometric dyes do not exhibit emission or excitation shift when binding to Ca^{2+}, which allows for faster $[Ca^{2+}]_i$ measurements with simple imaging protocols. These dyes usually work in the visible range that does not cause as much phototoxicity as ultraviolet light that is often used with ratiometric dyes. In addition, because these dyes can be excited with one wavelength and emit one wavelength, this eliminates the necessity of using complex equipment. The main disadvantage of non-ratiometric dyes is that their emission intensity is affected by the dye concentration, dye leakage and photobleaching. Thus, $[Ca^{2+}]_i$ measurements performed with non-ratiometric dyes tend to be less accurate. The time-based ratioing has been proposed to overcome these disadvantages. In this approach, the fluorescence intensity is calculated relative to a baseline fluorescence value. (Minta et al., 1989; Smith and Augustine, 1988)

Fluo-4 is an example of non-ratiometric dye with the absorption maximum at 494 nm, and emission maximum at 516 nm (Gee et al., 2000). When fluo-4 molecules bind to Ca^{2+}, its fluorescence intensity has more than a 100-fold increase.

2.2.6.3 Loading of dyes into cells

Acetoxymethyl (AM) ester loading has become one of the most popular techniques of dye loading due to its simplicity (Vetter, 2012). In this technique, a heavy anionic fluorescent Ca^{2+} probe that is unable to pass through a lipid bilayer of a cellular

membrane is attached to lipophilic AM groups. This makes the dyes membrane-permeable. Once in the cytoplasm, cellular esterases hydrolyze the AM tails trapping the dye inside the cell as it is not able to cross the cellular membrane again without the AM group. Many Ca^{2+}-fluorescent dyes, including fura-2 and fluo-4, are commercially available as "AM" forms. The protocols for cell loading are simple: the cells are incubated with the dye, and the excess dye is then washed from the extracellular media.

The disadvantages of the AM dyes are compartmentalization (Di Virgilio et al., 1990), incomplete AM esters hydrolyzation, and dye extrusion via anion transporters (Vetter, 2012).

The compartmentalization can be reduced by performing dye loading at room temperature rather than at 37 ^{o}C, while AM esters hydrolyzation is more effectively performed at physiological temperatures, i.e. 37 ^{o}C (Vetter, 2012). Dye extrusion can be reduced by using anion channels inhibitors, for example, probenecid (Di Virgilio et al., 1990), however, this can also alter cellular physiological processes. Conducting the imaging at room temperature can also minimize dye extrusion (Paredes et al., 2008).

To conclude, the optimal conditions of the dye loading need to be determined experimentally for each cell type. In general, loading cells with a Ca^{2+}-sensitive AM ester dyes and performing measurements as quickly as possible at room temperature tend to work for the majority of cell types.

2.2.6.4 Genetically encoded Ca^{2+} indicators (GECI)

GECIs are fluorescent $[Ca^{2+}]_i$ reporters that can be incorporated into the genome of tissues and even organisms and allow for long-term *in vivo* measurements of $[Ca^{2+}]_i$ (Koldenkova and Nagai, 2013). In contrast to fluorescent Ca^{2+} dyes, GECIs can be designed to express in specific cell compartments, populations or organs (Tian et al., 2012). GECIs are chimeric fluorescent proteins that consist of a Ca^{2+}-binding domain attached to one or two fluorescent proteins. The Ca^{2+} binding domain usually represents a part of a calmodulin or troponin C proteins. (Tian et al., 2012; Koldenkova and Nagai, 2013) Binding of Ca^{2+} to the Ca^{2+}-binding domain results in interaction of this domain with the fluorescent protein, which in turn changes fluorescence properties of the GECI (Tian et al., 2012).

2.2.6.5 Limitations of using Ca^{2+}-sensitive dyes

One of the main concerns about using Ca^{2+}-sensitive dyes in general is their buffering capacity. To produce the signal, Ca^{2+}-sensitive dyes bind to Ca^{2+} ions reducing Ca^{2+} concentration in the cytoplasm and changing the Ca^{2+} dynamics pattern. The dyes tend to lower the amplitude of Ca^{2+} spikes in the cells and increase the time of the signal decay. (McMahon and Jackson, 2018; Tian et al., 2012)

2.2.7 Cell detection on fluorescence images

The fluorescence images obtained in Ca^{2+} imaging experiments are often analyzed manually (Gomes et al., 2003; Dombeck et al., 2007; Niell and Smith, 2005; Stalmans and Himpens, 1998). The user defines cells by drawing cell boundaries or regions inside cells. This process is time-consuming and involves user-dependent errors (Lorenz et al., 2003; Mukamel et al., 2009).

Automated cell segmentation algorithms have been suggested to detect cells on static immunofluorescence images with labelled cell nuclei and cell-to-cell junctions (Yang et al., 2013), as well as on time-lapse Ca^{2+} images (Shen et al., 2018). In addition, algorithms have been proposed to detect Ca^{2+} signaling events rather than to segment individual cells (Picht et al., 2007; Wegner et al., 2006; Francis et al., 2014). To the best of our knowledge, no automatic detection algorithms have been developed to segment RPE cells on fluorescence images obtained with Ca^{2+}-sensitive dyes.

2.3 Wound healing

In the body, wound healing process takes place in several stages: haemostasis, inflammatory, proliferative, and maturation stages (Velnar et al., 2009; Weber et al., 2012). Haemostasis occurs directly after wounding. During haemostasis, blood vessels contract to prevent blood loss. In addition, coagulation cascade is activated. (Pool, 1997; Velnar et al., 2009) In the inflammatory phase, macrophages and neutrophils are attracted to the wounded area to eliminate bacteria, injured cells, and prevent further tissue damage (Broughton et al., 2006). During the proliferative stage, new blood vessels are formed, formation of granulation tissue takes place, and the cells produce new extracellular matrix (ECM) (Velnar et al., 2009). ECM serves as a scaffold for cells migrating into the wounded area. Fibroblasts attracted to the

wound secrete collagen that is essential for providing strength to the wound. (Weber et al., 2012) Re-epithelialization takes place in the proliferative phase (Velnar et al., 2009). The final maturation phase consists of wound contraction and remodeling of collagen layer from type III to type I (Weber et al., 2012).

2.3.1 Epithelial-mesenchymal transition (EMT) of epithelial cells

During wound healing, epithelial cells undergo epithelial-mesenchymal transition in order to migrate towards the wounded area. Epithelial cells develop migratory phenotype by losing intercellular junctions and apical-basal polarity. (Weber et al., 2012) It has been demonstrated that cells undergoing EMT lose such epithelial markers as occludins, claudins (TJ proteins), and cadherins (adherence junctions components) (Yilmaz and Christofori, 2009). This process is controlled by transforming growth factor β (TGF-β)-dependent pathway and Wnt/β-catenin pathway (Weber et al., 2012; Burke, 2008). At the same time, the cells gain mesenchymal markers (e.g., vimentin, fibroblast-specific protein, tenascin-C and other) (Weber et al., 2012).

In the eyes, RPE cells maintain highly regular cobblestone cell shape, however, when grown in a cell culture, RPE cells show the ability to de-epithelialize through EMT transition, expand, and then reverse back to the epithelial phenotype. (Burke et al., 1996; Burke, 2008) In addition, RPE cells undergo TGF-β dependent EMT in the conditions of chronic wounding (Shih et al., 2017).

Rho-associated coiled-coil kinases (ROCKs) regulate cytoskeletal rearrangements during EMT (Vardouli et al., 2005). Inhibition of ROCKs has been shown to prevent EMT. It is hypothesized that ROCK inhibition affects TGF-β contributing to scarring (Wynn, 2007; Croze et al., 2014). Croze et al. have shown that ROCK inhibition increased hESC-RPE cells attachment and enhanced cell spreading within the first hour after cell plating (Croze et al., 2014; Croze et al., 2016).

2.3.2 Ca^{2+} signaling during wound healing on uni- and multicellular levels

When an epithelial cell layer is damaged, the ionic gradient collapses along the wounded area. For example, affected cells uptake Cl^- ions, while Na^+ ions leak out of the cells following the concentration gradient (Martin-Granados and McCaig, 2014). Wound healing is a composite process that implies an interplay between ion channels to define conductance of ions across cellular membranes that are critical

for response to tissue injury (Franklin et al., 2017). Potassium (Zundler et al., 2016), sodium (Justet et al., 2013) and calcium channels (Lansdown, 2002) have been reported to be crucial for the wound healing.

Ca^{2+} signaling plays a major role not only in maintaining normal epithelial physiology, but also in the event of cell injury. Ca^{2+} in the extracellular medium is the necessary condition for cellular membrane sealing after wounding (Steinhardt et al., 1994). In addition, the studies where Ca^{2+} was directly injected into the cytoplasm showed that the injected liquid became encapsulated by intercellular membrane vesicles (Terasaki et al., 1997). These studies suggest that upon mechanical injury of plasma membrane (e.g., piercing), Ca^{2+} ions entering the cytoplasm through the membrane hole from the extracellular space down the concentration gradient prompt non-specific membrane fusion of internal vesicles. These fused vesicles seal the hole in the membrane preventing further Ca^{2+} entry. The blockade of kinesin and myosin proteins inhibits vesicles transportation, and as a result, fails membrane closure. (Bi et al., 1997)

Another consequence of plasma membrane piercing, aside from Ca^{2+} influx, is the efflux of the molecules that normally locate inside the cells into the extracellular media. For example, basic fibroblast growth factor (bFGF) that is stored in the nucleus and cytoplasm leaks to the extracellular space upon cell injury. It has been shown that the amount of bFGF leaking through the wounded cell was enough to cause the mitogenic effect on unwounded cells (McNeil et al., 1989). Another paracrine factor that acts as a signal to non-wounded neighboring cells about the injury event is ATP. ATP is stored at mM concentrations inside the cells, and once it leaks out, it creates abnormally high concentration of ATP around the injury site and diffuses to the non-wounded cells. (Woolley and Martin, 2000)

In case of more severe tissue wounds, when many cells are being mechanically injured, the initial Ca^{2+} influx into the damaged cells is considered to be the essential signal for the undamaged cells to rearrange their junctions and coordinate movement (Woolley and Martin, 2000). The mechanical injury of a cellular monolayer results in emergence of an intercellular Ca^{2+} wave that spreads from the wound edges towards the non-injured cells. The absence of extracellular Ca^{2+} significantly reduces cellular migration to the wounded area, while high extracellular Ca^{2+} concentration results in increased cell motility. (Tran et al., 1999)

2.3.3 Wounding and wound healing in RPE

Patients with wet form of AMD are often being treated by surgical removal of neovascularization. This procedure creates a local defect in the RPE cell layer and underlying Bruch's membrane. The inability of the cells to grow into the wounded area affects choriocapillaris and photoreceptors integrity and functionality. (Sugino et al., 2003; Nasir et al., 1997; Korte et al., 1989) Rapid RPE restitution, the process of fast proliferation and migration of RPE to heal the wounded areas, has been proposed to be beneficial for maintaining the remaining photoreceptors (Fleckner et al., 2000; Miura et al., 2003).

Wound healing has been studied in animal and human RPE, for example, bovine (Miura et al., 2003), chick (Hergott et al., 1993), rabbit (Oganesian et al., 1997), porcine (Tamiya, 2010), and hESC-RPE cells (Croze et al., 2016).

2.3.3.1 RPE wound healing *in vivo*

In *in vivo*, RPE wound healing has been studied in different animal models including rabbits. In rabbits, RPE wounds were made with subretinal hydraulic irrigation that caused minimal damage to Bruch's membrane, but significant damage to the RPE layer. Upon wounding, the cells changed their epithelial phenotype towards a migratory phenotype and slid from the periphery to the wound area. However, the authors stated that it was unclear whether the main role of repopulating the injured area belonged to the sliding migration of native peripheral RPE or to their hyperplastic descendants. The complete re-epithelialization of the wound occurred within 7 days, after which the cells gradually returned to the native phenotype. Multilayered RPE patches were observed together with the RPE monolayer. (Oganesian, 1997)

2.3.3.2 RPE wound healing in cell cultures

Wounding of RPE cells grown in cultures *in vitro* triggers changes in cell morphology close to the wound edges, while distant cells remain unchanged. The cells lose the cobblestone morphology and gain a migratory phenotype. The RPE cells proliferate and migrate into the wounded area to resurface the defect. (Verstraeten et al., 1990; Kaida et al., 2000; Grisanti, 1995) It has been reported that RPE cells can migrate as

cellular sheets or as single cells depending on the time they spent in the culture prior to wounding (Kaida et al., 2000).

Wound healing has been studied in hESC-RPE cultures. These cells migrate into the wounded area not always as cell sheets like other epithelia (Matsubayashi et al, 2004; Rosen and Misfeldt, 1980), but sometimes as single cells. (Croze et al., 2016) In addition, it has been shown that pan ROCK inhibition accelerated scrape wound healing in hESC-RPEs: the cells treated with pan ROCK inhibitors had higher proliferation rates and regained cobblestone morphology faster than in control cultures (Croze et al., 2016).

3 AIMS

The aim of this study was to investigate Ca^{2+} dynamics (mechanically induced and spontaneous $[Ca^{2+}]_i$ transients) in human RPE cells and to determine whether factors such as cellular maturation status and wounding affect it. The specific aims of the thesis are as follows:

- To develop biomedical engineering tools to assess mechanically induced and spontaneous Ca^{2+} activity in RPE cells. (**Study I-IV**) This will benefit biomechanistic studies, as well as possible assessment of cells in the clinical context.
- To use the developed tools for investigation and analysis of the effect of mechanical stimulation on RPE cells. (**Study I-IV**)
- To reveal the mechanism of intercellular Ca^{2+} wave propagation induced by mechanical stimulation experimentally and with mathematical modeling approach. (**Study I, II**)
- To determine whether maturation status affects spontaneous and mechanically induced $[Ca^{2+}]_i$ transients. (**Study III**) This knowledge can be applied in the future for evaluating cells intended for transplantation.
- To assess the effect of scrape wounds and wound healing on spontaneous and mechanically induced $[Ca^{2+}]_i$ transients to benefit understanding of RPE wound healing processes. (**Study IV**)

4 METHODS

The methods of Ca^{2+} imaging, wounding and wound healing assays, immunofluorescence staining, and PCR with de novo developed computational methods for the analysis of large amount of experimental data were applied to ARPE-19 and hESC-RPE cells to achieve the goals of the thesis. The flow chart of the methods used in this thesis are presented in **Fig. 5**.

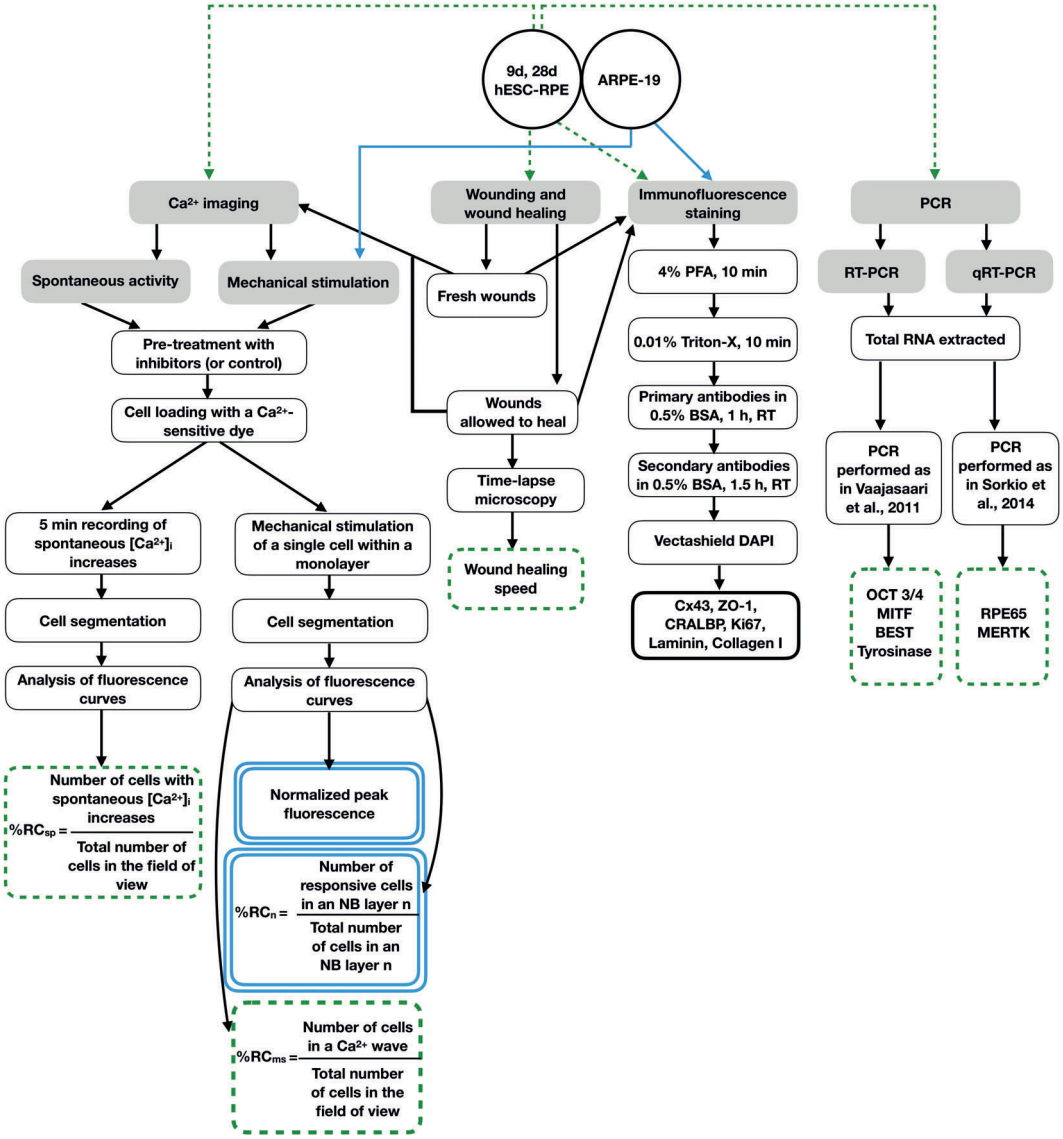

Figure 5. The flow chart of the methods used in the thesis. Green boxes (dotted frames) indicate results derived for hESC-RPE cells. Blue boxes (double frames) represent the results derived for ARPE-19 cells. 9d hESC-RPE – hESC-RPE cultured for 9 days; 28d hESC-RPE – hESC-RPE cultured for 28 days. All abbreviations can be found in the "Abbreviations" section.

4.1 Cell culturing

4.1.1 ARPE-19

A human immortalized RPE cell line ARPE-19 (**Study I, II**) was cultured in Dulbecco's modified Eagle's medium (DMEM) supplemented with 10% fetal bovine serum (FBS), 2 mM glutamax, and an antibiotic mixture of 100 U/ml penicillin/streptomycin. The cells were cultured at 37 ^{o}C in a humidified atmosphere containing 5% CO_2. For the experiments, cells were washed with Ca^{2+}- and Mg^{2+}-free phosphate buffered saline (PBS) solution, dissociated with trypsin-EDTA, and seeded on coverslips or glass-bottomed cell culture dishes at a density of ~ $1.5*10^5$ cells/cm^2.

4.1.2 hESC-RPE

4.1.2.1 Differentiation of hESC-RPE

The two hESC lines Regea08/017 (**Study IV**) and Regea08/023 (**Study III, IV**) derived and characterized, as described in Skottman, 2010, were used in this thesis. Briefly, the undifferentiated hESC lines were cultured on mitotically inactivated, mitomycin-treated (10 μg/ml) human foreskin fibroblasts feeder cells. Then, hESCs were differentiated towards RPE cells in RPEbasic medium (Vaajasaari et al., 2011) as cell aggregates for 49-147 days. Pigmented areas of floating aggregates were manually chosen, dissociated with trypsin–EDTA, plated with methods described previously (Vaajasaari et al., 2011), and cultured for 28-174 days to expand the number of cells.

4.1.2.2 Culturing of hESC-RPE for the experiments

After expansion, the hESC-RPEs were dissociated with 1x Trypsin–EDTA and plated on Ormocomp-treated (Käpylä et al., 2014), collagen IV (ColIV)-coated coverslips (7 mm in diameter) at a density of 10^5 cells/cm^2. The cells were cultured for a period of 9 ± 1 (**Study III, IV**), 16 ± 1 (**Study IV**), 28 ± 1 (**Study III, IV**), or

35 ± 1 (**Study IV**) days in RPEbasic medium. The medium was replenished three times a week.

4.2 Ca^{2+} imaging

4.2.1 General Ca^{2+} imaging procedures

For Ca^{2+} imaging experiments (**Study I-IV**), the cell culture medium was substituted with Hanks balanced salt solution (HBSS) containing: 137 mM NaCl, 5 mM KCl, 0.44 mM KH_2PO_4, 20 mM HEPES, 4.2 mM $NaHCO_3$, 5 mM glucose, 1.2 mM $MgCl_2$, and 2 mM $CaCl_2$. pH was set to 7.37 with NaOH; osmolarity was adjusted to 335 ± 5 mOsm/kg with sucrose.

The Ca^{2+}-sensitive dyes fura-2-AM (**Study I, II**) and fluo-4-AM (**Study III, IV**) were used to estimate changes in $[Ca^{2+}]i$ under different conditions. The cells were washed with HBSS once, then incubated with either 8 μM fura-2-AM in HBSS for 40 min at 37 °C, or with 4 μM fluo-4-AM in HBSS for 1 h at room temperature (RT). Then, the cells were washed with HBSS at least thrice.

4.2.2 Assessment of blocker effects on Ca^{2+} dynamics

To assess the effect of different drugs on intra- and intercellular Ca^{2+} dynamics, the cells were pre-incubated with inhibitors in HBSS solution after the Ca^{2+}-sensitive dye loading and before the recording of Ca^{2+} dynamics. The list of the used inhibitors and their expected effects are presented in **Table 1**.

Table 1. Blockers used in Ca^{2+} imaging experiments

Reagent	Concentration, μm	Incubation time, min	Expected effect	Study
18-α-GA	30	30	Blockage of Cx43 GJ	I, III
Quinidine	3, 30, 300	10	Non-specific GJ blockage	I
1-Heptanol	1000	50	Non-specific GJ blockage	I
Suramin	50	25-30	P2 receptor blockage	I, III
Thapsigargin	2	10	Depletion of intracellular Ca^{2+} stores	I, III
18-α-GA + suramin	30 + 50	25-30	Blockage of GJ and P2 receptors	II

4.2.2.1 Recording protocol

The cellular Ca^{2+} dynamics was recorded with an inverted fluorescence microscope Olympus IX51 and ANDOR iXion 885 camera. Fluorescence dyes were excited with Polychrome V with a bandwidth of 15 nm. The recording protocols for fura-2-AM and fluo-4-AM are presented in **Table 2**. Fura-2-AM was used as a ratiometric dual-excitation dye.

Table 2. Ca^{2+} imaging recording protocols

	Fura-2-AM	**Fluo-4-AM**
Excitation wavelength, nm	340 and 380 (<60 ms interval)	490
Emission collection wavelength, nm	>510	510-560
Exposure time, ms	25 and 50	20
Frames per second	1 (340 and 380 nm image pair)	2
Binning	1x1	2x2

The background fluorescence was recorded from empty coverslips.

4.2.3 Recording of mechanically induced Ca^{2+} activity in cells

To induce intercellular Ca^{2+} waves the ARPE-19 or hESC-RPE monolayers were mechanically stimulated. For that, a single cell in a monolayer was punctured (**Study I, II**) or touched (**Study III, IV**) with a glass micropipette. The micropipette was made from a glass capillary with a Narishige pipette puller. Then, it was set on a Luigs & Neumann SM 5–9 vertical microinjection system and gradually lowered to touch an individual cell. The recording of fluorescence reflecting $[Ca^{2+}]_i$ was started at least 20 s before the mechanical stimulation had been performed.

4.2.4 Recording of spontaneous Ca^{2+} activity in cells

The spontaneous $[Ca^{2+}]_i$ increases were recorded from resting, non-stimulated, hESC-RPE monolayers for a period of 5 min (600 frames).

4.2.5 Ca^{2+} imaging data analysis

4.2.5.1 Analysis of mechanically induced Ca^{2+} waves in ARPE-19 cells (Study I and II)

ARPE-19 Ca^{2+} dynamics was analyzed with TiLLvisION (v.4.5.65) and Matlab (R2010b, Mathworks). First, cells in the field of view were manually segmented in TiLLvisION, and each cell was assigned with a number. Then, cells in the field of view were divided into cell layers depending on their position: cells that surrounded the mechanically stimulated cell were denoted as neighboring cell layer 1 (NB1), cells immediately surrounding NB1 were denoted as NB2, and so on (**Study I, Fig. 1**). In TiLLvisION, the fluorescence intensities that emitted due to excitation at 340 and 380 nm (F340 and F380) were determined for individual cells. In Matlab, for each segmented cell, the ratio F340/F380 was determined after background correction $F340/380 = \frac{\mathrm{F340} - F340(background)}{F380 - F380(background)}$. Then, normalized fluorescence (NF) was calculated as the fluorescence value at each time point divided by the mean fluorescence prior to the mechanical stimulation. Intercellular Ca^{2+} wave spreading was described by the maximum NF (peak NF) and the percentage of responsive cells (%RC). A cell was considered to propagate the wave if it had peak NF value above 1.5.

4.2.5.2 Analysis of hESC-RPE Ca^{2+} dynamics (Study III and IV)

The recorded time series were managed offline with Matlab (R2013A, MathWorks) algorithms developed for this purpose and Fiji. The flow-chart with data analysis procedures is presented in the **Fig. 1** of **Study III**.

Cell segmentation of cobblestone-shaped hESC-RPE cells was performed with our semi-automatic segmentation method. The tool utilized various image processing techniques that allowed to remove acquisition artefacts, enhance separation of cytoplasm and nuclei, increase contrast, which overall improved the quality of cell center detection. First, the initial set of cell centroids was identified in the averaged fluorescence images after pre-processing using the Matlab *imfindcircles* function. Second, two complementary images were created by performing Fourier transform and histogram equalization, and the three images (initial and complementary) were passed through a multi-threshold process, after which additional three sets of cell centroids coordinates were extracted. Finally, the unique

cell centers coordinates were found using the four sets of cell centroids. Then, cell boundaries were approximated as fixed-sized circles around the detected cell centers. (**Study III, Supplementary material, Fig. 2** and **Study III, Fig. 1**) For fusiform cells (immature hESC-RPE), cell segmentation was manually performed in Fiji. Examples of images before and after cell segmentation are demonstrated in **Fig. 2** of **Study III**.

In Fiji, average fluorescence intensity of each segmented cell was calculated. For that, the mean pixels' intensity in each segmented cell area was determined from fluorescence images at every time point (usually 600 frames). In Matlab, the background correction of fluorescence curves has been performed, and then smoothened with the moving average algorithm. A baseline fluorescence level was then detected for each cell. Next, the bleaching correction was performed, and, finally, the fluorescence curves were normalized to basal fluorescence value. The fluorescence peaks were then detected in Matlab with the threshold amplitude set to 10% higher than the basal fluorescence level. (**Study III, Fig. 1; Study III, Supplementary material**)

To assess the spontaneous Ca^{2+} activity of a cellular monolayer, the percentage of cells with spontaneous $[Ca^{2+}]_i$ increases in the field of view was calculated during a 5 minute time period (abbreviated as %RCsp – percentage of responsive cells). In experiments with wounded hESC-RPE monolayers, the %RCsp was estimated in different areas relatively to the wound position (**Study IV, Fig. 6**).

To characterize the intercellular Ca^{2+} wave propagation emerging in response to the mechanical stimulation, cells that took part in a mechanically induced Ca^{2+} wave spreading were identified. Two cells were considered to spread an intercellular Ca^{2+} wave if they had fluorescence peaks, the time difference between these peaks was less than 4 s, and the distance between the cells was less than 2-3 characteristic cell sizes. The extent of the Ca^{2+} wave propagation was characterized by the following features:

1. Percentage of cells in the field of view, which propagate the Ca^{2+} wave (percentage of responsive cells - %RCms; **Study III**);
2. Absolute number of cells participating in the Ca^{2+} wave (**Study IV**)
3. Area of a monolayer covered by the Ca^{2+} wave (**Study IV**)

4.3 Immunofluorescence

The localization of RPE proteins and the presence of extracellular matrix proteins was investigated with indirect immunofluorescence staining as described in **Studies I-IV**. Briefly, RPE cells cultured on coverslips or glass-bottomed cell culture dishes were fixed in 4% paraformaldehyde (PFA) for 10 min. Then, the cells were permeabilized with 0.01% Triton-X in PBS for 10 min at RT, and unspecific binding sites were blocked with 3% bovine serum albumin (BSA) for 1 h. Next, the cells were incubated with primary antibodies diluted in 0.5% BSA-PBS for 1 h at RT. Then, the cells were subjected to secondary antibodies dissolved in 0.5% BSA-PBS for 1.5 h at RT. Finally, the cells were mounted with Vectashield mount with 4', 6' diamidino-2-phenylidole (DAPI). The lists of the used primary antibodies is presented in **Table 3**.

Table 3. Primary antibodies used in immunofluorescence studies

Abbreviation	**Protein name**	**Function in RPE**	**Study**
Cx43	Connexin 43	GJ component	I, III
ZO-1	Zonula occludens protein 1	TJ component	I-IV
CRALBP	Cellular retinaldehyde-binding protein	Retinoid carrier in visual cycle	III
Ki67	Antigen Ki67	Proliferating cell marker	IV
Lam	Laminin	ECM protein	IV
Col I	Collagen I	ECM protein	IV

Images were taken with Zeiss LSM 780 confocal microscope (Zeiss, Jena, Germany) using a 63x oil immersion objective or with Olympus IX51 fluorescence microscope using a 20x air objective.

4.4 Analysis of gene expression

4.4.1 RT-PCR

Reverse transcription–polymerase chain reaction (RT-PCR) was used in **Studies III** and **IV** to assess the transcription of RPE-specific genes, and, thus, validate the maturation status of hESC-RPE samples cultured for Ca^{2+} imaging experiments. The total RNA was extracted with a NucleoSpin XS kit according to the manufacturer's instructions. The RT-PCR protocol was completed as previously described in Vaajasaari et al. 2011. The list of the analyzed genes and the used primers is presented in **Table 4**.

Table 4. The expression of the genes studies in hESC-RPE

Abbreviation	Gene name	$T_{annealing}$	Protein function	Study
GAPDH	glyceraldehyde-3-phosphate dehydrogenase	55	a house-keeping gene. Used as an endogenous control	III, IV
OCT ¾	octamer-binding transcription factor	55	a pluripotency gene and a marker of undifferentiated hESCs	III, IV
MITF	microphthalmia-associated transcription factor	52	regulates cell differentiation and melanogenesis	III, IV
BEST	bestrophin	60	forms calcium-sensitive chloride channels in the RPE	IV
Tyrosinase	tyrosinase	52	catalyzes the conversion of tyrosine to melanin	III

4.4.2 Quantitative RT-PCR

Quantitative RT-PCR (qRT-PCR) with TaqMan Gene Expression Assays (Applied Biosystems Inc.) was used in **Study IV** to analyze expression of RPE-specific genes *RPE65* and *MERTK*. *GAPDH* was used as an endogenous control. Samples and negative controls were measured in triplicates similarly as described in Sorkio et al., 2014. *GAPDH* expression level of 9-day-cultured cells was used as a calibrator.

4.5 Scrape-loading/dye-transfer assay

Scrape-loading/dye-transfer assay was used in **Studies I** and **III** to assess GJ intercellular communication in ARPE-19 and hESC-RPE monolayers. Briefly, the cell culture medium was substituted with Alexa Fluor 568 hydrazide (1:1000 in PBS) that can pass through GJs (Weber et al., 2004). The cells were then scraped with a scalpel, incubated with the dye for 15 min at RT, and washed with PBS. The samples were imaged with an Olympus IX51 fluorescent microscope with a 10x air objective to detect the dye spreading. In experiments, where GJ blockage properties of 18-α - glycyrrhetinic acid (18-α-GA) were investigated, the cells were pre-incubated with 18-α-GA, as in Ca^{2+} imaging experiments, prior to scrape-loading.

4.6 Cell viability test

Cell viability was assessed with Live/Dead Viability/Cytotoxicity kit for Mammalian cells in **Studies I** and **III** to evaluate the possible toxicity effect of drugs used in Ca^{2+} imaging experiments. Briefly, the cells were incubated with a mixture of 0.25 μM Calcein-AM and 0.5 μM ethidium homodimer-1 for 30 min at RT. Viable cells were visualized as green and dead cells were visualized as red under Olympus IX51 fluorescence microscope.

4.7 Assessment of wound healing in hESC-RPE monolayers

4.7.1 Wounding of hESC-RPE monolayers

In **Study IV**, hESC-RPEs were mechanically wounded by performing a linear wound with a 10 µl plastic pipette tip on day 9 or day 28 of culture on coverslips. The experiments with wounded monolayers started either 15 min or 7 days after the wounding.

4.7.2 Time-lapse microscopy

The wound healing process was assessed by continuous visualization (time-lapse microscopy) in Nikon BioStation CT. For this, the cells were cultured at 37 °C and 5% CO_2. The phase contrast images of control and wounded areas were automatically taken every 1-3 hours during 7-8 days with a 10x objective.

4.7.3 Assessment of wound healing speed and time of hESC-RPEs

Wound healing time and speed were calculated using the samples without visible damage of the ColIV coverslip coating. The wound healing speed (s) was computed as the initial wound size (p, in pixels) divided by the full healing time (t, hours): $s = \frac{p}{t}$. Wound healing time was considered to be the time in hours required for the hESC-RPE monolayer to fully cover the cell-free area with the cells.

4.8 Mathematical modeling of Ca^{2+} waves propagation in ARPE-19 cells

4.8.1 Model assumptions

The mathematical model of Ca^{2+} dynamics emerging in response to a mechanical stimulus was constructed based on the following assumptions:

1. Cells close to the MS site experience stretch caused by the stimulation, allowing Ca^{2+} influx through stretch-sensitive Ca^{2+} channels (SSCC). NB layers 2-4 also experience minor stretch, which decreases with the distance from the MS site.

2. The MS cell secretes a signaling molecule (ATP or UTP) to extracellular space leading to production of IP3.

3. IP3 causes release of Ca^{2+} from ER to cytoplasm via IP3R3 receptor.

4. Increasing $[Ca^{2+}]_i$ activates RyR, resulting in additional Ca^{2+} release from ER.

5. Ca^{2+} is pumped out of the cytoplasm through SERCA and PMCA. IP3 degrades in the cytoplasm.

6. IP3 and Ca^{2+} can diffuse between neighboring cells via GJs.

The $[Ca^{2+}]_i$ changes were calculated at each NB layer as a sum of the following Ca^{2+} fluxes:

$$\frac{d[Ca^{2+}]_i}{dt} = J_{SSCC} + J_{IP_3R_3} + J_{RyR} + J_{Leak} + J_{GJ} - J_{Pump}$$

where the subscripts indicate the flux source. (**Table 5**)

Table 5. Ca^{2+} fluxes forming $[Ca^{2+}]_i$ at each time point in an ARPE-19 Ca^{2+} wave propagation model

Abbreviation	Flux	Direction of the flux
J_{sscc}	Flux through stretch-sensitive Ca^{2+} channels	In
J_{IP3R3}	Flux from ER caused by activation of IP3R3 receptor	In
J_{RyR}	Flux from ER caused by activation of RyR receptor	In
J_{pump}	Flux through SERCA and PMCA	Out
J_{leak}	Leak flux from ER and extracellular space	In
J_{GJ}	Flux through GJs	In

In – the flux is directed into the cellular cytoplasm; *Out* – the flux is directed outside of the cytoplasm

Each flux represents a partial differential equation. The model was constructed using Matlab SimBiology tool (R2012a, The MathWorks, Natick, MA).

The detailed model description can be found in **Study II**.

4.8.2 Model parametrization

The experimental data of $[Ca^{2+}]_i$ dynamics (fluorescence curves) from control cells and cells with blocked GJs were used for the model parametrization (**Tables 2, 3** in **Study II**). Parameters were fitted with Matlab SimBiology Parameter Fit Task.

The model uses stretch intensity, extracellular ligand concentration, IP3R3 phosphorylation rate, and Ca^{2+} and IP3 fluxes through GJs as location-specific parameters.

4.8.3 Sensitivity analysis

The sensitivity analysis was performed by changing certain parameters (**Table 2**, **Study II**) and evaluating the following features of the Ca^{2+} waves: peak amplitude, time to peak, Ca^{2+} wave width at a half maximum, and Ca^{2+} concentration at the end of the Ca^{2+} wave at NB layers 1, 5, and 10.

4.8.4 Model prediction of suramin effect

This model was used to investigate a possible mechanism of suramin action on ARPE-19 cells utilizing the experimental data of mechanically induced Ca^{2+} waves in monolayers with blocked GJs and P2 receptors. The sensitivity analysis of $P2Y_2$ regulation parameters and G-protein cascade parameters was performed for a dataset recorded for the cells with blocked GJs. Finally, the model was fitted to the dataset derived from cells with blocked GJs and P2 receptors by refitting $P2Y_2$ and G-protein cascade parameters.

4.9 Ethical considerations

Tampere University has the approval of the National Authority for Medicolegal Affairs Finland (TEO) to study human embryos (Dnro 1426/32/300/05). The supportive statement of the Ethical Committee of the Pirkanmaa Hospital District allows to derive, culture, and differentiate hESC lines from surplus human embryos (R05116). No new lines were derived for this study.

4.10 Statistics

Statistical tests used in different studies are presented in **Table 6**.

Table 6. Statistical analysis

Study	Compared values	Statistical test
I	Mean NF	Two-sample unpaired Student's t-test
III	Normalized RCsp	Two-sample Kolmogorov-Smirnov test
III	Normalized RCms	Two-sample Kolmogorov-Smirnov test
IV	Cell area	Two-sample unpaired Student's t-test
IV	Wound healing time	Two-sample unpaired Student's t-test
IV	Wound healing speed	Two-sample unpaired Student's t-test
IV	RCsp	Mann-Whitney test
IV	Number of cells participating in a Ca^{2+} wave	Mann-Whitney test
IV	Area of a Ca^{2+} wave	Mann-Whitney test

Mann-Whitney and Kolmogorov-Smirnov tests allowed for statistical analysis of experiments with low number of data points (less than 10). In the experiments where the large number of values was measured (more than 10) and when the data points were assumed to have normal distribution, the unpaired Student's t-test was used to compare "control" and "treated" datasets.

5 RESULTS

Present study focused on analyzing the mechanically induced intercellular Ca^{2+} waves and spontaneous $[Ca^{2+}]_i$ transients in RPE cells and their changes during maturation and wound healing. For this, methods for performing single-cell mechanical stimulation and tracking $[Ca^{2+}]_i$ changes in the monolayer of cells were developed. Because this work relied on analysis of fluorescence signals from a large number of cells (more than 80,000 cells were analyzed in **Study III** alone), semi-automatic algorithms for segmentation of cells in the fluorescence images were developed. Further analysis of fluorescence curves was also automatized using various Matlab scripts developed for this purpose. In addition, the mathematical model that describes the propagation of mechanically induced Ca^{2+} waves in RPE was created for this study.

First, assessment of intercellular Ca^{2+} waves and their mechanisms of emergence in ARPE-19 cells were investigated. (**Study I**)

Second, a mathematical model of Ca^{2+} waves spreading in ARPE-19 cells was developed. This was based on the experimental data from **Study I** that allowed for a deeper understanding of the mechanisms beyond the wave propagation. (**Study II**)

Third, the Ca^{2+} dynamics (intercellular Ca^{2+} waves and spontaneous $[Ca^{2+}]_i$ spikes) alterations during cellular maturation were investigated. For that, hESC-RPE cells were used. These cells undergo distinct maturation-related alterations within a short time span. (**Study III**)

Finally, the effects of wounding and wound healing on Ca^{2+} dynamics in hESC-RPE monolayers at different maturation stages were studied. (**Study IV**)

The flowchart summarizing the work performed in this thesis is presented in **Fig. 6**.

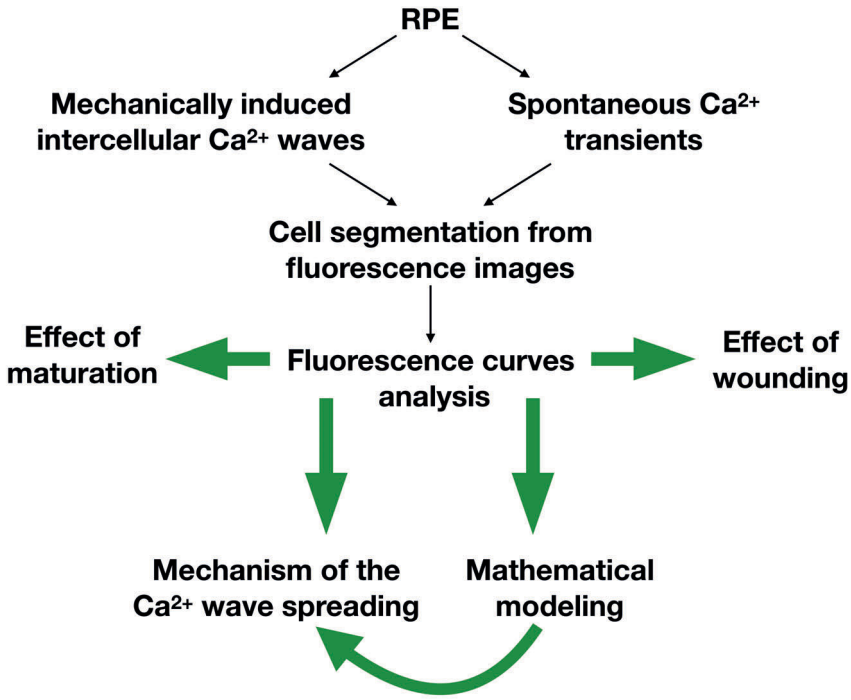

Figure 6. The flowchart of the main thesis outcomes

5.1 Cellular morphology and maturation status

The brightfield microscopy and immunofluorescence staining were used to assess the morphology of ARPE-19 and hESC-RPE cells.

ARPE-19 cells (**Study I, Fig. 2; Study II**), 9-day-cultured hESC-RPE (**Study III, Fig. 3A; Study IV, Fig. 1A, E**) and 7-day post-wounded hESC-RPE (**Study IV, Fig 6D, J**) had fusiform morphology with little or no pigmentation. hESC-RPE cells cultured for 28 or 35 days had predominantly cobblestone morphology with significant pigmentation (**Study III, Fig. 3B; Study IV, Fig. 1G, H, K, L**).

Immunofluorescence labeling showed the presence of a GJ protein Cx43 and a tight junction component ZO-1 in both ARPE-19 cells (**Study I, Fig. 2B; Study II, Fig. 4**) and hESC-RPE (**Study III, Fig. 3E, F; Study IV, Fig. 2A-C, G-I**). ZO-1 was also present in the healed hESC-RPE cells. (**Study IV, Fig. 2D-F, J-L**) In addition, we demonstrated hESC-RPE cells to express RPE-specific protein CRALBP (**Study III, Fig. 3C, D**) and to secrete extracellular proteins laminin and

Collagen I (ColI) in control conditions. (**Study IV, Fig. 3A-C, G-I**) The increased production of ColI was observed after wounding. (**Study IV, Fig. 3J-L**) The marker of dividing cells Ki67 was found in 9- and 16-day cultured hESC-RPE cells (**Fig. 7**), and sometimes close to the wound edges in the hESC-RPE monolayers that were cultured for 28 days, wounded, and then allowed to heal for 7 days. (**Study IV, Fig. 2 D-F**)

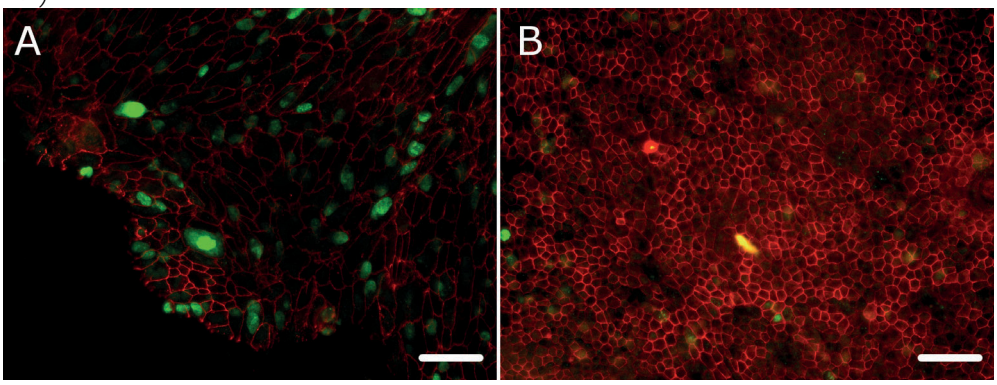

Figure 7. The immunofluorescence images of hESC-RPE cells showing ZO-1 (red) and Ki67 (green). A. Freshly wounded 9-day-cultured hESC-RPE B. 16-day-cultured hESC-RPE. Scale bar: 50 µm

The results of immunofluorescence staining for hESC-RPE cells of different ages are summarized in **Table 7**.

Table 7. Immunofluorescence staining results for hESC-RPE cells.

Protein	**9d.**	**16d.**	**28d.**	**35d.**
Cx43 (GJ component)	+ (III)	N/A	+ (III)	N/A
CRALBP	+ (III)	+ (unpublished)	+(III)	N/A
ZO-1	+ (III)	+ (unpublished)	+ (III)	+ (IV)
Ki67	+ (unpublished)	+ (unpublished)	occur rarely (unpublished)	- (IV)
Laminin	+ (unpublished)	+ (IV)	+ (unpublished)	+ (unpublished)
Col I	N/A	+ (IV)	N/A	N/A

"9d." – 9-day-cultured hESC-RPE cells; "16d." – 16-day-cultured hESC-RPE cells; "28d." – 28-day-cultured hESC-RPE cells; "35d." – 35-day-cultured hESC-RPE cells. "+" – expression was observed; "-" - expression was not observed; N/A – data was not collected. Study number is indicated in the parentheses.

RT-PCR analysis showed that hESC-RPE cells did not express a pluripotent gene marker *OCT ¾*, but expressed RPE-specific markers *MITF*, *tyrosinase*, and *bestrophin*. The results of RT-PCR analysis are presented in **Table 8**. (**Study III, Fig. 3G; Study IV, Fig. 1A, B**)

Table 8. RT-PCR results for hESC-RPE cells.

Gene	**9d.**	**16d.**	**28d.**	**35d.**
Oct 3/4	- (III)	N/A	- (III)	N/A
MITF	+ (III, IV)	+ (IV)	+ (III, IV)	+ (IV)
Tyrosinase	+ (III, IV)	+ (IV)	+ (III, IV)	+ (IV)
Bestrophin	+ (IV)	+ (IV)	+ (IV)	+ (IV)

"9d." – 9-day-cultured hESC-RPE cells; "16d." – 16-day-cultured hESC-RPE cells; "28d." – 28-day-cultured hESC-RPE cells; "35d." – 35-day-cultured hESC-RPE cells. "+" – expression was observed; "-" expression was not observed; N/A – data was not collected. Study number is indicated in the parentheses.

In **Study IV**, we also performed qRT-PCR for *RPE65* (an RPE-specific protein) and *MERTK* (a protein that controls phagocytosis). (**Study IV, Fig. 1C, D**) 28-day-cultured cells had a higher mRNA expression of these proteins compared to 9-day-cultured cells.

5.2 Ca^{2+}waves in ARPE-19 cells

5.2.1 Mechanical stimulation

When a single cell within a monolayer was touched with a glass micropipette, the $[Ca^{2+}]_i$ increase was initiated and propagated in a wave-like manner from the stimulation site. (**Study I, Fig. 3A**) The averaged kinetics of normalized fluorescence (NF) reflecting the kinetics of $[Ca^{2+}]_i$ increases in NB layers 1-11 is shown in **Study I, Fig. 3B**. The cells located close to the stimulation point had larger peak NF and reached them faster compared to distant cells. In addition, the wave propagation speed decreased with distance from the site of stimulation. The wave spread to 13.7 ± 2.1 cell layers away from the MS cell.

5.2.2 The mechanism of the Ca^{2+} wave spreading

5.2.2.1 The origin of $[Ca^{2+}]_i$ transients

The $[Ca^{2+}]_i$ transients triggered by the single-cell mechanical stimulation could originate from extracellular Ca^{2+} influx, or from the intracellular Ca^{2+} stores.

To assess the influence of extracellular Ca^{2+}, the mechanical stimulation was done in Ca^{2+}-free extracellular medium, while the impact of ER was studied by inducing Ca^{2+} waves after the depletion of ER with thapsigargin.

Ca^{2+}-free conditions resulted in lower peak NF in cells close to the stimulation site, and larger peak NF in distant cells. (**Study I, Fig. 4A**) The mathematical model of the Ca^{2+} wave spreading suggested that cells close to the site of stimulation have an influx of Ca^{2+} through SSCC. (**Study II**) Thapsigargin dramatically reduced the Ca^{2+} wave spreading: the peak NF and %RC were lower than in control in cells close to the MS site, and the Ca^{2+} wave was completely blocked farther NB layer 4. (**Study I, Fig. 4A, B**)

5.2.2.2 The route of Ca^{2+} waves propagation

Intercellular Ca^{2+} waves, that arise spontaneously or as a result of mechanical stimulation, can propagate either through extracellular media or intracellularly via GJs between cells.

Scrape-loading/dye-transfer assay confirmed that ARPE-19 cells have functional GJs (**Study I, Fig. 5A**) and that 18-α-GA can be used as an effective GJ blocker (**Study I, Fig. 5B**).

The blockade of GJs with 18-α-GA resulted in reduced peak NF in all NB layers. Cells closer to the MS point had the most prominent peak NF decrease, and the effect attenuated with the distance. (**Study I, Fig. 5C**)

Other unspecific GJ blockers 1-heptanol and quinidine were tested. 1-heptanol did not block the Ca^{2+} wave, while quinidine blocked the wave completely.

According to our mathematical model of Ca^{2+} wave spreading, all cells conduct IP3 and Ca^{2+} via GJs, and the flux through GJs decreases with the distance.

The presence of the extracellular route of propagation was assessed by inducing Ca^{2+} waves in disconnected cell clusters (**Study I, Fig. 6A**). When the wave was induced in a cluster, it was able to propagate through cell-free gaps. The propagation

speed (4.2 ± 0.2 μm/s) and %RC were lower compared to confluent ARPE-19 monolayers (**Study I, Fig. 6B**).

The mathematical model suggested that the MS cell secretes a ligand. The ligand diffuses mediating $[Ca^{2+}]_i$ transients in neighboring cells, and the ligand concentration decreases with the distance. In addition, cellular sensitivity to the extracellular ligand depends on the IP3 receptor phosphorylation rate. IP3 receptor phosphorylation rate increases with the distance attenuating $[Ca^{2+}]_i$ transients. (**Study II**)

To investigate the possible participation of P2 receptors in Ca^{2+} wave propagation, ARPE-19 monolayers were incubated with suramin, the P2 receptor blocker, prior to mechanical stimulation. Suramin significantly reduced %RC further NB layer 4. (**Study I, Fig. 4B**)

The contribution of P2Y receptors was studied by inducing mechanical stimulation in the presence of suramin and absence of Ca^{2+}. Suramin lowered %RC beyond NB layer 4 in Ca^{2+}-free conditions. (**Study I, Fig. 4B**).

All the above-mentioned inhibitors effects were summarized in **Table 9**.

Table 9. Properties of mechanically stimulated Ca^{2+} waves in ARPE-19 cells (**Study I**)

	Cells close to MS site		**Cells distant from MS site**	
Speed to reach NF peak	0.65 ± 0.16 NF units/s		0.04 ± 0.004 NF units/s	
Propagation speed	16.7-33.3 μm/s		7.1-14.3 μm/s	
	Peak NF	**%RC in NBs**	**Peak NF**	**%RC in NBs**
Ca^{2+}-free extracellular medium vs. Control	↓	≈	↑	≈
Thapsigargin vs. Control (ER depletion)	↓	↓	No wave	No wave
18-α-GA vs. Control (Cx43 blocker)	↓	≈	↓	≈
1-Heptanol vs. Control (unspecific GJ blocker)	≈	≈	≈	≈
Quinidine vs. Control (considered as a potential GJ blocker)	No wave	No wave	No wave	No wave
Suramin vs. Control (P2 receptors blocker)	≈	≈	≈	↓
Suramin + Ca^{2+}-free vs. Ca^{2+}-free	N/A	≈	N/A	↓

↓ - decrease was observed; ↑ - increase was observed; ≈ - no significant change is observed; N/A – data was not collected

5.2.2.3 Possible mechanism of suramin effect

The Ca^{2+} wave properties were compared between the experimental dataset recorded from the cells with blocked GJs (18-α-GA-treated cells) to the experimental dataset derived from cells with blocked GJs and P2 receptors (18-α-GA and suramin-treated cells). The results are presented in **Table 10**.

Table 10. Comparison between the two experimental datasets (**Study II**)

$[Ca^{2+}]_i$ curve feature	**Dataset 1 (GJs and P2-receptors both blocked) compared to Dataset 2 (GJs blocked)**
Time to peak in NB1	Lower in Dataset 1
Time to peak in NB5 and NB10	Higher in Dataset 1
Ca^{2+} wave width at half-maximum	Lower in Dataset 1
End $[Ca^{2+}]_i$	Lower in Dataset 1

Finally, it was investigated how the observed differences between $[Ca^{2+}]_i$ curves in the two datasets could be accounted for by changing $P2Y_2$ receptor model parameters. The increase of $P2Y_2$ unphosphorylated receptor dissociation constant and $P2Y_2$ receptor phosphorylation rate parameters induced the changes in $[Ca^{2+}]_i$ curves similar to those in the experimental data. (**Study II, Fig. 7B, C**) The values of these parameters were higher in the dataset recorded from the cells with blocked GJs and P2-receptors.

5.2.2.4 Sensitivity analysis of parameters

The sensitivity analysis discovered the following parameters to affect the shape of the Ca^{2+} dynamics curves: stretch, extracellular ligand concentration, IP3 receptor phosphorylation rate, IP3 flux via GJs in NB1. The results of the analysis are summarized in **Table 11**.

Table 11. Sensitivity analysis of parameters in mechanically induced Ca^{2+} wave spreading model (**Study II**)

Parameter change	**Changes in $[Ca^{2+}]_i$ curves shapes**
Stretch ↓	Time to peak in NB1 ↓
Extracellular ligand concentration↑	Time to peak ↓
IP3 receptor phosphorylation rate ↓	Peak amplitude ↑ Time to peak ↓ Ca^{2+} wave width at half-maximum ↓ or ↑ depending on NB layer End $[Ca^{2+}]_i$ ↑
IP3 input to NB1 via GJs ↑	Ca^{2+} wave width at half-maximum ↑ End $[Ca^{2+}]_i$ ↑

↓ - decrease; ↑ - increase

5.3 Mechanically induced Ca^{2+} waves and spontaneous $[Ca^{2+}]_i$ transients in hESC-RPE cells

5.3.1 Spontaneous $[Ca^{2+}]_i$ transients in 9- and 28-day-cultured hESC-RPE

Both 9- and 28-day-cultured cells exhibited spontaneous random $[Ca^{2+}]_i$ transients in single cells that rarely propagated as a wave between small cell clusters. The 28-day-cultured cells had more than twice higher spontaneous Ca^{2+} activity (%RCsp) compared to 9-day-cultured hESC-RPEs.

Removal of extracellular Ca^{2+} reduced %RCsp in 9-day-cultured cells and almost fully blocked spontaneous $[Ca^{2+}]_i$ activity in 28-day-cultured cells. Depletion of ER with thapsigargin almost completely abolished spontaneous $[Ca^{2+}]_i$ transients in cells of both ages.

Suramin and 18-α-GA did not affect %RCsp.

5.3.2 Mechanically induced Ca^{2+} waves in 9- and 28-day-cultured hESC-RPE

Mechanical stimulation of a cell in a hESC-RPE monolayer caused emergence of an intercellular Ca^{2+} wave. In 9-day-cultured cells, Ca^{2+} waves spread much farther from the stimulation point compared to 28-day-cultured cells. (**Study III, Fig. 5**) Suramin and thapsigargin reduced %RCms in 9-day-cultured cells, while in 28-day-cultured hESC-RPE suramin had no effect, and thapsigargin completely blocked Ca^{2+} waves. Removal of extracellular Ca^{2+} or the treatment of the cells with 18-α-GA did not affect the wave spreading.

The scrape-loading/dye-transfer assay was performed with both 9- and 28-day-cultured cells, showing homogenous dye distribution across the cells in control conditions. (**Study III, Fig. 7A, C**) 18-α-GA was able to block the hydrazide dye uptake. (**Study III, Fig. 7B, D**)

5.3.3 Wound healing in 9- and 28-day-cultured cells

5.3.3.1 Wound healing speed

The process of wound healing was followed with time-lapse phase contrast microscopy. The analysis of the image stacks revealed that cells wounded on day 9 of culture healed faster and better than those wounded on day 28. (**Study IV, Fig. 5A-C, E-F**)

Analysis of healed samples showed that ColIV was critical for successful healing. When ColIV coating was damaged during the wounding procedure, the percentage of the healed samples had more than a two-fold decrease.

5.3.3.2 Spontaneous $[Ca^{2+}]_i$ transients in wounded and healed hESC-RPE molonayers

The spontaneous $[Ca^{2+}]_i$ increases in 9- and 28-day-cultured freshly wounded and 7-day-healed samples were assessed. 9-day-cultured monolayers that were studied 15 minutes after wounding had more than a two-fold increase in %RCsp in the areas close to the wound edge compared to the non-wounded control areas.

In samples that were wounded on day 28 of culture and then allowed to heal for 7 days, the cells within the healed areas had almost a 2-fold decrease in %RCsp compared to the control.

5.3.3.3 Mechanically induced Ca^{2+} waves in wounded and healed hESC-RPE monolayers

Finally, the ability of cells to propagate mechanically induced intercellular Ca^{2+} waves was studied in wounded and healed hESC-RPE monolayers. The monolayers that were wounded on day 28 of culture and then healed for 7 days had much wider Ca^{2+} waves covering almost 9-fold larger areas compared to control. (**Study IV, Fig. 7E, F**)

6 DISCUSSION

Intercellular communication has vital importance in cellular functionality as it allows cells to operate concordantly as a tissue. Ca^{2+} is an ion that controls a number of essential cellular processes from cell differentiation to cell death. In addition, intercellular communication strongly depends on Ca^{2+} signaling. In many cell types, mechanical stimulation triggers changes in intra- and intercellular Ca^{2+} dynamics and, thus, is often used to study Ca^{2+}-dependent intercellular communication. (Rottingen and Iversen, 2000)

In this study, the analysis of mechanically induced Ca^{2+} waves as well as spontaneous Ca^{2+} activity in RPE cells were investigated under various experimental conditions. To assess the Ca^{2+} activity from a large number of cells, semi-automated algorithms were developed to perform cell segmentation from the fluorescence images and to analyze fluorescence curves from individual cells.

In this thesis, for the first time, it was demonstrated that RPE cells exhibit intercellular Ca^{2+} waves and spontaneous $[Ca^{2+}]_i$ transients that depend on cellular maturation status and alter due to wounding and wound healing. Furthermore, the routes of the Ca^{2+} wave propagation were experimentally investigated, and the gathered data was further applied to create a mathematical model of Ca^{2+} wave spreading in RPE cells.

6.1 Mechanically induced intercellular Ca^{2+} waves in ARPE-19 and hESC-RPE

6.1.1 The method of mechanical stimulation

Mechanically induced Ca^{2+} waves have been studied in a number of cell types, including epithelial cells (Stalmans and Himpens, 1998; Churchill et al., 1996), endothelial cells (D'hondt et al., 2007; Moerenhout et al., 2001), osteosarcoma cells (Gomez et al., 2001), chondrocytes (D'Andrea and Vittur, 1996), but, according to our knowledge, not in human RPE.

In this study, we performed mechanical stimulation by touching cells, loaded with a fluorescent Ca^{2+}-sensitive dye, with a glass micropipette. In our experience, such stimulation can result in membrane stretching or in membrane perforation.

In most studies, mechanical stimulation has been done without making a membrane perforation (Frame and de Feijter, 1997; Stalmans and Himpens, 1998; Gomes et al., 2005; D'hondt et al., 2007; Moerenhout et al., 2001). The main disadvantage of this stimulation method lies in the difficulty to control the amount of pressure applied to different cells. In addition, cells may vary in microvilli or cilia size, which will introduce further complications to pressure calibration. On the other hand, it is advantageous that cytoplasmic content that can affect Ca^{2+} wave spreading (such as ATP) does not leak out of the stimulated cell, which facilitates the investigation of the Ca^{2+} wave propagation routes. Thus, when the experimental data suggests paracrine propagation route, it can be safely assumed that the cell secrets a ligand rather than it passively leaks out through the introduced membrane hole. In this thesis, we used the described method of mechanical stimulation (without making a membrane perforation) for inducing intercellular Ca^{2+} waves in hESC-RPE cells. (**Study III, IV**) The stimulation method without cell perforation has been chosen because cell injury has been investigated separately for hESC-RPE cells in **Study IV**.

Here, in **Studies I** and **II**, the ARPE-19 cells were stimulated by making a membrane perforation in a cell. During the stimulation, the lowering of the pipette towards the cell of interest was stopped as soon as a dark spot appeared. The benefit of this method lies in better control of the stimulus application: the membrane perforation could be visually seen under the fluorescent microscope as it appeared as the dark spot and resulted in rapid bleaching of the stimulated cell due to dye leakage. The perforation method of stimulation has been chosen for ARPE-19 cells because the conditions when cells are mechanically injured mimic cell wounding that can happen under physiological conditions. The main hindrance of this method lies in the outflow of the cytoplasmic content, which complicates investigation of the Ca^{2+} wave spreading mechanisms (Woolley and Martin, 2000).

6.1.2 Assessment of intercellular Ca^{2+} wave propagation from the fluorescence images time-series

The experiments involving mechanically induced Ca^{2+} waves imply analysis of fluorescence signals from a large number of cells. Most studies investigating Ca^{2+} signaling with fluorescent probes use manual cell segmentation, which is a very time-

consuming process (Gomes et al., 2003; Dombeck et al., 2007; Niell and Smith, 2005; Stalmans and Himpens, 1998). In **Studies I-IV**, manual cell segmentation has been used for the analysis of mechanically induced Ca^{2+} waves in fusiform RPE.

An automatic cell segmentation is a demanding area of research. For the analysis of Ca^{2+} dynamics in cells with cobblestone morphology, we developed a semi-automatic algorithm for cell detection. This tool automatically found cell centers in fluo-4-AM microscope fluorescence images of cobblestone-shaped RPE. The algorithm used the averaged images obtained from Ca^{2+} imaging time-series. These images went through various transformation processes, such as noise removal, Fourier transform, adaptive histogram equalization. The cell centers were found by using a combination of Matlab's in-built function for finding circular structures and a multi-threshold process. The cell centers recognized by the algorithm could be manually altered in the images where the detection was not accurate enough. Then, the cells were approximated as user-defined fixed-sized circles. This method was quite time-efficient: the cells from the entire field of view (which is 500-900 cobblestone RPE cells) could be segmented within several minutes. In contrast, manual cell segmentation of fusiform ARPE-19 cells could be done within 15 minutes for only 300-400 cells per a field of view. Because the algorithm decreased the required manual user's input, it overall increased the number of cells segmented per a unit of time. In addition, the analysis of single-cell fluorescence curves extracted from the fluorescence images, as well as further meta-analysis of the Ca^{2+} dynamics, was partially automatized by using MatLab scripts. Moreover, in **Studies III** and **IV** the mechanically induced intercellular Ca^{2+} waves were also programmed to be detected automatically in MatLab using user-defined thresholds. (**Study III, Supplementary data**) Our method of cell detection allowed us to significantly reduce the time-consuming process of manual cell segmentation. This, combined with automatization of fluorescence curve analysis and the Ca^{2+} wave detection with Matlab scripts, provided means to thoroughly investigate Ca^{2+} wave propagation taking into account the majority of cells in the field of view in **Studies III** and **IV**.

6.1.3 Ca^{2+} wave spreading in control conditions

The effect of mechanical stimulation has been studied in several rat RPE cultures: healthy Long-Evans RPE (LE-RPE), dystrophic Royal College of Surgeons RPE (RCS-RPE), and immortalized RPE-J cell line (Stalmans and Himpens, 1997; Stalmans and Himpens, 1998; Stalmans and Himpens, 1999; Himpens et al., 1999;

Gomes et al., 2003). In LE-RPE and RPE-J, mechanical stimulation resulted in a $[Ca^{2+}]_i$ transient that spread to 2-3 neighboring cell layers (Gomes et al., 2003; Stalmans and Himpens, 1997). The authors have shown that the amplitude of $[Ca^{2+}]_i$ spikes and the speed of the Ca^{2+} wave propagation was lower in dystrophic RCS-RPE compared to control LE-RPE (Stalmans and Himpens, 1998). In some epithelia, for example, in rat liver epithelium the mechanically induced Ca^{2+} waves spread up to 8 cell layers away from the stimulation site (Frame and de Feijter, 1997).

After evaluating the morphology and $[Ca^{2+}]_i$ dynamics with the developed image analysis tools, we found remarkably different results of Ca^{2+} wave propagation in ARPE-19 (**Study I**) and fusiform 9-day-cultured hESC-RPE compared to more mature 28- and 35-day-cultured hESC-RPE (**Study III, IV**). In ARPE-19 and 9-day-cultured hESC-RPE, mechanical stimulation resulted in wide-spreading intercellular Ca^{2+} waves. In contrast, in 28- and 35-day-cultured hESC-RPEs the wave propagation was restricted to just a few cells away from the stimulation site. The morphology of our immature 9-day-cultured hESC-RPE was very similar to that of ARPE-19 cells: the cells had fusiform morphology and low pigmentation level. Therefore, it was not surprising that cells with immature morphology had strong intercellular Ca^{2+} waves. The 28- and 35-day-cultured hESC-RPEs usually had a typical mature RPE morphology with cobblestone cells shape and significant pigmentation. Accordingly, their response to mechanical stimulation was very similar to that of rat RPE (Gomes, 2003; Stalmans and Himpens, 1997), i.e., Ca^{2+} waves that spread only a few cells away from the stimulation site. Interestingly, in rare cases, 28-day-cultured hESC-RPEs had strong Ca^{2+} waves similarly to ARPE-19 and 9-day-cultured hESC-RPEs. In these samples, cells around the stimulation site had quite large variation in size. This may indicate their immature state despite the fact that they had been cultured for 28 days prior to experiments. In this thesis, the maturation status of hESC-RPE was estimated from the entire coverslip that was used in an experiment with RT-PCR (**Study III, IV**). For future studies, it would be beneficial to utilize techniques, such as spatial RNA sequencing (Ståhl et al., 2016), to estimate the maturation status of individual cells involved in the Ca^{2+} wave spreading and omit the rest of the cells on the coverslip. In contrast with bulk RNA analysis, this would allow for direct correlation between the individual cell maturation state and the ability to propagate the wave. This information would be especially valuable when combined with our technique for Ca^{2+} wave propagation analysis that allows to assess $[Ca^{2+}]_i$ dynamics in single cells.

It is also worth mentioning that all the Ca^{2+} dynamics measurements were done using fluorescent Ca^{2+} probes, which act as Ca^{2+} buffers and, thus, may disturb Ca^{2+}

signaling patterns occurring in cells. This limitation cannot be overcome as all the available probes, including the genetically encoded ones, sense Ca^{2+} by binding it, and, consequently, decrease the concentration of the cytoplasmic Ca^{2+} available for physiological action. (McMahon and Jackson, 2018)

6.1.4 Ca^{2+} wave propagation in the absence of extracellular Ca^{2+}

The contribution of extracellular Ca^{2+} to Ca^{2+} wave spreading is often assessed by performing mechanical stimulation in the absence of extracellular Ca^{2+}. Previous studies have demonstrated that Ca^{2+} waves in different cell types vary greatly in Ca^{2+}-free media. For example, calf pulmonary endothelial (Moerenhout et al., 2001) and ovine lens epithelial cells (Churchill et al., 1996) did not require extracellular Ca^{2+} for the wave propagation, while rat RPE (Stalmans and Himpens, 1997) and osteosarcoma cells (Gomez et al., 2001) were completely inhibited in Ca^{2+}-free conditions. In our experiments, the absence of extracellular Ca^{2+} was not able to block the mechanically induced Ca^{2+} wave propagation neither in ARPE-19 (**Study I**), nor in hESC-RPE cells (**Study III**). However, ARPE-19 cells had lower amplitudes of $[Ca^{2+}]_i$ transients in neighboring cell layers 1-3 (**Study I**). This can be taken as an indication that cells close to the stimulation site do recruit extracellular Ca^{2+}, but it is not the only source of Ca^{2+} for $[Ca^{2+}]_i$ increases. Our mathematical model of Ca^{2+} wave spreading in ARPE-19 cells suggests that cells in the vicinity of the stimulation site, have an influx of extracellular Ca^{2+} through the stretch-sensitive Ca^{2+} channels (**Study II**). Moreover, the absence of extracellular Ca^{2+} increased the percentage of responsive cells, especially in distant cell layers. In rare cases, Ca^{2+} waves spread up to 3 layers farther than in control. Thus, in ARPE-19 cells the Ca^{2+}-free conditions seem to promote the wave spreading. Zero-extracellular Ca^{2+} conditions increase the opening of connexin hemi-channels and trigger ATP-release in the neighboring cells and thus may explain the enhanced Ca^{2+} wave spreading (Braet et al., 2003). On the other hand, with hESC-RPE cells, where we calculated the overall number of cells engaged in the wave spreading and not peak NF values in single cells, we did not find any statistically significant difference between Ca^{2+} wave spreading in control conditions and in the absence of extracellular Ca^{2+} (**Study III**). It is, thus, still possible that extracellular Ca^{2+} may affect $[Ca^{2+}]_i$ increases in individual hESC-RPE cells.

6.1.5 Ca^{2+} wave spreading after depletion of ER

Another source of Ca^{2+} that cells can use to increase $[Ca^{2+}]_i$ is the endoplasmic reticulum. Thapsigargin is a drug that is commonly used to deplete endoplasmic reticulum via inhibition of SERCA that pumps Ca^{2+} from cytoplasm to endoplasmic reticulum (Thastrup et al., 1990). It has been reported that depletion of endoplasmic reticulum leads to partial or complete inhibition of mechanically induced intercellular Ca^{2+} waves in ovine lens epithelia (Churchill et al., 1999), rat RPE (Stalmans and Himpens, 1998), rat osteosarcoma cells (Gomez et al., 2001), and other cell types. In concordance with the literature, we demonstrated that in ARPE-19 cells and 28-day-cultured hESC-RPE application of thapsigargin almost completely blocked the mechanically induced Ca^{2+} waves (**Study I, III**). In ARPE-19, the cells close to the stimulation site had a residual Ca^{2+} wave that is consistent with the finding that these cells utilize extracellular Ca^{2+} as we showed in experiments with Ca^{2+}-free extracellular medium (**Study I**). Also, in 9-day-cultured hESC-RPE, thapsigargin inhibited the wave propagation but the wave could not be fully blocked (**Study III**). As stated above, we demonstrated that 9-day-cultured hESC-RPE are not likely to recruit extracellular Ca^{2+} for $[Ca^{2+}]_i$ increases. Thus, it is possible that they utilize another source of Ca^{2+}, for example, mitochondria or melanosomes (Islam, 2012). In this study, either the thapsigargin or Ca^{2+}-free medium were utilized, but these were not used in combination. Thus, before searching for another source of intracellular Ca^{2+}, it would be necessary to perform additional control experiments in which the cells would be stimulated in Ca^{2+}-free medium in the presence of thapsigargin.

6.1.6 Assessment of the gap junctional wave propagation route

Mechanically induced Ca^{2+} waves can propagate via GJ and paracrine routes. The GJ propagation route has been shown in airway epithelia (Boitano et al., 1992), lens epithelia (Churchill et al., 1996), articular chondrocytes (D'Andrea et al., 1996), corneal endothelia (Gomes et al., 2006), and rat RPE (Himpens et al., 1999). Paracrine route of propagation has been demonstrated in mammary epithelia (Enomoto et al., 1994), corneal endothelia (Moerenhout et al., 2001), and liver epithelia (Frame and de Feijter, 1997).

In this thesis, the scrape-loading/dye transfer assay was used to assess the functionality of GJs in ARPE-19 and hESC-RPE cells. Here, we confirmed that ARPE-19 cells have functional GJ intercellular communication (**Study I**). The

pattern of the scrape-loading/dye transfer assay was similar to reported by Hutnik et al. (Hutnik et al., 2008) with bright edges near the scrape wound that faded with increasing distance from the edges. In hESC-RPE cells, unlike ARPE-19, the dye uptake in scrape-loading/dye transfer assay appeared more homogenous, which may indicate that the dye did not spread via GJs but instead diffused through the extracellular medium via spontaneous openings of Cx43 hemi-channels. To exclude this possibility, an experiment where the dye is directly injected into a cell could be performed (Abbaci et al., 2008).

The 18-α-GA was tested in scrape-loading/dye transfer assay in ARPE-19 cells and hESC-RPE, where it effectively blocked GJ communication (or possible spontaneous hemi-channels openings in hESC-RPE) at a concentration of 30 μM.

In ARPE-19 cells, the blockade of GJs resulted in lower amplitudes of $[Ca^{2+}]_i$ transients, especially in the cells close to the stimulation site, which may indicate the necessity of functional GJs for Ca^{2+} wave spreading (**Study I**). The residual $[Ca^{2+}]_i$ transients could occur either due to ligand stimulation via paracrine route or due to incomplete blockade of GJs. Even though 18-α-GA has been used in a number of studies as a GJ blocker (Frame and de Feijter, 1997; D'Andrea and Vittur, 1996; Huo, et al., 2010; Verwey and Edwards, 2010; Johnston et al., 2016) it may also affect the unopposed Cx43 hemi-channels (Stout et al., 2004) decreasing ATP release from the cells. In the future, the emergence of more specific blockers that affect separately GJs and hemi-channels would be beneficial.

In hESC-RPE, 18-α-GA did not affect the Ca^{2+} wave propagation, as shown by the unchanged percentage of cells that participated in the wave (**Study III**). It was challenging to assess the effect of the blocker on 28-day-cultured hESC-RPE because the mechanically induced Ca^{2+} waves were minute. There is still a possibility that the blocker affects individual $[Ca^{2+}]_i$ transients in single cells.

The distance of intercellular Ca^{2+} wave propagation upon mechanical stimulation has been shown to depend on the number of GJs (Scemes and Giaume, 2006; Charles et al., 1992). Interestingly, in astrocytes, the distance of the wave propagation was decreased with the increased number of GJs (Scemes and Giaume, 2006), while in glioma cells, the effect was the opposite (Charles et al., 1992). We can speculate that these controversies could be explained by the initial amount of IP3 or Ca^{2+} in the stimulated cell. If the concentration of IP3 in the stimulated cell is low, and the cell is connected to few neighboring cells because of the low number of GJs, the amount of IP3 diffusing from the stimulated cell could be enough for the few neighboring cells to propagate the Ca^{2+} wave. However, if the number of GJs is increased, the stimulated cell distributes the low amount of IP3 among many cells,

and that amount is not enough to sustain the Ca^{2+} wave. This may explain the experimental results shown with astrocytes. In the case when the stimulated cell has high amount of IP3, the more cells it is connected to (i.e., the more GJs expression is), the more cells can participate in the wave spreading because the amount of IP3 is enough to stimulate a relatively large number of cells. This may explain the Ca^{2+} wave observations in glioma cells. In this thesis, the large amount of GJ channels in ARPE-19 cells could be responsible for far-spreading intercellular Ca^{2+} waves. However, this hypothesis and the amount of IP3 required has to be tested experimentally.

6.1.7 Assessment of the paracrine propagation route

In ARPE-19 cells, the mechanical stimulation of a single cell in disconnected cell clusters resulted in a Ca^{2+} wave that was able to pass over the cell-free spots (**Study I**). This clearly indicated the presence of a paracrine route of Ca^{2+} wave spreading.

The blockade of P2 receptors with suramin in confluent ARPE-19 monolayers resulted in significantly reduced percentage of responsive cells in ARPE-19, especially in distant cells (**Study I**), while it slightly inhibited Ca^{2+} wave propagation in 9-day-cultured hESC-RPEs and did not affect the wave spreading in 28-day-cultured hESC-RPE (**Study III**). These results demonstrated again the similarities of intercellular Ca^{2+} dynamics between ARPE-19 and immature hESC-RPE cells. In addition, it was concluded that paracrine route involving ATP (or UTP) ligand is present in ARPE-19 and immature hESC-RPE. This yet undetermined signaling molecule could be secreted by the mechanically stimulated cell, or by both the stimulated and neighboring cells. Our mathematical model of the Ca^{2+} wave propagation in ARPE-19 cells suggests that neighboring cells do not secrete signaling molecules on their own. If this wished to be confirmed experimentally, it would require direct measurements of the secreted ATP with ATP-biosensors, similarly as in Pearson et al., 2005. However, other molecules, such as UTP, must also be considered as possible ligands.

If aiming to assert whether mature hESC-RPE lack paracrine route of Ca^{2+} wave propagation, more control experiments would be required. Here, it would be beneficial to perform experiments, where cells are directly stimulated with ATP both in presence and absence of suramin. This would allow for estimation of the inhibition rate and adjustment of suramin concentration.

In ARPE-19 cells, mechanical stimulation after pre-treatment of cells with both 18-α-GA and suramin was performed for the development of the mathematical model (**Study II**). Even the usage of the two blockers was not able to fully inhibit the Ca^{2+} wave spreading. It can be speculated that the residual Ca^{2+} waves could occur via a paracrine route that does not involve P2 receptors, or due to incomplete inhibition of GJ communication and P2 receptors.

6.2 Mathematical modeling of mechanically induced Ca^{2+} wave spreading in ARPE-19 cells

The mathematical model of the mechanically induced Ca^{2+} waves propagation in ARPE-19 cells (**Study II**) was developed based on experimental data from **Study I** and additional experimental data. The data provided for the model were normalized fluorescence curves averaged from single cells at various neighboring cell layers under control conditions and after blockade of GJs, P2 receptors (**Study I**) as well as after inhibition of both GJs and P2 blockers. It was not possible to perform experimental calibration of the fura-2-AM dye to correlate normalized fluorescence values with $[Ca^{2+}]_i$ because it had to be done at the time of the actual experiments, which were not initially planned to be used in the mathematical modeling. Moreover, it has been noticed that *in vitro* calibration leads to much poorer reproducibility of the measurements and leads to less reliable amplitude results (Fowler & Tiger, 1997). Thus, in **Study II** the fluorescent curves were considered to directly reflect $[Ca^{2+}]_i$ dynamics in the cells. However, in the future studies, it would be compulsory to experimentally confirm that the fluorescent dye fura-2-AM produced the signal that could be linearly correlated with $[Ca^{2+}]_i$ at all $[Ca^{2+}]_i$ concentrations under our experimental conditions. If the correlation between the fluorescence signal and $[Ca^{2+}]_i$ is not linear at all $[Ca^{2+}]_i$, it may affect the peak amplitude of $[Ca^{2+}]_i$ dynamics curves and, more importantly, the shape of the curves.

The mathematical model was constructed in Matlab using components from previously published models of Ca^{2+} wave propagation (Lemon et al., 2003; LeBeau et al., 1999; Keizer & Levine, 1996), as well as components designed in **Study II**, for example, the stretch. The model contains static and location-dependent parameters. The majority of the static parameters were selected according to previously published Ca^{2+} signaling models (Lemon et al., 2003; LeBeau et al., 1999; Keizer & Levine, 1996) with some parameters being optimized to match the experimental data. The parameters of stretch and consequent activation of stretch-sensitive Ca^{2+} channels,

extracellular ligand concentration, and the phosphorylation rate of IP3R3 were adjusted separately in each cell layer. The intracellular Ca^{2+} concentration was optimized to match the experimental data in each neighboring cell layer.

6.2.1 The potential mechanism of mechanically induced Ca^{2+} wave spreading in RPE cells

The mathematical model (**Study II**) suggests that both the mechanically stimulated cell and cells from the neighboring cell layers 1 to 4 experience stretch. The stretch causes the influx of Ca^{2+} from the extracellular space through the stretch-sensitive Ca^{2+} channels. This is in agreement with the experimental data that shows the reduced peak normalized fluorescence values in cells close to the stimulation site in the absence of extracellular Ca^{2+} (**Study I**).

It has been demonstrated that in response to various stimuli epithelial cells secrete ATP (Reigada and Mitchell, 2005; Mitchell, 2001) that can diffuse through the extracellular media and is degraded by ectonucleotidases (Reigada et al., 2005). Our mathematical model in **Study II** predicted that the amplitude of $[Ca^{2+}]_i$ increase and the time to reach the peak amplitude was defined by the ligand concentration. This prediction is in agreement with the experimental findings of Sullivan et al. (1997) that showed direct correlation of $[Ca^{2+}]_i$ transients amplitude with the concentration of ATP used to induce the response in cultured RPE. In addition, the mathematical model of Ca^{2+} wave spreading in airway epithelial shows a similar trend (Warren et al., 2010). It is, however, challenging to confirm experimentally whether only the stimulated cell secretes a signaling molecule, or the cells that experience the stretch, or all the neighboring cells. In addition, because the mechanical stimulation was done by making a perforation in cellular membrane, it is possible that other signaling factors leaked from the stimulated cell. The experimental data provided for the model does not allow for precise prediction of the processes occurring in the stimulated cells.

It can be speculated that the molecules that passively leak or secreted from the stimulated cell spread through the extracellular media and interact, for example, with $P2Y_2$ receptors on neighboring cells producing IP3. Thereafter, IP3 activates the IP3R3 receptor on the endoplasmic reticulum releasing Ca^{2+}. (LeBeau et al., 1999) Even though there is no direct evidence of the presence of the type 3 IP3R receptor in ARPE-19 cells, the IP3R3 receptor has been found in other epithelia, such as

intestinal epithelium (Maranto, 1994) or airway epithelium (Sugiyama et al., 1996) and has been used in the modeling Ca^{2+} wave propagation (Warren et al., 2010).

The initial $[Ca^{2+}]_i$ increase caused by IP3 activates ryanodine receptor on the endoplasmic reticulum resulting in further elevation of $[Ca^{2+}]_i$ (Keizer et al., 1996). ARPE-19 cells have been shown to express ryanodine receptors on endoplasmic reticulum (Wimmers et al., 2008). The described paracrine stimulation is likely to induce a much stronger effect compared to the stimulation caused by the stretch of cell layers 1-4 because of the leak of the signaling molecules through the perforation in the stimulated cell membrane. It is challenging, however, to determine the relative contribution of the two stimulation factors (diffusion of paracrine molecules and stretch) to the $[Ca^{2+}]_i$ increase because performing the mechanical stimulation without a membrane perforation would only eliminate the leaking signaling molecules but will not block their possible secretion from the mechanically stimulated cell.

The presence of functional GJs in ARPE-19 cells has been confirmed experimentally in **Study I**, as well as in Hutnik et al., 2008. IP3 and free cytosolic Ca^{2+} have been demonstrated to diffuse into the cytoplasm of neighboring cells via GJs (Romanello and D'Andrea, 2001; Christ et al., 1992) spreading the intercellular Ca^{2+} wave.

Finally, the $[Ca^{2+}]_i$ decreases as the sarcoendoplasmic reticulum ATPase (SERCA) and plasma membrane Ca^{2+} ATPase (PMCA) pump the Ca^{2+} out of the cytoplasm, and IP3 degrades in the cytoplasm. The resting $[Ca^{2+}]_i$ is maintained through the Ca^{2+} leak currents.

The built scheme based on the modeling and experimental data of the mechanically induced Ca^{2+} wave propagation in ARPE-19 cells is presented in **Fig. 8**.

In **Study III**, we have demonstrated that immature hESC-RPE cells propagate mechanically induced intercellular Ca^{2+} waves in a similar manner as ARPE-19 cells covering large areas. Thus, it can be speculated that a similar mechanism could be possible for immature hESC-RPE cells.

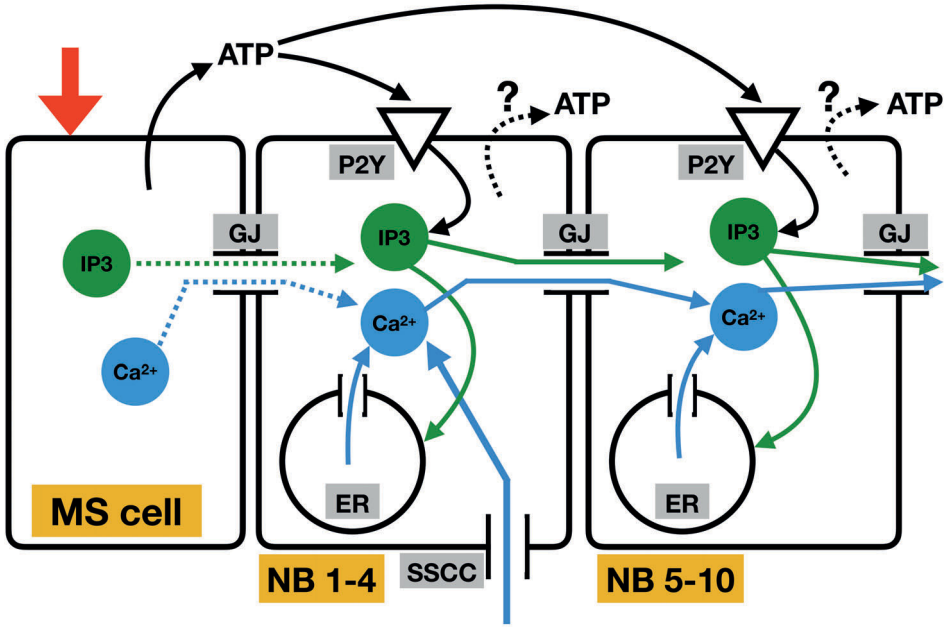

Figure 8. The scheme of the mechanically induced intercellular Ca^{2+} wave propagation in ARPE-19 cells. Solid lines – fluxes of Ca^{2+}, IP3, and ATP; dotted lines – possible fluxes of Ca^{2+}, IP3, and ATP. The mechanically stimulated cell (MS cell) secretes a signaling molecule (e.g., ATP) that interacts with P2Y receptors on the neighboring cell as it diffuses along the monolayer. This results in the production of IP3 and consequent release of Ca^{2+} from the ER. The IP3 and Ca^{2+} can pass to the neighboring cells via GJs increasing the $[Ca^{2+}]_i$ there. In addition, cells close to the site of stimulation (NB 1-4) experience stretch from the mechanical stimulation and allow extracellular Ca^{2+} through the SSCCs. The Abbreviations can be found in the "Abbreviations" section.

6.2.2 Prediction of the suramin effect

With our model, we attempted to predict the suramin effect on ARPE-19 cells. The model was able to reproduce the experimental data with blocked GJs and P2 receptors when unphosphorylated receptor dissociation constant was increased together with the phosphorylation rate of $P2Y_2$ receptors. Thus, the model suggests that suramin may disrupt ligand binding and enhance desensitization of $P2Y_2$ receptors. This finding contradicts previous observations where suramin has been

considered to disrupt the coupling between $P2Y_2$ receptors and the G-protein (Chung and Kermode, 2005), and needs to be confirmed experimentally.

The mathematical model presented in this thesis is the first Ca^{2+} signaling RPE model that describes Ca^{2+} dynamics after mechanical stimulation. It was able to reproduce experimental curves of RPE cells Ca^{2+} dynamics after mechanical stimulation in control conditions and after application of GJ and P2 receptor blockers. The model can be further improved, for example, by including voltage-gated Ca^{2+} channels. In addition, it would be beneficial to test the effect of the signaling molecule secretion by neighboring cells.

6.3 Spontaneous $[Ca^{2+}]_i$ transients in hESC-RPE cells

Spontaneous $[Ca^{2+}]_i$ transients have been demonstrated in various cell types, including neurons (Catsicas et al., 1998), muscles (Dabertrand et al., 2008), and glial cells (Mathiesen et al., 2013). In this thesis, for the first time, spontaneous $[Ca^{2+}]_i$ transients in hESC-RPEs were observed (**Study III**). The observations are in agreement with previously published studies on chick RPE (Pearson et al., 2004). Pearson et al. have reported that these increases are crucial for proliferation and differentiation of retinal progenitor cells (Pearson et al., 2005).

Here, it was demonstrated that when hESC-RPE matured gaining more pigmentation and shifting their morphology from fusiform towards cobblestone, the percentage of cells with spontaneous $[Ca^{2+}]_i$ transients increased. The cells with spontaneous $[Ca^{2+}]_i$ increases were randomly distributed and did not depend on the activity of neighboring cells. In rare cases, the transient $[Ca^{2+}]_i$ increases propagated as spontaneous Ca^{2+} waves to a few neighboring cells (**Study III**).

Studies on other cell types have shown that cells may require both extracellular and intracellular Ca^{2+} stores for spontaneous $[Ca^{2+}]_i$ increases (e.g., in smooth muscle cells (Dabertrand et al., 2008)) or only extracellular Ca^{2+} (e.g., in developing chick retina (Catsicas et al., 1998)). In our experiments, 28-day-cultured hESC-RPE cells required both Ca^{2+} sources to be available: if at least one Ca^{2+} source was blocked, the spontaneous $[Ca^{2+}]_i$ transients were almost completely inhibited (**Study III**). In 9-day-cultured cells, ER depletion completely abolished spontaneous $[Ca^{2+}]_i$ transients, while absence of extracellular Ca^{2+} significantly inhibited, but not completely blocked them (**Study III**). This indicates that the mechanisms of $[Ca^{2+}]_i$ transients may change during hESC-RPE maturation. In the future studies, it would be interesting to assess the possible difference in amplitudes of $[Ca^{2+}]_i$ transients in

9- and 28-day-cultured cells using a ratiometric Ca^{2+}-sensitive dye, e.g., fura-2-AM, that is more suitable for quantitative measurements.

It has been demonstrated that GJ blockers inhibited spontaneous intercellular Ca^{2+} waves but not transient $[Ca^{2+}]_i$ increases in single cells in chick embryo RPE and retina (Catsicas et al., 1998; Pearson et al., 2004). In our experiments, application of 18-α-GA, on average, was not able to block spontaneous $[Ca^{2+}]_i$ transients neither in 9-, nor in 28-day-cultured hESC-RPEs (**Study III**) that is in agreement with the literature data.

In developing chick retina, ATP has been reported to be released by "trigger" RPE cells that comprised 5 to 10% of the total amount of cells with spontaneous $[Ca^{2+}]_i$ transients (Pearson et al., 2004; Pearson et al., 2005). The ATP was responsible for the induction of spontaneous intercellular Ca^{2+} waves. The spontaneously arising intercellular Ca^{2+} waves were successfully inhibited by various GJ blockers, including 18-α-GA. 18-α-GA is not only known to inhibit Cx43 GJs, but also unopposed Cx43 hemi-channels. (Stout et al., 2004) Thus, the authors stated that "trigger" RPE cells produced spontaneous intercellular Ca^{2+} waves by releasing ATP through Cx43 hemi-channels. (Pearson et al., 2005) Because in our hESC-RPEs we saw spontaneous intercellular Ca^{2+} waves that involved 6-8% of cells with spontaneous $[Ca^{2+}]_i$ transients (**Study III**), it would be of interest to correlate this number with the application of 18-α-GA. Even though on average, the application of 18-α-GA did not affect the percentage of cells with spontaneous $[Ca^{2+}]_i$ transients, we saw large variation in different replicates (**Study III**). It is possible that 18-α-GA only affected the samples with spontaneous intercellular Ca^{2+} waves.

Inhibition of P2 receptors with suramin has been shown to constrain spontaneous intercellular Ca^{2+} waves but not transient $[Ca^{2+}]_i$ increases in individual cells. (Pearson et al., 2005) In hESC-RPE cells suramin did not affect percentage of cells with spontaneous $[Ca^{2+}]_i$ transients (**Study III**), that is in agreement with the previously published data.

6.4 RPE wound healing

RPE wound healing is a complex process that takes place in the eye, for example, after surgical interventions in AMD, and that is poorly understood (Bonilha, 2008; Carr et al., 2013).

In previous studies, it has been demonstrated that RPE attachment depended on the cellular morphology or differentiation state: the cells with lower pigmentation

level attached to the substrata better than those with high pigmentation (Schwartz et al., 2012). In this thesis, 9-day-cultured hESC-RPE cells were demonstrated to seal scrape wounds faster than more mature 28-day-cultured cells, which is in agreement with Schwartz et al., 2012 study (**Study IV**). It has been reported that the ability of RPE cells to attach *in vitro* to donors' Bruch's membranes strongly depends on donor's age (Gullapalli et al., 2005; Afshari & Fawcett, 2009). Our study confirmed that substratum was crucial for cellular wound healing. If the ColIV layer, the layer essential for maintaining cell proliferation and spreading on glass coverslips, was damaged during wounding, the cells showed significantly lower ability to seal the wounds. (**Study IV**) It is worth noting, however, that our results apply to hESC-RPEs cultured on coverslips with artificial Ormocomp coating, thus, they may not be extrapolated directly to *in vivo* conditions.

In this thesis for the first time, it was shown that wounding affects Ca^{2+} dynamics of hESC-RPE cells. It was demonstrated that in 9-day-cultured hESC-RPE samples, cells close to the fresh wound edges had higher percentage of cells with spontaneous $[Ca^{2+}]_i$ transients (**Study IV**). Thus, hESC-RPEs changed their intercellular Ca^{2+} dynamics because of the injury. Possibly, these changes occurred due to the initial intercellular Ca^{2+} wave that was triggered by wounding as scrape wounds are known to trigger intercellular Ca^{2+} waves that act as an initial signal to start the wound healing process (Woolley and Martin, 2000). This hypothesis has to be tested experimentally by performing the cellular monolayer injury and recording Ca^{2+} dynamics simultaneously to assess the initial Ca^{2+} wave and consequent changes of $[Ca^{2+}]_i$. Here, the more mature 28-day-cultured cells did not exhibit increase in the percentage of cells with spontaneous $[Ca^{2+}]_i$ transients (**Study IV**). In **Study III** it was shown that the %RCsp in 35-day-cultured cells was at the same level as in 28-day-cultured hESC-RPEs, therefore, it is possible that the wounded monolayer was unable to elevate the number of cells with spontaneous $[Ca^{2+}]_i$ transients. An alternative explanation is that in 28-day-cultured cells, the initial intercellular Ca^{2+} wave triggered by the wounding is not able to propagate as far as in 9-day-cultured cells (as was shown in the experiments with single cell mechanical stimulation in **Study III**). Thus, the changes in Ca^{2+} dynamics would be visible in the lower number of cells compared to 9-day-cultured cells.

When the cells were injured on day 9 of culture and then allowed to heal for 7 days, the cells in the healed areas did not have significant differences in spontaneous and mechanically induced Ca^{2+} activities compared to the undamaged neighboring cells (**Study IV**). The morphology of the cells in the wound area was similar to that of the surroundings. However, when 28-day-cultured cells were injured and then

healed for 7 days, the cells in the healed zones had fusiform morphology, reduced percentage of cells with spontaneous $[Ca^{2+}]_i$ transients, and wide-spreading mechanically induced intercellular Ca^{2+} waves (**Study IV**). Hence, the cells in the healed zone resembled the morphology and Ca^{2+} dynamics of immature hESC-RPE cells. (**Study IV**)

6.5 Future prospects

The main goals of this research were to gain deeper understanding of human RPE Ca^{2+} dynamics, to develop tools for analyzing Ca^{2+} dynamics from a large number of cells, and to elucidate factors that affect normal $[Ca^{2+}]_i$ behavior in cells, such as maturation or wounding. Here, ARPE-19 and hESC-RPE were used as RPE cell models, and according to experiments presented in this thesis, immature hESC-RPEs have similar Ca^{2+} dynamics as ARPE-19 cells. The Ca^{2+} dynamics of mature hESC-RPEs cells is different than that of immature hESC-RPEs and ARPE-19 cells. Still, these results need to be directly confirmed with native human RPE by performing comparable experiments on spontaneous and mechanically induced Ca^{2+} activity.

The results reported in this dissertation revealed that hESC-RPE cells at different maturation stages vary drastically both in mechanically induced and spontaneous Ca^{2+} activities. This knowledge may benefit the development of assays for assessment of RPE cellular maturation status. Such assays can be used along with routine gene expression measurements, for example, prior to transplantations or in drug-testing, to select the appropriate maturation level of the cells.

The experiments on hESC-RPE wound healing demonstrated the importance of cellular maturation status on the speed and success of the wound healing process. In addition, it was shown that spontaneous $[Ca^{2+}]_i$ transients undergo significant changes around the wound edge. This knowledge could benefit the research of RPE wound healing, for example, after CNV excision. Because the experiments on wound healing in hESC-RPE cell cultures had good reproducibility and predictable rate of wound closure, these models are suitable for drug testing.

In order to utilize the measurements of Ca^{2+} dynamics in any test systems, the analysis of the Ca^{2+} dynamics data must be fast, efficient, replicable, and reliable. Thus, it is crucial to continue the development of tools for automatic cell segmentation, including fusiform cells, analysis of fluorescence curves, and detection

of intercellular Ca^{2+} waves. Such tools could also be applied to other epithelia and other types of fluorescent reporters.

7 CONCLUSIONS AND MAIN FINDINGS

In this dissertation, we investigated mechanically induced and spontaneous $[Ca^{2+}]_i$ transients in human RPE cells. In addition, we studied the effect of cellular maturation, scrape wounding and consequent wound healing on Ca^{2+} dynamics. The major contributions and conclusions were:

- The methods to efficiently investigate Ca^{2+} dynamics in a large number of cells were developed.
- The mechanical stimulation of a single cell in a monolayer was demonstrated to trigger an intercellular Ca^{2+} wave in human RPE cells.
- In immortalized human RPE ARPE-19 cells, the mechanically induced intercellular Ca^{2+} waves were shown to propagate via gap junctional and paracrine routes.
- In hESC-RPE cells, maturation status was shown to dramatically affect spontaneous and mechanically induced $[Ca^{2+}]_i$ transients. In less mature, fusiform, hESC-RPE the lower spontaneous and higher mechanically induced Ca^{2+} activity was detected compared to more mature, cobblestone, hESC-RPE cells.
- In hESC-RPE cells, the fresh scrape wounds were shown to increase the percentage of cells with spontaneous $[Ca^{2+}]_i$ transients close to wound edges. The cells in healed areas of hESC-RPE monolayers were demonstrated to resemble Ca^{2+} dynamics of immature hESC-RPEs.
- The wound healing capacity of immature hESC-RPE cells was shown to be greater than that of mature hESC-RPE cells.

The results of this thesis provide insights for better understanding of RPE Ca^{2+} signaling, which is essential in assessing cellular functionality in transplantation and wound healing studies, as well as in drug discovery and toxicology tests.

8 REFERENCES

Aasen, T., Raya, A., Barrero, M.J., Garreta, E., Consiglio, A., Gonzalez, F., Vassena, R., Bilić, J., Pekarik, V., Tiscornia, G., Edel, M., Boué, S. & Belmonte, J.C.I. (2008). Efficient and Rapid Generation of Induced Pluripotent Stem Cells from Human Keratinocytes, Nature Biotechnology, Vol. 26(11), pp. 1276–1284.

Abbaci, M., Barberi-Heyob, M., Blondel, W., Guillemin, F. & Didelon, J. (2008). Advantages and Limitations of Commonly Used Methods to Assay the Molecular Permeability of Gap Junctional Intercellular Communication, Biotechniques, Vol. 45(1), pp. 33-52, 56-62.

AbouAlaiwi, W.A., Takahashi, M., Mell, B.R., Jones, T.J., Ratnam, S., Kolb, R.J. & Nauli, S.M. (2009). Ciliary Polycystin-2 is a Mechanosensitive Calcium Channel Involved in Nitric Oxide Signaling Cascades, Circulation Research, Vol. 104(7), pp. 860-869.

Afshari, F.T. & Fawcett, J.W. (2009). Improving RPE Adhesion to Bruch's Membrane, Eye, Vol. 23(10), pp. 1890-1893.

Ahmado, A., Carr, A.-J., Vugler, A.A., Semo, M., Gias, C., Lawrence, J.M., Chen, L.L., Chen, F.K., Turowski, P., da Cruz, L. & Coffey, P.J. (2011). Induction of Differentiation by Pyruvate and DMEM in the Human Retinal Pigment Epithelium Cell Line ARPE-19, Investigative Ophthalmology & Visual Science, Vol. 52(10), pp. 7148-7159.

Alberts, B., Johnson, A., Lewis, J., Raff, M., Roberts, K. & Walter, P. (2015). Molecular Biology of the Cell, 6th edition. Garland Science, New York.

Allbritton, N.L., Meyer, T. & Stryer, L. (1992). Range of Messenger Action of Calcium Ion and Inositol 1,4,5-trisphosphate, Science, Vol. 258(5089), pp. 1812-1815.

Amirpour, N., Nasr-Esfahani, M.H., Esfandiari, E., Razavi, S. and Karamali, F. (2013). Comparing Three Methods of Co-culture of Retinal Pigment Epithelium with Progenitor Cells Derived Human Embryonic Stem Cells, International Journal of Preventive Medicine, Vol. 4(11), pp. 1243-1250.

Atwood, J.L. (ed) (2017). Comprehensive Supramolecular Chemistry II. Elsevier, USA.

Ban, Y. & Rizzolo, L.J. (2000). Regulation of Glucose Transporters During Development of the Retinal Pigment Epithelium, Developmental Brain Research, Vol. 121(1), pp. 89-95.

Batat, P., Vives, G., Bofinger, R., Chang, R.-W., Kauffmann, B., Oda, R., Jonusauskas, G. & Mcclenaghan, N.D. (2012). Dynamics of Ion-Regulated Photoinduced Electron Transfer in BODIPY-BAPTA Conjugates, Photochemical Photobiological Sciences, Royal Society of Chemistry, Vol. 11(11), pp. 1666-1674.

Bauer, H.C., Krizbai, I.A., Bauer, H. & Traweger, A. (2014). "You Shall Not Pass"—Tight Junctions of the Blood Brain Barrier, Frontiers in Neuroscience, Vol. 8(392), pp. 1-21.

Benhar, I., London, A. & Schwartz, M. (2012). The Privileged Immunity of Immune Privileged Organs: The Case of the Eye, Frontiers of Immunology, Vol. 3(296), pp. 1-6.

Beltramello, M., Piazza, V., Bukauskas, F.F., Pozzan, T. & Mammano, F. (2005). Impaired Permeability to Ins(1,4,5)P3 in a Mutant Connexin Underlies Recessive Hereditary Deafness, Nature Cell Biology, Vol. 7(1), pp. 63–69.

Benedicto, I., Lehmann, G.,L., Ginsberg, M., Nolan, D.J., Bareja, R., Elemento, O., Salfati, Z., Alam, N.M., Prusky, G.T., Llanos, P., Rabbany, S.Y., Maminishkis, A., Miller, S.S., Rafii, S. & Rodriguez-Boulan, E. (2017). Concerted Regulation of Retinal Pigment Epithelium Basement Membrane and Barrier Function by Angiocrine Factors, Nature Communications, Vol. 8, pp. 15374.

Bennett, M.R., Farnell, L. & Gibson, W.G. (2005). A Quantitative Model of Purinergic Junctional Transmission of Calcium Waves in Astrocyte Networks, Biophysical Journal, Vol. 89(4), pp. 2235-2250.

Bennis, A., Jacobs, J.G., Catsburg, L.A.E., Ten Brink, J.B., Koster, C, Schlingemann, R.O., van Meurs, J., Gorgels, T.G.M.F., Moerland, P.D., Heine, V.M. & Bergen, A.A. (2017). Stem Cell Derived Retinal Pigment Epithelium: The Role of Pigmentation as Maturation Marker and Gene Expression Profile Comparison with Human Endogenous Retinal Pigment Epithelium, Stem Cell Reviews and Reports, Vol. 13(5), pp. 659-669.

Berridge, M.J., Lipp, P. & Bootman, M.D. (2000). The Versatility and Universality of Calcium Signaling, Nature Reviews Molecular Cell Biology, Vol. 1(1), pp. 11-21.

Berridge, M.J., Bootman, M.D. & Roderick, H.L. (2003). Calcium Signalling: Dynamics, Homeostasis and Remodelling, Nature Reviews Molecular Cell Biology, Vol. 4(7), pp. 517-529.

Beutner, D., Voets, T., Neher, E. & Moser, T. (2001). Calcium Dependence of Exocytosis and Endocytosis at the Cochlear Inner Hair Cell Afferent Synapse, Neuron, Vol. 29(3), pp. 681-690.

Bhutto, I.A., McLeod, D.S., Hasegawa, T., Kim, S.Y., Merges, C., Tong, P. & Lutty, G.A. (2006). Pigment Epithelium-Derived Factor (PEDF) and Vascular Endothelial Growth Factor (VEGF) in Aged Human Choroid and Eyes with Age-Related Macular Degeneration, Experimental Eye Research, Vol. 82(1), pp. 99–110.

Bi, G.Q., Morris, R.L., Liao, G., Alderton, J.M., Scholey, J.M. & Steinhardt, R.A. (1997). Kinesin and Myosin-Driven Steps of Vesicle Recruitment for Ca^{2+}-Regulated Exocytosis, Journal of Cell Biology, Vol. 138(5), pp. 999-1008.

Binder, S., Stanzel, B.V., Krebs, I. & Glittenberg, C. (2007). Transplantation of the RPE in AMD, Progress in Retinal and Eye Research, Vol. 26(5), pp. 516-554.

Boitano, S., Dirksen, E.R. & Sanderson, M.J. (1992). Intercellular Propagation of Calcium Waves Mediated by Inositol Trisphosphate, Science, Vol. 258(5080), pp. 292-295.

Bonilha, V.L. (2008). Age and Disease-Related Structural Changes in the Retinal Pigment Epithelium, Clinical Ophthalmology, Vol. 2(2), pp. 413–424.

Bootman, M.D., Rietdorf, K., Hardy, H., Dautova, Y., Corps, E., Pierro, C., Stapleton, E., Kang, E. & Proudfoot, D. (2012). Calcium Signalling and Regulation of Cell Function, Encyclopedia of Life Sciences, pp. 1-14.

Braet, K., Aspeslagh, S., Vandamme, W., Willecke, K., Martin, P.E.M., Evans, W.H. & Leybaert, L. (2003). Pharmacological Sensitivity of ATP Release Triggered by Photoliberation of Inositol - 1,4,5 - Trisphosphate and Zero Extracellular Calcium in Brain Endothelial Cells, Cellular Physiology, Vol. 197(2), pp. 205-213.

Brohawn, S.G., Su, Z. & MacKinnon, R. (2014). Mechanosensitivity is Mediated Directly by the Lipid Membrane in TRAAK and TREK1 K+ Channels, Proceedings of the National Academy of Sciences of the United States of America, Vol. 111(9), pp. 3614-3619.

Buchholz, D.E., Hikita, S.T., Rowland, T.J., Friedrich, A.M., Hinman, C.R., Johnson, L.V. & Clegg, D.O. (2009). Derivation of Functional Retinal Pigmented Epithelium from Induced Pluripotent Stem Cells, Stem Cells, Vol. 27(10), pp. 2427–2434.

Burke, J.M., Skumatz, C.M., Irving, P.E. & McKay, B.S. (1996). Phenotypic Heterogeneity of Retinal Pigment Epithelial Cells In Vitro and In Situ, Experimental Eye Research, Vol. 62(1), pp. 63-73.

Burke, J.M. (2008). Epithelial Phenotype and the RPE: is the Answer Blowing in the Wnt?, Progress in Retinal and Eye Research, Vol. 27(6), pp. 579-595.

Carr, A.-J., Vugler, A., Lawrence, J., Chen, L.L., Ahmado, A., Chen, F.K., Semo, M., Gias, C., da Cruz, L., Moore, H.D., Walsh, J. & Coffey, P.J. (2009). Molecular Characterization and Functional Analysis of Phagocytosis by Human Embryonic Stem Cell-Derived RPE Cells Using a Novel Human Retinal Assay, Molecular Vision, Vol. 15, pp. 283-295.

Carr, A.-J.F., Smart, M.J.K., Ramsden, C.M., Powner, M.B., da Cruz, L. & Coffey, P.J. (2013). Development of Human Embryonic Stem Cell Therapies for Age-Related Macular Degeneration, Trends in Neurosciences, Vol. 36(7), pp. 385-395.

Catterall, W.A. (2011). Voltage-Gated Calcium Channels, Cold Spring Harbor Perspectives in Biology, Vol. 3(8), pp. a003947.

Catsicas, M., Bonness, V., Becker, D. & Mobbs, P. (1998). Spontaneous Ca^{2+} Transients and Their Transmission in the Developing Chick Retina, Current Biology, Vol. 8(5), pp. 283–288.

Chalfie, M. (2009). Neurosensory Mechanotransduction, Nature Reviews Molecular Cell Biology, Vol. 10(1), pp. 44-52.

Charles, A.C., Merrill, J.E., Dirksen, E.R. & Sanderson, M.J. (1991). Intercellular Signaling in Glial Cells: Calcium Waves and Oscillations in Response to Mechanical Stimulation and Glutamate, Neuron, Vol. 6(6), pp. 983-992.

Charles, A.C., Kodali, S.K. & Tyndale, R.F. (1996). Intercellular Calcium Waves in Neurons, Molecular and Cellular Neuroscience, Vol. 7, pp. 337-353.

Cheng, H., Lederer, W.J. & Cannell, M.B. (1993). Calcium Sparks: Elementary Events Underlying Excitation-Contraction Coupling in Heart Muscle, Science, Vol. 262(5134), pp. 740-744.

Christ, G.J., Moreno, A.P., Melman, A. & Spray, D.C (1992). Gap Junction-Mediated Intercellular Diffusion of Ca^{2+} in Cultured Human Corporal Smooth Muscle Cells, American Journal of Physiology, Vol. 263(2), pp. 373–383.

Chung, W. & Kermode, J.C. (2005). Suramin Disrupts Receptor-G Protein Coupling by Blocking Association of G Protein α and $\beta\gamma$ Subunits, Journal of Pharmacology and Experimental Therapeutics, Vol. 313(1), pp. 191-198.

Churchill, G.C., Atkinson, M.M. & Louis, C.F. (1996). Mechanical Stimulation Initiates Cell-to-Cell Calcium Signaling in Ovine Lens Epithelial Cells, Journal of Cell Science, Vol. 109(2), pp. 355-365.

Cideciyan, A.V., Aleman, T.S., Swider, M., Schwartz, S.B., Steinberg, J.D., Brucker, A.J., Maguire, A.M., Bennett, J., Stone, E.M. & Jacobson, S.G. (2004). Mutations in ABCA4 Result in Accumulation of Lipofuscin Before Slowing of the Retinoid Cycle: a Reappraisal of the Human Disease Sequence, Human Molecular Genetics, Vol. 13(5), pp. 525–534.

Clair, C., Chalumeau, C., Tordjmann, T., Poggioli, J., Erneux, C., Dupont, G. & Combettes, L. (2001). Investigation of the Roles of Ca^{2+} and InsP(3) Diffusion in the Coordination of Ca^{2+} Signals Between Connected Hepatocytes, Journal of Cell Science, Vol. 114(11), pp. 1999–2007.

Clegg, D.O., Hikita, S.T., Hu, Q., Buchholz, D., Rowland, T.J., Pennington, B., Croze, R., Leach, L., Tsie, M., Conti, L. & Johnson, L.V. (2013). Derivation of Retinal Pigmented Epithelial Cells for the Treatment of Ocular Disease. Stem Cells Handbook, Humana Press, New York, pp. 411-418.

Colegio, O.R., Van Itallie, C.M., McCrea, H.J., Rahner, C. & Anderson, J.M. (2002). Claudins Create Charge-Selective Channels in the Paracellular Pathway Between Epithelial Cells, American Journal of Physiology - Cell Physiology, Vol. 283(1), pp. 142-147.

Colin, W.T. & Tovey, S.C. (2010). IP3 Receptors: Toward Understanding Their Activation, Cold Spring Harbor Perspectives in Biology, Vol. 2(12), pp. a004010.

Contreras, L., Drago, I., Zampese, E. & Pozzan, T. (2010). Mitochondria: The Calcium Connection, Biochimica et Biophysica Acta – Bioenergetics, Vol. 1797(6-7), pp. 607-618.

Corey, D.P. & Hudspeth, A.J. (1979). Response Latency of Vertebrate Hair Cells, Biophysical Journal, Vol. 26(3), pp. 499-506.

Coste, B., Mathur, J., Schmidt, M., Earley, T.J., Ranade, S., Petrus, M.J., Dubin, A.E., & Patapoutian, A. (2010). Piezo1 and Piezo2 are Essential Components of Distinct Mechanically Activated Cation Channels, Science, Vol. 330(6000), pp. 55-60.

Croze, R.H., Buchholz, D.E., Radeke, M.J., Thi, W.J., Hu, Q., Coffey, P.J. & Clegg, D.O. (2014). ROCK Inhibition Extends Passage of Pluripotent Stem Cell-Derived Retinal Pigmented Epithelium, Stem Cells Translational Medicine, Vol. 3(9), pp. 1066-1078.

Croze, R.H., Thi, W.J. & Clegg, D.O. (2016). ROCK Inhibition Promotes Attachment, Proliferation, and Wound Closure in Human Embryonic Stem Cell-Derived Retinal Pigmented Epithelium, Translational Vision Science & Technology, Vol. 5(6), pp. 7.

D'Andrea, P. & Vittur, F. (1996). Gap Junctions Mediate Intercellular Calcium Signaling in Cultured Articular Chondrocytes, Cell Calcium, Vol. 20(5), pp. 389-397.

D'hondt, C., Ponsaerts, R., Srinivas, S.P., Vereecke, J. & Himpens, B. (2007). Thrombin Inhibits Intercellular Calcium Wave Propagation in Corneal Endothelial Cells by Modulation of Hemichannels and Gap Junctions, Investigative Ophthalmology & Visual Science, Vol. 48(1), pp. 120-133.

Dabertrand, F., Mironneau, J., Macrez, N. & Morel, J. (2008). Full Length Ryanodine Receptor Subtype 3 Encodes Spontaneous Calcium Oscillations in Native Duodenal Smooth Muscle Cells, Cell Calcium, Vol. 44(2), pp. 180–189.

da Cruz, L., Fynes, K., Georgiadis, O., Kerby, J., Luo, Y.-H., Ahmado, A., Vernon, A., Daniels, J.T., Nommiste, B., Hasan, S.M., Gooljar, S.B., Carr, A.-J.F., Vugler, A., Ramsden, C.M., Bictash, M., Fenster, M., Steer, J., Harbinson, T., Wilbrey, A., Tufail, A., Feng, G., Whitlock, M., Robson, A.G., Holder, G.E., Sagoo, M.S., Loudon, P.T., Whiting, P. & Coffey, P.J. (2018). Phase 1 Clinical Study of an Embryonic Stem Cell–Derived Retinal Pigment Epithelium Patch in Age-Related Macular Degeneration, Nature Biotechnology, Vol. 36(4), pp. 328–333.

Deng, X., Zhu, D., Spee, C. & Hinton, D.R. (2010). A 3d Co-Culture System Facilitates Photoreceptor-Like Differentiation of Human Retinal Progenitor Cells, ARVO Annual Meeting Abstract, Vol. 51, pp. 5950.

Di Virgilio, F., Steinberg, T.H. & Silverstein, S.C. (1990). Inhibition of Fura-2 Sequestration and Secretion with Organic Anion Transport Blockers, Cell Calcium, Vol. 11(2-3), pp. 57–62.

Dombeck, D.A., Khabbaz, A.N., Collman, F., Adelman, T.L. & Tank, D.W. (2007). Imaging Large-Scale Neural Activity with Cellular Resolution in Awake, Mobile Mice, Neuron, Vol. 56(1), pp. 43-57.

Dunn, K.C., Aotaki-Keen, A.E., Putkey, F.R. & Hjelmeland, L.M. (1996). ARPE-19, a Human Retinal Pigment Epithelial Cell Line with Differentiated Properties, Experimental Eye Research, Vol. 62(2), pp. 155-170.

Dustin, L.B. (2000). Ratiometric Analysis of Calcium Mobilization, Clinical and Applied Immunology Reviews, Vol. 1(1), pp. 5–15.

Dutot, M., Liang, H., Pauloin, T., Brignole-Baudouin, F., Baudouin, C., Warnet, J.M. & Rat, P. (2008). Effects of Toxic Cellular Stresses and Divalent Cations on the Human P2X7 Cell Death Receptor, Molecular Vision, Vol. 14, pp. 889-897.

Enomoto, K., Furuya, K., Yamagishi, S., Oka, T. & Maeno, T. (1994). The Increase in the Intracellular Ca^{2+} Concentration Induced by Mechanical Stimulation is Propagated Via Release of Pyrophosphorylated Nucleotides In Mammary Epithelial Cells, Pflügers Archiv European Journal of Physiology, Vol. 427(5-6), pp. 533-542.

Fanning, A.S., Jameson, B.J., Jesaitis, L.A. & Anderson, J.M. (1998). The Tight Junction Protein ZO-1 Establishes a Link between the Transmembrane Protein Occludin and the Actin Cytoskeleton, The Journal of Biological Chemistry, Vol. 273(45), pp. 29745–29753.

Feldman, E.L., Randolph, A.E., Johnston, G.C., DelMonte, M.A. & Greene, D.A. (1991). Receptor-Coupled Phosphoinositide Hydrolysis in Human Retinal Pigment Epithelium, Journal of Neurochemistry, Vol. 56(6), pp. 2094–2100.

Feng, W., Yasumura, D., Matthes, M.T., LaVail, M.M. & Vollrath, D. (2002). Mertk Triggers Uptake of Photoreceptor Outer Segments During Phagocytosis by Cultured Retinal Pigment Epithelial Cells, Journal of Biological Chemistry, Vol. 277(19), pp. 17016-17022.

Ferrari, M.B., Ribbeck, K., Hagler, D.J. & Spitzer, N.C. (1998). A Calcium Signaling Cascade Essential for Myosin Thick Filament Assembly in Xenopus Myocytes, Vol. 141(6), pp. 1349-1356.

Ferreira-Martins, J., Rondon-Clavo, C., Tugal, D., Korn, J.A., Rizzi, R., Padin-Iruegas, M.E., Ottolenghi, S., De Angelis, A., Urbanek, K., Ide-Iwata, N., D'Amario, D., Hosoda, T., Leri, A., Kajstura, J., Anversa, P. & Rota, M. (2009). Spontaneous Calcium Oscillations Regulate Human Cardiac Progenitor Cell Growth, Circulation Research, Vol. 105(8), pp. 764-774.

Fleckner, M.R., Hochman, M.A., Buzney, S.M., Weiter, J.J., Tolentino, F.I. & Khadem, J.J. (2000). Complications of Surgery for Subfoveal Choroidal Neovascularization, International Ophthalmology Clinics, Vol. 40(1), pp. 201–214.

Forest, D.L., Johnson, L.V. & Clegg, D.O. (2015). Cellular Models and Therapies for Age-Related Macular Degeneration, Disease Models & Mechanisms, Vol. 8(5), pp. 421-427.

Fowler, C.J. & Tiger, G. (1997). Calibration of Fura-2 Signals Introduces Errors into Measurement of Thrombin-Stimulated Calcium Mobilisation in Human Platelets, Clinica Chimica Acta, Vol. 265(2), pp. 247-261.

Fragoso, G. & Lopez-Colome, A.M. (1999). Excitatory Amino Acid-Induced Inositol Phosphate Formation in Cultured Retinal Pigment Epithelium. Visual Neuroscience, Vol. 16(2), pp. 263–269.

Frame, M.K. & de Feijter, A.W. (1997). Propagation of Mechanically Induced Intercellular Calcium Waves via Gap Junctions and ATP Receptors in Rat Liver Epithelial Cells, Experimental Cell Research, Vol. 230(2), pp. 197-207.

Francis, M., Waldrup, J., Qian, X. & Taylor, M.S. (2014). Automated Analysis of Dynamic Ca^{2+} Signals in Image Sequences, Journal of Visualized Experiments, Vol. 88, pp. e51560.

Franklin, B.M., Voss, S.R. & Osborn, J.L. (2017). Ion Channel Signaling Influences Cellular Proliferation and Phagocyte Activity During Axolotl Tail Regeneration, Mechanisms of Development, Vol. 146, pp. 42-54.

Fronk, A.H. & Vargis, E. (2016). Methods for Culturing Retinal Pigment Epithelial Cells: A Review of Current Protocols and Future Recommendations, Journal of Tissue Engineering, Vol. 7, pp. 1–23.

Gama, A. & Schmitt, F. (2012). Cadherin Cell Adhesion System in Canine Mammary Cancer: A Review, Veterinary Medicine International, Vol. 2012, pp. 357187.

Gee, K., Brown, K., Chen, W., Bishop-Stewart, J., Gray, D. & Johnson, I. (2000). Chemical and Physiological Characterization of Fuo-4 Ca(2+)-Indicator Dyes, Cell Calcium 27(2), pp. 97-106.

Gerasimenko, J.V., Tepikin, A.V., Petersen, O.H. & Gerasimenko, O.V. (1998). Calcium Uptake via Endocytosis with Rapid Release from Acidifying Endosomes, Current Biology, Vol. 8(24), pp. 1335-1338.

Giepmans, B.N.G. & Moolenaar, W.H. (1998). The Gap Junction Protein Connexin43 Interacts with the Second PDZ Domain of the Zona Occludens-1 Protein, Current Biology, Vol. 8(16), pp. 931-934.

Gomes, P., Malfait, M., Himpens, B. & Vereecke, J. (2003). Intercellular Ca^{2+}-Transient Propagation in Normal and High Glucose Solutions in Rat Retinal Epithelial (RPE-J) Cells During Mechanical Stimulation, Cell Calcium, Vol. 34(2), pp. 185-192.

Gomes, P., Srinivas, S.P., Vereecke, J. & Himpens, B. (2005). ATP-dependent Paracrine Intercellular Communication in Cultured Bovine Corneal Endothelial Cells, Investigative Ophthalmology & Visual Science, Vol. 46(1), pp. 104-113.

Gomes, P., Srinivas, S.P., Vereecke, J. & Himpens, B. (2006). Gap Junctional Intercellular Communication in Bovine Corneal Endothelial Cells, Experimental Eye Research, Vol. 83(10), pp. 1225-1237.

Grisanti, S. & Guidry, C. (1995). Transdifferentiation of Retinal Pigment Epithelial Cells from Epithelial to Mesenchymal Phenotype, Investigative Ophthalmology & Visual Science, Vol. 36(2), pp. 391-405.

Guha, S., Baltazar, G.C., Coffey, E.E., Tu, L.-A., Lim, J.C., Beckel, J.M., Eysteinsson, T., Lu, W., O'Brien-Jenkins, A., Patel, S., Laties, A.M. & Mitchell, C.H. (2013). Lysosomal Alkalinization, Lipid Oxidation, Impaired Autophagy and Reduced Phagosome Clearance Triggered by P2X7 Receptor Activation in Retinal Pigmented Epithelial Cells, FASEB Journal, Vol. 27(11), pp. 4500–4509.

Guha, S., Coffey, E.E., Lu, W., Lim, J.C., Beckel, J.M., Laties, A.M. & Mitchell, C.H. (2014). Approaches for Detecting Lysosomal Alkalinization and Impaired Degradation in Fresh and Cultured RPE Cells: Evidence for a Role in Retinal Degenerations, Experimental Eye Research, Vol. 126, pp. 68-76.

Guharay, F. & Sachs, F. (1984). Stretch-Activated Single Ion Channel Currents in Tissue-Cultured Embryonic Chick Skeletal Muscle, The Journal of Physiology, Vol. 352(1), pp. 685-701.

Gullapalli, V.K., Sugino, I.K., Van Patten, Y., Shah, S. & Zarbin, M.A. (2005). Impaired RPE Survival on Aged Submacular Human Bruch's Membrane, Experimental Eye Research, Vol. 80(2), pp. 235-248.

Hamill, O.P. (2006). Twenty Odd Years of Stretch-Sensitive Channels, Pflügers Archiv: European Journal of Physiology, Vol. 453(3), pp. 333–351.

Harris, A.L. (2007). Connexin Channel Permeability to Cytoplasmic Molecules, Progress in Biophysics and Molecular Biology, Vol. 94(1–2), pp. 120-143.

Hartsock, A. & Nelson, W.J. (2008). Adherens and Tight Junctions: Structure, Function and Connections to the Actin Cytoskeleton, Biochimica et Biophysica Acta – Biomembranes, Vol. 1778(3), pp. 660-669.

Hattori, M., Suzuki, A.Z., Higo, T., Miyauchi, H., Michikawa, T., Nakamura, T., Inoue, T. & Mikoshiba, K. (2004). Distinct Roles of Inositol 1,4,5-Trisphosphate Receptor Types 1 and 3 in Ca2+ Signaling, Journal of Biological Chemistry, Vol. 279(12), pp. 11967-11975.

Hergott, G.J., Nagai, H. & Kalnins, V.I. (1993). Inhibition of Retinal Pigment Epithelial Cell Migration and Proliferation with Monoclonal Antibodies Against the Beta 1 Integrin Subunit During Wound Healing in Organ Culture, Investigative Ophthalmology & Visual Science, Vol. 34(9), pp. 2761–2768.

Himpens, B., Stalmans, P., Gomez, P., Malfait, M. & Vereecke, J. (1999). Intra- and Intercellular Ca^{2+} Signaling in Retinal Pigment Epithelial Cells During Mechanical Stimulation, The FASEB Journal, Vol. 13, pp. 63–68.

Homolya, L., Steinberg, T.H. & Boucher, R.C. (2000). Cell to Cell Communication in Response to Mechanical Stress via Bilateral Release of Atp and Utp in Polarized Epithelia, Journal of Cell Biology, Vol. 150(6), pp. 1349-1360.

Hongisto, H., Jylhä, A., Nättinen, J., Rieck, J., Ilmarinen, T., Veréb, Z., Aapola, U., Beuerman, R., Petrovski, G., Uusitalo, H. & Skottman, H. (2017). Comparative Proteomic Analysis of Human Embryonic Stem Cell-Derived and Primary Human Retinal Pigment Epithelium, Scientific Reports, Vol. 7(1), pp. 6016.

Hu, J. & Bok, D. (2001). A Cell Culture Medium that Supports the Differentiation of Human Retinal Pigment Epithelium into Functionally Polarized Monolayers, Molecular Vision, Vol. 7, pp. 14-19.

Hughes, B.A. & Takahira, M. (1996). Inwardly Rectifying K+ Currents in Isolated Human Retinal Pigment Epithelial Cells, Investigative Ophthalmology & Visual Science, Vol. 37(6), pp. 1125-1139.

Humeau, J., Bravo-San Pedro, J.M., Vitale, I., Nuñez, L., Villalobos, C., Kroemer, G. & Senovilla, L. (2018). Calcium Signaling and Cell Cycle: Progression or Death, Cell Calcium, Vol. 70, pp. 3-15.

Huo, B., Lu, X.L., Costa, K.D., Xu, Q. & Guo, X.E. (2010). An ATP-dependent Mechanism Mediates Intercellular Calcium Signaling in Bone Cell Network under Single Cell Nanoindentation, Cell Calcium, Vol. 47(3), pp. 234-241.

Hutnik, C.M.L., Pocrnich, C.E., Liu, H., Laird, D.W. & Shao, Q. (2008). The Protective Effect of Functional Connexin43 Channels on a Human Epithelial Cell Line Exposed to Oxidative Stress, Investigative Ophthalmology & Visual Science, Vol. 49(2), pp. 800-806.

Idelson, M., Alper, R., Obolensky, A., Shushan, B.E., Hemo, I., Yachimovich-Cohen, N., Khaner, H., Smith, Y., Wiser, O., Gropp, M., Cohen, M.A., Even-Ram, S., Berman-Zaken, Y., Matzrafi, L., Rechavi, G., Banin, E. & Reubinoff, B. (2010). Directed Differentiation of Human Embryonic Stem Cells into Functional Retinal Pigment Epithelium Cells, Cell - Stem Cell, Vol. 5(4), pp. 396–408.

Islam, M.S. (ed) (2012). Calcium signaling, Advances in Experimental Medicine and Biology, Vol. 740. Springer, Dordrecht, Heidelberg, New York, London.

Johnston, N.R., Mitchell, R.K., Haythorne, E., Pessoa, M.P., Semplici, F., Ferrer, J., Piemonti, L., Marchetti, P., Bugliani, M., Bosco, D., Berishvili, E., Duncanson, P., Watkinson, M., Broichhagen, J., Trauner, D., Rutter, G.A. & Hodson, D.J. (2016). Beta Cell Hubs Dictate Pancreatic Islet Responses to Glucose, Cell Metabolism, Vol. 24(3), pp. 389-401.

Justet, C., Evans, F., Vasilskis, E., Hernández, J.A. & Chifflet, S. (2013). ENaC Contribution to Epithelial Wound Healing is Independent of the Healing Mode and of Any Increased Expression in the Channel, Cell and Tissue Research, Vol. 353(1), pp. 53–64.

Kaempf, S., Walter, P., Salz, A.K. and Thumann, G. (2008). Novel Organotypic Culture Model of Adult Mammalian Neurosensory Retina in Co-Culture with Retinal Pigment Epithelium, Journal of Neuroscience Methods, Vol. 173(1), pp. 47-58.

Kaida, M., Cao, F., Skumatz, C.M., Irving, P.E. & Burke, J.M. (2000). Time at Confluence for Human RPE Cells: Effects on the Adherens Junction and in Vitro Wound Closure, Investigative Ophthalmology & Visual Science, Vol. 41(10), pp. 3215-3224.

Kawano, S., Shoji, S., Ichinose, S., Yamagata, K., Tagami, M. & Hiraoka, M. (2002). Characterization of Ca^{2+} Signaling Pathways in Human Mesenchymal Stem Cells, Cell Calcium, Vol. 32(4), pp. 165-174.

Kennedy, B.G. & Mangini, N.J. (1996). Plasma Membrane Calcium-ATPase in Cultured Human Retinal Pigment Epithelium, Experimental Eye Research, Vol. 63(5), pp. 547–556.

Kennedy, B.G., Echtenkamp, S.F., Kostrominova, T., Alloosh, M. & Mangini, N.J. (2007). Calcium Transport in Retinal Pigment Epithelium of the Ossabaw Swine, Investigative Ophthalmology & Visual Science, Vol. 48(13), p. 2535.

Kew, J.N.C. & Kemp, J.A. (2005). Ionotropic and Metabotropic Glutamate Receptor Structure and Pharmacology, Psychopharmacology, Vol. 179(1), pp. 4-29.

Keizer, J. & Levine, L. (1996). Ryanodine receptor adaptation and Ca^{2+}-induced Ca^{2+} release-dependent Ca^{2+}oscillations, Biophysical Journal, Vol. 71(6), pp. 3477-3487.

Kinnunen, K., Petrovski, G., Moe, M.C., Berta, A. & Kaarniranta, K. (2012). Molecular Mechanisms of Retinal Pigment Epithelium Damage and Development of Age ‐ Related Macular Degeneration, Acta Ophthalmologica, Vol. 90(4), pp. 299-309.

Klein, R., Peto, T., Bird, A. & Vannewkirk, M.R. (2004). The Epidemiology of Age-Related Macular Degeneration, American Journal of Ophthalmology, Vol. 137(3), pp. 486-495.

Klettner, A., Kauppinen, A., Blasiak, J., Roider, J., Salminen, A. & Kaarniranta, K. (2013). Cellular and Molecular Mechanisms of Age-Related Macular Degeneration: from Impaired Autophagy to Neovascularization, The International Journal of Biochemistry & Cell Biology, Vol. 45(7), pp. 1457-1467.

Klimanskaya, R., Hipp, J., Rezai, K.A., West, M., Atala, A. & Lanza, R. (2004). Derivation and Comparative Assessment of Retinal Pigment Epithelium from Human Embryonic Stem Cells Using Transcriptomics, Cloning and Stem Cells, Vol. 6(3), pp. 217-245.

Kolb, H., Nelson, R. & Fernandez, E. (1995). Webvision: The Organization of the Retina and Visual System. Webvision, Salt Lake City.

Koldenkova, V.P. & Nagai, T. (2013). Genetically Encoded Ca2 + Indicators: Properties and Evaluation, Biochimica et Biophysica Acta - Molecular Cell Research, Vol. 1833(7), pp. 1787-1797.

Korkka, I., Viheriälä, T., Juuti-Uusitalo, K., Uusitalo-Järvinen, H., Skottman, H., Hyttinen, J. & Nymark, S. (2018). Functional Voltage-Gated Calcium Channels Are Present in Human Embryonic Stem Cell-Derived Retinal Pigment Epithelium, Stem Cells Translational Medicine, Vol. 9999, pp. 1-15.

Korte, G.E., Burns, M.S. & Bellhorn, R.W. (1989). Epithelium-Capillary Interactions in the Eye: The Retinal Pigment Epithelium and the Choriocapillaris, International Review of Cytology, Vol. 114, pp. 221-248.

Kruman, I.I. & Mattson, M.P. (1999). Pivotal Role of Mitochondrial Calcium Uptake in Neural Cell Apoptosis and Necrosis, Journal of Neurochemistry, Vol. 72(2), pp. 529-540.

Kuznetsova, A.V., Kurinov, A.M. & Aleksandrova, M.A. (2014). Cell Models to Study Regulation of Cell Transformation in Pathologies of Retinal Pigment Epithelium, Journal of Ophthalmology, Vol. 2014, pp. 801787.

Käpylä, E., Sorkio, A., Teymouri, S., Lahtonen, K., Vuori, L., Valden, M., Skottman, H., Kellomäki, M. & Juuti-Uusitalo, K. (2014). Ormocomp-Modified Glass Increases Collagen Binding and Promotes the Adherence and Maturation of Human Embryonic Stem Cell-Derived Retinal Pigment Epithelial Cells, Langmuir, Vol. 30(48), pp. 14555–14565.

la Cour, M. (1985). The Retinal Pigment Epithelium Controls the Potassium Activity in the Subretinal Space, Acta Ophthalmologica Supplement, Vol. 173, pp. 9-10.

Lagunowich, L.A. & Grunwald, G.B. (1989). Expression of Calcium-Dependent Cell Adhesion During Ocular Development: A Biochemical, Histochemical and Functional Analysis, Developmental Biology, Vol. 135(1), pp. 158-171.

Laird, D.W. & Revel, J.P. (1990). Biochemical and Immunochemical Analysis of the Arrangement of Connexin43 in Rat Heart Gap Junction Membranes, Journal of Cell Science, Vol. 97(1), pp. 109-117.

Lansdown, A.B. (2002). Calcium: A Potential Central Regulator in Wound Healing in the Skin, Wound Repair and Regeneration, Vol. 10(5), pp. 271-285.

Leach, L.L. & Clegg, D.O. (2015). Concise Review: Making Stem Cells Retinal: Methods for Deriving Retinal Pigment Epithelium and Implications for Patients with Ocular Disease, Stem Cells, Vol. 33(8), pp. 2363-2373.

Leach, L.L., Croze, R.H., Hu, Q., Nadar, V.P., Clevenger, T.N., Pennington, B.O., Gamm, D.M. & Clegg, D.O. (2016). Induced Pluripotent Stem Cell-Derived Retinal Pigmented Epithelium: A Comparative Study Between Cell Lines and Differentiation Methods, Journal of Ocular Pharmacology and Therapeutics, Vol. 32(5), pp. 317-330.

LeBeau, A.P., Yule, D.I., Groblewski, G.E. & Sneyd, J. (1999). Agonist-Dependent Phosphorylation of the Inositol 1,4,5-Trisphosphate Receptor, The Journal of General Physiology, Vol. 113(1), pp. 851–872.

Lemon, G., Gibson, W.G. & Bennett, M.R. (2003). Metabotropic Receptor Activation, Desensitization and Sequestration-II: Modelling the Dynamics of the Pleckstrin Homology Domain, Journal of Theoretical Biology, Vol. 223(1), pp. 113-129.

Leybaert, L. & Sanderson, M.J. (2012). Intercellular Ca^{2+} Waves: Mechanisms and Function, Physiological Reviews, Vol. 92(3), pp. 1359-1392.

Liao, J.-L., Yu, J., Huang, K., Hu, J., Diemer, T., Ma, Z., Dvash, T., Yang, X.-J., Travis, G.H., Williams, D.S., Bok, D. & Fan, G. (2010). Molecular Signature of Primary Retinal Pigment Epithelium and Stem-Cell-Derived RPE Cells, Human Molecular Genetics, Vol. 19(21), pp. 4229–4238.

Lloyd-Evans, E., Waller-Evans, H., Peterneva, K. & Platt, F.M. (2010). Endolysosomal Calcium Regulation and Disease, Biochemical Society Transactions, Vol. 38(6), pp. 1458-1464.

Loh, Y.-H., Agarwal, S., Park, I.-H., Urbach, A., Huo, H., Heffner, G.C., Kim, K., Miller, J.D., Ng, K. & Daley, G.Q. (2009). Generation of Induced Pluripotent Stem Cells from Human Blood, Blood, Vol. 113, pp. 5476-5479.

Lorenz, J.J., Lorenz, M.G. & Barker, J.L. (2003). Pixel-Based Criteria-Oriented Analysis of Time-Lapse Ca^{2+}-Fluorescence Images, Journal of Neuroscience Methods, Vol. 127(2), pp. 157-166.

Lukyanenko, V. & Györke, S. (1999). Ca^{2+} Sparks and Ca^{2+} Waves in Saponin-Permeabilized Rat Ventricular Myocytes, The Journal of Physiology, Vol. 521(3), pp. 575–585.

Malik, N. & Rao, M.S. (2013). A Review of the Methods for Human iPSC Derivation, Pluripotent Stem Cells - Methods in Molecular Biology (Methods and Protocols), Vol 997. Humana Press, Totowa, NJ.

Maminishkis, A., Chen, S., Jalickee, S., Banzon, T., Shi, G., Wang, F.E., Ehalt, T., Hammer, J.A. & Miller, S.S. (2006). Confluent Monolayers of Cultured Human Fetal Retinal Pigment Epithelium Exhibit Morphology and Physiology of Native Tissue, Investigative Ophthalmology & Visual Science, Vol. 47(8), pp. 3612-3624.

Mandai, M., Watanabe, A., Kurimoto, Y., Hirami, Y., Morinaga, C., Daimon, T., Fujihara, M., Akimaru, H., Sakai, N., Shibata, Y., Terada, M., Nomiya, Y., Tanishima, S., Nakamura, M., Kamao, H., Sugita, S., Onishi, A., Ito, T., Fujita, K., Kawamata, S., Go, M.J., Shinohara, C., Hata, K., Sawada, M., Yamamoto, M., Ohta, S., Ohara, Y., Yoshida, K., Kuwahara, J., Kitano, Y., Amano, N., Umekage, M., Kitaoka, F., Tanaka, A., Okada, C., Takasu, N., Ogawa, S., Yamanaka, S. & Takahashi, M. (2018). Autologous Induced Stem-Cell–Derived Retinal Cells for Macular Degeneration, The New England Journal of Medicine, Vol. 376(11), pp. 1038-1046.

Mangini, N.J., Haugh-Scheidt, L., Valle, J.E., Cragoe Jr., E.J., Ripps, H. & Kennedy, B.G. (1997). Sodium–Calcium Exchanger in Cultured Human Retinal Pigment Epithelium, Experimental Eye Research, Vol. 65(6), pp. 821–834.

Mannagh, J., Arya, D.V. & Irvine, A.R.Jr. (1973). Tissue Culture of Human Retinal Pigment Epithelium, Investigative Ophthalmology & Visual Science, Vol. 12(1), pp. 52-64.

Maranto, A.R. (1994). Primary Structure, Ligand Binding, and Localization of the Human Type 3 Inositol 1,4,5-Trisphosphate Receptor Expressed in Intestinal Epithelium, The Journal of Biological Chemistry, Vol. 269(2), pp. 1222-1230.

Martin-Granados, C. & McCaig, C.D. (2014). Harnessing the Electric Spark of Life to Cure Skin Wounds, Advances in Wound Care, Vol. 3(2), pp. 127-138.

Marmorstein, A.D. (2001). The Polarity of the Retinal Pigment Epithelium, Traffic, Vol. 2(12), pp. 867-872.

Mathiesen, C., Brazhe, A., Thomsen, K. & Lauritzen, M. (2013). Spontaneous Calcium Waves in Bergman Glia Increase with Age and Hypoxia and May Reduce Tissue Oxygen, Journal of Cerebral Blood Flow & Metabolism, Vol. 33(2), pp. 161–169.

Matsubayashi, Y., Ebisuya, M., Honjoh, S. & Nishida, E. (2004). ERK Activation Propagates in Epithelial Cell Sheets and Regulates Their Migration During Wound Healing, Current Biology, Vol. 14(8), pp. 731-735.

Matthews, B.D., Overby, D.R., Mannix, R. & Ingber, D.E. (2006). Cellular Adaptation to Mechanical Stress: Role of Integrins, Rho, Cytoskeletal Tension and Mechanosensitive Ion Channels, Journal of Cell Science, Vol. 119(3), pp. 508-518.

Mazzoni, F., Safa, H. & Finnemann, S.C. (2014). Understanding Photoreceptor Outer Segment Phagocytosis: Use and Utility of RPE Cells in Culture, Experimental Eye Research, Vol. 126, pp. 51-60.

McMahon, S.M. & Jackson, M.B. (2018). An Inconvenient Truth: Calcium Sensors are Calcium Buffers, Trends in Neurosciences, Vol. 41(12), pp. 880-884.

McNeil, P.L., Muthukrishnan, L., Warder, E. & D'Amore, P.A. (1989). Growth Factors are Released by Mechanically Wounded Endothelial Cells, Journal of Cell Biology, Vol. 109(2), pp. 811-822.

Meyer, J.S., Shearer, R.L., Capowski, E.E., Wright, L.S., Wallace, K.A., McMillan, E.L., Zhang, S.C. & Gamm, D.M. (2009). Modeling Early Retinal Development with Human Embryonic and Induced Pluripotent Stem Cells, Proceedings of the National Academy of Sciences, Vol. 106(39), pp. 16698–16703.

Micaroni, M. (2012). Calcium Around the Golgi Apparatus: Implications for Intracellular Membrane Trafficking in Calcium Signaling, Advances in Experimental

Medicine and Biology, Vol. 740. Springer, Dordrecht, Heidelberg, New York, London.

Miller, S.S. & Steinberg, R.H. (1977) Active Transport of Ions across Frog Retinal Pigment Epithelium, Experimental Eye Research, Vol. 25(3), pp. 235-248.

Minta, A., Kao, J.P. & Tsien, R.Y. (1989). Fluorescent Indicators for Cytosolic Calcium Based on Rhodamine and Fuorescein Chromophores, Journal of Biological Chemistry, Vol. 264(14), pp. 8171-8178.

Mitchell, C.H. (2001). Release of ATP by a Human Retinal Pigment Epithelial Cell Line: Potential for Autocrine Stimulation Through Subretinal Space, The Journal of Physiology, Vol. 534(1), pp. 193-202.

Miura, Y., Yanagihara, N., Imamura, H., Kaida, M., Moriwaki, M., Shiraki, K. & Miki, T. (2003). Hepatocyte Growth Factor Stimulates Proliferation and Migration During Wound Healing of Retinal Pigment Epithelial Cells in Vitro, The Japanese Journal of Ophthalmology, Vol. 47(3), pp. 268-275.

Moerenhout, M., Himpens, B. & Vereecke, J. (2001). Intercellular Communication upon Mechanical Stimulation of CPAE-Endothelial Cells is Mediated by Nucleotides, Cell Calcium, Vol. 29(2), pp. 125-136.

Moiseyev, G., Chen, Y., Takahashi, Y., Wu, B.X. & Ma, J.X. (2005). RPE65 is the Isomerohydrolase in the Retinoid Visual Cycle, Proceedings of the National Academy of Sciences, Vol. 102(35), pp. 12413-12418.

Morales, S.A., Telander, D.G., Mareninov, S., Nagy, A., Wadehra, M., Braun, J. & Gordon, L.K. (2012). Anti-EMP2 Diabody Blocks Epithelial Membrane Protein 2 (EMP2) and FAK Mediated Collagen Gel Contraction in ARPE-19 Cells, Experimental Eye Research, Vol. 102, pp. 10-16.

Mukamel, E.A., Nimmerjahn, A. & Schnitzer, M.J. (2009). Automated Analysis of Cellular Signals from Large-Scale Calcium Imaging Data, Neuron, Vol. 63(6), pp. 747-760.

Nasir, M.A., Sugino, I. & Zarbin, M.A. (1997). Decreased Choriocapillaris Perfusion Following Surgical Excision of Choroidal Neovascular Membranes in Age-Related Macular Degeneration, British Journal of Ophthalmology, Vol. 81(6), pp. 481–489.

Niell, C.M. & Smith, S.J. (2005). Functional Imaging Reveals Rapid Development of Visual Response Properties in the Zebrafish Tectum, Neuron, Vol. 45(6), pp. 941-951.

Newman, E.A. (2001). Propagation of Intercellular Calcium Waves in Retinal Astrocytes and Müller Cells, Journal of Neuroscience, Vol. 21(7), pp. 2215-2223.

Nezu, A., Tanimura, A., Morita, T. & Tojyo, Y. (2010). Visualization of Ins(1,4,5)P3 Dynamics in Living Cells: Two Distinct Pathways for Ins(1,4,5)P3 Generation Following Mechanical Stimulation of HSY-EA1 Cells, Journal of Cell Science, Vol. 123(13), pp. 2292-2298.

Nommiste, B., Fynes, K., Tovell, V.E., Ramsden, C., da Cruz, L. & Coffey, P. (2017). Stem Cell-Derived Retinal Pigment Epithelium Transplantation for Treatment of Retinal Disease, Progress in Brain Research, Vol. 231, pp. 225-244.

North, R.A. & Jarvis, M.F. (2013). P2X Receptors as Drug Targets, Molecular Pharmacology, Vol. 83(4), pp. 759-769.

Oganesian, A., Bueno, E., Yan, Q., Spee, C., Black, J., Rao, N.A. & Lopez, P.F. (1997). Scanning and Transmission Electron Microscopic Findings During RPE Wound Healing in Vivo, International Ophthalmology, Vol. 21(3), pp. 165–175.

Oshima, A. (2014). Structure and Closure of Connexin Gap Junction Channels, Federation of European Biochemical Societies, Vol. 588(8), pp. 1230-1237.

Palatinus, J.A., O'Quinn, M.P., Barker, R.J., Harris, B.S., Jourdan, J. & Gourdie, R.G. (2010). ZO-1 Determines Adherens and Gap Junction Localization at Intercalated Disks, American Journal of Physiology – Heart and Circulatory Physiology, Vol. 300(2), pp. 583-594.

Pande, G., Kumar, N.A. & Manogaran, P.S. (1996). Flow Cytometric Study of Changes in the Intracellular Free Calcium During the Cell Cycle, Cytometry, Vol. 24(1), pp. 55-63.

Paredes, R.M., Etzler, J.C., Watts, L.T., Zheng, W. & Lechleiter, J.D. (2008). Chemical Calcium Indicators, Methods, Vol. 46(3), pp. 143-151.

Pearson, R., Catsicas, M., Becker, D. & Mobbs, P. (2002). Purinergic and Muscarinic Modulation of the Cell Cycle and Calcium Signaling in the Chick Retinal Ventricular Zone, Journal of Neuroscience, Vol. 22(17), pp. 7569-7579.

Pearson, R.A., Catsicas, M., Becker, D.L., Bayley, P., Lüneborg, N.L. & Mobbs, P. (2004). Ca^{2+} Signalling and Gap Junction Coupling Within and Between Pigment Epithelium and Neural Retina in the Developing Chick, European Journal of Neuroscience, Vol. 19(9), pp. 2435-2445.

Pearson, R.A., Dale, N., Llaudet, E. & Mobbs, P. (2005). ATP Released Via Gap Junction Hemichannels from the Pigment Epithelium Regulates Neural Retinal Progenitor Proliferation, Neuron, Vol. 46(5), pp. 731-744.

Peng, S., Rahner, C. & Rizzolo, L.J. (2003). Apical and Basal Regulation of the Permeability of the Retinal Pigment Epithelium, Investigative Ophthalmology & Visual Science, Vol. 44(2), pp. 808-817.

Periasamy, M. & Kalyanasundaram, A. (2007). SERCA Pump Isoforms: Their Role in Calcium Transport and Disease, Muscle and Nerve, Vol. 35(4), pp. 430-442.

Peterson, W.M., Meggyesy, C., Yu, K. & Miller, S.S. (1997). Extracellular ATP Activates Calcium Signaling, Ion, and fluid Transport in Retinal Pigment Epithelium, The Journal of Neuroscience, Vol. 17(7), pp. 2324–2337.

Picht, E., Zima, A.V., Blatter, L.A. & Bers, D.M. (2007). SparkMaster: Automated Calcium Spark Analysis with ImageJ, American Journal of Physiology-Cell Physiology, Vol. 293(3), pp. C1073-C1081.

Pinton, P., Giorgi, C., Siviero, R., Zecchini, E. & Rizzuto, R. (2008). Calcium and Apoptosis: ER-Mitochondria Ca^{2+} Transfer in the Control of Apoptosis, Oncogene, Vol. 27(50), pp. 6407-6418.

Qin, S. & Rodrigues, G.A. (2012). Roles of αvβ5, FAK and MerTK in Oxidative Stress Inhibition of RPE Cell Phagocytosis, Experimental Eye Research, Vol. 94(1), pp. 63-70.

Ramsden, C.M, Powner, M.B., Carr, A.-J.F., Smart, M.J.K., da Cruz, L. & Coffey, P.J. (2013). Stem Cells in Retinal Regeneration: Past, Present and Future, Development, Vol. 140(12), pp. 2576-2585.

Ranade, S.S., Syeda, R. & Patapoutian, A. (2015). Mechanically Activated Ion Channels, Vol. 88(2), pp. 1162-1179.

Rawes, V., Kipling, D., Kill, I. R. & Faragher, R.G.A. (1997). The Kinetics of Senescence in Retinal Pigmented Epithelial Cells: a Test for the Telomere Hypothesis of Ageing?, Biochemistry, Vol. 62(11), pp. 1291–1295.

Reigada, D. & Mitchell, C.H. (2005). Release of ATP from Retinal Pigment Epithelial Cells Involves Both CFTR and Vesicular Transport, American Journal of Physiology-Cell Physiology, Vol. 288(1), pp. C132–C140.

Resende, R.R., Adhikari, A., da Costa, J.L., Lorençon, E., Ladeira, M.S., Guatimosim, S., Kihara, A.H. & Ladeira, L.O. (2010). Influence of Spontaneous Calcium Events on Cell-Cycle Progression in Embryonal Carcinoma and Adult Stem Cells, Biochimica et Biophysica Acta, Vol. 1803(2), pp. 246–260.

Rizzolo, L.J (2007). Development and Role of Tight Junctions in the Retinal Pigment Epithelium, International Review of Cytology, Vol. 258, pp. 195-234.

Romanello, M. & D'Andrea, P. (2001). Dual Mechanism of Intercellular Communication in HOBIT Osteoblastic Cells: A Role for Gap-Junctional Hemichannels, Journal of Bone and Mineral Research, Vol. 16(8), pp. 1465–1476.

Rosen, P. & Misfeldt, D.S. (1980). Cell Density Determines Epithelial Migration in Culture, Proceedings of the National Academy of Sciences, Vol. 77(8), pp. 4760-4763.

Rosenthal, R., Malek, G., Salomon, N., Peill-Meininghaus, M., Coeppicus, L., Wohlleben, H., Wimmers, S., Bowes Rickman, C. & Strauss, O. (2005). The Fibroblast Growth Factor Receptors, FGFR-1 and FGFR-2, Mediate Two Independent Signalling Pathways in Human Retinal Pigment Epithelial Cells, Biochemical and Biophysical Research Communications, Vol. 337(1), pp. 241-247.

Rosenthal, R., Bakall, B., Kinnick, T., Peachey, N., Wimmers, S., Wadelius, C., Marmorstein, A. & Strauss, O. (2006). Expression of Bestrophin-1, the Product of the VMD2 Gene, Modulates Voltage-Dependent Ca^{2+} Channels in Retinal Pigment Epithelial Cells, FASEB Journal, Vol. 20(1), pp. 178-180.

Rottingen, J. & Iversen, J. (2000). Ruled by Waves? Intracellular and Intercellular Calcium Signalling, Acta Physiologica Scandinavica, Vol. 169(3), pp. 203-219.

Rowland, T.J., Buchholz, D.E. & Clegg, D.O. (2012). Pluripotent Human Stem Cells for the Treatment of Retinal Disease, Journal of Cellular Physiology, Vol. 227(2), pp. 457-466.

Ryan, J.S., Baldridge, W.H. & Kelly, M.E. (1999). Purinergic Regulation of Cation Conductances and Intracellular Ca^{2+} in Cultured Rat Retinal Pigment Epithelial Cells, Journal of Physiology, Vol. 520(3), pp. 745–759.

Ryan, S., Schachat, A., Wilkinson, C., Hinton, D., Sadda, S. & Wiedemann, P. (2012). Retina, 5th Edition. Saunders, Elsevier, United States.

Sachs, F. (2010). Stretch-Activated Ion Channels: What Are They?, Physiology, Vol. 25(1), pp. 50–56.

Salceda, R. & Riesgo-Escovar, R.J. (1990). Characterization of Calcium Uptake in Chick Retinal Pigment Epithelium, Pigment Cell and Melanoma Research, Vol. 3(3), pp. 141-145.

Samuel, W., Jaworski, C., Postnikova, O.A., Kutty, R.K., Duncan, T., Tan, L.X., Poliakov, E., Lakkaraju, A. & Redmond, T.M. (2017). Appropriately Differentiated ARPE-19 Cells Regain Phenotype and Gene Expression Profiles Similar to those of Native RPE Cells, Molecular Vision, Vol. 23, pp. 60-89.

Sanderson, M.J., Charles, A.C. & Dirksen, E.R. (1990). Mechanical Stimulation and Intercellular Communication Increases Intracellular Ca^{2+} in Epithelial Cells, Cell Regulation, Vol. 1(8), 585-596.

Sanderson, M.J., Charles, A.C., Boitano, S. & Dirksen, E.R. (1994). Mechanisms and Function of Intercellular Calcium Signaling, Molecular and Cellular Endocrinology, Vol. 98(2), pp. 173-187.

Sankaranarayanan, S. & Ryan, T.A. (2001). Calcium Accelerates Endocytosis of Vsnares at Hippocampal Synapses, Nature Neuroscience, Vol. 4(2), pp. 129–136.

Scemes, E. & Giaume, C. (2006). Astrocyte Calcium Waves: What They Are and What They Do, Glia, Vol. 54(7), pp. 716-725.

Schlosser, S.F., Burgstahler, A.D. & Nathanson, M.H. (1996). Isolated Rat Hepatocytes Can Signal to Other Hepatocytes and Bile Duct Cells by Release of Nucleotides, Proceedings of the National Academy of Sciences, Vol. 93(18), pp. 9948-9953.

Schwartz, S.D., Hubschman, J.-P., Heilwell, G., Franco-Cardenas, V., Pan, C.K., Ostrick, R.M., Mickunas, E., Gay, R., Klimanskaya, I., & Lanza, R. (2012). Embryonic Stem Cell Trials for Macular Degeneration: A Preliminary Report, Lancet, Vol. 379(9817), pp. 713–720.

Schwartz, S.D., Tan, G., Hosseini, H. & Nagiel, A. (2016). Subretinal Transplantation of Embryonic Stem Cell–Derived Retinal Pigment Epithelium for the Treatment of Macular Degeneration: An Assessment at 4 Years, Investigative Ophthalmology & Visual Science, Vol. 57(5), pp. ORSFc1-9.

Sheu, S.J., Wu, S.N. & Hu, D.N. (2005). Stretch-Stimulated Activity of Large Conductance Calcium-Activated Potassium Channels in Human Retinal Pigment Epithelial Cells, Journal of Ocular Pharmacology and Therapeutics, Vol. 21(6), pp. 429-435.

Shibahara, S., Takeda, K., Yasumoto, K., Udono, T., Watanabe, K., Saito, H. & Takahashi, K. (2001). Microphthalmia-Associated Transcription Factor (MITF): Multiplicity in Structure, Function, and Regulation, Journal of Investigative Dermatology Symposium Proceedings, Vol. 6(1), pp. 99-104.

Shih, Y.H., Radeke, M.J., Radeke, C.M. & Coffey, P.J. (2017). Restoration of Mesenchymal RPE by Transcription Factor-Mediated Reprogramming, Investigative Ophthalmology & Visual Science, Vol. 58(1), pp. 430-441.

Shirinifard, A., Glazier, J.A., Swat, M., Gens, J.S., Family, F., Jiang, Y. & Grossniklaus, H.E. (2012). Adhesion Failures Determine the Pattern of Choroidal Neovascularization in the Eye: A Computer Simulation Study, Plos Computational Biology, Vol. 8(5), pp. e1002440.

Simmons, L., Ambrose, W.M., Takezawa, T. & Swaroop, A. (2011). Evaluation of Photoreceptor and Retinal Pigment Epithelium Three-dimensional Co-culture Model, ARVO Annual Meeting Abstract, Vol. 52, pp. 438.

Skottman, H. (2010). Derivation and Characterization of Three New Human Embryonic Stem Cell Lines in Finland, In Vitro Cellular & Developmental Biology – Animal, Vol. 46(3-4), pp. 206-209.

Smith, S.J. & Augustine, G.J. (1988). Calcium Ions, Active Zones and Synaptic Transmitter Release, Trends in Neurosciences, Vol. 11(10), pp. 458–464.

Sorkio, A., Hongisto, H., Kaarniranta, K., Uusitalo, H., Juuti-Uusitalo, K. & Skottman, H. (2014). Structure and Barrier Properties of Human Embryonic Stem Cell–Derived Retinal Pigment Epithelial Cells Are Affected by Extracellular Matrix Protein Coating, Tissue Engineering Part A, Vol. 20(3-4), pp. 622-634.

Sparrow, J.R. & Boulton M. (2005). RPE Lipofuscin and its Role in Retinal Pathobiology, Experimental Eye Research, Vol. 80(5), pp. 595-606.

Sparrrow, J.R., Hicks, D. & Hamel, C.P. (2010). The Retinal Pigment Epithelium in Health and Disease, Current Molecular Medicine, Vol. 10(9), pp. 802-823.

Stalmans, P. & Himpens, B. (1997). Confocal Imaging of Ca^{2+} Signaling in Cultured Rat Retinal Pigment Epithelial Cells During Mechanical and Pharmacologic Stimulation, Investigative Ophthalmology & Visual Science, Vol. 38(1), pp. 176-187.

Stalmans, P. & Himpens, B. (1998). A Decreased Ca^{2+}-Wave Propagation is Found Among Cultured RPE Cells from Dystrophic RCS Rats, Investigative Ophthalmology & Visual Science, Vol.39(8), pp. 1493-1502.

Stalmans, P. & Himpens, B. (1999). Properties of Intra- and Intercellular Ca^{2+}-Wave Propagation Elicited by Mechanical Stimulation in Cultured RPE Cells, Cell Calcium, Vol. 25(6), pp. 391–399.

Steinberg, R.H. (1985). Interactions Between the Retinal Pigment Epithelium and the Neural Retina, Documenta Ophthalmologica, Vol. 60(4), pp. 327-346.

Steinhardt, R.A., Bi, G. & Alderton, J.M. (1994). Cell Membrane Resealing by a Vesicular Mechanism Similar to Neurotransmitter Release, Science, 26(5145), pp. 390-393.

Strauss, O. (2005). The Retinal Pigment Epithelium in Visual Function, Physiological Reviews, Vol. 85(3), pp. 845-881.

Stone, L.S. & Molliver, D.C. (2009). In Search of Analgesia: Emerging Poles of GPCRs in Pain, Molecular Interventions, Vol. 9(5), pp. 234-251.

Stout, C., Goodenough, D.A. & Paul, D.L. (2004). Connexins: Functions without Junctions, Current Opinion in Cell Biology, Vol. 16(5), pp. 507-12.

Ståhl, P.L., Salmén, F., Vickovic, S., Lundmark, A., Navarro, J.F., Magnusson, J., Giacomello, S., Asp, M., Westholm, J.O., Huss, M., Mollbrink, A., Linnarsson, S., Codeluppi, S., Borg, Å., Pontén, F., Costea, P.I., Sahlén, P., Mulder, J., Bergmann, O., Lundeberg, J. & Frisén, J. (2016). Visualization and Analysis of Gene Expression in Tissue Sections by Spatial Transcriptomics, Science, Vol. 353(6294), pp. 78-82.

Suchyna, T.M, Nitsche, J.M., Chilton, M., Harris, A.L., Veenstra, R.D. & Nicholson, B.J. (1999). Different Ionic Selectivities for Connexins 26 and 32 Produce Rectifying Gap Junction Channels, Biophysical Journal, Vol. 77(6), pp. 2968-2987.

Sugino, I.K., Wang, H., & Zarbin, M.A. (2003). Age-Related Macular Degeneration and Retinal Pigment Epithelium Wound Healing, Molecular Neurobiology, Vol. 28(2), pp. 177-194.

Sugiyama, T., Yamamoto-Hino, M., Wasano, K., Mikoshiba, K. & Hasegawa, M. (1996). Subtype-specific Expression Patterns of Inositol 1,4,5-Trisphosphate Receptors in Rat Airway Epithelial Cells, The Journal of Histochemistry and Cytochemistry, Vol. 44(11), pp. 1237-1242.

Sullivan, D.M., Erb, L., Anglade, E., Weisman, G.A., Turner, J.T. & Csaky, K.G. (1997). Identification and Characterization of P2Y2 Nucleotide Receptors in Human Retinal Pigment Epithelial Cells, Journal of Neuroscience Research, Vol. 49(1), pp. 43–52.

Sáez, J.C., Connor, J.A., Spray, D.C. & Bennett, M.V. (1989). Hepatocyte Gap Junctions are Permeable to the Second Messenger, Inositol 1,4,5-Trisphosphate, and to Calcium Ions, Proceedings of the National Academy of Sciences, Vol. 86(8), pp. 2708-2712.

Sáez, J.C., Contreras, J.E., Bukauskas, F.F., Retamal, M.A. & Bennett, M.V.L (2003). Gap Junction Hemichannels in Astrocytes of the CNS, Acta Physiologica, Vol. 179(1), pp. 9-22.

Takahashi, K. & Yamanaka, S. (2006). Induction of Pluripotent Stem Cells from Mouse Embryonic and Adult Fibroblast Cultures by Defined Factors, Cell, Vol. 126(4), pp. 663-676.

Takahashi, K., Tanabe, K., Ohnuki, M., Narita, M., Ichisaka, T., Tomoda, K. & Yamanaka, S. (2007). Induction of Pluripotent Stem Cells from Adult Human Fibroblasts by Defined Factors, Cell, Vol. 131(5), pp. 861-872.

Tamiya, S., Liu, L. & Kaplan, H.J. (2010). Epithelial–Mesenchymal Transition and Proliferation of Retinal Pigment Epithelial Cells Initiated upon Loss of Cell–Cell Contact, Investigative Ophthalmology & Visual Science, Vol. 51(5), pp. 2755–2763.

Tanna, P., Strauss, R.W., Fujinami, K. & Michaelides, M. (2017). Stargardt Disease: Clinical Features, Molecular Genetics, Animal Models and Therapeutic Options, British Journal of Ophthalmology, Vol. 101(1), pp. 25-30.

Terasaki, M., Miyake, K., & McNeil, P.L. (1997). Large Plasma Membrane Disruptions are Rapidly Resealed by Ca^{2+}-Dependent Vesicle-Vesicle Fusion Events, Journal of Cell Biology, Vol. 139(1), pp. 63-74.

Terry, L.E., Alzayady, K.J., Furati, E. & Yule, D.I. (2018). Inositol 1,4,5-trisphosphate Receptor Mutations Associated with Human Disease, Messenger (Los Angel), Vol. 6(1-2), pp. 29-44.

Thastrup, O., Cullen, P.J., Drøbak, B.K., Hanley, M.R. & Dawson, A.P. (1990). Thapsigargin, a Tumor Promoter, Discharges Intracellular Ca^{2+} Stores by Specific Inhibition of the Endoplasmic Reticulum Ca^{2+}-ATPase, Proceedings of the National Academy of Sciences, Vol. 87(7), pp. 2466-2470.

Tian, L., Hires, S.A & Looger, L.L. (2012). Imaging Neuronal Activity with Genetically Encoded Calcium Indicators, Cold Spring Harbor Protocols, Vol. 2012(6), pp. 647-656.

Tovell, V.E. & Sanderson, J. (2008). Distinct P2Y Receptor Subtypes Regulate Calcium Signaling in Human Retinal Pigment Epithelial Cells, Investigative Ophthalmology & Visual Science, Vol. 49(1), pp. 350-357.

Tran, P.O.T., Hinman, L.E., Unger, G.M. & Sammak, P.J. (1999). A Wound-Induced $[Ca^{2+}]_i$ Increase and Its Transcriptional Activation of Immediate Early Genes Is Important in the Regulation of Motility, Experimental Cell Research, Vol. 246(2), pp. 319–326.

Travis, G.H., Golczak, M., Moise, A.R. & Palczewski, K. (2007). Diseases Caused by Defects in the Visual Cycle: Retinoids as Potential Therapeutic Agents, Annual Review of Pharmacology and Toxicology, Vol. 47, pp. 469-512.

Ulrich, A.B. & Pour, P.M. (2001). Cell Lines, Encyclopedia of Genetics, pp. 310-311.

Vaajasaari, H., Ilmarinen, T., Juuti-Uusitalo, K., Rajala, K., Onnela, N., Narkilahti, S., Suuronen, R., Hyttinen, J., Uusitalo, H. & Skottman, H. (2011). Toward the Defined and Xeno-Free Differentiation of Functional Human Pluripotent Stem Cell-Derived Retinal Pigment Epithelial Cells, Molecular Vision, Vol. 17, pp. 558–575.

Vainio, I., Juuti-Uusitalo, K.M., Skottman, H., Hyttinen, J.A.K. & Nymark, S. (2014). Characterization of Calcium Currents in Stem Cell Derived Retinal Pigment Epithelium, ARVO Annual Meeting Abstract, Vol. 55, pp. 6339.

Van Itallie, C., Rahner, C. & Anderson, J.M (2001). Regulated Expression of Claudin-4 Decreases Paracellular Conductance through a Selective Decrease in Sodium Permeability, The Journal of Clinical Investigation, Vol. 107(10), pp. 1319-1327.

Vardouli, L., Moustakas, A. & Stournaras, C. (2005). LIM-kinase 2 and Cofilin Phosphorylation Mediate Actin Cytoskeleton Reorganization Induced by Transforming Growth Factor-Beta, Journal of Biochemistry, Vol. 280(12), pp. 11448-11457.

Veenstra, R.D., Wang, H.-Z., Beyer, E.C. & Brink, P.R. (1994). Selective Dye and Ionic Permeability of Gap Junction Channels Formed by Connexin45, Circulation Research, Vol. 75(3), pp. 483-490.

Verstraeten, T.C., Buzney, S.M., Macdonald, S.G. & Neufeld, A.H. (1990). Retinal Pigment Epithelium Wound Closure In Vitro. Pharmacologic Inhibition, Investigative Ophthalmology & Visual Science, Vol. 31(3), pp. 481-488.

Verwey, L.J. & Edwards, T.M. (2010). Gap Junctions and Memory: An Investigation Using a Single Trial Discrimination Avoidance Task for the Neonate Chick, Neurobiology of Learning and Memory, Vol. 93(2), pp. 189-195.

Vetter, I. (2012). Development and Optimization of FLIPR High Throughput Calcium Assays for Ion Channels and GPCRs, in Calcium Signaling, Advances in Experimental Medicine and Biology, Vol 740. Springer, Dordrecht, Heidelberg, New York, London.

von Kügelgen, I. & Hoffmann, K. (2016). Pharmacology and Structure of P2Y Receptors, Neuropharmacology, Vol. 104, pp. 50-61.

Warren, N.J., Tawhai, M.H. & Crampin, E.J. (2010). Mathematical Modelling of Calcium Wave Propagation in Mammalian Airway Epithelium: Evidence for Regenerative ATP Release, Experimental Physiology, Vol. 95(1), pp. 232–249.

Weber, C.E., Li, N.Y., Wai, P.Y. & Kuo, P.C. (2012). Epithelial-Mesenchymal Transition, TGF-β, and Osteopontin in Wound Healing and Tissue Remodeling After Injury, Journal of Burn Care & Research, Vol. 33(3), pp. 311–318.

Weber, P.A., Chang, H.C., Spaeth, K.E., Nitsche, J.M. & Nicholson, B.J. (2004). The Permeability of Gap Junction Channels to Probes of Different Size is Dependent on Connexin Composition and Permeant-Pore Affinities, Biophysical Journal, Vol. 87(2), pp. 958-973.

Wegner, F.V., Both, M. & Fink, R.H. (2006). Automated Detection of Elementary Calcium Release Events Using the á Trous Wavelet Transform, Biophysical Journal, Vol. 90(6), pp. 2151-2163.

Wei, C., Wang, X., Zheng, M. & Cheng, H. (2012). Calcium Gradients Underlying Cell Migration, Current Opinion in Cell Biology, Vol. 24(2), pp. 254-261.

Wimmers, S., Karl, M.O. & Strauss, O. (2007). Ion Channels in the RPE, Progress in Retinal and Eye Research, Vol. 26(3), pp. 263-301.

Wimmers, S. & Strauss, O. (2007). Basal Calcium Entry in Retinal Pigment Epithelial Cells is Mediated by TRPC Channels, Investigative Ophthalmology & Visual Science, Vol. 48(12), pp. 5767-5772.

Wimmers, S., Coeppicus, L., Rosenthal, R. & Strauss, O. (2008). Expression Profile of Voltage-Dependent Ca^{2+} Channel Subunits in The Human Retinal

Pigment Epithelium, Graefe's Archive for Clinical and Experimental Ophthalmology, Vol. 246(5), pp. 685-692.

Woolley, K. & Martin, P. (2000). Conserved Mechanisms of Repair: from Damaged Single Cells to Wounds in Multicellular Tissues, BioEssays, Vol. 22(10), 911-919.

Wynn, T.A. (2007). Common and Unique Mechanisms Regulate Fibrosis in Various Fibroproliferative Diseases, The Journal of Clinical Investigation, Vol. 117(3), pp. 524-529.

Xia, S. & Ferrier, J. (1992). Propagation of a Calcium Pulse Between Osteoblastic Cells, Biochemical and Biophysical Research Communications, Vol. 186(3), pp. 1212-1219.

Yang, D., Elner, S.G., Clark, A.J., Hughes, B.A., Petty, H.R. & Elner, V.M. (2011). Activation of P2X Receptors Induces Apoptosis in Human Retinal Pigment Epithelium, Investigative Ophthalmology & Visual Science, Vol. 52(3), pp. 1522-1530.

Yang, Z., Bogovic, J.A., Carass, A., Ye, M., Searson, P.C. & Prince, J.L. (2013). Automatic Cell Segmentation in Fluorescence Images of Confluent Cell Monolayers Using Multi-Object Geometric Deformable Model, Proceedings of SPIE-the International Society for Optical Engineering, Vol. 8669, pp. 10.1117/12.2006603.

Yilmaz, M. & Christofori, G. (2009). EMT, the Cytoskeleton, and Cancer Cell Invasion, Cancer and Metastasis Reviews, Vol. 28(1-2), pp. 15–33.

Ying, X., Minamiya, Y., Fu, C. & Bhattacharya, J. (1996). Ca^{2+} waves in Lung Capillary Endothelium, Circulation Research, Vol. 79(4), pp. 898-908.

Zeiss, C.J. (2010). Animals as Models of Age-Related Macular Degeneration - an Imperfect Measure of the Truth, Veterinary Pathology, Vol. 47(3), pp. 396–413.

Zhang, Y., Tang, W., Ahmad, S., Sipp, J.A., Chen, P. & Lin, X. (2005). Gap Junction-Mediated Intercellular Biochemical Coupling in Cochlear Supporting Cells is Required for Normal Cochlear Functions, Proceedings of the National Academy of Sciences, Vol. 102(42), pp. 15201-15206.

Zhao, P.Y.C., Peng, S., Ediriwickrema, L., Qiu, C., Davis, K.J., Adelman, R.A. & Rizzolo, L.J. (2014). Co-culture of Stem Cell Derived Retinal Progenitors and Retinal Pigment Epithelium Promotes Tissue Maturity, ARVO Annual Meeting Abstract, Vol. 55, pp. 3995.

Zhao, P.Y., Gan, G., Peng, S., Wang, S.B., Chen, B., Adelman, R.A. & Rizzolo, L.J. (2015). TRP Channels Localize to Subdomains of the Apical Plasma Membrane in Human Fetal Retinal Pigment Epithelium, Investigative Ophthalmology & Visual Science, Vol. 56(3), pp. 1916-1923.

Zhou, T., Benda, C., Duzinger, S., Huang, Y., Li, X., Li, Y., Guo, X., Cao, G., Chen, S., Hao, L., Chan, Y.-C., Ng, K.-M., Ho, J.C., Wieser, M., Wu, J., Redl, H., Tse, H.-F., Grillari, J., Grillari-Voglauer, R., Pei, D. & Esteban, M.A. (2011). Generation of Induced Pluripotent Stem Cells from Urine, Journal of the American Society of Nephrology, Vol. 22(7), pp. 1221-1228.

Zundler, S., Caioni, M., Müller, M., Strauch, U., Kunst, C. & Woelfel, G. (2016). K+ Channel Inhibition Differentially Regulates Migration of Intestinal Epithelial Cells in Inflamed vs. Non-Inflamed Conditions in a PI3K/Akt-Mediated Manner, PLoS One, Vol. 11(1), pp. e0147736.

PUBLICATIONS

PUBLICATION I

Intercellular Ca^{2+} Wave Propagation in Human Retinal Pigment Epithelium Cells Induced by Mechanical Stimulation

Abu Khamidakh, A.E., Juuti-Uusitalo, K., Larsson, K., Skottman, H. & Hyttinen, J.

2013, Experimental Eye Research, Vol. 108, pp. 129-139
https://doi.org/10.1016/j.exer.2013.01.009

Experimental Eye Research 108 (2013) 129–139

Contents lists available at SciVerse ScienceDirect

Experimental Eye Research

journal homepage: www.elsevier.com/locate/yexer

Intercellular Ca^{2+} wave propagation in human retinal pigment epithelium cells induced by mechanical stimulation

A.E. Abu Khamidakh [a,b,*], K. Juuti-Uusitalo [b,c], K. Larsson [b,c], H. Skottman [b,c], J. Hyttinen [a,b,**]

[a] Department of Biomedical Engineering, Tampere University of Technology, PL 692, 33101 Tampere, Finland
[b] BioMediTech, Tampere, Finland
[c] IBT – The Institute of Biomedical Technology, Biokatu 12, 33014 Tampere, University of Tampere, Finland

ARTICLE INFO

Article history:
Received 6 July 2012
Accepted in revised form 14 January 2013
Available online 22 January 2013

Keywords:
retinal pigment epithelium
ARPE-19
calcium wave
mechanical stimulation

ABSTRACT

Ca^{2+} signaling is vitally important in cellular physiological processes and various drugs also affect Ca^{2+} signaling. Thus, knowledge of Ca^{2+} dynamics is important toward understanding cell biology, as well as the development of drug-testing assays. ARPE-19 cells are widely used for modeling human retinal pigment epithelium functions and drug-testing, but intercellular communication has not been assessed in these cells. In this study, we investigated intercellular Ca^{2+} communication induced by mechanical stimulation in ARPE-19 cells. An intercellular Ca^{2+} wave was induced in ARPE-19 monolayer by point mechanical stimulation of a single cell. Dynamic changes of intracellular Ca^{2+} concentration ($[Ca^{2+}]_i$) in the monolayer were tracked with fluorescence microscopy imaging using Ca^{2+}-sensitive fluorescent dye fura-2 in presence and absence of extracellular Ca^{2+}, after depletion of intracellular Ca^{2+} stores with thapsigargin, and after application of gap junction blocker α-glycyrrhetinic acid and P2-receptor blocker suramin. Normalized fluorescence values, reflecting amplitude of $[Ca^{2+}]_i$ increase, and percentage of responsive cells were calculated to quantitatively characterize Ca^{2+} wave propagation. Mechanical stimulation of a single cell within a confluent monolayer of ARPE-19 cells initiated an increase in $[Ca^{2+}]_i$, which propagated to neighboring cells in a wave-like manner. Ca^{2+} wave propagated to up to 14 cell tiers in control conditions. The absence of extracellular Ca^{2+} reduced $[Ca^{2+}]_i$ increase in the cells close to the site of mechanical stimulation, whereas the depletion of intracellular Ca^{2+} stores with thapsigargin blocked the wave spreading to distant cells. The gap junction blocker α-glycyrrhetinic acid reduced $[Ca^{2+}]_i$ increase in the cell tiers close to the site of mechanical stimulation, indicating involvement of gap junctions in Ca^{2+} wave propagation. The P2-receptor blocker suramin reduced the percentage of responsive cells participating in Ca^{2+} wave spreading beyond the fourth cell tier, showing the necessity of P2-receptors for Ca^{2+} wave propagation. In disconnected, i.e., subconfluent, ARPE-19 cell clusters Ca^{2+} wave spreading was considerably less efficient compared to that in confluent ARPE-19 monolayer at the same distances. ARPE-19 cells showed repeatable and robust Ca^{2+} dynamics after mechanical stimulus. The ARPE-19 cells exhibited two different mechanisms of Ca^{2+} wave propagation dependent on the cell location: in the cells close to the site of mechanical stimulation the Ca^{2+} wave propagated mainly through gap junctions and required Ca^{2+} from both intracellular Ca^{2+} stores and extracellular media, while farther away the propagation was more dependent on the purinergic receptors and did not require extracellular Ca^{2+}. The proposed method could provide a tool to assess the drug-induced changes in intercellular communication in *in vitro* assays in human retinal pigment epithelial cells.

1. Introduction

Ca^{2+} is a major signaling molecule that dictates cellular fate in the secretion of growth factors (Barg, 2003), cell differentiation (Black and Smith, 1989), and cell death (Mattson and Chan, 2003). Intercellular communication (IC) is also strongly dependent on Ca^{2+} signaling (Rottingen and Iversen, 2000). IC is a fundamental property of cells that allows them to work as a biological tissue.

* Corresponding author. Department of Biomedical Engineering, Tampere University of Technology, Biokatu 6, 4-211, PL 692, 33101 Tampere, Finland. Tel.: +358 465 451 005.
** Corresponding author. Department of Biomedical Engineering, Tampere University of Technology, PL 692, 33101 Tampere, Finland. Tel.: +358 408 490 020.
E-mail addresses: amna.abukhamidakh@tut.fi (A.E. Abu Khamidakh), kati.juuti-uusitalo@uta.fi (K. Juuti-Uusitalo), kim.larsson@uta.fi (K. Larsson), heli.skottman@uta.fi (H. Skottman), jari.hyttinen@tut.fi (J. Hyttinen).

0014-4835/$ – see front matter © 2013 Elsevier Ltd. All rights reserved.
http://dx.doi.org/10.1016/j.exer.2013.01.009

Drugs influence IC through various routes, such as membrane receptors (Baurand and Gachet, 2003), Ca^{2+} pumps (Brini and Carafoli, 2009), and ion channels (Overington et al., 2006). Thus, information about Ca^{2+} dynamics can be used in the development of drug testing assays.

Mechanical stimulation is known to induce a rapid increase in the intracellular Ca^{2+} concentration ($[Ca^{2+}]_i$), which spreads from mechanically stimulated cells to neighboring cells in a wave-like manner. Ca^{2+} waves have been shown to occur in different types of cells: neurons (Charles et al., 1996), glial cells (Charles et al., 1991), osteoblasts (Xia and Ferrier, 1992), hepatocytes (Schlosser et al., 1996), epithelial cells (Churchill et al., 1996; Stalmans and Himpens, 1998), and endothelial cells (D'hondt et al., 2007). Thus, mechanical stimulation of a single cell can be utilized to study IC.

Ca^{2+} waves can be induced by two separate routes: intracellularly via gap junctions (GJ) or via the extracellular medium, the so-called paracrine route. GJ are intercellular protein channels that allow controlled direct exchange of molecules. The pore size of GJ channels allows for diffusion of molecules of less than 1000 Da (such as ions [Na^+, K^+, Ca^{2+}, H^+], inositol 1,4,5-trisphosphate [IP3], and nucleotides (Evans and Martin, 2002; Goodenough et al., 1996; Sáez et al., 2003)). GJ are made of six connexins and form a structure called a connexon that pierces the plasma membrane of one cell and docks with a connexon of the neighboring cell, creating an intercellular channel (Giepmans et al., 2003). GJ play an essential role in coordinating tissue functions (Mese et al., 2006). Paracrine IC, in contrast to GJ IC, does not require cell-to-cell apposition. Paracrine IC involves the release of signaling molecules from the cell into the extracellular medium. Signaling molecules activate neighboring cells as they diffuse.

ATP is probably the most studied paracrine factor involved in Ca^{2+} wave propagation. This has been examined in several cell types such as epithelial, endothelial, glioblastoma, and glioma cells (Cotrina et al., 1998; Gomes et al., 2005; Klepeis et al., 2004). Investigations conducted on airway epithelial cells suggest that IP_3, which is elevated by mechanical stimulation, acts as a messenger in cell-to-cell communication (Boitano et al., 1992; Sanderson et al., 1990). These studies demonstrate that IP_3-sensitive Ca^{2+} stores are needed for Ca^{2+} wave propagation. It has been proposed that IP_3 can either diffuse via GJ from mechanically stimulated cells (Sanderson et al., 1994) or is generated in cells due to purinergic receptor activation by ATP released from mechanically stimulated cells (Jorgensen et al., 1997; Nezu et al., 2010).

In this work, we examined the intercellular Ca^{2+} signaling transduction mechanism in a human retinal pigment epithelium (RPE) cell line, ARPE-19. The RPE is the outermost retinal layer lying just outside the neurosensory retina. The RPE forms a barrier that controls the transcellular water and ion transport between choroid and neural retina. This balance maintains photoreceptors microenvironment (Steinberg, 1985; Strauss, 2005). The RPE also plays a major role in renewal of photoreceptors, exerting phagocytosis on rods and cones outer segments, and reisomerization and transport of 11-cis retinal (Boulton and Dayhaw-Barker, 2001; Strauss, 2005).

Ca^{2+} is known to be involved in most of the crucial RPE functions, such as controlling of water and ion balance in subretinal space during dark and light adaptation (Fain et al., 2001), triggering of phagocytosis and secretion of growth factors (Wimmers et al., 2007).

Tissues undergo mechanical stress in several pathologic conditions. RPE cells in the back of the eye encounter mechanical stress, which can lead to retinal detachment, e.g., in proliferative diabetic retinopathy or proliferative vitreoretinopathy (Seko et al., 1999). The most abrupt form of mechanical stress in retina is the retinal tear. It can arise spontaneously, but is often associated to treatments for age-related macular degeneration, i.e., intravitreal injections or photodynamic therapy. The RPE cells are subjected to the mechanical stress also after the tear, during the healing of the RPE (Barkmeier and Carvounis, 2011). Mechanical stimulation allows activating Ca^{2+} signaling and study stress-induced physiological processes in RPE cells.

The ARPE-19 cell line is widely used to model basic RPE cell functions (Abe et al., 2003; Alizadeh et al., 2001; Dunn et al., 1998; Milbury et al., 2007; Narayan et al., 2003; Slomiany and Rosenzweig, 2004; Wrona et al., 2004) and to study drug effects on RPE cells (Luthra et al., 2006; Majumdar et al., 2004). However, until now the characteristics of intercellular Ca^{2+} communication in ARPE-19 cells has not been elucidated. The purpose of this study was to investigate the characteristics of Ca^{2+} wave propagation in ARPE-19 cells. In this study, we assessed Ca^{2+} wave spreading after mechanical stimulation in various culture conditions, including application of chemicals affecting this phenomenon, to explore the processes that mediate coordinated cellular responses.

2. Materials and methods

2.1. Cell culture

Studies were performed using commercial human RPE immortalized cell line (ARPE-19 cells [ATCC Manassas, VA, U.S.A.]). Cells were cultured in Dulbecco's modified Eagle's medium (DMEM; Gibco Invitrogen, Carlsbad, CA, USA) supplemented with 10% fetal bovine serum (PAA Laboratories, Cölbe, German), 2 mM glutamax (Life Technologies, Carlsbad, CA, USA), and an antibiotic mixture of 100 U/ml penicillin/streptomycin (Cambrex Bio Science, Walkersville, MD, USA). The cells were cultured at 37 °C in a humidified atmosphere containing 5% CO_2 until they were 80% confluent. For experiments, the cells were seeded on a cell culture dish with a glass bottom (diameter 35 mm, height 5 mm, glass bottom thickness 175μm ± 15 μm; Greiner Bio One Cat.-No.: 627861) or on glass coverslips (No 1.5, Warner Instruments) at a density of 150,000 cells/cm^2. Prior to seeding, the cells were washed with Ca^{2+} and Mg^{2+}-free phosphate buffered saline (PBS) solution (Lonza Group Ltd., Basal, Switzerland) and dissociated with trypsin–EDTA (Lonza Group Ltd.). Cells were cultured to confluence for 2 days after seeding.

2.2. Functional studies

2.2.1. Media and chemicals for functional studies

For the measurements, the culture medium of the cells was replaced with HEPES buffered salt solution (HBSS) containing in (mM): 137 NaCl, 5 KCl, 0.44 KH_2PO_4, 20 HEPES, 4.2 $NaHCO_3$, 5 glucose, 1.2 $MgCl_2$, 2 $CaCl_2$ (pH = 7.37, osmolarity = 330–340 mOsm/kg). The pH was adjusted with 3M NaOH, and osmolarity was adjusted with 2.5M sucrose.

HBSS, excluding 2 mM $CaCl_2$, was used in nominal free Ca^{2+} experiments.

The contribution of intracellular Ca^{2+} stores to Ca^{2+} wave propagation was studied by treating the cells with 2 μM thapsigargin (Sigma–Aldrich, St. Louis, MO, USA) for 10 min to deplete the intracellular Ca^{2+}-stores.

The spreading of the Ca^{2+} wave through GJ was studied in the presence of GJ inhibitors: α-glycyrrhetinic acid (Sigma–Aldrich), quinidine (Sigma–Aldrich), and 1-heptanol (Sigma–Aldrich).

In these experiments, cells were incubated for 30 min in 30 μM α-glycyrrhetinic acid, 10 min in 3, 30 and 300 μM of quinidine and 50 min in 1 mM 1-heptanol prior to the measurements. All solutions were based on HBSS (pH adjusted to 7.37, osmolarity – to 330–340 mOsm/kg). 30 μM α-glycyrrhetinic acid was prepared from the stock solution of α-glycyrrhetinic acid in DMSO. The

control solution for this experiment contained an equal amount of DMSO. In all cases, except for quinidine, measurements were performed without an inhibitor wash-out to maintain their effect. Quinidine was washed out before the measurements, because of its fluorescent properties under the experimental conditions of Ca^{2+} imaging. Measurements with quinidine were performed immediately after the wash-out.

Propagation of the Ca^{2+} wave via purinergic receptors was studied with a P2-receptor blocker suramin (Sigma–Aldrich). The cells were preincubated with 50 μM suramin for 25 min prior to mechanical stimulation in normal or Ca^{2+}-free conditions or in presence of 2 μM thapsigargin.

Concentrations and treatment times for thapsigargin, GJ blockers, and suramin used for the experiments are summarized in Table 1.

2.2.2. Cell viability test

Cell viability was assessed in ARPE-19 cells under control conditions and after treatment with GJ blockers, suramin, and thapsigargin with the Live/Dead Viability/Cytotoxicity kit for Mammalian cells (Invitrogen). Briefly, the cells were rinsed with Dulbecco's PBS and incubated at room temperature for 40 min with a mixture of 0.25 μM calcein AM (green fluorescence) and 0.5 μM ethidium homodimer-1 (red fluorescence, EthD-1). A fluorescence microscope (Olympus IX51) was used to image the viable cells (green fluorescence) and dead cells (red fluorescence) with a 10× long working distance objective. The experiments were performed two times.

2.2.3. Scrape loading/dye transfer assay

GJ intercellular communication was assessed with the scrape loading/dye transfer assay (El-Fouly et al., 1987). ARPE-19 cells were grown in the same manner as for live cell Ca^{2+} imaging. After medium was removed, cells were scraped with a surgical scalpel, and Alexa Fluor 568 hydrazide (Invitrogen, 1:1000), that can pass through gap junctional channels (Weber et al., 2004), dissolved in HBSS was added. After 15 min incubation the cells were rinsed with Dulbecco's PBS (Lonza Group Ltd., Basal, Switzerland), and visualized immediately with fluorescence microscope (Olympus IX51) using a 20× air objective.

To test the effectiveness of GJ blocker α-glycyrrhetinic acid, the cells were incubated with 30 μM α-glycyrrhetinic acid for 30 min prior the scrape loading/dye transfer test, and 30 μM α-glycyrrhetinic acid was added to the hydrazide-containing solution.

Experiments were repeated twice in several biological replicates.

2.2.4. Mechanical stimulation for inducing a Ca^{2+} wave

Mechanical stimulation was induced with a glass micropipette mounted on a Luigs & Neumann SM 5–9 vertical micro-injection system. The pipette was intermittently lowered, thereby stimulating the cell of interest. The pipette for the stimulation was made by melting a glass capillary (Harvard Apparatus Ltd; PG150T-7.5, 1.5 mm × 1.16 mm × 7.5 cm) with a Narishige patch clamp puller and Microforge for flame polishing of capillary tips. The tip was sealed by melting.

In our experiments, we chose to perform the stimulation with membrane perforation to achieve an equivalent stimulation strength across all experiments. Furthermore, stimulation was visually controlled by the appearance of a black dot on fluorescence images, indicating perforation (data not shown).

2.2.5. Ca^{2+} imaging

ARPE-19 cells were loaded with the Ca^{2+}-sensitive dye fura-2-acetoxymethyl ester (fura-2 AM; Invitrogen, Molecular Probes). Fura-2 AM was dissolved in DMSO (Sigma–Aldrich) and added to the HBSS. The cells were incubated with 8 μM fura-2 AM for 40 min at 37 °C. After loading, the cells were washed 10 times with HBSS without fura-2 AM before adding the final volume of HBSS or modified HBSS (Ca^{2+}-free, thapsigargin, GJ blockers or suramin containing HBSS).

Ca^{2+} wave spreading was inspected with an Olympus IX51 fluorescence microscope and ANDOR iXion 885 camera. Cells were excited at 340 nm and 380 nm with Polychrome V. Fluorescence emission was collected at 510 nm.

2.2.6. Data analysis

The ratio images (i.e., 340–380 nm image pairs) were recorded at a speed of 1 image per second and processed offline with TiLLvisION (v.4.5.65) and in house MatLab (R2010b, Mathworks) software.

Cell boundaries were defined in TiLLvisION software. Each cell was numbered, starting from the mechanically stimulated (MS) cell and then to all visible neighboring (NB) cells in the field of view. The NB cells immediately surrounding MS cell were defined as the first NB cell layer (NB layer 1), cells immediately surrounding the first layer were defined as the second NB layer (NB layer 2), and so on (Fig. 1). Emitted fluorescence intensities from the respective excitations were averaged for each cell.

The ratio of emitted fluorescence intensities resulting from excitation at 340 and 380 nm (F_{340}/F_{380}) was determined for each cell after background correction. Normalized fluorescence (NF) was then obtained by dividing the fluorescence value by the mean fluorescence value before the point of mechanical stimulation.

Table 1
Reagents used in Ca^{2+} imaging experiments.

Reagent	Concentration, μM	Treatment time, min	Wash out
Thapsigargin	2	10	–
α-glycyrrhetinic acid	30	30	–
Quinidine	3, 30, 300	10	+
1-Heptanol	1000	50	–
Suramin	50	25	–

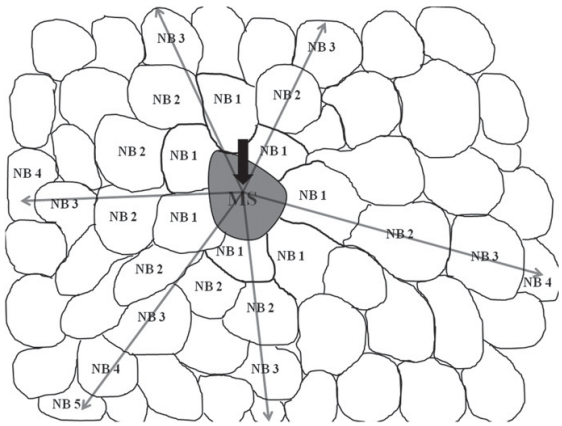

Fig. 1. Definition of neighboring (NB) cell layers on a confluent cell monolayer. Labels: MS – the mechanically stimulated cell, NB layer 1 – first neighboring layer is in direct contact with MS; NB layer 2 – second neighboring layer is in direct contact with NB layer 1, and so on.

Intercellular wave propagation was characterized by the maximum NF (peak NF) and the percentage of responsive cells (%RC). Cells with peak NF < 1.5 were considered not responsive. The results are expressed as mean $\pm$ SEM. The total number of responsive cells used to calculate mean NF in NB cell layer number X is indicated as n_x. All experiments were performed at least three times.

The time needed for the Ca^{2+} wave to propagate to one subsequent NB cell layer in interconnected cells was calculated as the time between NF peaks in two adjacent cell layers.

The speed of Ca^{2+} waves in disconnected cell clusters was estimated by dividing the distance between the MS cell and the NB cell in μm over the time between the NF peaks in these cells. In this case the speed is expressed in μm/s.

2.2.7. Statistics

Two-sample, unpaired Student's *t*-test (Matlab R2010b, Mathworks) was used to determine the statistical significance between the mean normalized fluorescence values in different groups. $P < 0.05$ was considered statistically significant.

2.3. Immunofluorescence staining

The morphology of the cells and the localization of connexin 43 were assessed with immunofluorescence labeling that was performed as previously described in Vaajasaari et al. (2011). Briefly, confluent cell cultures either grown on Greiner glass bottom dishes or coverslips were rinsed in PBS 3 times and fixed in 4% paraformaldehyde (Sigma–Aldrich) in 1× PBS (Lonza Group Ltd) for 10 min. After 3 rinses with PBS, the cells were permeabilized in 0.01% Triton X (Sigma–Aldrich) in PBS buffer for 10 min at room temperature. Thereafter, cells were washed 3 times in PBS and unspecific binding sites were blocked with 3% bovine serum albumin (Sigma–Aldrich) in PBS for 1 h. Then the cells were treated with primary antibodies rabbit-anti-human connexin 43 (Sigma, cat: C6219, 1:1000 dilution in 0.5% BSA-PBS) present in GJ labeling, mouse-anti-human ZO-1 (Gibco Invitrogen, cat: 33-9100, 1:250 dilution in 0.5% BSA-PBS) for protein present in tight junction labeling. After 1 h incubation at room temperature, the cells were washed three times with 1× PBS and thereafter subjected to secondary antibodies, Alexa Fluor 488 donkey-anti-rabbit and Alexa Fluor 568 donkey-anti-mouse IgG (both from Molecular Probes, Life Technologies, Paisley, UK, in 1:1500 dilution in 0.5% BSA-PBS). Actin filaments were stained with Phalloidin tetra methyl rhodamine B isothiocyanate (Sigma–Aldrich) in 1:300 dilution in 0.5% BSA-PBS) simultaneously with secondary antibodies. After 1 h incubation at room temperature, the cells were rinsed 3 times with PBS. Stained cells were mounted with Vectashield mount with 4′, 6′ diamidino-2-phenylidole (DAPI [Vector Laboratories Inc., Burlingame, CA, USA]), which stained the nuclei. Images were taken with Olympus IX51 microscope with a 40× objective.

3. Results

3.1. Morphology of ARPE-19 cells

In this study, monolayers of human ARPE-19 cells grown for 2 days after seeding were used in all experiments, except the experiment on non-interconnected cell clusters.

The confluent layer had Cx43-positive labeling, that can be seen on the edges of the cells (Fig. 2A and B), phalloidin localized both on cell edges and on stress fibers indicating that some of the cells had fusiform and some already a cobblestone morphology, respectively (Fig. 2A), and tight junctions were observed with ZO-1 labeling (Fig. 2B).

3.2. Mechanical stimulation induces a $[Ca^{2+}]_i$ increase, which propagates to neighboring cells

Mechanical stimulation of a single cell in a confluent monolayer initiated an increase in the intracellular Ca^{2+} concentration ($[Ca^{2+}]_i$), which propagated to neighboring cells in a wave-like manner seen in the fluorescence images in Fig. 3A.

The kinetics of fluorescence, reflecting $[Ca^{2+}]_i$ transients, in cells from NB layers 1–11 are shown in Fig. 3B. Each line graph represents mean NF values from 13 experiments (60–208 cells for each line graph). The decrease of peak NF and the increase in the response delay of NB cells with an increase in the NB cell layer number is evident from the graph. The rate of the decrease in NF after achieving the peak NF was similar in all NB layers. The rate of the increase in NF before achieving the peak NF decreased from 0.65 ± 0.16 NF units/s in NB layer 1 to 0.04 ± 0.004 NF units/s in NB layer 10. Ca^{2+} wave propagated to the subsequent NB layer within 1.5 s when spreading through NB layers 2–4, and within 3.5 s when spreading through NB layers 4–15. Taking into account cell size variability, the speed of Ca^{2+} wave propagation in NB layers 2–4 was in the range of 16.7–33.3 μm/s and in NB layers 4–15 − 7.1–14.3 μm/s.

Propagation of the Ca^{2+} wave was typically discontinuous within the cells with short delays separating rapid increases in

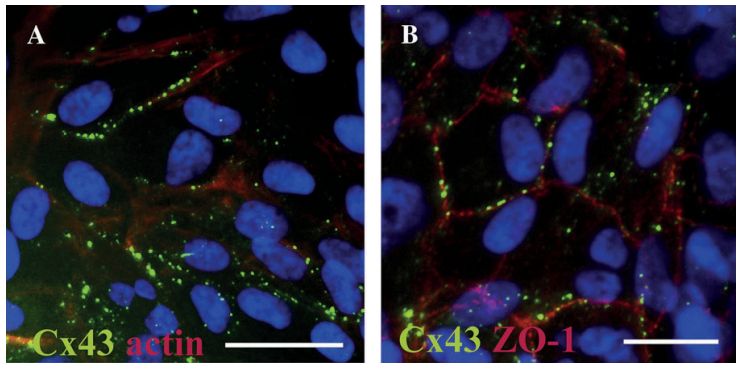

Fig. 2. Representative ARPE-19 cell monolayers used for live cell imaging. A – gap junction component Cx43 (green) and actin (red), B – Cx43 (green) and tight junction component ZO-1 (red). Scale bar: 20 μm.

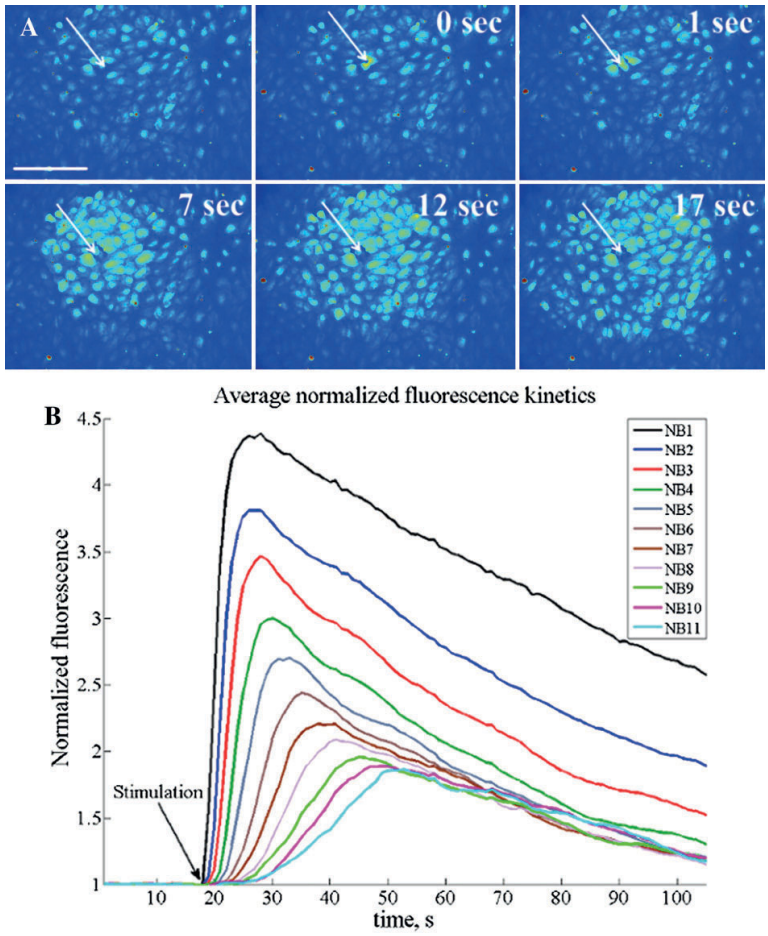

Fig. 3. Ca^{2+} wave propagation in ARPE-19 cell layers. A – pseudocolored fluorescence images of ARPE-19 monolayer at different time points after mechanical stimulation. The color represents fluorescence changes in fura-2 induced by $[Ca^{2+}]_i$ changes. The first image shows the fluorescence intensities before the stimulation. The second image (0 s) shows the moment of stimulation. The stimulated cell is indicated with a white arrow. Scale bar: 100 μm. B – Time course of the mean normalized fluorescence in NB layers 1–11. Black arrow indicates the time of mechanical stimulation.

individual cells, as seen in Fig. 3. The wave spread to 13.7 ± 2.1 cell layers away from the site of mechanical stimulation.

3.3. *The origin of $[Ca^{2+}]_i$ increase*

The increase in intracellular $[Ca^{2+}]_i$ induced by mechanical stimulation may originate from an extracellular Ca^{2+} influx, or Ca^{2+} release from intracellular Ca^{2+} stores, or both. To determine the contribution of extracellular and intracellular Ca^{2+} to transient $[Ca^{2+}]_i$ increases, we performed mechanical stimulation in Ca^{2+}-free medium and after the depletion of intracellular Ca^{2+}-stores with 2 μM thapsigargin (Fig. 4A and B).

Mechanical stimulation in Ca^{2+}-free extracellular medium still induced Ca^{2+} waves. The increases in $[Ca^{2+}]_i$ (represented by maxima of NF values) induced by mechanical stimulation in Ca^{2+}-free and control conditions are shown as line graphs in Fig. 4A. Mechanical stimulation in Ca^{2+}-free HBSS resulted in decreased peak NF values in the cells in NB layers 1–3 compared to control cells. The peak NF values, which occurred due to stimulation in Ca^{2+}-free conditions, in cells located farther than NB layer 5 were higher than in controls. The overlap of the two curves representing peak NF values for the cells in control and Ca^{2+}-free conditions is shown in Fig. 4A.

The rate of the cells that responded to mechanical stimulation is represented as a graph, where each point corresponds to the % RC in a certain NB layer (Fig. 4B). In the absence of extracellular Ca^{2+}, the waves typically spread to the same distance as in the control condition. In rare cases, $[Ca^{2+}]_i$ transients could be observed in up to 17 cell layers away from the site of mechanical stimulation, which is approximately three NB layers farther than that in controls.

The depletion of intracellular Ca^{2+} stores with thapsigargin, which inhibits Ca^{2+}-ATPase in the endoplasmic reticulum (Thastrup et al., 1990), resulted in dramatically reduced Ca^{2+} waves. Following 10 min Ca^{2+} depletion, the distance to which the Ca^{2+} wave propagated was decreased to NB layers 2–4. The peak NF values (Fig. 4A) and the %RC were significantly reduced in these NB cell layers (Fig. 4B).

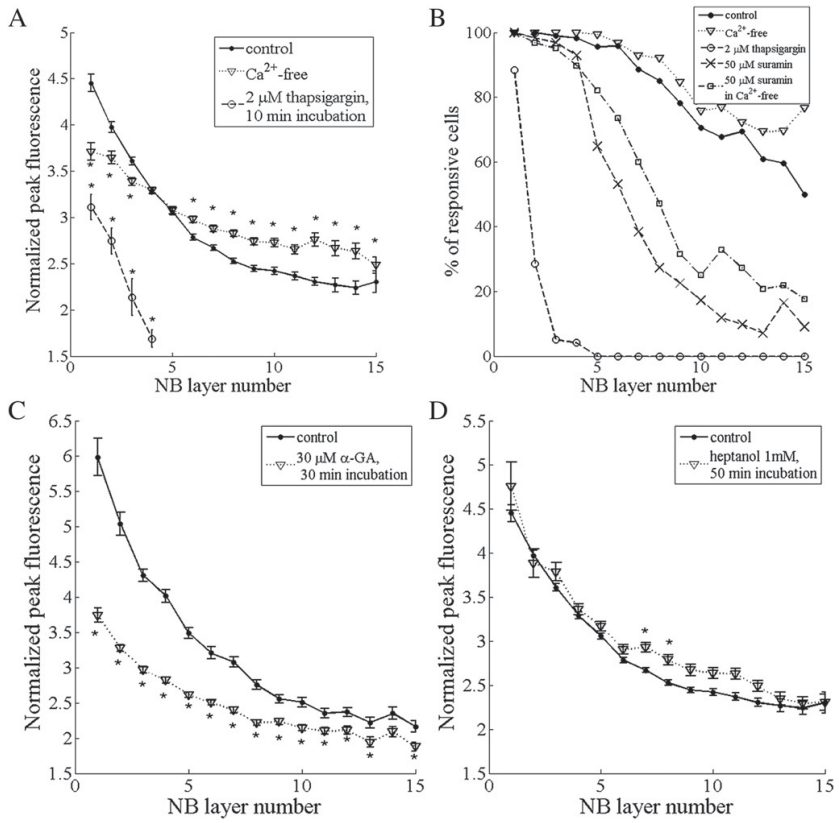

Fig. 4. Alterations of the Ca^{2+} wave spread in the absence of extracellular Ca^{2+}, after the depletion of intracellular Ca^{2+} stores, and in the presence of GJ and P2-receptor blockers. A – Mean normalized fluorescence (NF) peak values in control (n_{1-12} = 113–364, n_{13-15} = 22–48) and Ca^{2+}-free conditions ($n_{1,2,12-15}$ = 23–75, n_{3-11} = 113–184) for NB layers 1–15 and after the depletion of intracellular Ca^{2+} stores with 2 μM thapsigargin ($n_{1,2}$ = 28–59, $n_{3,4}$ = 2–6). B – Percentage of responsive cells in NB layers 1–15 in control, Ca^{2+}-free conditions, after the depletion of intracellular Ca^{2+} stores with 2 μM thapsigargin and after P2-receptor blockade with 50 μM suramin in absence and presence of extracellular Ca^{2+}. C – Mean NF peak values induced by stimulation in control conditions ($n_{1-3,13-15}$ = 12–43, n_{4-12} = 42–72) and after incubation with 30 μM α-GA ($n_{1-3,10-15}$ = 17–91, n_{4-9} = 107–143) for 30 min for NB layers 1–15. D – Mean NF peak values induced by stimulation in control conditions (n_{1-12} = 113–364, n_{13-15} = 22–48) and after incubation with 1 mM 1-heptanol ($n_{1-3,13-15}$ = 10–36, n_{4-11} = 48–74) for 50 min for NB layers 1–15. *statistically significant difference.

3.4. The route of Ca^{2+} wave propagation

Because Ca^{2+} waves can propagate either extracellularly via media or from cell to cell via GJ, we examined whether we could detect the most common component of GJ, connexin 43 (Cx43) in these cells. Expression of Cx43 was confirmed by immunofluorescence labeling, which showed an array on the edges of ARPE-19 cells (Fig. 2). The functionality of GJ was defined with dye scrape/loading assay (Fig. 5A).

To examine the involvement of GJ in the propagation of Ca^{2+} waves, we incubated ARPE-19 cells with the GJ inhibitors 18-α-glycyrrhetinic acid (18-α-GA), quinidine, and 1-heptanol prior to the mechanical stimulation.

18-α-GA influences Cx43 and disrupts GJ communications between cells (Guo et al., 1999). Our preliminary experiments with scrape loading/dye transfer assays indicated an effective inhibition of GJ by 18-α-GA as shown in Fig. 5B. Thus, we used it to block GJ in live Ca^{2+} imaging experiments. 18-α-GA reduced peak NF values in all NB cell layers (Fig. 4C). The effect was most prominent at NB layers 1–8, where the peak NF values were reduced by 20–37%. Beyond NB layer 8, the effect was less prominent. 18-α-GA did not reduce the distance of Ca^{2+} wave spreading or the %RC (data not shown).

1-Heptanol, which is a non-specific GJ blocker (Spray et al., 2002), did not affect the Ca^{2+} wave propagation and did not have a major effect on peak NF values (Fig. 4D), the %RC, or the distance of Ca^{2+} wave propagation (data not shown).

Quinidine has not been shown to interfere with Cx43 hemichannels, however, it is considered as a potential gap junction blocker. Moreover, quinidine has substantial non-specific effects on variety of cascades that might affect Ca^{2+} wave propagation (Juszczak and Swiergiel, 2009). In our experiments, the application of quinidine resulted in a complete inhibition of Ca^{2+} waves. The effect of quinidine was reversible, and the waves were restored after quinidine had been washed out.

To estimate a possible contribution of extracellular factors to Ca^{2+} waves propagation we assessed the spreading of Ca^{2+} waves in non-interconnected, i.e., subconfluent, cell clusters consisting of 3–10 cells. When a single cell within a cell cluster was exposed to mechanical stimulation, the Ca^{2+} wave spread to all the cells in the cluster. The clusters were typically small and contained no more than 3 to 6 NB layers (Fig. 6A). After a short time lag, an increase in the fluorescence occurred in some of the cells that were not physically connected to the group containing the MS cell. The speed of Ca^{2+} wave propagation was 4.2 ± 0.2 μm/s. The %RC in

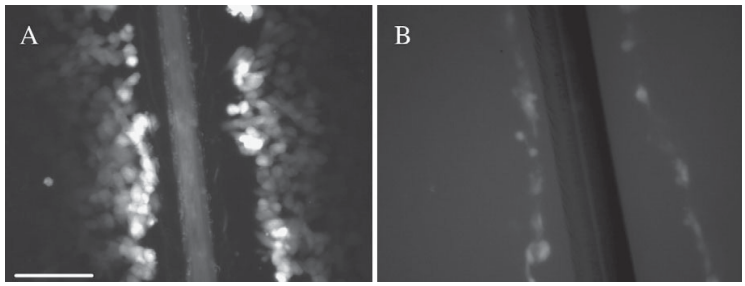

Fig. 5. Scrape loading/dye transfer assay with hydrazide. Cell-free lane is the line scraped with a surgical scalpel. A – control, B – after treatment with 30 μM 18-α-GA for 30 min. Scale bar: 100 μm.

disconnected cell clusters was significantly lower than that in confluent cells. The %RC at different distances from the MS cells in subconfluent and confluent layers is shown in Fig. 6B.

To examine the involvement of P2-receptors in Ca^{2+} wave propagation, we preincubated the cells with suramin, which has been reported to block P2-receptors (Dunn and Blakeley, 1988; Frame and de Feijter, 1997) prior to mechanical stimulation. Suramin treatment dramatically reduced %RC beyond NB layer 4 (Fig. 4B). Suramin did not affect NF values in responsive cells (data not shown).

To determine the contribution of P2Y receptors to Ca^{2+} wave propagation, we preincubated the cells with suramin in Ca^{2+}-free extracellular medium. Suramin caused a marked reduction of %RC beyond NB layer 4 under Ca^{2+}-free extracellular conditions (Fig. 4B).

The involvement of P2X receptors in Ca^{2+} wave propagation was studied with thapsigargin and suramin treatment before mechanical stimulation. This treatment did not have an effect on %RC compared to thapsigargin treatment alone (data not shown).

3.5. Cell viability

Microscopic observations revealed that treatment with 18-α-GA, 1-heptanol, quinidine, suramin and thapsigargin did not have an effect on ARPE-19 cell viability (Fig. 7).

4. Discussion

The RPE cells are essential in maintaining viability of photoreceptors (Bok, 1993; Steinberg, 1985; Strauss, 2005; Wimmers et al., 2007). Many of RPE functions are regulated by changes in intracellular free Ca^{2+}, for example, increases in intracellular free Ca^{2+} regulate water and ion transport (Joseph and Miller, 1992), phagocytic activities of RPE (Nguyen-Legros and Hicks, 2000), dark and light adaptation of photoreceptors cells (Lavallee et al., 2003) and secretion of growth factors (Barg, 2003).

Intracellular Ca^{2+} signals can spread to adjacent cells in a wave-like manner, thereby constituting an intercellular signal that can synchronize an otherwise uncoordinated response (Rottingen and Iversen, 2000). Thus, the characteristics of Ca^{2+} waves, such as speed, distance, and dynamics of propagation, provide important information about cell and tissue level functions.

Mechanically induced Ca^{2+} waves have been assessed in several cell types: epithelial cells (Churchill et al., 1996; Frame and de Feijter, 1997; Stalmans and Himpens, 1998), endothelial cells (D'hondt et al., 2007, Gomes et al., 2005; Moerenhout et al., 2001), articular chondrocytes (D'Andrea and Vittur, 1996), and osteosarcoma cells (Gomez et al., 2001). In human RPE cells, however, this has not been studied.

In most of previous papers, mechanical stimulation was performed by touching the cellular membrane without visible membrane damage (D'hondt et al., 2007, Frame and de Feijter, 1997; Gomes et al., 2005; Moerenhout et al., 2001; Stalmans and Himpens, 1998). We induced mechanical stimulation by making a small perforation in a single cell, so that stimulation could be visibly detected, the strength of the stimulus would be easier to control and we would know that equal stimuli were applied in all of our experiments.

Mechanically induced Ca^{2+} waves spread typically no further than 8 tiers: 4.2 ± 0.1 cell tiers for ovine lens epithelium (Churchill

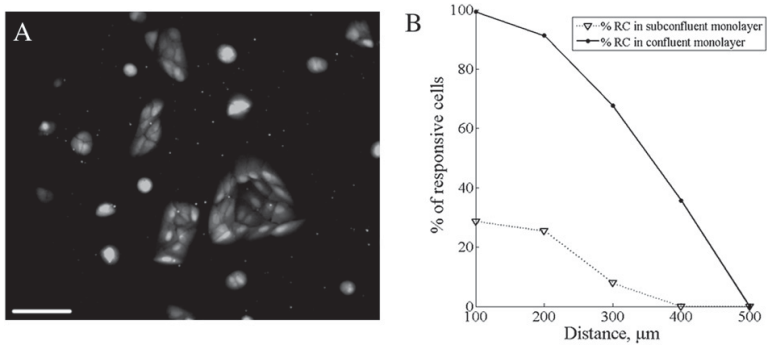

Fig. 6. Ca^{2+} wave spreading in disconnected cell clusters. A – a representative fluorescent image of subconfluent cells loaded with fura-2 dye. Scale bar: 100 μm. B – Percentage of responsive cells during Ca^{2+} wave propagation in subconfluent and confluent ARPE-19 cell layers at different distances from mechanically stimulated cell.

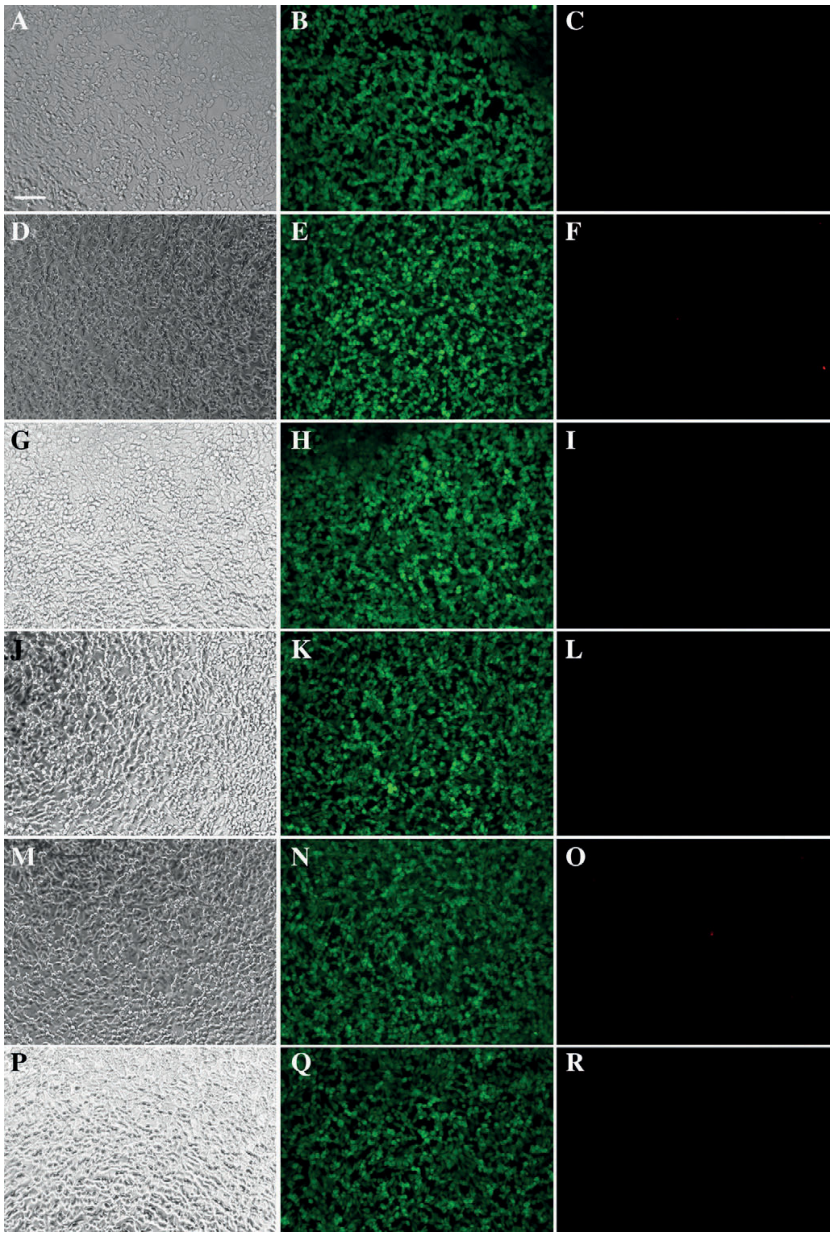

Fig. 7. Cell viability test performed after the following treatments: A–C – control; D–F – 30 μM glycyrrhetinic acid, 30 min incubation; G–I – 1 mM heptanol, 50 min incubation; J–L – 30 μM quinidine, 10 min incubation; M–O – 50 μM suramin, 25 min incubation; P–R – 2 μM thapsigargin, 10 min incubation. Representative images of the ARPE-19 cells taken with phase contrast microscopy (A, D, G, J, M, P), viable cells loaded with calcein-AM (B, E, H, K, N, Q) and dead cells loaded with ethidium bromide (C, F, I, L, O, R) taken with fluorescence microscopy. Scale bar: 100 μm.

et al., 1996), 4–6 cell tiers in corneal endothelial cells (D'hondt et al., 2007, Gomes et al., 2005), 2–3 cell tiers in Long-Evans rats RPE LE-RPE (Himpens et al., 1999), 2 cell tiers in immortalized rat RPE RPE-J cell line (Gomes et al., 2003) and 4–8 cell tires in rat liver epithelial cells (Frame and de Feijter, 1997). In our experiments, Ca^{2+} waves spread to up to 13.7 ± 2.1 cell layers, which is significantly farther compared to previously obtained data. Such a long wave spread distance can probably be attributed to the intrinsic properties of ARPE-19 cells, e.g., the high number of gap junctions observed by immunofluorescence labeling. This result is not likely to be associated with the membrane perforation that occurred after mechanical stimulation, because when we applied

mechanical stimulation without membrane perforation, the results were not appreciably different from those described above (data not shown).

In this study, the kinetics of normalized fluorescence, reflecting the Ca^{2+} kinetics, at different cell layers were different. Specifically, the rate of the increase in Ca^{2+} was dissimilar in various neighboring cell layers: the farther the neighboring cell layer from the site of mechanical stimulation, the slower the rate of the Ca^{2+} increase. This can be interpreted as that the cell receives more mixed stimulation farther away from the place of induction. This mixed stimulation occurs because the Ca^{2+} waves do not spread equally in different directions, thus the surrounding cells are not stimulated simultaneously. Moreover, even though the stimulus spread looks like a wave, the cells do not respond equally to the stimulation, which also contributes to the diversified stimulation from the surrounding cells.

To determine the contribution of extracellular Ca^{2+} to the increase in the intracellular Ca^{2+} concentration, we induced the wave in the absence of extracellular Ca^{2+}. Previous results on stimulation in Ca^{2+}-free conditions are controversial: it has been reported that the absence of extracellular Ca^{2+} was not required for Ca^{2+} wave propagation in ovine lens epithelial cells (Churchill et al., 1996) and calf pulmonary artery endothelium (Moerenhout et al., 2001), but in studies with LE- and RCS-rat RPE (Himpens et al., 1999; Stalmans and Himpens, 1998) and rat osteosarcoma cells (Gomez et al., 2001; Himpens et al., 1999; Moerenhout et al., 2001; Stalmans and Himpens, 1998), the absence of extracellular Ca^{2+} completely abolished Ca^{2+} waves. In our experiments, when mechanical stimulation was applied to the cells in Ca^{2+}-free extracellular medium, the Ca^{2+} wave still occurred. However, the increase in the intracellular Ca^{2+} concentration in the first three neighboring cell layers was slightly lower than in the controls. Thus, in the cells close to the mechanically stimulated cell, extracellular Ca^{2+} contributes to the increase in the intracellular Ca^{2+} concentration.

To assess the role of intracellular Ca^{2+} stores in Ca^{2+} wave propagation we depleted them with thapsigargin (Thastrup et al., 1990). Earlier it was reported that the depletion of intracellular Ca^{2+} stores leads to complete or partial inhibition of Ca^{2+} waves in LE- and RCS-rat RPE (Stalmans and Himpens, 1998), ovine lens epithelial (Churchill et al., 1996), calf pulmonary artery endothelial (Moerenhout et al., 2001), and rat osteosarcoma cells (Gomez et al., 2001). In our ARPE-19 cells, the depletion of intracellular Ca^{2+} stores led to complete inhibition of the wave after the fourth neighboring cell layer. Thus, the propagation of the Ca^{2+} wave farther than the fourth neighboring cell layer is strongly dependent on intracellular Ca^{2+} stores. A small increase in the intracellular Ca^{2+} concentration still occurred in some cells from the first four neighboring cell layers. The occurrence of a faint Ca^{2+} wave in the first four neighboring cell layers indicates that these cells may use Ca^{2+} from the extracellular medium, which can also be deduced from the results of the experiments in Ca^{2+}-free solution, in addition to Ca^{2+} from intracellular Ca^{2+} stores. These experiments show the differences in the Ca^{2+} wave propagation mechanism in cells located close to the site of mechanical stimulation and in distant cells.

The diffusion of signaling molecules is thought to occur either through extracellular medium or via gap junctions (Rottingen and Iversen, 2000). However, the molecules and mechanisms involved are not fully elucidated.

In many cell types, Ca^{2+} waves spread via gap junctions (Boitano et al., 1992; Churchill et al., 1996; D'Andrea and Vittur, 1996; Gomes et al., 2006; Himpens et al., 1999; Sanderson et al., 1990). The presence of gap junctions has been demonstrated in ARPE-19 cells in Hutnik et al. (2008). We also confirmed the presence of abundant gap junctions in ARPE-19 monolayers with immunofluorescence staining, as well as their functionality with scrape loading/dye transfer assay. To assess the possible contribution of gap junctions to the Ca^{2+} wave propagation, we used the gap junction blockers α-glycyrrhetinic acid, 1-heptanol, and quinidine.

α-Glycyrrhetinic acid is known to affect Cx43 integrity, which leads to uncoupling of gap junctions (Guo et al., 1999). In cultured articular chondrocytes, α-glycyrrhetinic acid completely blocks Ca^{2+} waves (D'Andrea and Vittur, 1996), and in corneal endothelial cells reduces the percentage of responsive cells (Gomes et al., 2006). It also blocks gap junctions in RPE cells (Kojima et al., 2008), and ARPE-19 cell line (Hutnik et al., 2008). We also confirmed that α-glycyrrhetinic acid blocks gap junctions in ARPE-19 cells. In our experiments, α-glycyrrhetinic acid reduced the $[Ca^{2+}]_i$ increase, but did not influence the distance of Ca^{2+} wave propagation. The effect of α-glycyrrhetinic acid was most prominent in the cells located close to the mechanically stimulated cell, indicating the importance of gap junctions in Ca^{2+} wave propagation in these cells. An incomplete inhibition of Ca^{2+} waves may be explained by only partial blockade of the gap junctions or by the effect of extracellular signaling molecules passing through the medium.

1-Heptanol has been reported as an unspecific gap junction blocker (Spray et al., 2002) and shown to reduce the percentage of responsive cells after mechanical stimulation in osteosarcoma cells (Gomez et al., 2001), corneal endothelium cells (Gomes et al., 2006; Moerenhout et al., 2001) and thymic nurse epithelial cells (Nihei et al., 2003). In our experiments, heptanol had only minor effects on Ca^{2+} wave propagation in ARPE-19 cells at a distance of neighboring cell layers 7 and 8, which can probably be attributed to cells daily variations.

Quinidine is commonly used as a gap junction blocker, however, little is known about its mechanism of action on gap junctions (Juszczak and Swiergiel, 2009). It has not been shown to interfere with Cx43 hemichannels. Moreover, quinidine is known to have vast non-specific effects on cells, such as inhibition of IP3 binding (Juszczak and Swiergiel, 2009) and even blockade of P2-receptors (Burnstock and Knight, 1978), thus, it was of interest to test the effect of quinidine on Ca^{2+} wave propagation. Quinidine fully blocked Ca^{2+} waves in our experiments with ARPE-19 cells. This may be a result of a non-specific quinidine action on IP3 binding, P2-receptors, as well as gap junctions.

The specific Cx43 blocker (α-glycyrrhetinic acid) partially inhibited Ca^{2+} wave propagation in ARPE-19, and quinidine completely blocked Ca^{2+} wave propagation. However, non-specific gap junction blocker 1-heptanol did not have an effect on Ca^{2+} wave propagation.

To determine the propagation of the signal through the extracellular medium, we performed mechanical stimulation on subconfluent, i.e., disconnected, ARPE-19 cell clusters. In disconnected rat liver epithelial cells (Frame and de Feijter, 1997) and corneal endothelial cells (Gomes et al., 2005), Ca^{2+} waves have been shown to spread in the same manner as in confluent cell layers, demonstrating that the waves can be triggered by extracellular stimulation factors. In our studies, mechanical stimulation induced a regular Ca^{2+} wave in the cells that were connected to the mechanically stimulated cell. In some cases, we observed stimulation of cells that were disconnected from the mechanically stimulated cell. However, the percentage of responsive cells never exceeded 30%, even if the disconnected cells were very close to the mechanically stimulated cell. Our results suggest that a factor passing through extracellular medium is involved in Ca^{2+} wave propagation, but, acting alone, it cannot induce a full scale Ca^{2+} wave in ARPE-19 cells. This result is different from previously reported findings in other cell types (Frame and de Feijter, 1997; Gomes et al., 2005).

To assess the involvement of purines (ATP, UTP) in the extracellular pathway of Ca^{2+} wave propagation, we studied the effect of

the P2-receptor blocker suramin. In mammary (Enomoto et al., 1994; Frame and de Feijter, 1997; Gomes et al., 2005; Moerenhout et al., 2001) and liver epithelial cells (Enomoto et al., 1994; Frame and de Feijter, 1997; Gomes et al., 2005; Moerenhout et al., 2001) and corneal endothelial cells (Enomoto et al., 1994; Frame and de Feijter, 1997; Gomes et al., 2005; Moerenhout et al., 2001), suramin has been shown to either completely abolish or significantly reduce Ca^{2+} wave spread. However, in airway epithelial cells, it did not influence the wave propagation (Hansen et al., 1993). In our studies, suramin dramatically reduced the percentage of the responsive cells beyond the fourth neighboring cell layer, but it did not have any effect on normalized fluorescence values in the responsive cells. This result indicates that purines play an important role in Ca^{2+} wave propagation beyond the forth neighboring cell layer.

The P2-receptors involved in Ca^{2+} wave propagation could be either P2Y, a G-protein coupled receptor, or P2X receptor, a ligand-gated ion channel (Ralevic and Burnstock, 1998). When we estimated the role of P2Y receptors by suramin application in the absence of extracellular Ca^{2+} the percentage of responsive cells located farther than the fourth neighboring cell layer was radically decreased compared to that in Ca^{2+}-free conditions. This indicates the involvement of P2Y receptors in Ca^{2+} wave propagation beyond neighboring cell layer four. Then when the contribution of P2X receptors to Ca^{2+} wave propagation was studied by the pre-treatment of cells with both suramin and thapsigargin, we saw no effect on %RC compared to thapsigargin treatment alone. These results demonstrated that P2X receptors are not likely to contribute to Ca^{2+} wave propagation between neighboring cell layers from one to four. Overall, our experiments with the blockade of P2-receptors indicate that P2Y receptors are important in Ca^{2+} wave propagation in distant cells, however, there are other strong mechanisms of Ca^{2+} wave propagation in the proximity of the site of mechanical stimulation as previously discussed. This result correlates with our findings on a α-glycyrrhetinic acid effect, which showed Ca^{2+} wave propagation to be highly dependent on gap junctions in the cells close to the site of mechanical stimulation. In addition, incomplete inhibition of the wave spread farther than the fourth neighboring cell layer after suramin application may indicate the rudimental propagation of the wave through gap junctions. This would also explain the higher normalized fluorescence peak values under Ca^{2+}-free conditions compared to control and slightly higher percentage of responsive cells after suramin treatment in Ca^{2+}-free conditions compared to suramin treatment in presence of Ca^{2+}, as low extracellular Ca^{2+} is known to increase Cx43 hemichannels permeability (Barbe et al., 2006).

Based on our results we can conclude that ARPE-19 cells exhibit a different mechanism of Ca^{2+} wave propagation in cells that are located close to the site of mechanical stimulation compared to distant cells. We can deduce that the Ca^{2+} wave propagates mainly through gap junctions in the cells close to the site of mechanical stimulation and requires Ca^{2+} from both intracellular Ca^{2+} stores and extracellular media, while in the distant cells the propagation is more dependent on purinergic receptors and does not require extracellular Ca^{2+}. The cells close to a mechanically stimulated cell may sense mechanical stretch, caused by a displacement of the stimulated cell in the moment of stimulation. Thus, these cells may sense membrane stretching and together with the Ca^{2+}-inducing signals from stimulated and neighboring cells the response is different from that of the distant cells.

5. Conclusions

Our results demonstrated the existence of repeatable and robust intercellular Ca^{2+} waves in human ARPE-19 cells induced by mechanical stimulation. Ca^{2+} kinetics in ARPE-19 cells are highly dependent on intracellular Ca^{2+} stores. We showed that the signaling molecules that mediate Ca^{2+} waves diffuse both via extracellular medium and intercellular gap junction channels. Gap junctions have the most prominent effect on the Ca^{2+} wave spreading in the cells close to the site of mechanical stimulation, while P2Y receptors are responsible for the wave propagation in distant cells.

Our experiments indicated good reproducibility of the Ca^{2+} wave after mechanical stimulation and we were able to describe intercellular communication and its changes induced by various drugs quantitatively from the obtained Ca^{2+} wave properties. Thus, the proposed method of assessing changes in the intercellular communication of Ca^{2+} dynamics could become a potential ARPE-19 cells-based drug-testing assay.

Acknowledgments

We thank Outi Melin, Hanna Koskenaho, Elina Konsén, Juha Heikkilä for their technical assistance. This study was financially supported by the Doctoral Programme of the President of the Tampere University of Technology and the Academy of Finland (grant numbers 252225, 218050 and 137801). Part of the data was presented at ARVO 2012 meeting, Fort Lauderdale, USA. Authors declare no conflict-of-interest or financial disclosures.

References

Abe, T., Sugano, E., Saigo, Y., Tamai, M., 2003. Interleukin-1β and barrier function of retinal pigment epithelial cells (ARPE-19): aberrant expression of junctional complex molecules. Investigative Ophthalmology & Visual Science 44, 4097–4104.

Alizadeh, M., Wada, M., Gelfman, C.M., Handa, J.T., Hjelmeland, L.M., 2001. Down-regulation of differentiation specific gene expression by oxidative stress in ARPE-19 cells. Investigative Ophthalmology & Visual Science 42, 2706–2713.

Barbe, M.T., Monyer, H., Bruzzone, R., 2006. Cell-cell communication beyond connexins: the pannexin channels. Physiology 21, 103–114.

Barg, S., 2003. Mechanisms of exocytosis in insulin-secreting B-cells and glucagon-secreting A-cells. Pharmacology and Toxicology 92, 3–13.

Barkmeier, A.J., Carvounis, P.E., 2011. Retinal pigment epithelial tears and the management of exudative age-related macular degeneration. Seminars in Ophthalmology 26, 94–103.

Baurand, A., Gachet, C., 2003. The P2Y1 receptor as a target for new antithrombotic drugs: a review of the P2Y1 antagonist MRS-2179. Cardiovascular Drug Reviews 21, 67–76.

Black, B., Smith, J., 1989. Regulation of goblet cell differentiation by calcium in embryonic chick intestine. The FASEB Journal 3, 2653–2659.

Boitano, S., Dirksen, E.R., Sanderson, M.J., 1992. Intercellular propagation of calcium waves mediated by inositol trisphosphate. Science 258, 292–295.

Bok, D., 1993. The retinal pigment epithelium: a versatile partner in vision. Journal of Cell Science Supplement 17, 189–195.

Boulton, M., Dayhaw-Barker, P., 2001. The role of the retinal pigment epithelium: topographical variation and ageing changes. Eye 15, 384–389.

Brini, M., Carafoli, E., 2009. Calcium pumps in health and disease. Physiological Reviews 89, 1341–1378.

Burnstock, G., Knight, G.E., 1978. Cellular distribution and functions of P2 receptor subtypes in different systems. In: Anonymous International Review of Cytology. Academic Press, pp. 31–304.

Charles, A.C., Kodali, S.K., Tyndale, R.F., 1996. Intercellular calcium waves in neurons. Molecular and Cellular Neuroscience 7, 337–353.

Charles, A.C., Merrill, J.E., Dirksen, E.R., Sanderson, M.J., 1991. Intercellular signaling in glial cells: calcium waves and oscillations in response to mechanical stimulation and glutamate. Neuron 6, 983–992.

Churchill, G.C., Atkinson, M.M., Louis, C.F., 1996. Mechanical stimulation initiates cell-to-cell calcium signaling in ovine lens epithelial cells. Journal of Cell Science 109, 355–365.

Cotrina, M.L., Lin, J.H.C., Alves-Rodrigues, A., Liu, S., Li, J., Azmi-Ghadimi, H., Kang, J., Naus, C.C.G., Nedergaard, M., 1998. Connexins regulate calcium signaling by controlling ATP release. Proceedings of the National Academy of Sciences 95, 15735–15740.

D'hondt, C., Ponsaerts, R., Srinivas, S.P., Vereecke, J., Himpens, B., 2007. Thrombin inhibits intercellular calcium wave propagation in corneal endothelial cells by modulation of hemichannels and gap junctions. Investigative Ophthalmology & Visual Science 48, 120–133.

D'Andrea, P., Vittur, F., 1996. Gap junctions mediate intercellular calcium signalling in cultured articular chondrocytes. Cell Calcium 20, 389–397.

Dunn, K.C., Marmorstein, A.D., Bonilha, V.L., Rodriguez-Boulan, E., Giordano, F., Hjelmeland, L.M., 1998. Use of the ARPE-19 cell line as a model of RPE polarity: basolateral secretion of FGF5. Investigative Ophthalmology & Visual Science 39, 2744–2749.

Dunn, P.M., Blakeley, A.G., 1988. Suramin: a reversible P2-purinoceptor antagonist in the mouse vas deferens. British Journal of Pharmacology 93, 243–245.

El-Fouly, M.H., Trosko, J.E., Chang, C., 1987. Scrape-loading and dye transfer: a rapid and simple technique to study gap junctional intercellular communication. Experimental Cell Research 168, 422–430.

Enomoto, K., Furuya, K., Yamagishi, S., Oka, T., Maeno, T., 1994. The increase in the intracellular Ca^{2+} concentration induced by mechanical stimulation is propagated via release of pyrophosphorylated nucleotides in mammary epithelial cells. Pflügers Archiv European Journal of Physiology 427, 533–542.

Evans, W.H., Martin, P.E.M., 2002. Gap junctions: structure and function (Review). Molecular Membrane Biology 19, 121–136.

Fain, G.L., Matthews, H.R., Cornwall, M.C., Koutalos, Y., 2001. Adaptation in vertebrate photoreceptors. Physiological Reviews 81, 117–151.

Frame, M.K., de Feijter, A.W., 1997. Propagation of mechanically induced intercellular calcium waves via gap junctions and ATP receptors in rat liver epithelial cells. Experimental Cell Research 230, 197–207.

Giepmans, B.N.G., Feiken, E., Gebbink, M.F.B.G., Moolenaar, W.H., 2003. Association of connexin43 with a receptor protein tyrosine phosphatase. Cell Communication and Adhesion 10, 201–205.

Gomes, P., Malfait, M., Himpens, B., Vereecke, J., 2003. Intercellular Ca^{2+}-transient propagation in normal and high glucose solutions in rat retinal epithelial (RPE-J) cells during mechanical stimulation. Cell Calcium 34, 185–192.

Gomes, P., Srinivas, S.P., Vereecke, J., Himpens, B., 2005. ATP-dependent paracrine intercellular communication in cultured bovine corneal endothelial cells. Investigative Ophthalmology & Visual Science 46, 104–113.

Gomes, P., Srinivas, S.P., Vereecke, J., Himpens, B., 2006. Gap junctional intercellular communication in bovine corneal endothelial cells. Experimental Eye Research 83, 1225–1237.

Gomez, P., Vereecke, J., Himpens, B., 2001. Intra- and intercellular Ca^{2+}-transient propagation in normal and high glucose solutions in ROS cells during mechanical stimulation. Cell Calcium 29, 137–148.

Goodenough, D.A., Goliger, J.A., Paul, D.L., 1996. Connexins, connexons, and intercellular communication. Annual Review of Biochemistry 65, 475–502.

Guo, Y., Martinez-Williams, C., Gilbert, K.A., Rannels, D.E., 1999. Inhibition of gap junction communication in alveolar epithelial cells by 18α-glycyrrhetinic acid. American Journal of Physiology – Lung Cellular and Molecular Physiology 276, L1018–L1026.

Hansen, M., Boitano, S., Dirksen, E.R., Sanderson, M.J., 1993. Intercellular calcium signaling induced by extracellular adenosine 5′-triphosphate and mechanical stimulation in airway epithelial cells. Journal of Cell Science 106, 995–1004.

Himpens, B., Stalmans, P., Gomez, P., Malfait, M., Vereecke, J., 1999. Intra- and intercellular Ca^{2+} signaling in retinal pigment epithelial cells during mechanical stimulation. The FASEB Journal 13 (Suppl.), S63–S68.

Hutnik, C.M.L., Pocrnich, C.E., Liu, H., Laird, D.W., Shao, Q., 2008. The protective effect of functional connexin43 channels on a human epithelial cell line exposed to oxidative stress. Investigative Ophthalmology & Visual Science 49, 800–806.

Jorgensen, N.R., Geist, S.T., Civitelli, R., Steinberg, T.H., 1997. ATP- and gap junction-dependent intercellular calcium signaling in osteoblastic cells. The Journal of Cell Biology 139, 497–506.

Joseph, D.P., Miller, S.S., 1992. Alpha-1-adrenergic modulation of K and Cl transport in bovine retinal pigment epithelium. The Journal of General Physiology 99, 263–290.

Juszczak, G.R., Swiergiel, A.H., 2009. Properties of gap junction blockers and their behavioural, cognitive and electrophysiological effects: animal and human studies. Progress in Neuro-Psychopharmacology and Biological Psychiatry 33, 181–198.

Klepeis, V.E., Weinger, I., Kaczmarek, E., Trinkaus-Randall, V., 2004. P2Y receptors play a critical role in epithelial cell communication and migration. Journal of Cellular Biochemistry 93, 1115–1133.

Kojima, A., Nakahama, K., Ohno-Matsui, K., Shimada, N., Mori, K., Iseki, S., Sato, T., Mochizuki, M., Morita, I., 2008. Connexin 43 contributes to differentiation of retinal pigment epithelial cells via cyclic AMP signaling. Biochemical and Biophysical Research Communication 366, 532–538.

Lavallee, C.R., Chalifoux, J.R., Moosally, A.J., Balkema, G.W., 2003. Elevated free calcium levels in the subretinal space elevate the absolute dark-adapted threshold in hypopigmented mice. Journal of Neurophysiology 90, 3654–3662.

Luthra, S., Narayanan, R., Marques, E.A., Chwa, M., Kim, D.W., Dong, J., Seigel, G.M., Neekhra, A., Gramajo, A.L., Brown, D.J., Kenney, M.C., Kuppermann, B.D., 2006. Evaluation of in vitro effects of Bevacizumab (Avastin) on retinal pigment epithelial, neurosensory retinal, and microvascular endothelial cells. Retina 26.

Majumdar, S., Macha, S., Pal, D., Mitra, A., 2004. Mechanism of ganciclovir uptake by rabbit retina and human retinal pigmented epithelium cell line ARPE-19. Current Eye Research 29, 127–136.

Mattson, M.P., Chan, S.L., 2003. Calcium orchestrates apoptosis. Nature Cell Biology 5, 1041–1043.

Mese, G., Richard, G., White, T.W., 2006. Gap junctions: basic structure and function. The Journal of Investigative Dermatology 127, 2516–2524.

Milbury, P.E., Graf, B., Curran-Celentano, J.M., Blumberg, J.B., 2007. Bilberry (*Vaccinium myrtillus*) anthocyanins modulate heme oxygenase-1 and glutathione S-transferase-pi expression in ARPE-19 cells. Investigative Ophthalmology & Visual Science 48, 2343–2349.

Moerenhout, M., Himpens, B., Vereecke, J., 2001. Intercellular communication upon mechanical stimulation of CPAE-endothelial cells is mediated by nucleotides. Cell Calcium 29, 125–136.

Narayan, S., Prasanna, G., Krishnamoorthy, R.R., Zhang, X., Yorio, T., 2003. Endothelin-1 synthesis and secretion in human retinal pigment epithelial cells (ARPE-19): differential regulation by cholinergics and TNF-α. Investigative Ophthalmology & Visual Science 44, 4885–4894.

Nezu, A., Tanimura, A., Morita, T., Tojyo, Y., 2010. Visualization of Ins(1,4,5)P3 dynamics in living cells: two distinct pathways for Ins(1,4,5)P3 generation following mechanical stimulation of HSY-EA1 cells. Journal of Cell Science 123, 2292–2298.

Nguyen-Legros, J., Hicks, D., 2000. Renewal of Photoreceptor Outer Segments and their Phagocytosis by the Retinal Pigment Epithelium. International Review of Cytology. Academic Press, pp. 245–313.

Nihei, O.K., Campos de Carvalho, A.C., Spray, D.C., Savino, W., Alves, L.A., 2003. A novel form of cellular communication among thymic epithelial cells: intercellular calcium wave propagation. American Journal of Physiology – Cell Physiology 285, C1304–C1313.

Overington, J.P., Al-Lazikani, B., Hopkins, A.L., 2006. How many drug targets are there? Nature Reviews Drug Discovery 5, 993–996.

Ralevic, V., Burnstock, G., 1998. Receptors for purines and pyrimidines. Pharmacological Reviews 50, 413–492.

Rottingen, J., Iversen, J., 2000. Ruled by waves? Intracellular and intercellular calcium signalling. Acta Physiologica Scandinavica 169, 203–219.

Sáez, J.C., Berthoud, V.M., Brañes, M.C., Martínez, A.d., Beyer, E.C., 2003. Plasma membrane channels formed by connexins: their regulation and functions. Physiological Reviews 83, 1359–1400.

Sanderson, M.J., Charles, A.C., Dirksen, E.R., 1990. Mechanical stimulation and intercellular communication increases intracellular Ca^{2+} in epithelial cells. Cell Regulation 1, 585–596.

Sanderson, M.J., Charles, A.C., Boitano, S., Dirksen, E.R., 1994. Mechanisms and function of intercellular calcium signaling. Molecular and Cellular Endocrinology 98, 173–187.

Schlosser, S.F., Burgstahler, A.D., Nathanson, M.H., 1996. Isolated rat hepatocytes can signal to other hepatocytes and bile duct cells by release of nucleotides. Proceedings of the National Academy of Sciences 93, 9948–9953.

Seko, Y., Seko, Y., Fujikura, H., Pang, J., Tokoro, T., Shimokawa, H., 1999. Induction of vascular endothelial growth factor after application of mechanical stress to retinal pigment epithelium of the rat in vitro. Investigative Ophthalmology & Visual Science 40, 3287–3291.

Slomiany, M.G., Rosenzweig, S.A., 2004. Autocrine effects of IGF-I-induced VEGF and IGFBP-3 secretion in retinal pigment epithelial cell line ARPE-19. American Journal of Physiology – Cell Physiology 287, C746–C753.

Spray, D.C., Rozental, R., Srinivas, M., 2002. Prospects for rational development of pharmacological gap junction channel blockers. Current Drug Targets 3, 455–464.

Stalmans, P., Himpens, B., 1998. A decreased Ca^{2+}-wave propagation is found among cultured RPE cells from dystrophic RCS rats. Investigative Ophthalmology & Visual Science 39, 1493–1502.

Steinberg, R.H., 1985. Interactions between the retinal pigment epithelium and the neural retina. Documenta Ophthalmologica 60, 327–346.

Strauss, O., 2005. The retinal pigment epithelium in visual function. Physiological Reviews 85, 845–881.

Thastrup, O., Cullen, P.J., Drøbak, B.K., Hanley, M.R., Dawson, A.P., 1990. Thapsigargin, a tumor promoter, discharges intracellular Ca^{2+} stores by specific inhibition of the endoplasmic reticulum Ca2(+)-ATPase. Proceedings of the National Academy of Sciences 87, 2466–2470.

Vaajasaari, H., Ilmarinen, T., Juuti-Uusitalo, K., Rajala, K., Onnela, N., Narkilahti, S., Suuronen, R., Hyttinen, J., Uusitalo, H., Skottman, H., 2011. Toward the defined and xeno-free differentiation of functional human pluripotent stem cell-derived retinal pigment epithelial cells. Molecular Vision 17, 558–575.

Weber, P.A., Chang, H., Spaeth, K.E., Nitsche, J.M., Nicholson, B.J., 2004. The permeability of gap junction channels to probes of different size is dependent on connexin composition and permeant-pore affinities. Biophysical Journal 87, 958–973.

Wimmers, S., Karl, M.O., Strauss, O., 2007. Ion channels in the RPE. Progress in Retinal and Eye Research 26, 263–301.

Wrona, M., Różanowska, M., Sarna, T., 2004. Zeaxanthin in combination with ascorbic acid or α-tocopherol protects ARPE-19 cells against photosensitized peroxidation of lipids. Free Radical Biology and Medicine 36, 1094–1101.

Xia, S., Ferrier, J., 1992. Propagation of a calcium pulse between osteoblastic cells. Biochemical and Biophysical Research Communications 186, 1212–1219.

PUBLICATION II

Computational Model of Ca^{2+} Wave Propagation in Human Retinal Pigment Epithelial ARPE-19 Cells

Vainio, I., Abu Khamidakh, A., Paci, M., Skottman, H., Juuti-Uusitalo, K., Hyttinen, J. & Nymark, S.

2015, PLoS One, Vol. 10(6), e0128434
https://doi.org/10.1371/journal.pone.0128434

PLOS ONE

RESEARCH ARTICLE

Computational Model of Ca^{2+} Wave Propagation in Human Retinal Pigment Epithelial ARPE-19 Cells

Iina Vainio[1,2]*, Amna Abu Khamidakh[1,2], Michelangelo Paci[1,2], Heli Skottman[3], Kati Juuti-Uusitalo[3], Jari Hyttinen[1,2], Soile Nymark[1,2]

1 Department of Electronics and Communications Engineering, Tampere University of Technology, Tampere, Finland, **2** Institute of Biosciences and Medical Technology, Tampere University of Technology, Tampere, Finland, **3** Institute of Biosciences and Medical Technology, University of Tampere, Tampere, Finland

* iina.vainio@tut.fi

OPEN ACCESS

Citation: Vainio I, Abu Khamidakh A, Paci M, Skottman H, Juuti-Uusitalo K, Hyttinen J, et al. (2015) Computational Model of Ca^{2+} Wave Propagation in Human Retinal Pigment Epithelial ARPE-19 Cells. PLoS ONE 10(6): e0128434. doi:10.1371/journal.pone.0128434

Academic Editor: Zsolt Ablonczy, Medical University of South Carolina, UNITED STATES

Received: October 24, 2014

Accepted: April 27, 2015

Published: June 12, 2015

Data Availability Statement: All relevant data are within the paper.

Funding: This study was financially supported by the Academy of Finland (grant numbers 252225, 260375, 218050 and 137801), TEKES- the finnish funding agency for innovation (Human Spare Part Project), and Doctoral Programme of the President of the Tampere University of Technology. The funders had no role in study design, data collection and analysis, decision to publish, or preparation of the manuscript.

Abstract

Objective

Computational models of calcium (Ca^{2+}) signaling have been constructed for several cell types. There are, however, no such models for retinal pigment epithelium (RPE). Our aim was to construct a Ca^{2+} signaling model for RPE based on our experimental data of mechanically induced Ca^{2+} wave in the *in vitro* model of RPE, the ARPE-19 monolayer.

Methods

We combined six essential Ca^{2+} signaling components into a model: stretch-sensitive Ca^{2+} channels (SSCCs), P_2Y_2 receptors, IP_3 receptors, ryanodine receptors, Ca^{2+} pumps, and gap junctions. The cells in our epithelial model are connected to each other to enable transport of signaling molecules. Parameterization was done by tuning the above model components so that the simulated Ca^{2+} waves reproduced our control experimental data and data where gap junctions were blocked.

Results

Our model was able to explain Ca^{2+} signaling in ARPE-19 cells, and the basic mechanism was found to be as follows: 1) Cells near the stimulus site are likely to conduct Ca^{2+} through plasma membrane SSCCs and gap junctions conduct the Ca^{2+} and IP_3 between cells further away. 2) Most likely the stimulated cell secretes ligand to the extracellular space where the ligand diffusion mediates the Ca^{2+} signal so that the ligand concentration decreases with distance. 3) The phosphorylation of the IP_3 receptor defines the cell's sensitivity to the extracellular ligand attenuating the Ca^{2+} signal in the distance.

Competing Interests: The authors have declared that no competing interests exist.

Conclusions

The developed model was able to simulate an array of experimental data including drug effects. Furthermore, our simulations predict that suramin may interfere ligand binding on P_2Y_2 receptors or accelerate P_2Y_2 receptor phosphorylation, which may partially be the reason for Ca^{2+} wave attenuation by suramin. Being the first RPE Ca^{2+} signaling model created based on experimental data on ARPE-19 cell line, the model offers a platform for further modeling of native RPE functions.

Introduction

Epithelial tissue covers and lines all internal and external body surfaces. These cell layers have multiple functions depending on their location, and many of these functions are controlled by Ca^{2+} activity[1]. Retinal pigment epithelium (RPE), a monolayer of pigmented polarized cells, is crucial for the maintenance of visual functions. Located in the back of the eye between photoreceptors and choriocapillaries, RPE forms a vital part of the blood-retinal barrier (BRB)[2]. The physiology of RPE is tightly coupled with the activity of the various ion channels, such as Ca^{2+} channels that are associated with several important RPE functions including transepithelial transport of ions and water, dark adaption of photoreceptor activity, phagocytosis, secretion, and differentiation[3]. In RPE, as well as in other epithelia, local deformation of the cell membrane initiates a significant Ca^{2+} wave [4–6]. Such deformation of the cell membrane can occur in clinically important pathological conditions such as retinal tear resulting from complications after photodynamic therapy[7], intravitreal bevacizumab injection[8], or intravitreal pegaptanib injection[9]. Intercellular Ca^{2+} signaling is also linked to the initial stages of wound repair: excessive mechanical stimulation causes cell death and thus initiates Ca^{2+} waves that create Ca^{2+} gradients which play an important role in cell migration[1]. In addition, Ca^{2+} waves also regulate the local transepithelial ion transport to maintain the spatial ion gradients across the epithelium[1]. We recently demonstrated in RPE that an easily induced and repeatable Ca^{2+} wave could be produced by mechanical stimulation[5]. This provides an experimental way to study Ca^{2+} activity in the epithelial monolayer.

In silico models of various cellular processes are becoming an increasingly important part of biological research, including drug discovery and toxicology studies. The importance of this was recently emphasized in a review of cardiotoxicity testing [10]. Computational models of Ca^{2+} signaling, specifically, have been developed for many cell types including pancreatic and parotid acinar cells[11], astrocytes[12], and hepatocytes[13]. Epithelial Ca^{2+} signaling, however, differs from other cell types because the epithelium forms a highly polarized cell monolayer that comprises organized apical and basal cell membranes. The epithelial cells are tightly connected with tight junctions and gap junctions between the cells[14]. At present, there are only a few epithelial Ca^{2+} signaling models available, for example for the urothelial monolayer[15] and for the airway epithelium[16]. RPE has many unique functions compared to other epithelia as it supports the complex processes of vision. Indeed, in the treatment of many eye diseases, RPE is either the drug target or it hinders drug penetration and provides a barrier between most of the eye and the blood stream. Hence, computational models of the functions of RPE, including Ca^{2+} dynamics, are well warranted.

The aim of this study, therefore, is to provide a deeper understanding of the study of Ca^{2+} activity by introducing a detailed computational model of RPE Ca^{2+} dynamics. The computational model described in this paper is based on our experimental data on a mechanically

induced Ca^{2+} wave in ARPE-19 cells, a commercial immortalized human RPE cell line that is widely used to assess RPE cell functions *in vitro* [17–19], regardless of its limitations in cellular morphology, organization and function [20].

The computational model is mostly based on the experimental data of Abu Khamidakh et al. 2013[5]. In addition, the model comprises our new unpublished α-glycyrrhetinic acid (GA)-suramin-treated data. We constructed the model by combining previously published cell Ca^{2+} dynamics model components of P_2Y_2 receptors [21], inositol 1,4,5-trisphosphate (IP_3) receptors [22], ryanodine receptors [23], Ca^{2+} pumps and gap junctions to a new model component of mechanical stretch. Furthermore, we connected the epithelial cells to each other in the model to enable the diffusion of the molecules and propagation of the stretch. We developed the model based on two experimental data sets: the GA-treated data, where gap junctions (GJs) were blocked by α-glycyrrhetinic acid and untreated control data, where GJs define the connections between the cells. The varying conditions the cells are exposed to due to the mechanical stimulation were modeled by defining three location-specific variables: stretch, extracellular ligand concentration, and IP_3 receptor phosphorylation rate. In addition, we validated the model by simulating the combined blocking effect of GJs and P_2 receptors by GA and suramin. This way, we obtained the first RPE Ca^{2+} signaling model, and we could reveal a deeper understanding of Ca^{2+} activity.

Materials and Methods

Experimental data

In this study, the experimental data of Abu Khamidakh et al. 2013[5] was complemented with new experimental data. Passage numbers for confluent cultures of human RPE immortalized cells (ARPE-19 cell line [ATCC Manassas, VA, U.S.A.]) were p. 23, 24, 30 for GA-treated dataset, p. 23, 24, 28, 30 for control data set and p. 29, 30, 31 for GA-suramin-treated data set. These ARPE-19 cultures were used for Ca^{2+} imaging, by loading them with the Ca^{2+}-sensitive dye fura-2-acetoxymethyl ester. Single cell mechanical stimulation, membrane perforation of one cell, was induced with a glass micropipette. The intracellular Ca^{2+} concentration transient travelled over the ARPE-19 monolayer starting from the mechanically stimulated (MS) cell, and spreading to the neighboring (NB) cells (Fig 1). The NB cells immediately surrounding the MS cell were defined as the first NB cell layer (NB layer 1 = NB_1); cells immediately surrounding the first layer were defined as the second NB layer (NB layer 2 = NB_2) and so on. The ratio of the emitted fluorescence intensities resulting from excitation at 340 and 380 nm (F_{340}/F_{380}) was determined for each cell after background correction. Normalized fluorescence (NF), which reflects the changes in intracellular Ca^{2+} concentration, was then obtained by dividing the fluorescence value by the mean fluorescence value before the mechanical stimulation.[5] The experimental work produced data in NF units. The computational model, however, is presented in absolute calcium concentrations. Due to the lack of absolute reference we consider the model predictions only relative.

Three data sets were simulated with the model. Firstly, in the GA-treated data set the gap junctions (GJs) were blocked by α-glycyrrhetinic acid (GA) (Sigma-Aldrich, St. Louis, MO, USA). Secondly, the model was verified with an untreated control data set that was based on the previous model—only the GJ model component was added. Thirdly, the model was applied to predict a combined blocking effect of GA and P_2 receptor blocker suramin (Sigma-Aldrich) with GA-suramin-treated data set. Each data set was averaged from at least three separate experiments.

The experiments with GA-suramin-treated ARPE-19 cells were not included in the original paper of Abu Khamidakh et al. 2013[5]. The experimental details concerning the ARPE-19 cells as well as the experimental solutions, infrastructure, and protocols are presented in[5] with the following exception: the cells were incubated in a solution containing 30μM GA

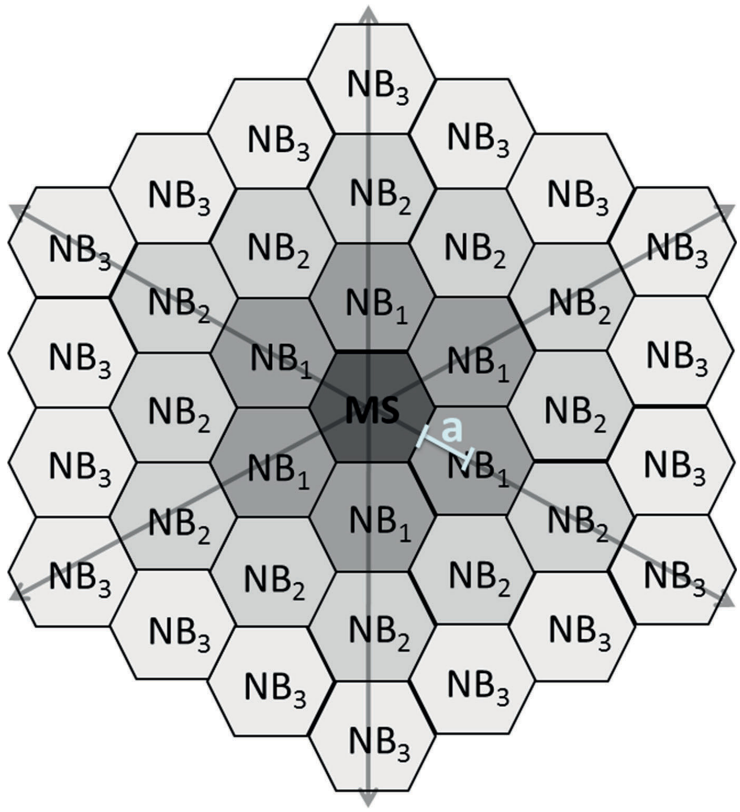

Fig 1. Numbering of the cell layers. Schematic representation of the location of the mechanically stimulated (MS) cell with respect to the neighboring (NB) cell layers: NB_1 is the first layer which is in direct contact with the MS cell; NB_2 is the second layer which is in direct contact with NB_1, and so forth. White line segment marks an apothem (a) of a hexagon.

doi:10.1371/journal.pone.0128434.g001

(incubation time 30 min) and 50μM suramin (incubation time 25 min) prior to mechanical stimulation. To receive representative data for each NB layer, the raw data was averaged so that the NF graphs were aligned by the starting time of mechanical stimulation, and the mean values were calculated for each NB with a one-second sampling rate. This was previously done for the control data set[5], but the averaging was performed also here for the GA-treated and GA-suramin-treated data sets.

Indirect immunofluorescence staining. ARPE-19 cells (p. 24, 27, 44, three cover slips from each passage) were cultured on glass coverslips for two days. For immunofluorescence staining, the samples were washed three times with PBS and fixed for 15 min with 4% paraformaldehyde (pH 7.4; Sigma-Aldrich) at room temperature (RT). After three subsequent washes with PBS, the samples were permeabilizing by a 15 min incubation in 0.1% Triton X-100 in PBS (Sigma-Aldrich) at RT. This was followed again by three PBS washes, after which the samples were incubated with 3% bovine serum albumin (BSA; Sigma-Aldrich) at RT for 1 h. Primary antibody Zonula Occludens (ZO-1) 1:100 (33–9100, Life Technologies) was diluted in 3% BSA PBS and incubated for 1 h at RT. Samples were then washed four times with PBS, and

followed by 1h incubation at RT with secondary antibody donkey anti-mouse Alexa Fluor 568 (A10037, Life Technologies) diluted 1:400 in 3% BSA in PBS. The washes with PBS were repeated again and nuclei were stained with 4′, 6′ diamidino-2-phenylidole (DAPI) included in the mounting medium (P36935, Life Technologies).

Confocal microscopy and image processing. Zeiss LSM780 LSCM on inverted Zeiss Cell Observer microscope (Zeiss, Jena, Germany) with Plan-Apochromat 63x/1.4 oil immersion objective was used for confocal microscopy. Voxel size was set to x = y = 66nm and z = 200nm, pixel stacks were set to 1024x1024, and approximately 50–80 slices were acquired with line average of 2. DAPI and Alexa-568 were excited with 405nm and 561nm lasers and detected with emission windows of 410–495nm and 570–642nm, respectively. The images saved in czi format were processed with ImageJ (Rasband, W.S., ImageJ, U. S. National Institutes of Health, Bethesda, Maryland, USA, http://imagej.nih.gov/ij/, 1997–2014.) and assembled using Adobe Photoshop CS6 (Adobe Systems, San Jose, USA).

Construction of the model

The Ca^{2+} model was constructed by combining six subcellular model components that included the stretch component designed in this study and the P_2Y_2 receptor models of Lemon et al. 2003[21], the IP_3 receptor type 3 (IP_3R_3) of LeBeau et al. 1999[22], and the ryanodine receptor (RyR) of Keizer & Levine 1996[23]. The GJ model component connected the neighboring cells. These model components with corresponding numbering and their rationale, hypothesized Ca^{2+} wave propagation mechanisms as well as model equations (see chapter Detailed model equations) that were used for the NB layers and data sets are summarized in Table 1. The basis for the mathematical implementation is presented in Fig 2 as a schematic model.

Parameters and parameterization

The model parameters are represented in Table 2 and the parameters specific for each NB layer in Table 3. Most of the parameters were adopted from the models of Lemon et al. 2003[21], LeBeau et al. 1999[22], and Keizer & Levine 1996[23]. Typically, the volumes of ARPE-19 cells [5,24,25] and RPE cells[26,27] are variable. The cell width was approximated to be 14μm from the corner-to-corner of a hexagon and the height was 12μm[5].The cytoplasmic volume was approximated to be about 70% of the total cell volume[28]. Thus, a cytoplasmic volume (v) of $1.07\ 10^{-15}\ m^3$ was used in the simulations. The initial values, the values at time of mechanical stimulation, were taken mostly from the model of Lemon et al. 2003[21]. The initial value 0.12μM for intracellular Ca^{2+} concentration ($[Ca^{2+}]_i$) is an arbitrary value approximating the baseline Ca^{2+} concentration determined from GA-treated data set for NB_5-NB_{10} layers using Matlab SimBiology Toolbox.

The rest of the parameters were fitted with Matlab SimBiology Parameter Fit Task: First, the parameter values, excluding SSCC and GJ model components, were fitted with GA-treated data set in NB5 layer. This layer has in general the largest Ca^{2+} response from those NB layers that do not experience any stretch due to mechanical stimulation, according to our assumption. Secondly, the SSCC model component parameters, excluding the location-specific stretch (θ) parameter (see below), were fitted with the same GA-treated data set in NB1 layer that is assumed to have the largest stretch. These values were then used in all simulations for all data sets and NB layers. For the control data set with gap junctions, all other parameters were kept unchanged but the GJ related diffusion parameters, $D_{Ca^{2+}}$, D_{IP_3}, $In_{Ca^{2+}}$ and In_{IP_3}, were fitted using NB1 layer. As a boundary condition we assumed that there is no outflow of IP_3 and Ca^{2+} outside the epithelium, thus Out_{IP_3} and $Out_{Ca^{2+}}$ were assigned to be zero.

Table 1. Model design.

Mechanism	Number	Component	Rationale	Equations	NB layer	Data set
Mechanical stimulus applied to MS cell may stretch ARPE-19 cells near the site of stimulation [5] resulting in the opening of SSCCs that conduct Ca^{2+} from the extracellular space to the cytoplasm. It is shown that ARPE-19 cells can secrete ligand to the extracellular space as a response to stimuli [38].	I	Stretch-sensitive Ca^{2+} channel (SSCC)	Cultured rat RPE expresses SSCCs on plasma membrane [4,53]. In ARPE-19 $[Ca^{2+}]_i$ wave was seen in NB_1-NB_4 layers even when the ER was depleted[5], indicating a Ca^{2+} influx mechanism independent of the ER, possibly the SSCCs.	7–9[a]	1–4	GA-treated, Control, GA-suramin-treated
The ligand, likely ATP or UTP [3,30,38,54], interacts with G-protein coupled purinergic receptor type P_2Y_2 on the cell membrane leading to the production of inositol 1,4,5-trisphosphate (IP_3) to the cytoplasm in a ligand concentration dependent manner.	II	Purinergic P_2Y_2 receptor (P_2Y_2)	The presence of P_2Y_2 receptors has been shown in cultured human RPE[30], bovine and human fetal RPE as well as in Long-Evans rats[55]	10–16[b]	1–10	GA-treated, Control, GA-suramin-treated[e]
IP_3 diffuses across the cytoplasm to the endoplasmic reticulum (ER), where it interacts with IP_3R_3 resulting in a release of Ca^{2+} from the ER[22].	III	IP_3 receptor type 3 (IP_3R_3)	Currently there is no direct evidence about the subtype of IP_3R expressed in ARPE-19. Hence, the data from other epithelia [56], [57], and[58] and an epithelial model [16] was utilized to choose the subtype 3 (IP_3R_3).	17–21[c]	1–10	GA-treated, Control, GA-suramin-treated
As the cytoplasmic Ca^{2+} concentration increases, RyRs become activated releasing more Ca^{2+} to the cytoplasm from the ER[23].	IV	Ryanodine receptor (RyR)	RyRs, locating on the membrane of ER participate in Ca^{2+} signaling in rat RPE[4], and ARPE-19[51].	22–24[d]	1–10	GA-treated, Control, GA-suramin-treated
The cytoplasmic Ca^{2+} concentration is decreased by the pumping activities of SERCA and PMCA. IP_3 is degraded in the cytoplasm. Ca^{2+} leak currents maintain the cytoplasmic Ca^{2+} baseline level.	V	Sarco/endoplasmic reticulum ATPase (SERCA), plasma membrane Ca^{2+} ATPase (PMCA), Leak	The presence of SERCA has been shown by blocking it to deplete the ER from Ca^{2+} in ARPE-19 cells[5] and rat RPE [53]. PMCA has been identified on the plasma membrane of cultured human RPE[59].	25	1–10	GA-treated, Control, GA-suramin-treated
GJs form intercellular connections between neighboring cells allowing diffusion of Ca^{2+} and IP_3 between the NB layers.	VI	Gap junction (GJ)	GJs form intercellular connections in ARPE-19[5], and rat RPE[4,60] enabling Ca^{2+} wave to spread over the monolayer.	26–28	1–10	Control

[a]Designed in this study

[b]Lemon et al. 2003[21]

[c]LeBeau et al. 1999[22]

[d]Keizer & Levine 1996[23]

[e]Parameter values of k_p modified

Hypothesized mechanisms and model components for Ca^{2+} wave propagation after mechanical stimulation with corresponding equations, NB layers, and data sets.

doi:10.1371/journal.pone.0128434.t001

Location-dependent parameters

Three parameters were assumed to vary according to the location of the cell with respect to the MS cell: stretch (θ) activating the stretch-sensitive Ca^{2+} channels (SSCCs), the extracellular ligand concentration ([L])[6,16,29,30], and the phosphorylation rate of IP_3R_3 (α_4)[22]. Ca^{2+}

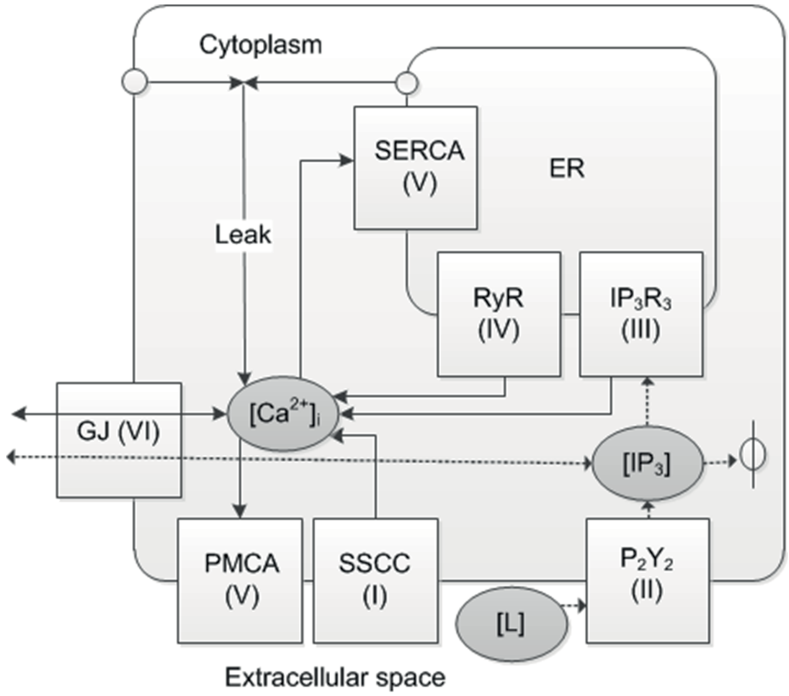

Fig 2. Schematic diagram of the Ca^{2+} signaling model. Solid arrows represent Ca^{2+} fluxes and dashed arrows IP_3 dynamics. Roman numerals denote the model components I-VI. Abbreviations: $[Ca^{2+}]_i$ = cytoplasmic Ca^{2+} concentration, [L] = extracellular ligand concentration, $[IP_3]$ = cytoplasmic IP_3 concentration, SSCC = stretch-sensitive Ca^{2+} channel, P_2Y_2 = purinergic receptor type P_2Y_2, IP_3R_3 = IP_3 receptor type 3, RyR = ryanodine receptor, SERCA = sarco/endoplasmic reticulum Ca^{2+} ATPase, PMCA = plasma membrane Ca^{2+} ATPase, Leak = combinatory Ca^{2+} leak from the extracellular space and the endoplasmic reticulum (ER), GJ = gap junction, ϕ = degradation.

doi:10.1371/journal.pone.0128434.g002

concentration was modeled separately in each NB layer. The distance (x) defines the distance of the NB layer from the MS cell centre that was calculated using the idealized hexacon RPE cell architecture (Fig 1) as

$$x = a2n = \frac{s}{2\tan\left(\frac{180}{6}\right)}2n, \quad (1)$$

where a is an apothem of the hexagon, 6 is the number of corners in the hexagon, s = 7μm is the length of the hexagon side and n = 1, 2, 3. . .10 according to the NB layer numbering.

The stretch component was present in cell layers NB1-NB4. Stretch (θ) was parameterized in the GA-treated data set separately for each NB layer. The obtained parameters resulted in an exponentially decaying function corresponding to the decay of an amplitude envelope of a damped wave in a membrane [31]. This function was then used for modeling the stretch

$$\theta = 0.3426e^{-0.105x}, \quad (2)$$

where x is the distance from the MS cell ($R^2 = 0.9878$).

Table 2. Constant parameters and initial conditions.

Parameter	Description	Value	Reference
I Stretch-sensitive Ca^{2+} channels (SSCCs)			
k_{SSCC}	Maximal SSCC flux rate	1.025 μM s^{-1}	fitted
k_f	SSCC forward rate constant	0.1382 s^{-1}	fitted
k_b	SSCC backward rate constant	0.04027 s^{-1}	fitted
k_θ	Stretch-relaxation parameter	0.08105 s^{-1}	fitted
II Metabotropic receptor P_2Y_2			
L_0	Bolus extracellular ligand concentration at x = 0μm	1310 μM	fitted
D_{ATP}	Diffusion coefficient of A	236 μm^2 s^{-1}	[61]
$[R_T]$	Total number of P_2Y_2 receptors	$2 \cdot 10^4$	[62]
K_1	Unphosphorylated receptor dissociation constant	5 μM	[21]
K_2	Phosphorylated receptor dissociation constant	100 μM	[21]
k_r	Receptor recycling rate	$1.75 \cdot 10^{-4}$ s^{-1}	[21]
k_p	Receptor phosphorylation rate	0.03 s^{-1}	[21]
k_e	Receptor endocytosis rate	$6 \cdot 10^{-3}$ s^{-1}	[21]
ξ	Fraction of mobile receptors	0.85	[21]
$[G_T]$	Total number of G-protein molecules	$1 \cdot 10^5$	[63]
k_{deg}	IP_3 degradation rate	1.25 s^{-1}	[64]
k_a	G-protein activation rate	0.017 s^{-1}	[21]
k_d	G-protein deactivation rate	0.15 s^{-1}	[21]
$[(PIP_2)_T]$	Total number of PIP_2 molecules	$5.0 \cdot 10^4$	[21]
r_r	PIP_2 replenishment rate	0.015 s^{-1}	[21]
δ	G-protein intrinsic activity parameter	$1.238 \cdot 10^{-3}$	[21]
K_3	Dissociation constant for Ca^{2+} binding to PLC	0.4 μM	[21]
α	Effective signal gain parameter	$2.781 \cdot 10^{-5}$ s^{-1}	[21]
N_a	Avogadro's constant	$6.02252 \cdot 10^{23}$	
v	Volume of the cytoplasmic space	$1.07 \cdot 10^{-15}$ m^3	see text
III IP_3 receptor type 3 (IP_3R_3)			
α_1	Maximum rate of k_1	40 μM s^{-1}	[22]
β_1	$[Ca^{2+}]_i$ for half-maximal k_1	0.8 μM	[22]
k_{-1}	Rate of O to S transition	0.88 s^{-1}	[22]
k_2	Rate of O to I_1 transition	0.5 s^{-1}	[22]
k_3	Rate of I_1 to S transition	0.5 s^{-1}	[22]
β_4	$[IP_3]$ for half-maximal k_4	0.01 μM	[22]
k_5	Rate of I_2 to S transition	0.02 s^{-1}	[22]
$k_{IP_3R_3}$	Maximum IP_3R_3 flux rate	155.8 μM s^{-1}	fitted
IV Ryanodine receptor (RyR)			
K_a	Keizer & Levine dissociation constant	0.37224 μM	[23]
K_b	Keizer & Levine dissociation constant	0.63601 μM	[23]
K_c	Keizer & Levine dissociation constant	0.05714 μM	[23]
k_{RyR}	Maximum RyR flux rate	16.04 μM s^{-1}	fitted
V Ca^{2+} pumps and leak current			
V_{Pump}	Maximal pump rate	5.341 μM s^{-1}	fitted
K_{Pump}	$[Ca^{2+}]_i$ for half-maximal V_{Pump}	0.5030 μM	fitted
J_{Leak}	Ca^{2+} leak current	0.1450 μM s^{-1}	fitted
VI Gap junctions (GJ)			
$D_{Ca^{2+}}$	Diffusion coefficient of Ca^{2+} through GJs	512.7 μm^2 s^{-1}	fitted
D_{IP_3}	Diffusion coefficient of IP_3 through GJs	913.9 μm^2 s^{-1}	fitted

(*Continued*)

Table 2. (*Continued*)

Parameter	Description	Value	Reference
$In_{Ca^{2+}}$	Ca^{2+} input to NB1	-0.003320 μM s^{-1}	fitted
In_{IP_3}	IP_3 input to NB1	0.5771 μM s^{-1}	fitted
$Out_{Ca^{2+}}$	Ca^{2+} output from NB10	0 μM s^{-1}	see text
Out_{IP_3}	IP_3 output from NB10	0 μM s^{-1}	see text
Initial conditions (time 0s)			
$[R^S]$	Total number of unphosphorylated surface receptors	17000	[21]
$[R^S_p]$	Total number of phosphorylated surface receptors	0	[21]
[G]	Basal number of G-protein molecules	14	[21]
$[IP_3]$	Basal IP_3 concentration	0.01 μM	[21]
$[PIP_2]$	Basal number of PIP_2 molecules	49997	[21]
$[Ca^{2+}]_i$	Basal cytoplasmic Ca^{2+} concentration	0.12 μM	see text

Most of the parameters were taken from the models of Lemon et al. 2003[21] for P_2Y_2 receptor, LeBeau et al. 1999[22] for IP_3R_3, and Keizer & Levine 1996[23] for RyR. Reference 'fitted' means that the parameter was optimized in this study.

doi:10.1371/journal.pone.0128434.t002

Ligand diffusion in the extracellular space is modelled according to thin film solution to Fick's diffusion law [32] as follows describing the ligand concentration (L) as a function of time (t)

$$L(x,t) = \frac{L_0}{\sqrt{4\pi D_{ATP} t}} e^{-x^2/(4Dt)}, \quad (3)$$

where L_0 is the initial bolus ligand concentration above the MS cell (at x = 0), D_{ATP} is the diffusion coefficient for ATP, and x describes the NB layer distance from the central MS cell.

IP_3R_3 phosphorylation rate (α_4) used in Eq 21 was fitted separately for each NB layer in GA-treated and control data sets, which resulted in shallowly rising exponential functions with respect to the distance of the cell from the MS cell (x). The equation for GA-treated data

Table 3. Location-dependent parameters with respect to the MS cell.

Parameter	Description	Equation	Range
x	Distance from the MS cell centre	1	From 12.12 μm (NB1) to 121.24 μm (NB10)
θ	Stretch	2 (exponential decay)	From 0.096 (NB1) to 1.014 10^{-6} (NB10)
L	Extracellular ligand concentration	3 (exponential decay)	From 26.14 μM (NB1) to 2.61 μM (NB10)
α_4	IP_3R_3 phosphorylation rate	4 (exponential rise)	From 0.0413 s^{-1} (NB1) to 0.1548 s^{-1} (NB10)
		5 (exponential rise)	From 0.0333 (NB1) to 0.1503 (NB10)
$J_{GJ,Ca^{2+}}$	Ca^{2+} flux through GJs	26	From 0.049 μM s^{-1} (NB1→NB2) to 1.8 10^{-6} μM s^{-1} (NB9→NB10)
J_{GJ,IP_3}	IP_3 flux through GJs	27	From 0.407 μM s^{-1} (NB1→NB2) to 0.022 μM s^{-1} (NB9→NB10)
A	Area of the cell membranes connecting NB layers	28	From 1512 μm^2 (NB1) to 10584 μm^2 (NB10)

doi:10.1371/journal.pone.0128434.t003

set (R^2 = 0.9740) is

$$\alpha_4 = 0.0357e^{0.0121x} \quad (4)$$

and for control data set (R^2 = 0.9798)

$$\alpha_4 = 0.0282e^{0.0138x}. \quad (5)$$

Similarly to θ and L, these functions were then used in simulations instead of values from separate fits.

Model simulations

The parameters were fitted with Matlab SimBiology (R2012a, The MathWorks, Natick, MA) to the experimental data using Parameter Fit task, where the maximum iterations was 100. The solver type was ode45 (Dormand-Prince) and the error model was constant error model. The time step in the simulations was set to Δt = 0.1 seconds.

Sensitivity analysis

Sensitivity analysis was performed to evaluate the uncertainty of selected parameters that were fitted in this study (parameters $k_{IP_3R_3}$, k_{RyR}, V_{Pump}, K_{Pump}, J_{Leak}, In_{IP_3}, $In_{Ca^{2+}}$, D_{IP_3} and D_{IP_3} from Table 2) or behaved as location-specific parameters (parameters θ, L and α_4 from Table 3). Values of these parameters were changed -25%, -10%, 0%, +10% and +25% in the model including all the model components I-VI for the control data set. The influence of these parameter were studied for NB layers NB1, NB5 and NB10 concentrating on the following features of the Ca^{2+} wave: peak amplitude, time to peak, Ca^{2+} wave width at half maximum, and Ca^{2+} concentration at the end of the Ca^{2+} wave (at 90 seconds' time point).

Model prediction of drug effect: suramin

With the model, we investigated the mechanism by which suramin influences the Ca^{2+} waves in ARPE-19 cells. First, we compared the peak amplitude, time to peak, Ca^{2+} wave width at half maximum, and Ca^{2+} concentration in the end of the Ca^{2+} wave at 90 seconds' time point between two experimental data sets: GA-treated and GA-suramin-treated data sets. Second, we made sensitivity analysis about the behaviour of P_2Y_2 receptor regulation parameters (K_1, K_2, k_r, k_p, k_e, ξ), since suramin is a known unspecific antagonist of P_2 receptors. Suramin has also been suggested to disrupt the coupling between the receptor in the cell membrane and the G-protein by blocking the association of the G-protein α and βγ subunits[33]. Hence, the G-protein cascade parameters k_a, k_d and δ were also evaluated. The sensitivity analysis was done in the model for GA-treated data set (including model components I-V) in NB1, NB5 and NB10 layers. The parameter values were changed in the model by -25% and +25% in order to compare the effects of parameter modifications to the observed differences in the experimental data between GA-treated and GA-suramin-treated data sets. All other parameters were kept unchanged. Third, based on the results of this approach, the model was fitted to the GA-suramin-treated data set by refitting those P_2Y_2 receptor and G-protein cascade parameters that were observed to change the Ca^{2+} curve similarly to the differences seen in the experimental data between GA-treated and GA-suramin-treated data sets. This was done with Matlab SimBiology Parameter Fit task for each NB layer.

Detailed model equations

Time dependent changes in intracellular Ca^{2+} concentration $[Ca^{2+}]_i$ are presented in the model as a combination of Ca^{2+} fluxes

$$\frac{d[Ca^{2+}]_i}{dt} = J_{SSCC} + J_{IP_3R_3} + J_{RyR} - J_{Pump} + J_{Leak} + J_{GJ,Ca^{2+}}, \quad (6)$$

where the subscripts indicate the source of the flux: stretch-sensitive Ca^{2+} channels (J_{SSCC}), inositol 1,4,5-trisphosphate (IP_3) receptor type 3 ($J_{IP_3R_3}$), and ryanodine receptor (J_{RyR}). J_{Pump} combines the Ca^{2+} pumping functions of sarco/endoplasmic reticulum ATPase (SERCA) and the plasma membrane Ca^{2+} ATPase (PMCA). Leak Ca^{2+} current (J_{Leak}) describes the total leakage from the extracellular space and the endoplasmic reticulum (ER) to the cytoplasm. $J_{GJ,Ca^{2+}}$ is the Ca^{2+} flux through gap junctions.

I Stretch-sensitive Ca^{2+} channels (SSCCs). Stretch-sensitive Ca^{2+} channels (SSCCs) on the cell membrane are activated, when exposed to mechanical stimulation. Their closure is caused either by relaxation in the mechanical force or by their adaption to that mechanical force[34]. The SSCC model is described with Eqs 7–9. In this study, a model for SSCCs was developed according to the kinetic diagram shown in Fig 3, where C_{SSCC} describes the proportion of the channels in the closed state. O_{SSCC} is the proportion of SSCCs in the open state defined as

$$\frac{dO_{SSCC}}{dt} = \theta k_f - (\theta k_f + k_b) O_{SSCC}, \quad (7)$$

where k_f is the forward rate constant and k_b is the backward rate constant. Ca^{2+} flux via SSCCs (J_{SSCC}) is expressed as

$$J_{SSCC} = k_{SSCC} O_{SSCC}, \quad (8)$$

where k_{SSCC} is the maximum Ca^{2+} flux rate via SSCCs. Parameter θ is dimensionless, and describes the quantity of stretch induced at the time of mechanical stimulation, which then decreases with time

$$\frac{d\theta}{dt} = -k_\theta \theta, \quad (9)$$

according to a stretch-relaxation parameter k_θ.

II Purinergic receptor P_2Y_2. The agonist-induced activation of the second messenger system, here P_2Y_2, is represented by Eqs 10–16[21].The kinetic diagram for the P_2Y_2 receptor is presented in Fig 3. Some of the ligand-bound P_2Y_2 receptors on the cell surface are phosphorylated irreversibly at rate k_p, which causes desensitization of the receptors. Phosphorylated receptors are internalized at a rate k_e, and these internalized receptors are then dephosphorylated and recycled back to the surface at rate k_r. G-proteins can only be activated by the unphosphorylated P_2Y_2 receptors $[R^S]$ defined by

$$\frac{d[R^S]}{dt} = k_r[R_T] - \left(k_r + \frac{k_p[L]}{K_1 + [L]}\right)[R^S] - k_r[R_p^S], \quad (10)$$

where $[R_T]$ denotes the total number of surface receptors, K_1 is the dissociation constant for unphosphorylated receptors, and [L] is the extracellular ligand concentration. The total

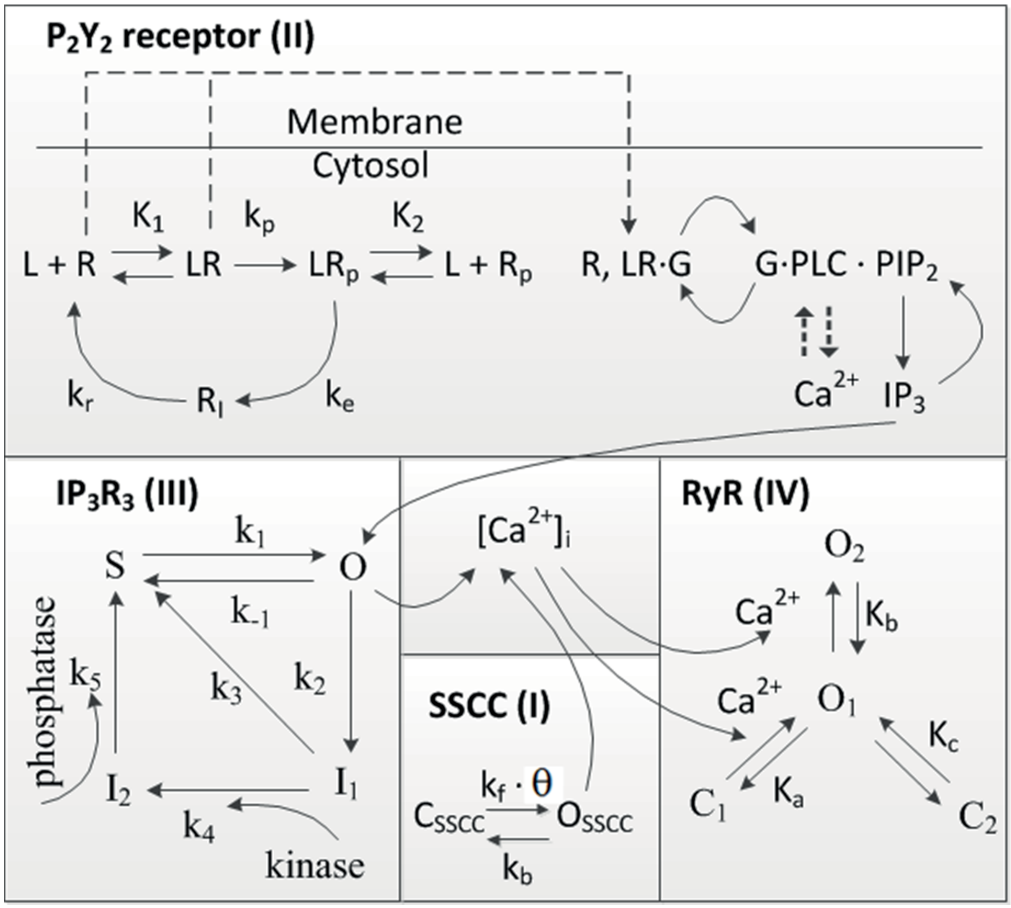

Fig 3. Kinetic diagram. Kinetics of the model component I (SSCC) were combined with the kinetics of model components II-IV from the original models of the P_2Y_2 receptor[21], IP_3R_3[22], and RyR[23].

doi:10.1371/journal.pone.0128434.g003

number of phosphorylated surface receptors $[R_p^S]$ is

$$\frac{d[R_p^S]}{dt} = [L]\left(\frac{k_p[R^S]}{K_1 + [L]} - \frac{k_e[R_p^S]}{K_2 + [L]}\right), \tag{11}$$

where K_2 is the dissociation constant for phosphorylated receptors. The binding of the ligand to the G-protein coupled receptor P_2Y_2 results in a cascade of events leading to the activation of enzyme phospholipase C (PLC). This enzyme then hydrolyses the phosphatidylinositol 4,5-bisphosphate (PIP_2) to IP_3. The activation rate (k_a) of the G-protein is proportional to two ratios: the ratio of the activities of the ligand unbound and bound receptor species (δ), and the ratio of the number of ligand bound receptors and the total number of receptors (p_r). Denoting the deactivation of G-protein to occur at a deactivation rate of k_d, the equations for the amount

of Gα · GTP labeled as [G] as well as for the ratio p_r can be expressed as

$$\frac{d[G]}{dt} = k_a(\delta + p_r)([G_T] - [G]) - k_d[G], \tag{12}$$

and

$$p_r = \frac{[L][R^S]}{\xi[R_T](K_1 + [L])}. \tag{13}$$

Equation for the concentration of IP_3 is

$$\frac{d[IP_3]}{dt} = r_h N_a^{-1} v^{-1}[PIP_2] - k_{\deg}[IP_3] + J_{GJ,IP_3}, \tag{14}$$

where k_{deg} is the degradation rate of IP_3 and J_{GJ,IP_3} is the IP_3 flux through gap junctions. The rate coefficient for PIP_2 hydrolysis (r_h) includes the effective signal gain parameter (α) and the dissociation constant for Ca^{2+} binding to PLC (K_3) that can be expressed as

$$r_h = \alpha\left(\frac{[Ca^{2+}]_i}{K_3 + [Ca^{2+}]_i}\right)[G]. \tag{15}$$

Replenishment of PIP_2 is required for IP_3 production to be maintained over sustained periods of agonist stimulation. The equation for the number of PIP_2 molecules $[PIP_2]$ is

$$\frac{d[PIP_2]}{dt} = -(r_h + r_r)[PIP_2] - r_r N_a v[IP_3] + r_r[(PIP_2)_T], \tag{16}$$

where r_r represents the PIP_2 replenishment rate and $[(PIP_2)_T]$ the total number of PIP_2 molecules.[21]

III IP_3 receptor type 3 (IP_3R_3). The IP_3 receptor type 3 (IP_3R_3) function is represented by the Eqs 17–21[22]. The kinetic diagram for IP_3R_3 is shown in Fig 3. The IP_3-induced release of Ca^{2+} from the ER through IP_3R_3 ($J_{IP_3R_3}$) is

$$J_{IP_3R_3} = k_{IP_3R_3} O^4, \tag{17}$$

where $k_{IP_3R_3}$ is the maximum rate of Ca^{2+} release, and IP_3R_3 comprises four subunits that all must be in the open state (O) for the receptor to conduct. The steady-state proportion of open receptors (O) is

$$O = \frac{\phi[IP_3]}{\frac{k_{-1}+k_2}{k_1}\phi + [IP_3]}, \tag{18}$$

Where ϕ function controls the sensitivity of IP_3R_3 to $[IP_3]$, and it can be expressed as

$$\phi = \frac{1}{1 + \frac{k_2}{k_3+k_4}\left(1 + \frac{k_4}{k_5}\right)}, \tag{19}$$

with rate coefficients k_{-1}, k_2, k_3, and k_5 being constants. Coefficient k_1 describes a rate for IP_3R_3 transition from shut state (S) to open state (O)

$$k_1 = \frac{\alpha_1[Ca^{2+}]_i^{\,3}}{\beta_1^{\,3} + [Ca^{2+}]_i^{\,3}}, \tag{20}$$

where constant α_1 is the maximum rate of S to O transition, and β_1 is the $[Ca^{2+}]_i$ at which the rate is half of its maximum. Coefficient k_4 expresses the rate for IP_3R_3 from the first inactivated

state (I_1) to the second inactivated state (I_2). It can be expressed as

$$k_4 = \frac{\alpha_4[IP_3]}{\beta_4 + [IP_3]}, \tag{21}$$

where the I_1 to I_2 transition is agonist specific and involves a phosphorylation of IP_3R_3 by kinase activity. This is defined by parameter α_4 that denotes the maximum rate of I_1 to I_2 transition, while β_4 denotes the value of $[IP_3]$ at which the rate is half maximal.[22]

IV Ryanodine receptor (RyR). The ryanodine receptor (RyR) dynamics were modeled by Keizer & Levine 1996[23] with Eqs 22–24. In Fig 3 the kinetic diagram for RyR is illustrated. The Ca^{2+} release from the ER through RyR (J_{RyR}) is defined by the maximum RyR flux rate (k_{RyR}) multiplied by the open probability (P_{RyR}) as

$$J_{RyR} = k_{RyR} P_{RyR} \tag{22}$$

where

$$P_{RyR} = \left(\frac{w^{\infty}\left(1+\left(\frac{[Ca^{2+}]_i}{K_b}\right)^3\right)}{1+\left(\frac{K_a}{[Ca^{2+}]_i}\right)^4+\left(\frac{[Ca^{2+}]_i}{K_b}\right)^3} \right), \tag{23}$$

and where w^{∞} is the RyR sensitivity function

$$w^{\infty} = \left(\frac{1+\left(\frac{K_a}{[Ca^{2+}]_i}\right)^4+\left(\frac{[Ca^{2+}]_i}{K_b}\right)^3}{1+\frac{1}{K_c}+\left(\frac{K_a}{[Ca^{2+}]_i}\right)^4+\left(\frac{[Ca^{2+}]_i}{K_b}\right)^3} \right), \tag{24}$$

and K_a, K_b, and K_c are dissociation constants. [23]

V Sarco/endoplasmic reticulum Ca^{2+} ATPase (SERCA) and plasma membrane Ca^{2+} ATPase (PMCA). J_{Pump} combines the pumping functions of sarco/endoplasmic reticulum Ca^{2+} ATPase (SERCA) and plasma membrane Ca^{2+} ATPase (PMCA)

$$J_{Pump} = \frac{V_{Pump}[Ca^{2+}]_i^2}{K_{Pump}{}^2 + [Ca^{2+}]_i^2}, \tag{25}$$

where V_{Pump} indicates the maximum flux rate of the pumps and K_{Pump} states the $[Ca^{2+}]_i$ for half-maximal pumping rate.

VI Gap junctions (GJs). Gap junctions (GJs) and the Ca^{2+} flux via GJs ($J_{GJ,Ca^{2+}}$) are modeled as

$$J_{GJ,Ca^{2+}} = \frac{D_{Ca^{2+}}}{A_{n-1,n}}([Ca^{2+}]_{in-1} - [Ca^{2+}]_{in}) - \frac{D_{Ca^{2+}}}{A_{n,n+1}}([Ca^{2+}]_{in} - [Ca^{2+}]_{in+1}), \tag{26}$$

where n is the number of the NB layer. The NB layer n receives Ca^{2+} from the previous NB layer $n-1$ and delivers Ca^{2+} to the next NB layer $n+1$ according to the concentration gradient. Similarly, IP_3 flux through GJs (J_{GJ,IP_3}) is modelled as

$$J_{GJ,IP_3} = \frac{D_{IP_3}}{A_{n-1,n}}([IP_3]_{n-1} - [IP_3]_n) - \frac{D_{IP_3}}{A_{n,n+1}}([IP_3]_n - [IP_3]_{n+1}), \tag{27}$$

where n is the number of the NB layer. $D_{Ca^{2+}}$ is the diffusion coefficient for Ca^{2+} and D_{IP_3} is the diffusion coefficient for IP_3. These diffusion coefficients do not take into account the open probability, regulation, or density of the GJs as they describe the actual movement of Ca^{2+} and

IP_3 from one NB layer to the next NB layer. As an exception to other NB layers, the fluxes from MS cell to NB_1 layer are modelled by parameters $In_{Ca^{2+}}$ and In_{IP_3} for Ca^{2+} and IP_3, respectively. Similarly, the fluxes from NB_{10} layer to distant cell layers are modelled with parameters $Out_{Ca^{2+}}$ and Out_{IP_3}.

Parameter A describes the area of the cell membranes connecting the neighbouring NB layers in the monolayer. The value for A is received by multiplying the area of one hexagon side, that is the length of the hexagon side (l = 7μm) times the height of the cell (h = 12μm), by the number of hexagon edges between the two NB layers as

$$A_{n\to n+1} = ((3 + 2(n-1))6)lh, \tag{28}$$

where n is the number of the NB layer (n = 1, 2, 3. . ..10). Each NB layer has six cells with three connecting sides and (n-1) 6 cells with two connecting sides (see Fig 1). In other words, the area (A) increases with distance from the central MS cell.

Results

Polarization of the ARPE-19 monolayer

Polarization of the ARPE-19 monolayer was demonstrated by immunolabeling the tight junctions in the monolayer. Confocal microscopy image (Fig 4) shows that within 2 days the ARPE-19 cells have formed a monolayer where ZO-1 is localised continuously in the junctions of the cells, forming a homogeneous network. This can be taken as an indication of the polarization of the epithelial cell culture [35].

Ca^{2+} signal propagation mechanisms

The fittings of the model to the experimental data in the NB1-NB10 layers are illustrated in Fig 5A for the GA-treated data set and in Fig 5B for the control data set. The model simulations managed to catch very well the features of the experimental data in both data sets. In GA-treated data set (Fig 5A), the simulations closely followed the data in peak amplitude, time to peak, Ca^{2+} wave width at half maximum and end Ca^{2+} concentration in NB1-NB9 layers. In NB10 layer, however, time to peak was longer in the simulation results than in the data. In the control data set (Fig 5B), the Ca^{2+} wave features differed slightly between the model and the data, but overall the curve shape of the model followed the data reasonably well. R^2 values describing the goodness of fit are presented in Table 4. In GA-treated data set and control data set R^2 values were higher than 0.8 in NB1-NB9 and lower than 0.8 in NB10. Hence, 90% of the fits in GA-treated data set and control data set resulted in $R^2 > 0.8$.

The model includes the model components of SSCCs, P_2Y_2 receptors, IP_3R_3s, RyRs, Ca^{2+} pumps and GJs, and the parameters were either obtained from previous studies or defined in this study for ARPE-19. The basic fit was done in GA-treated data set for NB5, but the SSCC model component was fitted in NB1 (Table 2). Three location-specific parameters were defined in this study: stretch (θ), extracellular ligand concentration (L) and phosphorylation rate of IP_3R_3 (α4) (Table 3). The stretch (θ) and extracellular ligand concentration (L) decayed exponentially from NB1 towards the distant NB cell layers. The IP_3R_3 phosphorylation rate regulated by the kinase activity (α_4) increased following a shallow exponential, almost linear function, from NB1 to NB10. The corresponding values of α_4 with the distance were lower in the control data set (Eq 5) than in the GA-treated data set (Eq 4) indicating a possible role of IP_3 receptor phosphorylation rate as a regulator of Ca^{2+} signaling. The GJ model component was parameterized in control data set for NB1. GJs mediated the Ca^{2+} signal by allowing the diffusion of Ca^{2+} and IP_3 between adjacent cell layers so that the fluxes of these species decreased with

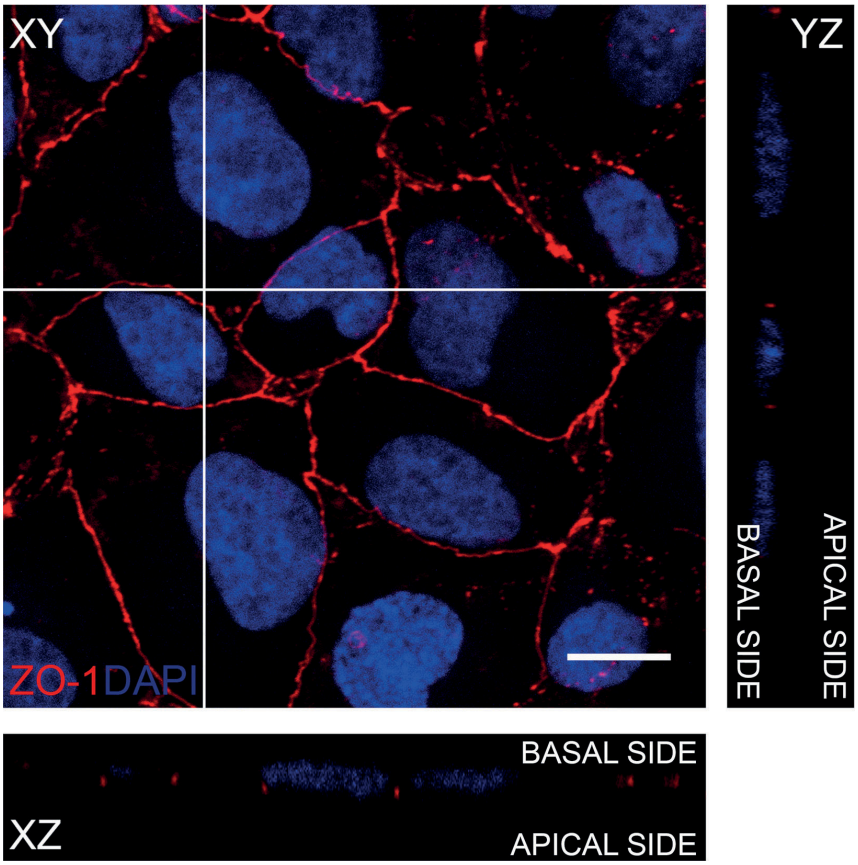

Fig 4. Polarization of the ARPE-19 monolayer. Z-projections (XZ and YZ) from apical side to basal side and maximum intensity projection of the XY plane in the ARPE-19 monolayer represent the localization of Zonula Occludens (ZO-1, red) in the confocal micrograph after immunofluorescence labeling with the nuclear label 4',6-diamidino-2-phenylindole (DAPI, blue). Scale bar is 10μm.

doi:10.1371/journal.pone.0128434.g004

distance from the MS cell due to the increasing area of the cell membranes connecting the NB layers (Table 3).

The resulting model of mechanical stimulus induced Ca^{2+} dynamics is: 1) Cells near the stimulus site conduct Ca^{2+} through plasma membrane SSCCs, and gap junctions conduct the Ca^{2+} and IP_3 between cells further away from stimulated cell. 2) The MS cell secretes one or several types of ligand to the extracellular space where the ligand diffusion mediates the Ca^{2+} signal so that the ligand concentration decreases with distance. 3) The phosphorylation of the IP_3 receptor defines the cell's sensitivity to the extracellular ligand attenuating the Ca^{2+} signal in the distance.

Results of the sensitivity analysis

The sensitivity of the four Ca^{2+} wave features described in Materials and Methods was studied for a set of parameters that were fitted in this study for NB1, NB5 and NB10 layers (Fig 6).

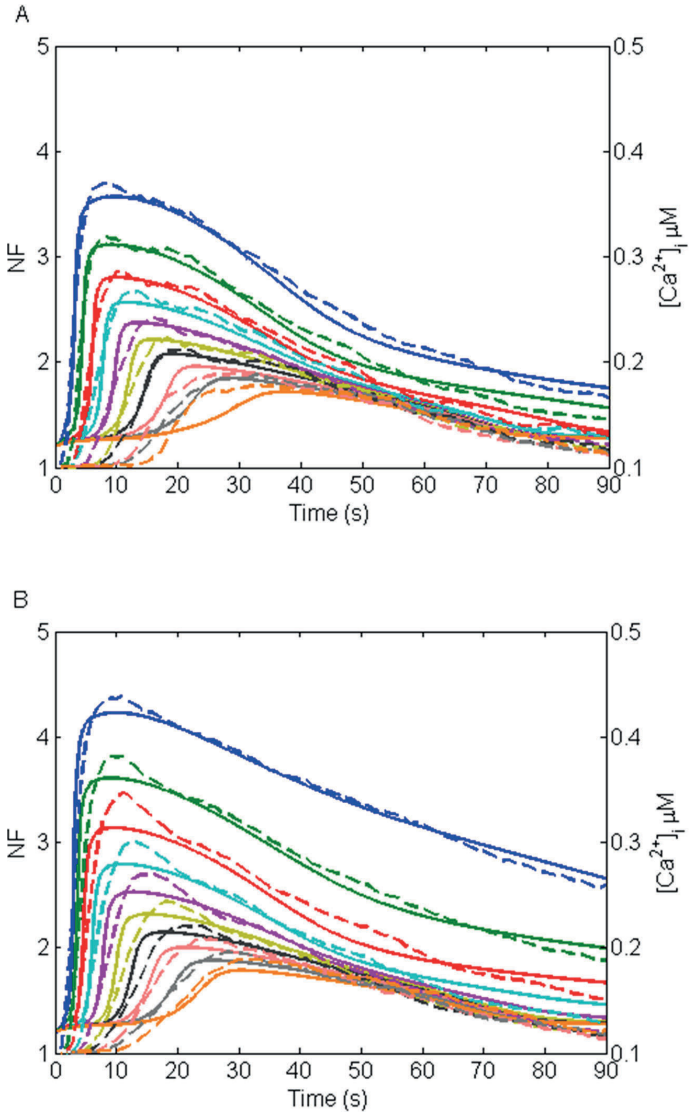

Fig 5. Fittings of the model to the experimental data. (A) GA-treated, and (B) control data sets with dashed lines representing the data in dimensionless NF units and solid lines representing the model simulations with arbitrary units representing $[Ca^{2+}]_i$ in μM concentrations. The uppermost curve pair (blue) represents NB1, the second uppermost NB2 (green), followed by NB3 (red), NB4 (light blue), NB5 (purple), NB6 (yellow), NB7 (black), NB8 (light red), NB9 (grey), and NB10 (orange).

doi:10.1371/journal.pone.0128434.g005

From the location-dependent parameters, θ, L and α_4, Ca^{2+} wave features were most sensitive to modifications in α_4 and the least sensitive to modifications in θ. Overall, decreasing the stretch parameter (θ) resulted in faster Ca^{2+} waves in NB1 (Fig 6B). Increasing the extracellular

Table 4. R^2 values indicating the goodness of fit between the model and the data.

Data set	NB1	NB2	NB3	NB4	NB5	NB6	NB7	NB8	NB9	NB10
GA-treated	0.9839	0.9815	0.9811	0.9651	0.9716	0.9627	0.9677	0.9326	0.8837	0.4561
Control	0.9665	0.9613	0.9454	0.9653	0.9686	0.9558	0.9508	0.9419	0.9108	0.6259
GA-suramin-treated	0.8633	0.8543	0.9344	0.9323	0.9414	0.9156	0.9253	0.7812	0.6110	0.2297

R^2 values are listed separately for each data set and NB layer.

doi:10.1371/journal.pone.0128434.t004

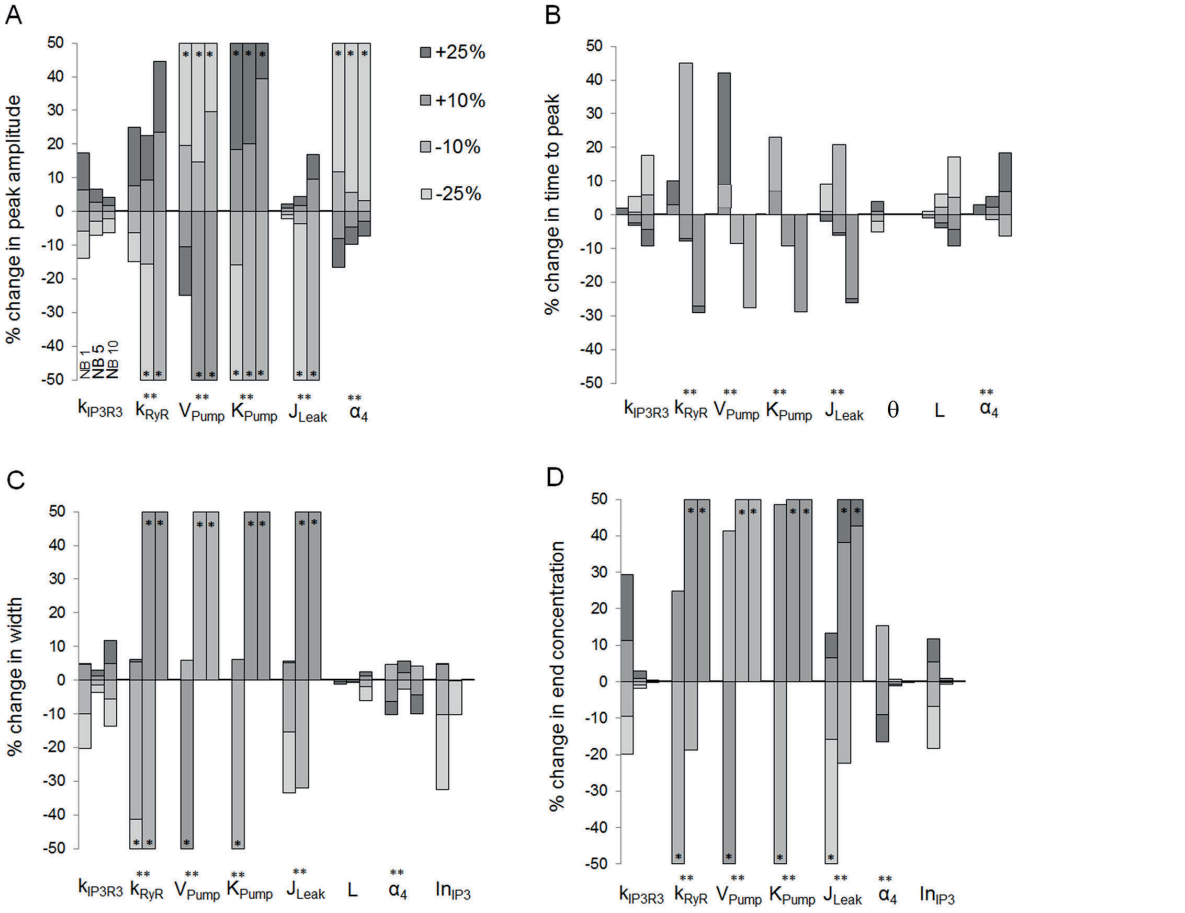

Fig 6. Sensitivity analysis of the model parameters. Percentage changes in Ca^{2+} wave (A) peak amplitude, (B) time to peak, (C) Ca^{2+} wave width at half maximum, and (D) end Ca^{2+} concentration at 90 seconds' time point due to changes in model parameters $k_{IP_3R_3}$, k_{RyR}, V_{Pump}, K_{Pump}, J_{Leak}, θ, L, α_4, In_{IP_3}, $In_{Ca^{2+}}$, D_{IP_3}, and $D_{Ca^{2+}}$ as marked in the x-axis. The analysis was carried out in NB layers NB1, NB5 and NB10 as denoted in (A) for parameter $k_{IP_3R_3}$. The amount of modification (-25%, -10%, +10% or +25%) is shown in the grayscale of the histogram. The histogram bar is marked with asterisk (*) if the change was greater than 50%, and with double asterisk (**) if parameter modification did not result typical Ca^{2+} waveform. Regarding each Ca^{2+} wave feature, the parameter is illustrated only if the change was more than 5%.

doi:10.1371/journal.pone.0128434.g006

ligand concentration (L) in turn decreased the time to peak (Fig 6B) and increased the Ca^{2+} wave width at half maximum (Fig 6C). The effects of the changes in IP_3 receptor phosphorylation rate (α_4) on Ca^{2+} wave features were complex: with decreasing α_4 Ca^{2+} wave peak amplitude increased (Fig 6A), time to peak decreased (Fig 6B), the Ca^{2+} wave width at half maximum increased or decreased depending on the NB layer (Fig 6C), and the end concentration increased (Fig 6D). The Ca^{2+} wave features were insensitive to gap junction related parameters $In_{Ca^{2+}}$, D_{IP_3} and $D_{Ca^{2+}}$ so that the tested modifications in their values resulted in less than 5% change in the features from the original conditions. Thus, they are not illustrated in Fig 6. However, increasing IP_3 input to NB1 via GJs (In_{IP_3}) increased the Ca^{2+} wave width at half maximum (Fig 6C) and end concentration (Fig 6D), and the sensitivity was significantly higher in NB1 layer than in the more distant NB layers. In general, the sensitivity of the model to the changes in tested parameters depended on the NB layer and thus on the distance to the MS cell. Few parameters, however, were independent of the location (parameters $k_{IP_3R_3}$, k_{RyR}, V_{Pump}, K_{Pump}, J_{Leak}), but changes in their values affected significantly the investigated Ca^{2+} wave features.

Possible suramin effect on attenuation of Ca^{2+} waves

Similarly to the general sensitivity analysis, the four Ca^{2+} wave features were compared between the experimental GA-treated and GA-suramin-treated data sets as well in NB1, NB5 and NB10 layers (Fig 7A). In the GA-suramin-treated data set, differences in peak amplitude were less than 10% compared to the GA-treated data set. However, time to peak decreased for NB1 and increased for NB5 and NB10 layers in the GA-suramin-treated data set. Furthermore, in this data set the Ca^{2+} wave width at half maximum and the end Ca^{2+} concentration were lower than in the GA-treated data set.

Since suramin is a known P_2 receptor blocker, we studied the sensitivity of the model to P_2Y_2 receptor parameters for the GA-treated data set (including model components I-V) by changing their values by ±25%. Similarly, G-protein cascade parameters were studied as well to consider the possible effect of suramin to disrupt the coupling between the receptor in the cell membrane and the G-protein. Our aim was to investigate the degree to which the observed differences in the Ca^{2+} wave features between GA-treated and GA-suramin-treated data sets could be accounted for by the changes in these parameters. The sensitivity analysis revealed that the modifications in P_2Y_2 unphosphorylated receptor dissociation constant (K_1) and P_2Y_2 receptor phosphorylation rate (k_p) indeed induced changes that were similar to the experimental observations (see Fig 7A): increase in K_1 modified the time to peak (Fig 7B) and increase in k_p narrowed the Ca^{2+} wave width at half maximum (Fig 7C). This would indicate disrupted ligand binding to the receptor or a higher phosphorylation rate of P_2Y_2 receptors as well as a faster desensitization of the receptors after ligand binding. P_2Y_2 receptor parameters K_2, k_r, k_e, ξ, on the contrary, had a negligible influence on Ca^{2+} wave behaviour: the modifications of these parameters by ±25% resulted only in less than 3% change on Ca^{2+} wave features, as was the case also for G-protein cascade parameter δ. G-protein cascade parameters G-protein activation rate (k_a) (Fig 7D) and G-protein deactivation rate (k_d) (Fig 7E) had diverse effects on the Ca^{2+} wave features: for example decreasing k_a and increasing k_d narrowed the Ca^{2+} wave width at half maximum in NB1 and NB5, but widened it in NB10. Thus, their behaviour did not follow the observations from the experimental data and therefore these factors were not considered to be responsible for the effects of suramin on the Ca^{2+} wave.

Fig 7F illustrates the fit of the model to the GA-suramin-treated data set after refitting the model parameters K_1 and k_p. The values of these parameters ranged as follows: K_1 values decreased from 8.83μM in NB1 to 5.15μM in NB10 and k_p values decreased from $0.19s^{-1}$ in NB1

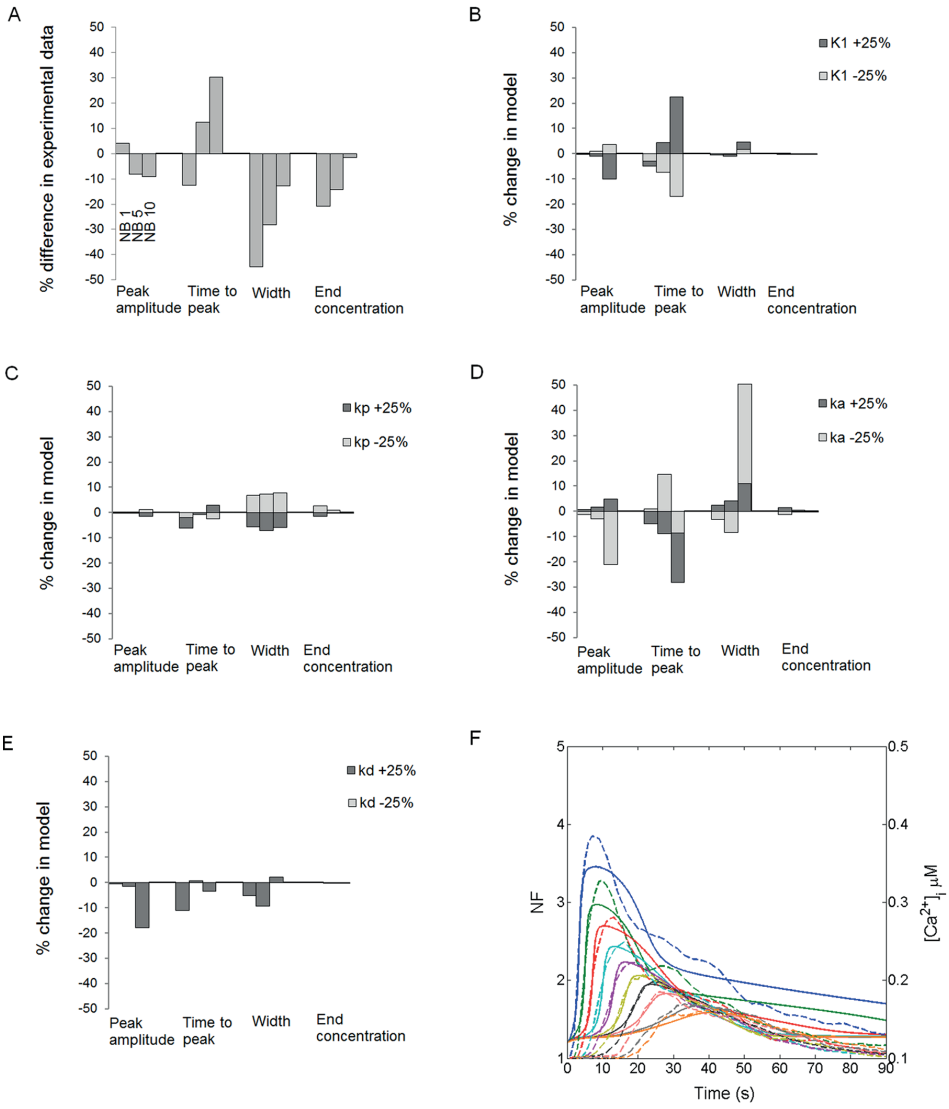

Fig 7. Suramin effects on Ca^{2+} wave. (A) Comparison of the peak amplitude, time to peak, Ca^{2+} wave width at half maximum, and end Ca^{2+} concentration at 90 seconds' time point in cell layers NB1, NB5 and NB10 between the experimental GA-treated and GA-suramin-treated data sets. The deviations of each Ca^{2+} wave feature in GA-suramin-treated data set from GA-treated data set are expressed as percentages. (B) Unphosphorylated P_2Y_2 receptor dissociation constant (K_1), (C) P_2Y_2 receptor phosphorylation rate (k_p), (D) G-protein activation rate (k_a), and (E) G-protein deactivation rate (k_d) were changed in the model for GA-treated data set either -25% or +25%, as denoted in the grayscale of the histogram, and the percentage change in each Ca^{2+} wave feature is illustrated. (F) Fitting of the model to the GA-suramin-treated data set. Dashed lines represent the data in dimensionless NF units, whereas solid lines represent the model simulations with arbitrary units representing $[Ca^{2+}]_i$ in μM concentrations. The uppermost curve pair (blue) represents NB1, the second uppermost NB2 (green), followed by NB3 (red), NB4 (light blue), NB5 (purple), NB6 (yellow), NB7 (black), NB8 (light red), NB9 (grey), and NB10 (orange).

doi:10.1371/journal.pone.0128434.g007

to $0.05s^{-1}$ in NB10. Overall, the values of K_1 and k_p were higher in the GA-suramin-treated data set than in the GA-treated data set. The simulated curves seem to fit well to the experimental data, except in NB1 layer at the end of the Ca^{2+} wave. In GA-suramin-treated data set, R^2 values were higher than 0.8 in NB1-NB7 and lower than 0.8 in NB8-NB10 (Table 4). 70% of the fits in GA-suramin-treated data set resulted in $R^2 > 0.8$ indicating that the model explains only partially the combined effect of GA and suramin on Ca^{2+} waves especially in the distant NB layers.

Discussion

The ARPE-19 cell line is an important biological model of human RPE despite its certain limitations [20]. This paper presents the first computational RPE model of Ca^{2+} signaling using the experimental data measured from the ARPE-19 monolayer after mechanical stimulation. We aimed to create a model that combines the most important Ca^{2+} signaling mechanisms in ARPE-19 cells so that the model can be used later in the development of more complicated RPE and epithelial models. Furthermore, the model was used to simulate and explain the Ca^{2+} signaling of epithelia, especially RPE, taking into account the following factors: 1) cells are on the monolayer; 2) they are connected to each other by GJs permeating Ca^{2+} and IP_3, and 3) the cells are most probably experiencing different stretching and chemical conditions depending on their distance from the mechanical stimulation site. To the best of our knowledge, this is the first time as Ca^{2+} signaling model has been implemented for the ARPE-19 monolayer. The model uses a set of location specific parameters including stretch, extracellular ligand concentration, and IP_3R_3 phosphorylation rate as well as the Ca^{2+} and IP_3 fluxes through GJs.

The identity of the extracellular ligand

The airway epithelium secretes the signal carriers ATP or UTP to the extracellular space in response to mechanical stimulation[16,36]. The connection of these ligands to Ca^{2+} signaling as extracellular signal mediators has been mathematically modeled[16]. It is likely that a similar function can be linked to ARPE-19 or RPE, where the ligand interacts with the cell membrane P_2Y_2 receptors. In our model, the ligand carried the signal in the extracellular space from the MS cell towards the distant NB cell layers after mechanical stimulation. According to our model, the extracellular ligand concentration decreased exponentially from NB1 towards NB10. We suggest, based on our modeling results, that the MS cell secretes ligand to the extracellular space. Epithelial cells such as ARPE-19 have been shown to secrete ATP under different stimuli[37,38]. On the other hand, the ligand degradation by ectonucleotidase activity[39] decrease the ligand concentration. The model predicts that the magnitude of the extracellular ligand concentration partly defines the nature of the cell response: higher and faster Ca^{2+} waves were observed with higher ligand concentrations. The ligand concentration was derived from diffusion equation, and the obtained exponential decay function fitted well to the experimental data. Experimental studies show that the Ca^{2+} wave peak amplitude value increases with increased ligand concentration in cultured human RPE[30] and in human airway epithelium[6]. Also, in the mathematical model of Warren et al. 2010[16], it was observed that the time to peak for human airway epithelium decreased as the ligand concentration increased. These observations are in good agreement with our model.

The role of IP_3 receptor phosphorylation rate

The phosphorylation of the IP_3 receptor represents an important regulatory mechanism for Ca^{2+} release[40–42]. It has been shown that the production of cyclic AMP (cAMP) through the

activation of the adenylyl cyclase pathway leads to the activation of protein kinase A that phosphorylates IP_3 receptors[43].

Our simulation results show that the maximal phosphorylation rate of IP_3R_3 (α_4) followed a shallow exponential, almost linear, increase from NB1 to NB10 in all three data sets. The parameter α_4 has previously been modeled as agonist specific only [22]. It is of note, however, that in addition to ATP or UTP and their interaction with P_2Y_2 receptors, also other types of ligand-receptor interactions may occur. One plausible explanation could be that MS cell secretes different types of ligands, because its cell membrane was broken in mechanical stimulation. This would further lead to complex biological interactions at the cellular level, which is seen as a chance of this parameter with cell location.

The need to model α_4 separately for the GA-treated data set and the control data set may be related to the functioning of the GJs, especially to their ability to alter ligand secretion in different cell types. Previous studies show that GJs participate in the regulation of the release of signaling molecules to the extracellular medium [44]. In astrocytes, as an example, GJs have been proposed to regulate the release of glutamate[45], an excitatory neurotransmitter and an important regulator of astrocyte Ca^{2+} oscillations[46].

Overall, α_4 parameter may reflect a number of ligands and cell mechanisms not modelled in this nor other epithelial Ca^{2+} models. The low α_4 values near the MS cell enable higher and faster Ca^{2+} waves at corresponding ligand concentrations compared to the distal cell layers, where higher levels of kinase activity attenuate and slow down the signal. This aligns well with the literature. In RPE, the addition of 8-Br-cAMP counteracted the elevation of $[Ca^{2+}]_i$ induced by connective tissue growth factor (CTGF)[47], and the cell migration inhibitor adrenomedullin increased intracellular cAMP and decreased $[Ca^{2+}]_i$[48]. The effect of the adenylyl cyclase pathway on IP_3R kinetics has been ignored in most of the previously published Ca^{2+} models e.g.[16,21,29], possibly because the kinase activity may not have been activated in those cell types or experimental conditions.

Gap junctions in Ca^{2+} wave propagation

GJs connect the adjacent cells together and allow the diffusion of signaling molecules between them. The diffusion through GJs has previously been modeled, for example, in airway epithelium[16]. In our model, GJs carried the Ca^{2+} signaling molecules between the NB layers based on the Ca^{2+} and IP_3 concentration gradients, and permeated Ca^{2+} and IP_3 selectively. As expected, NB layers near the MS cell were more sensitive to IP_3 input than the distant NB layers, and this was seen especially in the end Ca^{2+} concentration at 90 seconds' time point.

Possible Ca^{2+} wave attenuation mechanisms of suramin

In the GA-suramin-treated data set, the experimental data was reproduced in our model by increasing the unposphorylated receptor dissociation constant, which likely reflects disrupted ligand binding, and by increasing the phosphorylation rate of the P_2Y_2 receptors to enhance their desensitization. This may indicate that suramin targets on P_2Y_2 receptors as an unspecific P_2 receptor antagonist attenuating the Ca^{2+} wave. This intriguing model hypothesis driven from the model results needs to be confirmed experimentally. It is worth noting, however, that suramin has also been considered to disrupt the coupling between the receptor in the cell membrane and the G-protein by blocking the association of the G-protein α and $\beta\gamma$ subunits[33]. In our model, modifications in G-protein cascade parameters influenced the peak amplitude, time to peak and Ca^{2+} wave width at half maximum. Despite the observed diversity in their effects between the NB layers, it is possible that suramin targets the G-protein cascade as well, by acting as an attenuator of the Ca^{2+} wave.

Limitations of the model

Our work presents a computational model of epithelial Ca^{2+} signaling based on experimental work on the ARPE-19 cell line. This cell line is used extensively as a model of RPE, although it differs from it to some extent. The limitations of ARPE-19 compared to native human RPE arise, for example, from cell organization and metabolism[20]. Importantly for our study, ARPE-19 cell line in our experimental setup lacked pigmentation which resulted in a lack of the large Ca^{2+} stores, melanosomes, and needs to be taken into account when expanding our model to describe native RPE. In addition, we confirmed the polarity of the ARPE-19 monolayer with confocal microscopy. Trans-epithelial resistance (TER) that is a general measure of epithelial integrity was not measured due to technical challenges to perform the measurements on glass cover slips with our present equipment [49]. Nevertheless, the computational model created in this study describes the most important components of epithelial and ARPE-19 Ca^{2+} activity. Thus it provides a good basis to address the native RPE in the future, even though it, being based on an *in vitro* model of RPE, needs to be considered only as a model. To improve the model further, experimental data and model implementations on certain additional Ca^{2+} related mechanisms, such as P_2X receptors[50], voltage-sensitive Ca^{2+} channels[51] and Na^+/Ca^{2+} exchangers[52] would be well warranted. Finally, it is worth noting that the experimental work of Abu Khamidakh et al. 2013[5] did not produce absolute Ca^{2+} concentrations, and therefore our model also features only relative Ca^{2+} activity.

Conclusions

A full mathematical understanding of RPE and epithelial Ca^{2+} signaling would allow one to simulate cellular Ca^{2+} responses under several physiological, pathological, and experimental conditions. Our present model represents significant progress towards this goal since it is able to reproduce the experimental data from an RPE type epithelium, ARPE-19 cell line, in different conditions, simulate several epithelial Ca^{2+} signaling mechanisms, and predict drug responses in the epithelia. Our future work will include further development of the model especially focusing on the role of the voltage sensitive Ca^{2+} channels in the RPE.

Author Contributions

Conceived and designed the experiments: IV AA KJ SN JH. Performed the experiments: IV AA. Analyzed the data: IV AA SN. Contributed reagents/materials/analysis tools: IV AA HS JH. Wrote the paper: IV AA MP HS KJ JH SN.

References

1. Sanderson MJ, Charles AC, Boitano S, Dirksen ER. Mechanisms and function of intercellular calcium signaling. Mol Cell Endocrinol. 1994; 98: 173–187. PMID: 8143927
2. Konari K, Sawada N, Zhong Y, Isomura H, Nakagawa T, Mori M. Development of the blood-retinal barrier in vitro: Formation of tight junctions as revealed by occludin and ZO-1 correlates with the barrier function of chick retinal pigment epithelial cells. Exp Eye Res. 1995; 61: 99–108. PMID: 7556475
3. Wimmers S, Karl MO, Strauss O. Ion channels in the RPE. Prog Retin Eye Res. 2007; 26: 263–301. PMID: 17258931
4. Himpens B, Stalmans P, Gomez P, Malfait M, Vereecke J. Intra- and intercellular Ca2+ signaling in retinal pigment epithelial cells during mechanical stimulation. The FASEB Journal. 1999; 13: 63–68. PMID: 9872930
5. Abu Khamidakh AE, Juuti-Uusitalo K, Larsson K, Skottman H, Hyttinen J. Intercellular Ca2+ wave propagation in human retinal pigment epithelium cells induced by mechanical stimulation. Exp Eye Res. 2013; 108: 129–139. doi: 10.1016/j.exer.2013.01.009 PMID: 23352832

6. Hansen M, Boitano S, Dirksen ER, Sanderson MJ. Intercellular calcium signaling induced by extracellular adenosine 5′-triphosphate and mechanical stimulation in airway epithelial cells. Journal of Cell Science. 1993; 106: 995–1004. PMID: 8126116
7. Gelisken F, Inhoffen W, Partsch M, Schneider U, Kreissig I. Retinal pigment epithelial tear after photodynamic therapy for choroidal neovascularization. Am J Ophthalmol. 2001; 131: 518–520. PMID: 11292425
8. Garg S, Brod R, Kim D, Lane RG, Maguire J, Fischer D. Retinal pigment epithelial tears after intravitreal bevacizumab injection for exudative age-related macular degeneration. Clin Experiment Ophthalmol. 2008; 36: 252–256. doi: 10.1111/j.1442-9071.2008.01710.x PMID: 18412594
9. Singh RP, Sears JE. Retinal pigment epithelial tears after pegaptanib injection for exudative age-related macular degeneration. Am J Ophthalmol. 2006; 142: 160–162. PMID: 16815269
10. Rae Shi K. Revolution dawning in cardiotoxicity testing. Nature Reviews Drug Discovery. 2013; 12: 565–567. doi: 10.1038/nrd4083 PMID: 23903208
11. Sneyd J, Tsaneva-Atanasova K, Bruce JIE, Straub SV, Giovannucci DR, Yule DI. A model of calcium waves in pancreatic and parotid acinar cells. Biophys J. 2003; 85: 1392–1405. PMID: 12944257
12. Höfer T, Venance L, Giaume C. Control and plasticity of intercellular calcium waves in astrocytes: A modeling approach. The Journal of Neuroscience. 2002; 22: 4850–4859. PMID: 12077182
13. Wu D, Jia Y, Zhan X, Yang L, Liu Q. Effects of gap junction to Ca2+ and to IP3 on the synchronization of intercellular calcium oscillations in hepatocytes. Biophys Chem. 2005; 113: 145–154. PMID: 15617821
14. Rizzolo LJ. Development and role of tight junctions in the retinal pigment epithelium. Int Rev Cytol. 2007; 258: 195–234. PMID: 17338922
15. Appleby PA, Shabir S, Southgate J, Walker D. Cell-type-specific modelling of intracellular calcium signalling: A urothelial cell model. Journal of The Royal Society Interface. 2013; 10.
16. Warren NJ, Tawhai MH, Crampin EJ. Mathematical modelling of calcium wave propagation in mammalian airway epithelium: Evidence for regenerative ATP release. Experimental Physiology. 2010; 95: 232–249. doi: 10.1113/expphysiol.2009.049585 PMID: 19700517
17. Dunn KC, Marmorstein AD, Bonilha VL, Rodriguez-Boulan E, Giordano F, Hjelmeland LM. Use of the ARPE-19 cell line as a model of RPE polarity: Basolateral secretion of FGF5. Investigative Ophthalmology & Visual Science. 1998; 39: 2744–2749.
18. Glotin A, Debacq-Chainiaux F, Brossas J, Faussat A, Tréton J, Zubielewicz A, et al. Prematurely senescent ARPE-19 cells display features of age-related macular degeneration. Free Radical Biology and Medicine. 2008; 44: 1348–1361. doi: 10.1016/j.freeradbiomed.2007.12.023 PMID: 18226607
19. Yamamoto A, Akanuma S, Tachikawa M, Hosoya K. Involvement of LAT1 and LAT2 in the high- and low-affinity transport of L-leucine in human retinal pigment epithelial cells (ARPE-19 cells). J Pharm Sci. 2010; 99: 2475–2482. doi: 10.1002/jps.21991 PMID: 19890975
20. Ablonczy Z, Dahrouj M, Tang PH, Liu Y, Sambamurti K, Marmorstein AD, et al. Human retinal pigment epithelium cells as functional models for the RPE in vivo. Investigative Ophthalmology & Visual Science. 2011; 52: 8614–8620.
21. Lemon G, Gibson WG, Bennett MR. Metabotropic receptor activation, desensitization and sequestration—I: Modelling calcium and inositol 1,4,5-trisphosphate dynamics following receptor activation. J Theor Biol. 2003; 223: 93–111. PMID: 12782119
22. LeBeau AP, Yule DI, Groblewski GE, Sneyd J. Agonist-dependent phosphorylation of the inositol 1,4,5-trisphosphate receptor. The Journal of General Physiology. 1999; 113: 851–872. PMID: 10352035
23. Keizer J, Levine L. Ryanodine receptor adaptation and Ca2+(-)induced Ca2+ release-dependent Ca2+ oscillations. Biophys J. 1996; 71: 3477–3487. PMID: 8968617
24. Ahmado A, Carr A, Vugler AA, Semo M, Gias C, Lawrence JM, et al. Induction of differentiation by pyruvate and DMEM in the human retinal pigment epithelium cell line ARPE-19. Investigative Ophthalmology & Visual Science. 2011; 52: 7148–7159.
25. Dunn KC, Aotaki-Keen AE, Putkey FR, Hjelmeland LM. ARPE-19, a human retinal pigment epithelial cell line with differentiated properties. Exp Eye Res. 1996; 62: 155–170. PMID: 8698076
26. Peng S, Rahner C, Rizzolo LJ. Apical and basal regulation of the permeability of the retinal pigment epithelium. Investigative Ophthalmology & Visual Science. 2003; 44: 808–817.
27. Ross MH, Romrell LJ, Kaye GI. Histology a text and atlas. Baltimore: Lippincott Williams & Wilkins; 1995.
28. Feeney-Burns L, Hilderbrand ES, Eldridge S. Aging human RPE: Morphometric analysis of macular, equatorial, and peripheral cells. Investigative Ophthalmology & Visual Science. 1984; 25: 195–200.

29. Wang J, Huang X, Huang W. A quantitative kinetic model for ATP-induced intracellular oscillations. J Theor Biol. 2007; 245: 510–519. PMID: 17188305

30. Sullivan DM, Erb L, Anglade E, Weisman GA, Turner JT, Csaky KG. Identification and characterization of P2Y2 nucleotide receptors in human retinal pigment epithelial cells. J Neurosci Res. 1997; 49: 43–52. PMID: 9211988

31. Giancoli DC. Physics for scientists and engineers with modern physics (3rd edition): Prentice Hall; 2000.

32. Fall CP, Marland ES, Wager JM, Tyson JJ. Computational cell biology. New York: Springer; 2002.

33. Chung W, Kermode JC. Suramin disrupts receptor-G protein coupling by blocking association of G protein α and βγ subunits. Journal of Pharmacology and Experimental Therapeutics. 2005; 313: 191–198. PMID: 15626724

34. Hamill OP. Twenty odd years of stretch-sensitive channels. Pflugers Arch—Eur J Physiol. 2006; 453: 333–351.

35. Luo Y, Zhuo Y, Fukuhara M, Rizzolo LJ. Effects of culture conditions on heterogeneity and the apical junctional complex of the ARPE-19 cell line. Investigative Ophthalmology & Visual Science. 2006; 47: 3644–3655.

36. Homolya L, Steinberg TH, Boucher RC. Cell to cell communication in response to mechanical stress via bilateral release of atp and utp in polarized epithelia. The Journal of Cell Biology. 2000; 150: 1349–1360. PMID: 10995440

37. Reigada D, Mitchell CH. Release of ATP from retinal pigment epithelial cells involves both CFTR and vesicular transport. American Journal of Physiology—Cell Physiology. 2005; 288: C132–C140.

38. Mitchell CH. Release of ATP by a human retinal pigment epithelial cell line: Potential for autocrine stimulation through subretinal space. The Journal of Physiology. 2001; 534: 193–202. PMID: 11433002

39. Reigada D, Lu W, Zhang X, Friedman C, Pendrak K, McGlinn A, et al. Degradation of extracellular ATP by the retinal pigment epithelium. American Journal of Physiology—Cell Physiology. 2005; 289: C617–C624.

40. Chaloux B, Caron AZ, Guillemette G. Protein kinase A increases the binding affinity and the Ca2+ release activity of the inositol 1,4,5-trisphosphate receptor type 3 in RINm5F cells. Biology of the Cell. 2007; 99: 379–388. PMID: 17373911

41. Betzenhauser MJ, Fike JL, Wagner LE, Yule DI. Protein kinase A increases type-2 inositol 1,4,5-trisphosphate receptor activity by phosphorylation of serine 937. Journal of Biological Chemistry. 2009; 284: 25116–25125. doi: 10.1074/jbc.M109.010132 PMID: 19608738

42. Caron AZ, Chaloux B, Arguin G, Guillemette G. Protein kinase C decreases the apparent affinity of the inositol 1,4,5-trisphosphate receptor type 3 in RINm5F cells. Cell Calcium. 2007; 42: 323–331. PMID: 17320950

43. Wojcikiewicz RJH, Luo SG. Phosphorylation of inositol 1,4,5-trisphosphate receptors by cAMP-dependent protein kinase. Journal of Biological Chemistry. 1998; 273: 5670–5677. PMID: 9488697

44. Nielsen MS, Nygaard Axelsen L, Sorgen PL, Verma V, Delmar M, Holstein-Rathlou N. Gap junctions. 2012;Jul; 2(3): 1981–2035. doi: 10.1002/cphy.c110051 PMID: 23723031

45. Ye Z, Wyeth M, Baltan-Tekkok S, Ransom B. Functional hemichannels in astrocytes: A novel mechanism of glutamate release. J Neurosci. 2003;May 1; 23(9): 3588–3596. PMID: 12736329

46. De Pittà M, Goldberg M, Volman V, Berry H, Ben-Jacob E. Glutamate regulation of calcium and IP3 oscillating and pulsating dynamics in astrocytes. J Biol Phys. 2009; 35(4): 383–411. doi: 10.1007/s10867-009-9155-y PMID: 19669422

47. Guo C, Wang Y, Hu D, Han Q, Wang J, Hou X, et al. Modulation of migration and Ca2+ signaling in retinal pigment epithelium cells by recombinant human CTGF. Current Eye Research. 2009; 34:10: 852–862. doi: 10.3109/02713680903128935 PMID: 19895313

48. Huang W, Wang L, Yuan M, Ma J, Hui Y. Adrenomedullin affects two signal transduction pathways and the migration in retinal pigment epithelial cells. Investigative Ophthalmology & Visual Science. 2004; 45: 1507–1513.

49. Savolainen V, Juuti-Uusitalo K, Onnela N, Vaajasaari H, Narkilahti S, Suuronen R, et al. Impedance spectroscopy in monitoring the maturation of stem cell-derived retinal pigment epithelium. Annals of Biomedical Engineering. 2011; 39: 3055–3069. doi: 10.1007/s10439-011-0387-1 PMID: 21904797

50. Yang D, Elner SG, Clark AJ, Hughes BA, Petty HR, Elner VM. Activation of P2X receptors induces apoptosis in human retinal pigment epithelium. Investigative Ophthalmology & Visual Science. 2011; 52: 1522–1530.

51. Wimmers S, Halsband C, Seyler S, Milenkovic V, Strauss O. Voltage-dependent Ca2+ channels, not ryanodine receptors, activate Ca2+-dependent BK potassium channels in human retinal pigment epithelial cells. Mol Vis. 2008; 14: 2340–2348. PMID: 19096717

52. Loeffler KU, Mangini NJ. Immunohistochemical localization of na+/Ca2+ exchanger in human retina and retinal pigment epithelium. Graefe's Arch Clin Exp Ophthalmol. 1998; 236: 929–933. PMID: 9865624

53. Stalmans P, Himpens B. A decreased Ca2+-wave propagation is found among cultured RPE cells from dystrophic RCS rats. Investigative Ophthalmology & Visual Science. 1998; 39: 1493–1502.

54. Peterson WM, Meggyesy C, Yu K, Miller SS. Extracellular ATP activates calcium signaling, ion, and fluid transport in retinal pigment epithelium. The Journal of Neuroscience. 1997; 17: 2324–2337. PMID: 9065493

55. Maminishkis A, Jalickee S, Blaug SA, Rymer J, Yerxa BR, Peterson WM, et al. The P2Y2 receptor agonist INS37217 stimulates RPE fluid transport in vitro and retinal reattachment in rat. Investigative Ophthalmology & Visual Science. 2002; 43: 3555–3566.

56. Siefjediers A, Hardt M, Prinz G, Diener M. Characterization of inositol 1,4,5-trisphosphate (IP3) receptor subtypes at rat colonic epithelium. Cell Calcium. 2007; 41: 303–315. PMID: 16950509

57. Maranto AR. Primary structure, ligand binding, and localization of the human type 3 inositol 1,4,5-trisphosphate receptor expressed in intestinal epithelium. Journal of Biological Chemistry. 1994; 269: 1222–1230. PMID: 8288584

58. Sugiyama T, Yamamoto-Hino M, Wasano K, Mikoshiba K, Hasegawa M. Subtype-specific expression patterns of inositol 1,4,5-trisphosphate receptors in rat airway epithelial cells. Journal of Histochemistry & Cytochemistry. 1996; 44: 1237–1242.

59. Kennedy BG, Mangini NJ. Plasma membrane calcium-ATPase in cultured human retinal pigment epithelium. Exp Eye Res. 1996; 63: 547–556. PMID: 8994358

60. Stalmans P, Himpens B. Confocal imaging of Ca2+ signaling in cultured rat retinal pigment epithelial cells during mechanical and pharmacologic stimulation. Investigative Ophthalmology & Visual Science. 1997; 38: 176–187.

61. Shen J, Gimbrone MA Jr, Luscinskas FW, Dewey CF Jr. Regulation of adenine nucleotide concentration at endothelium-fluid interface by viscous shear flow. Biophys J. 1993; 64: 1323–1330. PMID: 8494987

62. Garrad RC, Otero MA, Erb L, Theiss PM, Clarke LL, Gonzalez FA, et al. Structural basis of agonist-induced desensitization and sequestration of the P2Y2 nucleotide receptor. Journal of Biological Chemistry. 1998; 273: 29437–29444. PMID: 9792648

63. Mahama PA, Linderman JJ. A monte carlo study of the dynamics of G-protein activation. Biophys J. 1994; 67: 1345–1357. PMID: 7811949

64. Fink CC, Slepchenko B, Loew LM. Determination of time-dependent inositol-1,4,5-trisphosphate concentrations during calcium release in a smooth muscle cell. Biophys J. 1999; 77: 617–628. PMID: 10388786

PUBLICATION III

Semi-Automatic Method for Ca^{2+} Imaging Data Analysis of Maturing Human Embryonic Stem Cells-Derived Retinal Pigment Epithelium

Abu Khamidakh, A.E., Santos, F.C.D., Skottman, H., Juuti-Uusitalo, K. & Hyttinen, J.

2016, Annals of Biomedical Engineering, Vol. 44(11), pp. 3408-3420
https://doi.org/10.1007/s10439-016-1656-9

Semi-automatic method for Ca^{2+} imaging data analysis of maturing human embryonic stem cells-derived retinal pigment epithelium

Amna E. Abu Khamidakh[1], Florentino Caetano dos Santos[1], Heli Skottman[2], Kati Juuti-Uusitalo[2], Jari Hyttinen[1]

1. Department of Electronics and Communications Engineering, Tampere University of Technology, BioMediTech, Biokatu 6, FM-1, 33520, Tampere, Finland.

2. University of Tampere, BioMediTech, Biokatu 12, FM-5, 33520, Tampere, Finland.

Abbreviated title: Ca^{2+} imaging of hESC-RPEs during maturation

Corresponding author (all stages of refereeing and publication): Amna E. Abu Khamidakh. Address: Biokatu 6, FM-1, 33520, Tampere, Finland; Tel: +358465451005; E-mail: amna.abukhamidakh@tut.fi

Corresponding author (post-publication): Jari Hyttinen. Address: Biokatu 6, FM-1, 33520, Tampere, Finland; Tel: +358408490020; E-mail: jari.hyttinen@tut.fi

Abstract and key terms

Ca^{2+} is a second messenger controlling vital cellular processes, including cell maturation. Changes in Ca^{2+} signaling during maturation of human embryonic stem cell-derived retinal pigment epithelial cells (hESC-RPE) have not been assessed previously. The aim of this study was to investigate maturation-dependent changes in transient intracellular Ca^{2+} ($[Ca^{2+}]_i$) increases in hESC-RPE. For this, we developed image analysis tools to evaluate cell-specific Ca^{2+} signals from the entire field of view. Spontaneous and mechanically induced transient $[Ca^{2+}]_i$ increases (STIs and MITIs) were analyzed in hESC-RPEs cultured for 9 (9d) or 28 (28d) days, altogether from more than 80.000 cells. Both cultures showed STIs: the longer culture time resulted in 2-fold increase of amount of cells with STIs. Mechanical stimulation induced intercellular Ca^{2+} waves in cells from both time points, but longer culture time reduced Ca^{2+} wave spreading. Depletion of intracellular Ca^{2+} stores decreased cell fraction with STIs and MITIs at both time points, and absence of extracellular Ca^{2+} had similar effect on cells with STIs. To conclude, hESC-RPE cells undergo significant Ca^{2+} signaling re-arrangements during a short maturation period increasing cell fraction with STIs, while decreasing coordinated cell response to mechanical stimulation. This knowledge and proposed analysis tools can be used for assessment of hESC-RPE maturation *in vitro*.

Key terms: hESC-RPE; intercellular calcium waves; mechanical stimulation; mechanically induced transient $[Ca^{2+}]_i$ increase; spontaneous transient $[Ca^{2+}]_i$ increase;

Abbreviations: spontaneous transient $[Ca^{2+}]_i$ increase – STI; mechanically induced transient $[Ca^{2+}]_i$ increase – MITI.

1. Introduction

The recently emerged technology of deriving cells from human pluripotent cells, including human embryonic stem cells (hESC), have provided a virtually unlimited supply of cells for transplantation purposes and *in vitro* drug-testing. Retinal pigment epithelial cells (RPE), a monolayer of cells critical for survival of eye photoreceptors, have been considered an excellent target for regenerative medicine approach in treating eye degenerative disorders, such as age-related macular degeneration.[3] Understanding of hESC-RPE maturation process *in vitro* is crucial for such applications.

Ca^{2+} is an important second messenger controlling vital cellular physiological processes, including cell differentiation and maturation. Increases of intracellular Ca^{2+} concentration ($[Ca^{2+}]_i$) are elementary events that provide this control.[29] Such $[Ca^{2+}]_i$ elevations exist in different time scales and may be restricted to a single cell or propagate between several cells, producing so -called Ca^{2+} waves, a phenomenon, where transient $[Ca^{2+}]_i$ increase that occurred in one cell propagates to neighboring cells. $[Ca^{2+}]_i$ elevations can activate signaling pathways in cytoplasm and nucleus stimulating or inhibiting gene expression and, thus, influence cell fate.[2] Transient increases of $[Ca^{2+}]_i$ can be spontaneous or occur as a result of various external stimulations, e.g., mechanically induced transient $[Ca^{2+}]_i$ increases (MITIs). Spontaneous transient increases of $[Ca^{2+}]_i$ (STIs) have been observed in many cell types, including smooth muscle cells[7], glia[18], cardiomyocytes[17], and neurons[4]. RPE cells from chicken embryos have been shown to exhibit STIs and spontaneous intercellular Ca^{2+} waves. The waves are mediated by ATP and spread between RPE

and neural retina, controlling proliferation and differentiation of retinal neural progenitor cells.[20,21]

Intercellular Ca^{2+} waves induced by mechanical stimulation have been detected in various cell types, for example, neurons[5], lens epithelial cells[6], corneal endothelial cells[8], as well as RPE cells[1,15]. Distinct Ca^{2+} dynamics at different differentiation stages has been shown in human osteoblasts[27], keratinocytes[9], neurons[22], chicken RPE[24] and other cell types[28]. Intercellular Ca^{2+} waves can propagate via two different routes: intracellularly via gap junctions (GJs), when signaling molecules pass from one cell to another through connexin channels, or via extracellular medium, involving, for example, activation of P2 receptors by ATP[2, 21].

Computational cell identification could allow fast and efficient assessment of Ca^{2+} signals in individual cells from the entire field of view. Usually, manual cell segmentation is used for analysis of single cell Ca^{2+} dynamics[1,8,21]. Automatic cell segmentation on fluorescent images is a challenging developing research area. It has been previously used to assess Ca^{2+} signals, for example, in brain cortex slices[19] and neuronal cell cultures[32]. For RPE cells, however, to the best of our knowledge, there are no such cell identification tools. Moreover, there are no studies on detection of STIs and MITIs in retinal pigment epithelial cells during maturation.

In this study, for the first time, we evaluated ability of hESC-RPE cells to trigger STIs and MITIs during maturation. We estimated fraction of cells in the monolayer with STIs and MITIs in pigmented hESC-RPEs at two different maturation stages. The Ca^{2+} dynamics was studied with live-cell Ca^{2+} imaging. We developed semi-automatic cell segmentation and Ca^{2+} dynamics analysis tools that allowed assessment of cell-

specific $[Ca^{2+}]_i$ increases in a whole field of view. In addition, localization of cell polarization-specific and mature RPE cell-specific proteins was evaluated with indirect immunofluorescence staining, gene expression was assessed with RT-PCR, and gap junctional functionality was estimated with scrape-loading/dye-transfer assay. The knowledge of Ca^{2+} dynamics alterations in hESC-RPE cell monolayers during maturation is important for better understanding of hESC-RPE physiology. Furthermore, it could facilitate development of new tools for assessment of hESC-RPE maturation status *in vitro.*

2. Materials and Methods

2.1. Differentiation of hESC-RPE Cells

In this study, we used hESC line Regea 08/023, which was derived and characterized in our laboratory at the University of Tampere, Finland, as described previously[25]. The hESC line was cultured on top of mitotically inactivated mitomycin (10 μg/ ml,Sigma-Aldrich, St. Louis, USA) treated human foreskin fibroblasts feeder cells (CRL-2429TM, ATCC, Manassas, VA, USA). The hESCs were cultured at 37°C and 5 % CO2 in hESC culture medium consisting of knock-out Dulbecco's Modified Eagle Medium (KO-DMEM) supplemented with 20% Knock-Out Serum Replacement (KO-SR), 2 mM Glutamax-I, 0.1 mM 2-mercaptoethanol (all from Life Technologies, Carlsbad, USA), 1% Non-Essential Amino Acids (NEAA), 50 U/ml Penicillin/Streptomycin (both from Lonza Group Ltd, Basel, Switzerland) and 8 ng/ml human basic fibroblast growth factor (bFGF,Peprotech, London, England). The culture medium was replenished five times a week and undifferentiated colonies were enzymatically passaged onto new feeder cells at ten-day intervals with TrypLE Select (Invitrogen, UK). The undifferentiated hESCs were induced to differentiate into RPE cells in suspension cultures in cell aggregates by reducing the KO-SR concentration to 15% and removing the bFGF. This medium is thereafter called RPEbasic[30]. Suspension cultured aggregates were matured for 49 to 147 days. The culture medium was replenished thrice in a week during that period. The pigmented areas of floating aggregates were manually selected, cut and dissociated with 1x Trypsin-EDTA (Lonza, Walkersville, USA)**.** The cells were filtered through a 100 μm BD Falcon cell strainer (BD Biosciences, San Jose, USA), and replated on human placental collagen IV (Col-IV; 5 $\mu g/cm^2$, Sigma-Aldrich) coated well-plate to expand cell

number. After expansion for 61 – 174 days, the hESC-RPEs were dissociated with 1x Trypsin-EDTA (Lonza) and cultured on Ormocomp-treated, Col-IV-coated coverslips. Culture time prior plating for experiments was in average 192 days (ranging from 110 to 296 days). This protocol has been previously used and determined to create mature and polarized RPE monolayers[16].

2.2. Cell Culturing for Experiments

For cell experiments, round 7 mm coverslips (Thermo Fisher Scientific, Inc., Leicestershire, UK) or square 13 mm coverslips (Zeiss, Jena, Germany) were treated with Ormocomp-I127 (Micro Resist Technology GmbH, Germany) and coated with Col-IV to enhance cell adherence and maturation, as described previously[16]. Mature hESC-RPE cells were seeded on Ormocomp-treated and Col-IV coated coverslips at a density of 10^5 cells/cm^2. Cells were cultured for a period of 9±1 (abbreviated further as 9d) or 28±1 (28d) days in RPEbasic medium. The medium was changed three times a week.

2.3. Media and Chemicals for Experiments

For Ca^{2+} imaging, we used extracellular HEPES-buffered salt solution (HBSS) containing (in mM): 137 NaCl, 5 KCl, 0.44 KH_2PO_4, 20 HEPES, 4.2 $NaHCO_3$, 5 glucose, 1.2 $MgCl_2$, 2 $CaCl_2$ (pH=7.37, osmolarity=335±5 mOsm/kg) (all components from Sigma-Aldrich). The pH and osmolarity were adjusted with 3 M NaOH and 2.5 M sucrose respectively.

To study the impact of extracellular Ca^{2+} on STIs and MITIs, the HBSS, excluding $CaCl_2$, was used. The effect of depletion of intracellular Ca^{2+} stores was studied by treating the cells with thapsigargin (2 μM, 10 min incubation, Sigma-Aldrich) [28]. The role of gap junctions (GJs) and P2 receptors was assessed with a GJ blocker 18-α-

glycyrrhetinic acid (18-α-GA; 30 μM, 30 min incubation; Sigma-Aldrich)[14] and a P2-receptor blocker suramin (50 μM, 30 min incubation; Sigma-Aldrich)[12]. 30 μM 18-α-GA was prepared from the stock solution of 18-α-GA in DMSO (Sigma-Aldrich). The control solution for this experiment contained an equal amount of DMSO.

All blocker solutions were based on HBSS. The blockers were maintained in the extracellular solution during the measurements to preserve their effect. Measurements were performed at room temperature (RT).

2.4. MITIs and STIs

For live-cell Ca^{2+} imaging experiments, hESC-RPE cells were loaded with Fluo-4-acetoxymethyl ester (Fluo-4 AM; 4 μM, 1 h incubation at RT, Life Technologies, Carlsbad, USA). The Fluo-4-AM dye was selected to be a Ca^{2+} indicator, as it has excitation maximum in the visible light range, which is less toxic for the cells than, for example, ultraviolet light. After dye loading, the cells were washed with HBSS thrice before adding the final volume of HBSS or modified HBSS, containing inhibitors. The coverslips were then mounted on a perfusion chamber (Warner Instruments, Hamden, USA) filled with HBSS and visualized with a 20x objective.

To induce a Ca^{2+} wave in a monolayer, mechanical stimulation of a single cell was done with a micropipette made from a glass capillary (Biomedical Instruments, Zöllnitz, Germany; 0.86 x 1.50 x 80mm) with a Narishige pipette puller. The micropipette was mounted on a Luigs & Neumann SM 5-9 vertical microinjection system (Luigs & Neumann, Ratingen, Germany) and intermittently lowered to touch a target cell membrane[1]. When the pipette touched cell surface, it resulted in temporary deformation of cell shape that was visible in the fluorescence light. If a cell membrane had been

damaged during the stimulation, the fluorescence dye leaked out of the stimulated cell by the end of the recordings.

Both STIs and MITIs were recorded with an Olympus IX51 fluorescence microscope (Olympus, Tokyo, Japan) and ANDOR iXion 885 camera (Oxford Instruments, Oxfordshire, UK). The dye was excited at 490 nm (bandwidth 15 nm) with Polychrome V (30% light intensity; TILL Photonics, Pittsburgh, USA) with an exposure time of 20 ms. Fluorescence emission was collected at 510-560 nm. The images were recorded at a rate of 2 frames per second with binning of 2x2 with Live Acquisition software v. 2.4.0.13 (FEI Munich GmbH). Time of recording was at least 5 min (600 frames). The corresponding bright field images were taken to assess cell morphology for each individual fluorescence time-series.

All experiments were performed at least 3 times. The average number of analyzed cells per field of view was 467±25 for 9d hESC-RPE and 606±15 for 28d hESC-RPE.

2.5. Data Analysis

Recorded images were processed offline with in-house Matlab (R2013A, MathWorks) algorithms and Fiji[23]. The detailed flow-chart with data analysis procedures is presented in **Figure 1**. For identification of cell centers, an averaged fluorescence image was created in Fiji, where each point in the resulting image was the mean of the values at that point in all the recorded time-series. Cell centers were detected from averaged fluorescence images with a Matlab in-house algorithm made for this purpose. The initial image was filtered to remove noise. Next, it was filtered by a morphological image opening with a disc-shaped kernel. Then, circular structures were detected with Matlabs' *imfindcircles* function, and the first set of cell centroids was extracted.

Additionally, Fourier transform and histogram equalization were performed to create two new images. These two images together with the initial image filtered for noise underwent a multi-threshold process, with a granularity of 0.05 in the 0 – 1 range. Next, cell centroids were extracted from these three images. Finally, unique center coordinates were derived from all four center coordinates lists. The automatically detected cell centers could be corrected manually at this stage. (**Supplementary data 1, Supplementary Matlab codes**) Coordinates of cell centers were exported into Fiji using a Balloon plugin[11], and cell boundaries were approximated as fixed-sized circles. For immature fusiform cells, cell segmentation was done manually in Fiji. An exemplary images before and after cell segmentation are presented in **Figure 2**. In Fiji, average fluorescence intensity of each cell was computed from the fluorescence time-series images at every recorded time point as mean value of pixels intensity in the cell area. In Matlab, the fluorescence curves were corrected for background, and the resulting curves were smoothened with a moving average algorithm (5 points span). Then, a baseline level was detected for each cell. Next, the fluorescence curves were corrected for bleaching and normalized to basal fluorescence value. Finally, fluorescence peaks were automatically detected. The threshold amplitude of peak detection was 10% higher than the basal fluorescence level. (**Supplementary data 2, Supplementary Matlab codes**)

To estimate the response to mechanical stimulation, we tracked cells participating in a mechanically induced Ca^{2+} wave. First, all cells in the field of view with at least one fluorescence peak were identified. Next, time difference between fluorescence peaks and distance between cell centers were computed. Finally, cell pairs with time difference

between peaks of less than 4 s, and distance between cells of less than 2 characteristic cell diameters were identified. Both cells from such selected pairs were considered to be involved in a Ca^{2+} wave. (**Supplementary data 3, Supplementary Matlab codes**) The extent of Ca^{2+} wave propagation was characterized by the percentage of responsive cells (RC_{ms}) in the field of view – the fraction of cells exhibiting MITIs.

In experiments with STIs recordings, the behavior of cellular monolayer was characterized by the percentage of cells exhibiting STIs (RC_{sp}) in the field of view and by number of peaks per cell (PPC). PPC_n – the percentage of responsive cells with *n* peaks – was calculated as the number of cells that had *n* peaks in their fluorescence curve divided by the total number of responsive cells in the field of view during a 5 min measurement. Spontaneously arising Ca^{2+} waves were tracked using the same algorithm as for detection of mechanically induced Ca^{2+} waves.

In experiments with drug treatments, RC_{sp} and RC_{ms} values for each treatment dataset were normalized to respective values in control measurements.

To test the predictability of activity peak occurrence in a cell monolayer, a correlation coefficient between δT (time difference between peaks in a pair of cells) and δL (distance between centers in a pair of cells) variables was calculated in Matlab. The results are expressed as mean ± standard error of mean.

2.6. Scrape-loading and Dye-transfer Assay

GJ functionality and blockade properties of 18-α-GA were assessed with scrape-loading and dye-transfer assay[10]. To perform this assay, the cells are scraped with a scalpel in presence of fluorescence dye that can pass through GJs, but cannot pass through cell

plasma membrane. The cells with damaged membrane uptake the dye and transfer it further to the intact cell layers via GJs, if GJs are functional.

In our control culture, the medium was removed, and cells were rinsed with Dulbecco's PBS (DPBS, Lonza). In the GJ blocking assessment, cells were preincubated with 18-α-GA (Sigma-Aldrich) similarly to Ca^{2+} imaging experiments. The Alexa Fluor 568 hydrazide (1:1000, Invitrogen, Carlsbad, USA) that can pass through GJs[31] was dissolved in DPBS, and added to the cells. Thereafter, an artificial gap between the cells was created with a scalpel, the cells were incubated with the dye for 15 min at RT, and rinsed with DPBS several times. The samples were visualized immediately with a fluorescent microscope (Olympus IX51) using a 10x air objective. Experiments were repeated at least twice.

2.7. Immunofluorescence Staining

Localization of GJ-forming Connexin 43 (Cx43), RPE cell-specific cellular Retinaldehyde-binding Protein (CRALBP) and tight junction-forming Zona Occludens Protein 1 (ZO-1) were assessed with indirect immunofluorescence labeling[1]. The list of the used primary and secondary antibodies is represented in **Table 1**. Images were taken with the Olympus IX51 microscope with a 20x air objective.

2.8. RT-PCR Analysis

After the Ca^{2+} imaging recordings, the total RNA was extracted with a NucleoSpin XS-kit (Macherey-Nagel, GmbH & Co, Düren, Germany) to verify the maturation status of used samples. For the RNA extraction, five separate 9d cultured samples and four separate 28d samples were pooled together to increase the RNA yield. The mRNA extraction and

RT-PCR analysis was done as described previously[26]. Annealing temperatures and used primers are presented in **Table 2**.

2.9. Cell Viability Test

Cell viability was assessed in hESC-RPE cells under control conditions and after drug treatments used in Ca^{2+} imaging experiments with Live/Dead Viability/Cytotoxicity kit for Mammalian cells (Invitrogen). Briefly, the cells were rinsed with DPBS and incubated with a mixture of 0.25 μM Calcein-AM and 0.5 μM ethidium homodimer-1 for 30 min at RT. A fluorescence microscope Olympus IX51 was used to register viable cells with green fluorescence and dead cells with red fluorescence with a 20x air objective. These experiments were performed at least twice.

2.10. Ethical Issues

BioMediTech at University of Tampere has the approval of the National Authority for Medicolegal Affairs Finland (TEO) to study human embryos (Dnro 1426/32/300/05) and a supportive statement of the Ethical Committee of the Pirkanmaa Hospital District to derive, culture, and differentiate hESC lines from surplus human embryos (R05116). No new lines were derived for this study.

2.11. Statistics

Two-sample Kolmogorov-Smirnov test was used to determine statistical significance between the RC_{sp} or RC_{ms} in different groups. $P<0.05$ was considered statistically significant.

3. Results

3.1. Morphology of 9d and 28d Cultured hESC-RPEs

Brightfield microscopy showed a clear difference in the morphology of 9d and 28d cultured cells. After 9 days of culture, cells had elongated fusiform morphology and low pigmentation (**Fig. 3A**). After 28 days of culture, hESC-RPEs acquired predominantly more compacted cobblestone morphology and more intense pigmentation (**Fig. 3B**). The indirect immunofluorescence staining showed that both 9d and 28d cultured cells were Cx43-, CRALBP- and ZO1-positive. However, 28d cultured cells had more prominent localization of these proteins on cell edges compared to 9d cultured hESC-RPEs (**Fig. 3C-F**).

The differentiation status of cells was evaluated with the RT-PCR. There, the Oct3/4, a pluripotency gene and a marker of undifferentiated hESC, was not expressed (**Fig. 3G**). MITF and tyrosinase were expressed in samples from both time points, verifying the maturation of hESC-RPE cells.

3.2. STIs in 9d and 28d Cultured hESC-RPEs

Both 9d and 28d cultured hESC-RPEs exhibited STIs. 28d cultured cells had 2.3-fold higher RC_{sp} (RC_{sp}=28±3%) compared to 9d cultured cells (RC_{sp}=12±2%; p <0.01) in control conditions (**Fig. 4A, S.video 1**). In cells of both ages, the majority of cells exhibiting STIs had one peak per cell during a 5 min period (PPC_1=67±2% in 9d, PPC_1=58±3% in 28d cultured cells). Longer culture time (35d cultured hESC-RPE) did not affect RC_{sp}. (**Supplementary Data 4, S. Fig. 6A**)

STIs were usually limited to one cell and in rare cases propagated to few neighboring cells. In 9d cultured cells, spontaneous Ca^{2+} waves, which involved 6±2% of cells with

STIs, were observed in 11 experiments out of 20. In these experiments, spontaneous Ca^{2+} waves propagated in small cell clusters (4±1 clusters/field of view in the 5 min measurement) consisting of 2.3±0.1 cells/cluster. In 28d cultured cells, small spontaneous Ca^{2+} waves, which involved 7.5±0.9% of cells with STIs, were detected in all 13 performed experiments. The waves propagated in cell clusters (7±1 clusters/ field of view in the 5 min measurement) consisting of 2.4±0.1 cells/cluster.

STIs occurred in randomly distributed cells. For 28d cultured cells, where RC_{sp} was the highest, correlation coefficient between time of peak occurrence and distance between cells was close to zero (-0.005 ± 0.003).

To investigate the contribution of extracellular Ca^{2+} to STIs, we performed experiments in Ca^{2+}-free medium. Following the removal of extracellular Ca^{2+}, RC_{sp} had a 2.3-fold decrease (p<0.05) in 9d cultured cells (**Fig. 4B**), while in 28d cultured cells STIs were almost completely abolished (p <0.01; **Fig. 4C**).

The involvement of intracellular Ca^{2+} stores in STIs was studied by depleting intracellular Ca^{2+} stores with thapsigargin. This drastically decreased (by 98%, p<0.05, for 9d cultured cells and by 96%, p<0.01, for 28d cultured) RC_{sp} in cells from both time points (**Fig. 4B, C**).

The necessity of GJs and P2 receptors was assessed by applying 18-α-GA or suramin to the cells to block GJs and P2 receptors respectively. RC_{sp} had high variations in different biological replicates. However, in average, these treatments did not lead to significant changes in RC_{sp} neither in 9d, nor in 28d cultured cells (**Fig. 4B, C**). DMSO, that was used to make a stock solution of 18-α-GA, did not affect RC_{sp}. (**Fig. 4B, C**)

3.3. MITIs in 9d and 28d Cultured hESC-RPEs

Mechanical stimulation of a single cell resulted in a MITI that propagated as a wave from the stimulated cell to neighboring cells. (**Fig. 5, S.video 2**) In 9d cultured hESC-RPEs, mechanically induced Ca^{2+} waves spread farther from the stimulation site (RC_{ms}=42±5%) than in 28d cultured hESC-RPEs (RC_{ms}=10±3%; p<0.001), as shown in **Figure 6A**. In 28d cultured cells, the occurrence and extent of waves depended on cell size variation around the site of mechanical stimulation. (**S. Fig. 4**) Longer culture time (35d cultured hESC-RPE) did not affect RC_{ms}. (**Supplementary Data 4, S. Fig. 6B**)

To expose the source of Ca^{2+} for MITIs, we performed mechanical stimulation in Ca^{2+}-free conditions and after depleting of intracellular Ca^{2+} stores with thapsigargin. Absence of extracellular Ca^{2+} did not affect RC_{ms} neither in 9d, nor in 28d cultured cells. The depletion of Ca^{2+} from endoplasmic reticulum inhibited Ca^{2+} wave propagation, reducing RC_{ms} by 95% (p<0.01) in 28d cultured cells and by 67% (p<0.05) in 9d cultured hESC-RPEs. (**Fig. 6B, C**)

Blockade of P2 receptors with suramin reduced RC_{ms} by 19% (p<0.05) in 9d cultured cells, while having no effect on 28d hESC-RPEs. Blockade of GJs with 18-α-GA did not affect RC_{ms} neither in 9d, nor in 28d cultured hESC-RPEs.

3.4. GJ Functionality

When the GJ functionality was inspected with scrape-loading/dye-transfer assay, both 9d and 28d cultured hESC-RPEs transferred hydrazide dye to cells located farther away from a cell-free lane, suggesting the presence of functional GJs (**Fig. 7A, C**). The dye transfer was inhibited with 18-α-GA (**Fig. 7B, D**).

3.5. Cell Viability

The cell viability or the number of dead cells was not affected by the drugs used in this study, as was shown with microscopic observation. (**Fig. 8**)

4. Discussion

Maturation is a complex process controlled by various factors. However, little is known about alterations of Ca^{2+} signaling during maturation. The knowledge of Ca^{2+} dynamics in RPE cells at different maturation stages could provide new insights for better assessment of RPE maturation *in vitro*.

In this study, we have detected STIs and MITIs in hESC-RPEs from thousands of cells with in-house analysis tools made for this purpose. For cell identification, we have used our semi-automatic tool. We automatically detected hESC-RPE cell centers from the cells with cobblestone morphology. Furthermore, the approximation of cells masks as fixed-size circles was successful to match cell shapes. For hESC-RPE cells with fusiform morphology, where cell shapes varied a lot, cell segmentation was done manually to properly identify cell area for analysis of Ca^{2+} dynamics. The automatized cell identification and fluorescence curves analysis allowed us to calculate the percentage of responsive cells taking into account the majority of cells in the field of view, altogether more than 80.000 cells.

STIs have been previously observed in RPE cells of developing chicken embryo[20]. There, STIs of RPE have been shown to control proliferation and differentiation of retinal neural progenitor cells.[20,21] Our data demonstrates single cell STIs in 9d and 28d cultured hESC-RPE cells. Furthermore, we have shown for the first time that longer hESC-RPE culture time increases percentage of cells exhibiting STIs. Our analysis shows that these cells are randomly distributed and are not dependent on activity of neighboring cells.

According to the literature, the source of Ca^{2+} for STIs is controversial: the smooth muscles cells recruit Ca^{2+} from both intracellular Ca^{2+} stores and extracellular Ca^{2+} [7], while in developing chick retina STIs rely mostly on extracellular Ca^{2+} [4]. Our cells from both time points require Ca^{2+} from intracellular Ca^{2+} stores and extracellular Ca^{2+} to trigger a STI.

GJ blockers 18-α-GA, carbenoxolone and retinoic acid in chick embryo RPE[20] and octanol in chick embryo retina[4] inhibit spontaneous intercellular Ca^{2+} waves, while not affecting STIs in single cells[20]. In line with the latter, in our experiments, blockade of GJs did not affect single cell STIs neither in 9d, nor in 28d cultured cells. Results, thus, indicate that the hESC-RPE cells have inherent ability to trigger their own STIs.

The blockade of P2 receptors in chick embryo has been shown to reduce the frequency of spontaneous intercellular Ca^{2+} waves, having no effect on single cell STIs[21]. In our hESC-RPEs, the blockade of P2 receptors did not affect the percentage of the cells having STIs neither in 9d, nor in 28d cultured cells. This indicates that hESC-RPE cells do not require activation of P2 receptors by extracellular ligands to trigger STIs, and the STIs are controlled by other mechanisms that remain to be explicated in further studies.

Our experiments with hESC-RPEs show a radical difference in responses of 9d and 28d cultured cells to a mechanical stimulation: 9d cultured cells responded with wide-spreading intercellular Ca^{2+} waves, while 28d cultured cells did not respond to this stimulation at all, or gave rise to small intercellular Ca^{2+} waves. In our earlier study, we have shown that mechanical stimulation induces wide-spreading intercellular Ca^{2+} waves in immortalized human RPE cell line ARPE-19[1]. In our hands, the morphology of ARPE-19 cells resembles the morphology of 9d cultured hESC-RPEs, and the waves

observed in 9d cultured hESC-RPEs were similar to those in ARPE-19, spreading far from the site of mechanical stimulation.

In rat RPE, the mechanical stimulation induced small intercellular Ca^{2+} waves spreading up to 2-3 cell tiers away from the stimulation site[13,15]. These findings are similar to our observations in 28d cultured hESC-RPEs. In rare cases, when the cells varied in size, and cobblestone morphology was not homogenous, mechanical stimulation resulted in wide-spreading Ca^{2+} waves. This diversity of responses might be due to moderate heterogeneity in maturation status of 28d cultured cells in the vicinity of mechanical stimulation site. When the cells had uniform cobblestone morphology with compacted cells, we could observe minor intercellular Ca^{2+} waves limited to few cells or no response at all. According to our knowledge, there have been no studies, where the correlation between RPE cell organization and calcium signaling in human retinal development has ever been assessed.

Previously, rat RPE has been reported to recruit extracellular Ca^{2+} in response to mechanical stimulation that is followed by Ca^{2+} release from intracellular Ca^{2+} stores[15]. In ARPE-19 cells, mechanically induced Ca^{2+} waves have been constrained by depletion of intracellular Ca^{2+} stores, while absence of extracellular Ca^{2+} has not been able to inhibit them[1]. In our 9d cultured hESC-RPEs, mechanically induced Ca^{2+} waves could not be completely blocked neither by depletion of intracellular Ca^{2+} stores, nor by extracellular Ca^{2+} removal. This data suggests that 9d cultured hESC-RPEs may use an alternative source of intracellular Ca^{2+} for MITIs, which needs to be elucidated in further studies. In 28d cultured hESC-RPEs, the residual Ca^{2+} waves relied on intracellular Ca^{2+} stores, but not on extracellular Ca^{2+}.

Blockade of GJs in rat RPE has been shown to inhibit mechanically induced Ca^{2+} waves by decreasing the amplitude of MITIs and the distance of wave spreading[15]. In ARPE-19 cells, it decreased the amplitude of MITIs, but not the distance of wave spreading[1]. Our 9d and 28d cultured hESC-RPEs expressed Cx43 and, according to the scrape-loading/dye-transfer assay, had functional GJs. The 18-α-GA did not alter the wave spreading after mechanical stimulation, suggesting that it is not dependent on GJs in hESC-RPEs.

Previously, we have shown that suramin reduces the distance of Ca^{2+} wave spreading in ARPE-19 cells[1]. Similar effects have been observed in spontaneous Ca^{2+} waves in developing chick RPE[21]. Here, in hESC-RPEs, suramin had a partial inhibitory effect on Ca^{2+} wave spreading in 9d cultured cells, indicating that P2 receptors may participate in Ca^{2+} wave spreading. Because suramin could not fully inhibit Ca^{2+} wave propagation, it is possible that other paracrine factors, such as NO or Ca^{2+} itself, contribute to mechanically induced Ca^{2+} wave spreading.

We show that hESC-RPE cells undergo drastic changes in Ca^{2+} activity during a short culture period. For the first time, our experiments demonstrate that during maturation, hESC-RPE cells increase their ability to spontaneously elevate $[Ca^{2+}]_i$, while losing their ability to propagate intercellular Ca^{2+} waves in response to mechanical stimulation. This knowledge and the simple tools and parameters presented in this study (RC_{sp} and RC_{ms}) could offer an additional method to estimate maturation status of hESC-RPE cells.

5. Acknowledgements

This work was supported by the Finnish Funding Agency for Technology and Innovation, Health Research Council of the Academy of Finland (grant numbers 252225, 218050 and 137801) and Tampere University of Technology President's Doctoral Program. The funders had no role in study design, data collection and analysis, decision to publish, or preparation of the manuscript. Outi Melin, Outi Heikkilä and Hanna Pekkanen are thanked for excellent technical assistance.

6. References

1. Abu Khamidakh, A.E., K. Juuti-Uusitalo, K. Larsson, H. Skottman, and J. Hyttinen. Intercellular Ca^{2+} wave propagation in human retinal pigment epithelium cells induced by mechanical stimulation. Exp Eye Res. 108:129-139, 2013.

2. Berridge, M., P. Lipp, and M. Bootman. The versatility and universality of calcium signaling. Nat. Rev. Mol. Cell Biol. 1:11-21, 2000.

3. Carr, A-J. F., M. J. K. Smart, C. M. Ramsden, M. B. Powner, L. da Cruz, and P.J. Coffey. Development of human embryonic stem cell therapies for age-related macular degeneration. Trends NeuroSci. 36:385-395, 2013.

4. Catsicas, M., V. Bonness, D. Becker, and P. Mobbs. Spontaneous Ca^{2+} transients and their transmission in the developing chick retina. Curr. Biol. 8:283-288, 1998.

5. Charles, A. C., S. K. Kodali, and R. F. Tyndale. Intercellular calcium waves in neurons. Mol. Cell. Neurosci. 7:337-353, 1996.

6. Churchill, G. C., M. M. Atkinson, and C. F. Louis. Mechanical stimulation initiates cell-to-cell calcium signaling in ovine lens epithelial cells. J. Cell Sci. 109:355-365, 1996.

7. Dabertrand, F., J. Mironneau, N. Macrez, and J. Morel. Full length ryanodine receptor subtype 3 encodes spontaneous calcium oscillations in native duodenal smooth muscle cells. Cell Calcium 44:180-189, 2008.

8. D'hondt, C., R. Ponsaerts, S. P. Srinivas, J. Vereecke, and B. Himpens. Thrombin inhibits intercellular calcium wave propagation in corneal endothelial cells by modulation of hemichannels and gap junctions. Invest. Ophthalmol. Vis. Sci. 48:120-133, 2007.

9. D'Souza, S. J. A., A. Pajak, K. Balazsi, and L. Dagnino. Ca^{2+} and BMP-6 signaling regulate E2F during epidermal keratinocyte differentiation. J. Biol. Chem. 276:23531-23538, 2001.

10. El-Fouly, M. H., J. E. Trosko, and C. Chang. Scrape-loading and dye transfer: A rapid and simple technique to study gap junctional intercellular communication. Exp. Cell Res. 168:422-430, 1987.

11. Federici, F., L. Dupuy, L. Laplaze, M. Heisler, and J. Haseloff. Integrated genetic and computation methods for in planta cytometry. Nat. Meth. 9:483-485, 2012.

12. Frame, M. K., and A. W. de Feijter. Propagation of mechanically induced intercellular calcium waves via gap junctions and ATP receptors in rat liver epithelial cells. Exp. Cell Res. 230:197-207, 1997.

13. Gomes, P., M. Malfait, B. Himpens, and J. Vereecke. Intercellular Ca^{2+}-transient propagation in normal and high glucose solutions in rat retinal epithelial (RPE-J) cells during mechanical stimulation. Cell Calcium 34:185-192, 2003.

14. Guo, Y., C. Martinez-Williams, K. A. Gilbert, and D. E. Rannels. Inhibition of gap junction communication in alveolar epithelial cells by 18α-glycyrrhetinic acid. Am. J. Physiol. Lung Cell Mol. Physiol. 276:1018-1026, 1999.

15. Himpens, B., P. Stalmans, P. Gomez, M. Malfait, and J. Vereecke. Intra- and intercellular Ca^{2+} signaling in retinal pigment epithelial cells during mechanical stimulation. FASEB J. 13:63-68, 1999.

16. Käpylä, E., A. Sorkio, S. Teymouri, K. Lahtonen, L. Vuori, M. Valden, H. Skottman, M. Kellomäki, and K. Juuti-Uusitalo. Ormocomp-modified glass increases collagen

binding and promotes the adherence and maturation of human embryonic stem cell-derived retinal pigment epithelial cells. Langmuir 30:14555-14565, 2014.
17. Lukyanenko, V., and S. Györke. Ca^{2+} sparks and Ca^{2+} waves in saponin-permeabilized rat ventricular myocytes. J. Physiol. (Lond.) 521:575-585, 1999.
18. Mathiesen, C., A. Brazhe, K. Thomsen, and M. Lauritzen. Spontaneous calcium waves in Bergman glia increase with age and hypoxia and may reduce tissue oxygen. J. Cereb. Blood Flow Metab. 33:161-169, 2013.
19. Mukamel, E. A., A. Nimmerjahn, and M. J. Schnitzer. Automated analysis of cellular signals from large-scale calcium imaging data. Neuron 63:747-760, 2009.
20. Pearson, R. A., M. Catsicas, D. L. Becker, P. Bayley, N. L. Lüneborg, and P. Mobbs. Ca^{2+} signalling and gap junction coupling within and between pigment epithelium and neural retina in the developing chick. Eur. J. Neurosci. 19:2435-2445, 2004.
21. Pearson, R. A., N. Dale, E. Llaudet, and P. Mobbs. ATP released via gap junction hemichannels from the pigment epithelium regulates neural retinal progenitor proliferation. Neuron 46:731-744, 2005.
22. Resende, R. R., A. S. Alves, L. R. G. Britto, and H. Ulrich. Role of acetylcholine receptors in proliferation and differentiation of P19 embryonal carcinoma cells. Exp. Cell Res. 314:1429-1443, 2008.
23. Schindelin, J., I. Arganda-Carreras, E. Frise, V. Kaynig, M. Longair, T. Pietzsch, S. Preibisch, C. Rueden, S. Saalfeld, B. Schmid, J. Tinevez, D. J. White, V. Hartenstein, K. Eliceiri, P. Tomancak, and A. Cardona. Fiji: an open-source platform for biological-image analysis. Nat. Meth. 9:676-682, 2012.

24. Sekiguchi-Tonosaki, M., M. Obata, A. Haruki, T. Himi, and J. Kosaka. Acetylcholine induces Ca^{2+} signaling in chicken retinal pigmented epithelial cells during dedifferentiation. Am. J. Physiol., Cell Physiol. 296:1195-1206, 2009.

25. Skottman, H. Derivation and characterization of three new human embryonic stem cell lines in Finland. In Vitro Cell. Dev. Biol. Anim. 46(3-4):206-9, 2010.

26. Sorkio, A., P. J. Porter, K. Juuti-Uusitalo, B. Meenan, H. Skottman, and G. Burke. Surface modified biodegradable electrospun membranes as a carrier for human embryonic stem cell derived retinal pigment epithelial cells. Tissue Eng. Part A 21:2301-2314, 2015.

27. Sun, S., Y. Liu, S. Lipsky, and M. Cho. Physical manipulation of calcium oscillations facilitates osteodifferentiation of human mesenchymal stem cells. FASEB J. 21:1472-1480, 2007.

28. Thastrup, O., P. J. Cullen, B. K. Drøbak, M. R. Hanley, and A. P. Dawson. Thapsigargin, a tumor promoter, discharges intracellular Ca^{2+} stores by specific inhibition of the endoplasmic reticulum Ca^{2+}-ATPase. Proc. Natl. Acad. Sci. 87:2466-2470, 1990.

29. Tonelli, F. P., A. Santos, D. Gomes, S. da Silva, K. Gomes, L. Ladeira, and R. Resende. Stem Cells and Calcium Signaling. Adv. Exp. Med. Biol. 740: 891–916, 2012.

30. Vaajasaari, H., T. Ilmarinen, K. Juuti-Uusitalo, K. Rajala, N. Onnela, S. Narkilahti, R. Suuronen, J. Hyttinen, H. Uusitalo, and H. Skottman. Toward the defined and xeno-free differentiation of functional human pluripotent stem cell–derived retinal pigment epithelial cells. Mol. Vis. 17:558-575, 2011.

31. Weber, P. A., H. Chang, K. E. Spaeth, J. M. Nitsche, and B. J. Nicholson. The permeability of gap junction channels to probes of different size is dependent on connexin composition and permeant-pore affinities. Biophys. J. 87:958-973, 2004.
32. Wong, L. C., B. Lu, K. W. Tan, and M. Fivaz. Fully-automated image processing software to analyze calcium traces in populations of single cells. Cell Calcium 48:270–274, 2010.

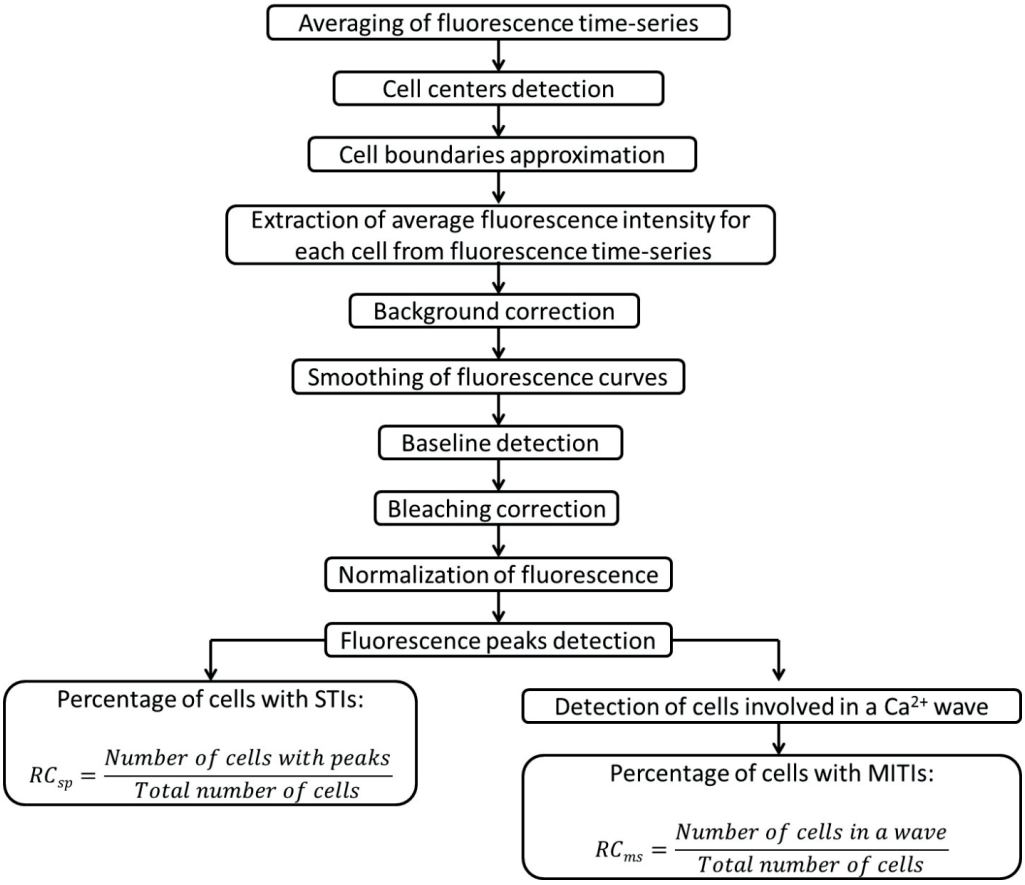

Fig. 1: Image analysis flow chart for semi-automatic cell detection in the fluorescence images and analysis of fluorescence kinetics from these cells**.**

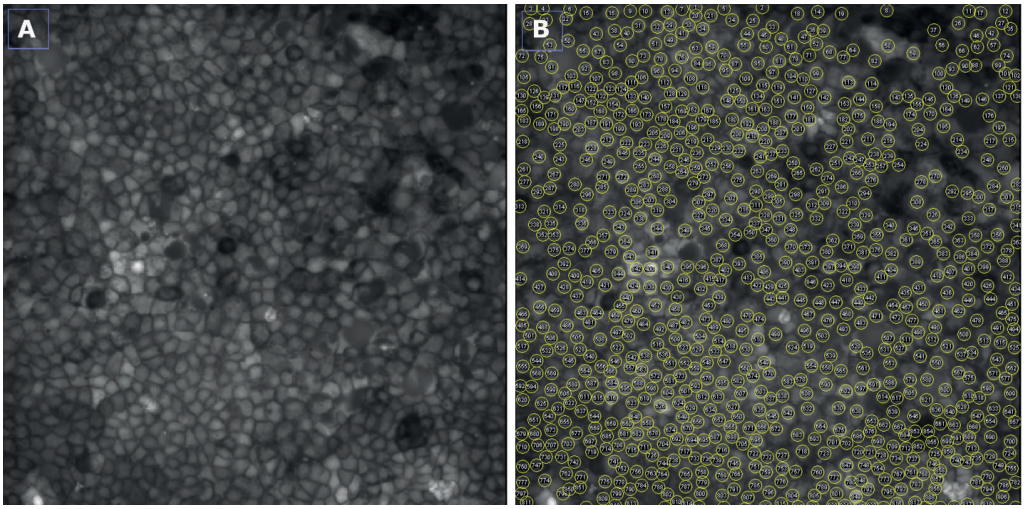

Fig. 2: Example of cell segmentation results. A – fluorescence image before cell segmentation. B – fluorescence image after cell segmentation. Circles indicate semi-automatically detected single cells. Each cell is assigned with a number.

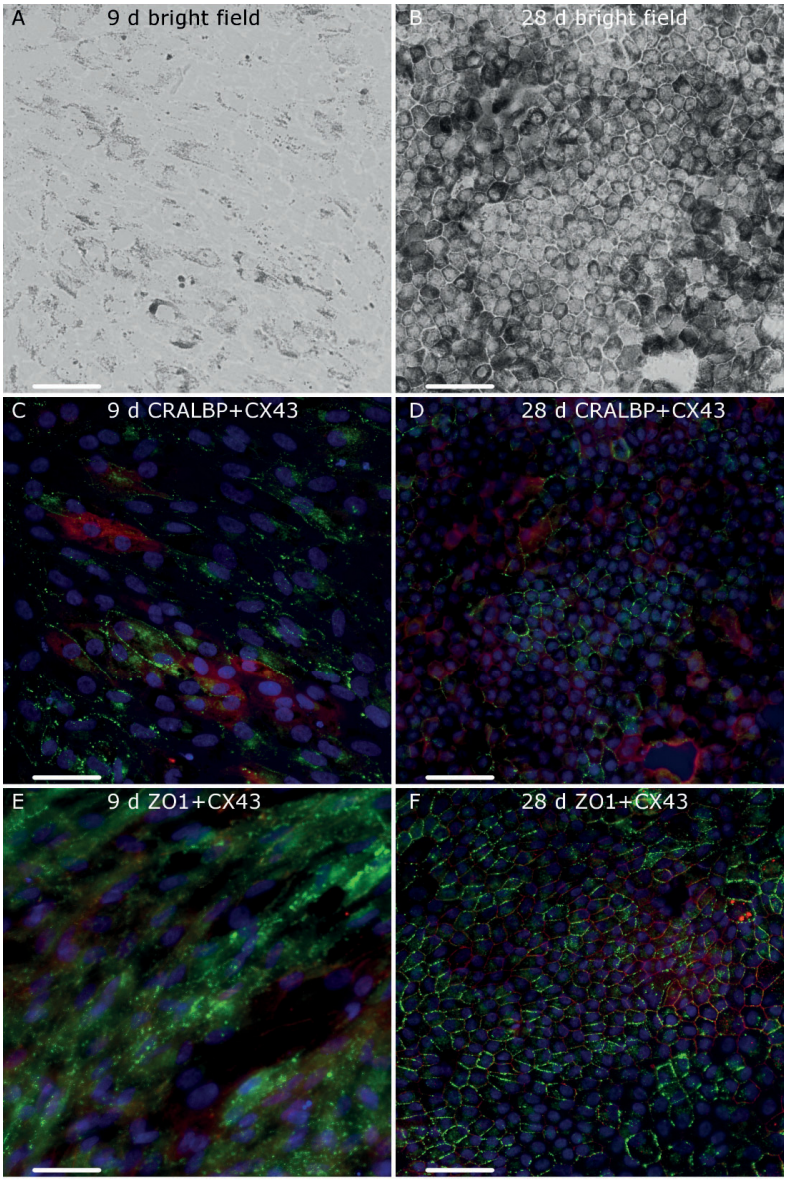
A
9 d bright field
B
28 d bright field
C
9 d CRALBP+CX43
D
28 d CRALBP+CX43
E
9 d ZO1+CX43
F
28 d ZO1+CX43

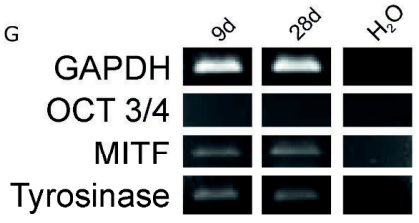
G
9d
28d
H2O
GAPDH
OCT 3/4
MITF
Tyrosinase

Fig. 3: Morphology and gene expression analysis of 9d and 28d cultured hESC-RPE monolayers. A – bright field image of 9d cultured hESC-RPEs; B – bright field image of 28d cultured hESC-RPEs; C – a GJ component CX43 (green), CRALBP, a protein present in mature cells, (red) and nuclei stain DAPI (blue) in 9d cultured hESC-RPEs; D –CX43 (green), CRALBP (red) and DAPI (blue) in 28d cultured hESC-RPEs; E – CX43 (green), a tight junction component ZO1 (red) and DAPI (blue) in 9d cultured hESC-RPEs; F – CX43 (green), ZO1 (red) and DAPI (blue) in 28d cultured hESC-RPEs; Scale bar: 50 μm; G - reverse transcription (RT-PCR) analysis of expression of a house-keeping gene GAPDH, pluripotency marker OCT ¾ and RPE-specific markers MITF and tyrosinase of 9d and 28d cultured hESC-RPEs. Water was used as a negative control.

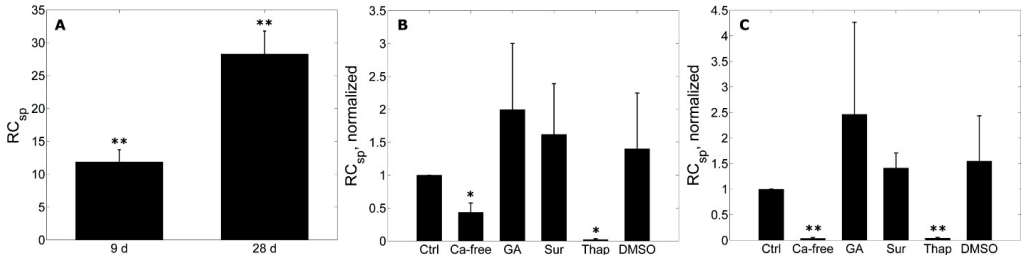

Fig. 4: RC_{sp} in 9d and 28d cultured hESC-RPE in control conditions, in absence of extracellular Ca^{2+}, after depletion of intracellular Ca^{2+} stores, in presence of GJ or P2 receptor blockers. Number of analyzed cells – n_c; number of analyzed samples – n_s. Statistical significance: $p < 0.05$ marked with *; $p < 0.01$ - **. A - RC_{sp} of 9d (n_c=10528, n_s=20) and 28d cultured hESC-RPE cells (n_c=8754, n_s=13) in control conditions; B – RC_{sp} normalized to control, in 9d cultured hESC-RPEs: in Ca^{2+}-free conditions (“Ca-free”; n_c=1062, n_s=3), after blockade of GJs with 30 μM 18-α-GA (“GA”; n_c=1252, n_s=3),

in presence of 50 μM P2 receptor blocker suramin ("Sur"; n_c=1220, n_s=3), after depletion of intracellular Ca^{2+} stores with 2 μM thapsigargin ("Thap"; n_c=1299, n_s=3), after DMSO treatment (in concentration equal to that used to dissolve 18-α-GA; "DMSO"; n_c=1122, n_s=3); C - RC_{sp} normalized to control, in 28d cultured hESC-RPEs: in Ca^{2+}-free conditions (n_c=3377, n_s=6), after 30 μM 18-α-GA treatment (n_c=3192, n_s=6), in presence of 50 μM suramin (n_c=3217, n_s=6), after application of 2 μM thapsigargin (n_c=3989, n_s=6), and after DMSO treatment (n_c=3309, n_s=6).

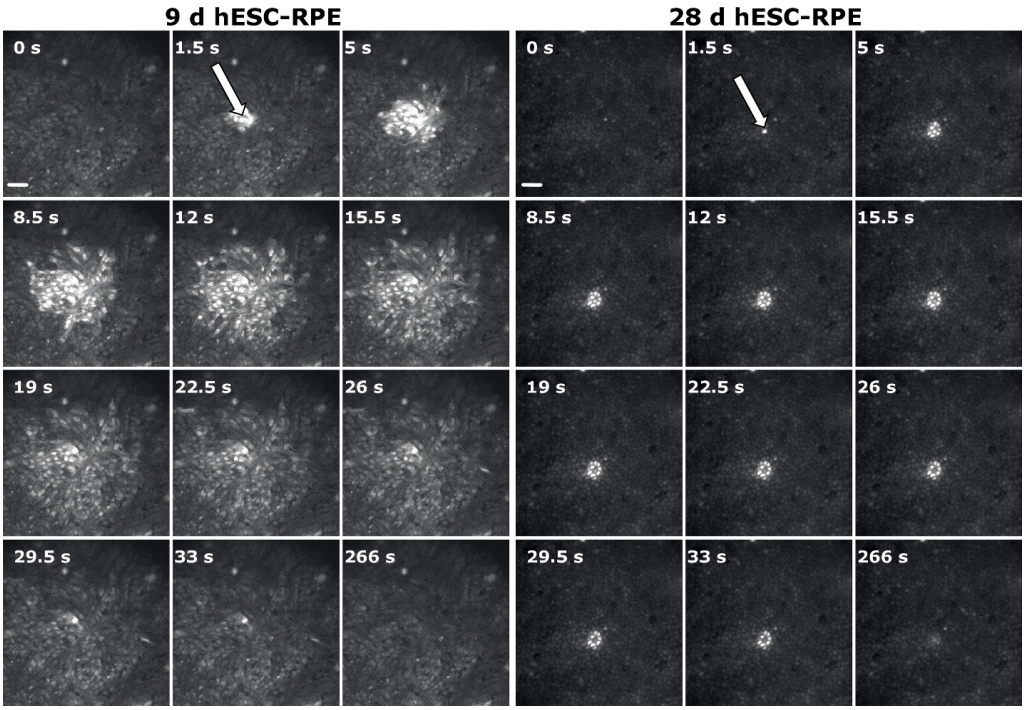

Fig. 5: Mechanically induced Ca^{2+} wave propagation in hESC-RPE monolayers loaded with intracellular Ca^{2+} indicator Fluo-4-AM. The fluorescence images of 9d and 28d cultured hESC-RPEs show relative levels of free intracellular Ca^{2+} concentration at

different time points after mechanical stimulation. The white arrow indicates a mechanical stimulation site. Scale bar: 50 μm.

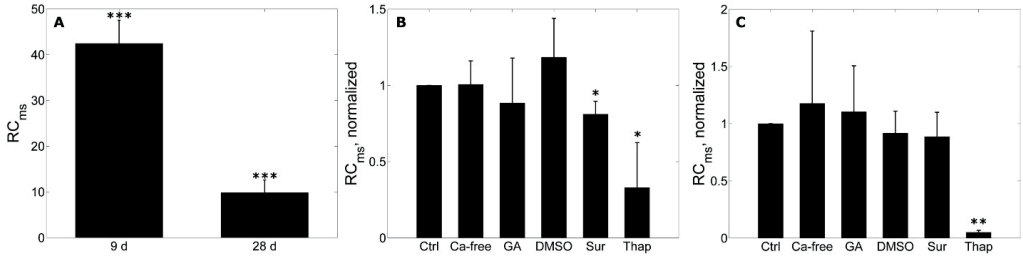

Fig. 6: RC_{ms} in 9d and 28d cultured hESC-RPEs in control conditions, in absence of extracellular Ca^{2+}, after depletion of intracellular Ca^{2+} stores, in presence of GJ or P2 receptor blockers. Statistical significance: $p < 0.05$ marked with *; $p < 0.01$ - **; $p < 0.001$ - ***. A - RC_{ms} of 9d (n_c=10669, n_s=21) and 28d cultured hESC-RPEs (n_c=5629, n_s=9) in control conditions; B – RC_{ms} normalized to control, in 9d cultured hESC-RPEs: in Ca^{2+}-free conditions ("Ca-free"; n_c=959, n_s=3), after blockade of GJs with 30 μM 18-α-GA ("GA"; n_c=1266, n_s=3), after DMSO treatment ("DMSO"; n_c=1102, n_s=3), in presence of 50 μM P2 receptor blocker suramin ("Sur"; n_c=1174, n_s=3), after depletion of intracellular Ca^{2+} stores with 2 μM thapsigargin ("Thap"; n_c=1512, n_s=3); C - RC_{ms} normalized to control, in 28d cultured hESC-RPEs: in Ca^{2+}-free conditions (n_c=3285, n_s=6), after 30 μM 18-α-GA treatment (n_c= 3216, n_s=5), after DMSO treatment (n_c=3498, n_s=6), in presence of 50 μM suramin (n_c=3363, n_s=6), and after application of 2 μM thapsigargin (n_c=4260, n_s=6).

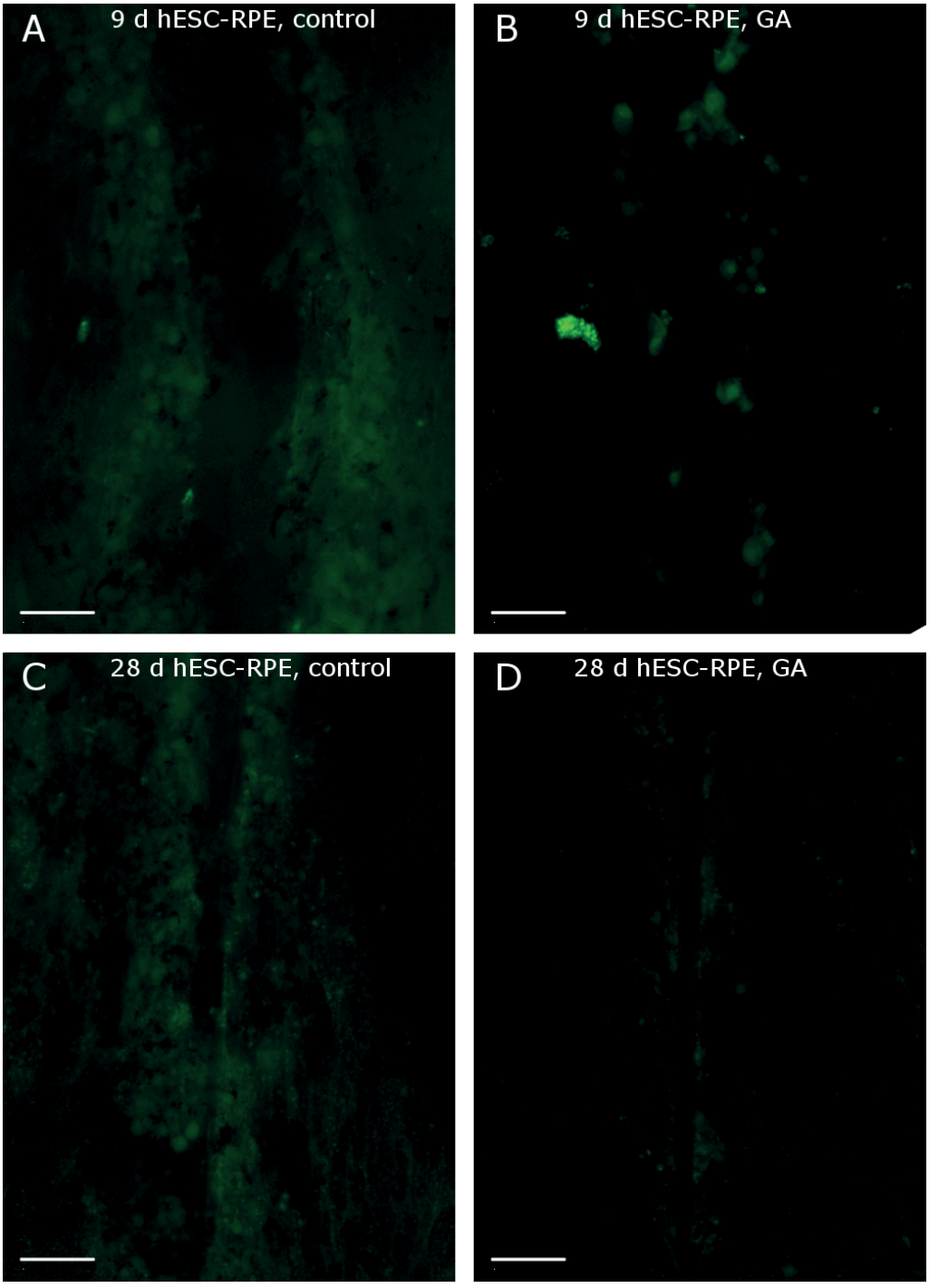
A
9 d hESC-RPE, control
B
9 d hESC-RPE, GA
C
28 d hESC-RPE, control
D
28 d hESC-RPE, GA

Fig. 7: Scrape loading/dye transfer assay with hydrazide in 9d and 28d cultured cells in control conditions (A, C) and after treatment with 30 μM 18-α-GA for 30 min (B, D). Cell-free lane is the line scraped with a surgical scalpel. Scale bar: 50 μm.

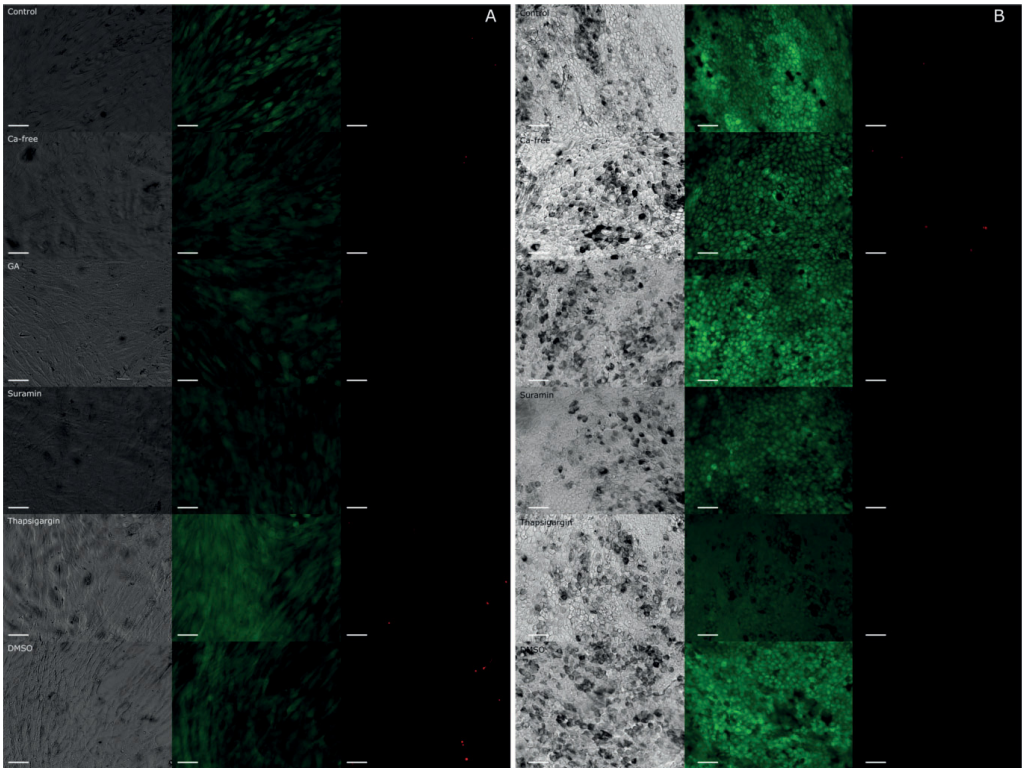

Fig. 8: Cell viability test of 9d (A) and 28d cultured hESC-RPEs (B) performed after the following treatments: control; Ca^{2+}-free conditions; 30 μM 18-α-GA, 30 min; 50 μM suramin, 30 min; 2 μM thapsigargin, 10 min; DMSO in concentration equal to that used to dissolve 18-α-GA, 30 min. Representative images of the 9d and 28d cultured hESC-RPEs taken with bright field microscopy (left panel in A and B), viable cells loaded with Calcein-AM (middle panel in A and B) and dead cells loaded with ethidium bromide (right panel in A and B) taken with fluorescence microscopy. Scale bar: 50 μm.

Tables

Table 1: Primary and secondary antibodies used for immunofluorescence staining.

Page 12.

Antibodies	Dilution	Manufacturer
I Ab: Rabbit-anti-human Cx43	1:500	Sigma-Aldrich, St. Louis, USA
I Ab: Mouse-anti-human ZO-1	1:250	Life Technologies, Carlsbad, USA
I Ab: Mouse-anti-human CRALBP	1:500	Abcam, Cambridge, USA
II Ab: Alexa Fluor 488 donkey-anti-rabbit	1:800	Molecular Probes, Leicestershire, UK
II Ab: Alexa Fluor 568 donkey-anti-mouse	1:800	Molecular Probes, Leicestershire, UK

Abbreviations: I Ab – primary antibody, II Ab – secondary antibody.

Table 2: Reverse-transcriptase–PCR primer sequences and used annealing temperatures. Page 13.

	Primer sequences (5' > 3')		
Gene	**Forward**	**Reverse**	**Ta**
GAPDH	GTT CGA CAG TCA GCC GCA TC	GGA ATT TGC CAT GGG TGG A	55
OCT 3/4	CGTGAAGCTGGAGAAGGAGA AGCTG	AAGGGCCGCAGCTTACACA TGTTC	55
MITF	AAG TCC TGA GCT TGC CAT GT	GGC AGA CCT TGG TTT CCA TA	52
tyrosinase	TGC CAA CGA TCC TAT CTT CC	GAC ACA GCA AGC TCA CAA GC	52

Abbreviations: Ta – annealing temperature, GADPH - glyceraldehyde 3-phosphate dehydrogenase, OCT3/4 - octamer-binding transcription factor, MITF - microphthalmia-associated transcription factor.

PUBLICATION IV

Wound Healing of Human Embryonic Stem Cell-Derived Retinal Pigment Epithelial Cells is Affected by Maturation Stage

Abu Khamidakh, A.E., Rodriguez-Martinez, A., Kaarniranta, K., Kallioniemi, A., Skottman, H., Hyttinen, J. & Juuti-Uusitalo, K.

2018, Biomedical Engineering Online, Vol. 17(102), pp. 1-20
https://doi.org/10.1186/s12938-018-0535-z

Abu Khamidakh *et al. BioMed Eng OnLine (2018) 17:102*
https://doi.org/10.1186/s12938-018-0535-z

BioMedical Engineering OnLine

RESEARCH

Open Access

Wound healing of human embryonic stem cell-derived retinal pigment epithelial cells is affected by maturation stage

Amna E. Abu Khamidakh[1], Alejandra Rodriguez-Martinez[2], Kai Kaarniranta[3,4], Anne Kallioniemi[2], Heli Skottman[2], Jari Hyttinen[1] and Kati Juuti-Uusitalo[2*]

*Correspondence:
kati.juuti-uusitalo@staff.uta.fi
[2] Faculty of Medical and Life Sciences, BioMediTech, University of Tampere, Arvo Ylpön Katu 34, Tampere, Finland
Full list of author information is available at the end of the article

Abstract

Background: Wound healing of retinal pigment epithelium (RPE) is a complex process that may take place in common age-related macular degeneration eye disease. The purpose of this study was to evaluate whether wounding and wound healing has an effect on Ca^{2+} dynamics in human embryonic stem cell (hESC)-RPEs cultured different periods of time.

Methods: The 9-day-cultured or 28-day-cultured hESC-RPEs from two different cell lines were wounded and the dynamics of spontaneous and mechanically induced intracellular Ca^{2+} activity was measured with live-cell Ca^{2+} imaging either immediately or 7 days after wounding. The healing time and speed were analyzed with time-lapse bright field microscopy. The Ca^{2+} activity and healing speed were analysed with image analysis. In addition the extracellular matrix deposition was assessed with confocal microscopy.

Results: The Ca^{2+} dynamics in hESC-RPE monolayers differed depending on the culture time: 9-day-cultured cells had higher number of cells with spontaneous Ca^{2+} activity close to freshly wounded edge compared to control areas, whereas in 28-day-cultured cells there was no difference in wounded and control areas. The 28-day-cultured, wounded and 7-day-healed hESC-RPEs produced wide-spreading intercellular Ca^{2+} waves upon mechanical stimulation, while in controls propagation was restricted. Most importantly, both wave spreading and spontaneous Ca^{2+} activity of cells within the healed area, as well as the cell morphology of 28-day-cultured, wounded and thereafter 7-day-healed areas resembled the 9-day-cultured hESC-RPEs.

Conclusions: This acquired knowledge about Ca^{2+} dynamics of wounded hESC-RPE monolayers is important for understanding the dynamics of RPE wound healing, and could offer a reliable functionality test for RPE cells. The data presented in here suggests that assessment of Ca^{2+} dynamics analysed with image analysis could be used as a reliable non-invasive functionality test for RPE cells.

Keywords: Image analysis, hESC-RPE, RPE, Cell maturation, Wound healing, Spontaneous $[Ca^{2+}]_i$ increases, Mechanical stimulation, Ca^{2+} waves, Mechanically induced intercellular Ca^{2+} waves

Background

The retinal pigment epithelial (RPE) cells form a monolayer of tightly packed cells which lay between neurosensory retina and the choroid [1]. The RPEs absorb stray light, transport the nutrients from the choroidal side to neural retina, regulate visual cycle and secrete various trophic factors maintaining retinal homeostasis [2].

In pathological conditions RPE dysfunction may lead to the cell layer disruption and choroidal neovascularization as observed in wet age-related macular degeneration (AMD) [3]. AMD is the leading cause of irreversible blindness among the elderly in Western countries. AMD can be divided into dry and wet forms with ~ 80 and ~ 20% prevalence, respectively. No efficient treatment exists today for dry AMD. Wet AMD development is strongly associated with the vascular endothelial growth factor (VEGF)-derived aberrant blood vessels sprout from the choroidal capillaries that penetrate through the Bruch's membrane and RPE into subretinal space. If left untreated, choroidal neovascularization evokes hemorrhage, retinal edema, and increased damage to retinal cells, fibrosis and permanent visual loss due to the undergoing wound healing process. VEGF is the principal therapy target for inhibiting the detrimental neovascularization process, i.e. by intravitreal administration of ranibizumab or bevacizumab or VEGF Trap [4]. Also the intravitreal injection itself may be traumatic and lead to RPE tear and wound healing.

The functionality of RPE after wounding has been assessed in various animal models, for example, rabbit [5, 6], chick [7], porcine [8], bovine RPE [9] and in donor human RPE cells, [10, 11] and human ESC-RPE cells [12]. These studies demonstrated that RPE cells on the wound edge undergo dedifferentiation, changing their phenotype towards the phenotype of migrating cells: the cells evolve cytoskeletal reorganization and partially or completely lose their pigmentation [5, 6, 8, 13].

Ca^{2+} is an important second messenger which mediates vital cellular functions from cell proliferation to cell death. The calcium transients triggered after ATP stimulation are used as a functionality assessment for stem cell derived RPE cells [14, 15]. In addition, Ca^{2+} is known to play an important role in the wound healing process [16].

Immediately following tissue wounding, intracellular Ca^{2+} concentration ($[Ca^{2+}]_i$) increases in the cells located at the edge of the wound. This $[Ca^{2+}]_i$ increase then spreads to neighboring cells, forming so-called intercellular Ca^{2+} wave, which activates undamaged cells, triggers reorganization of cell junctions and coordinates cell motility [17, 18].

In RPE cells, Ca^{2+} controls important physiological processes, such as dark/light adaptation of photoreceptors, phagocytosis, trans-epithelial transport of fluid and ions, secretion of growth factors, as well as and differentiation [19].

RPE cells exhibit spontaneous $[Ca^{2+}]_i$ increases that are important for communication with retina [20, 21]. We have recently shown that human RPE cells have distinct spontaneous Ca^{2+} activity at different maturation stages. The immature RPEs, where the majority of the cells have fusiform morphology and low level of pigmentation, have lower amount of cells with spontaneous $[Ca^{2+}]_i$ increases compared with more mature, cobblestone-shaped, highly-pigmented cells [22].

It has been demonstrated that upon mechanical stimulation of a single cell within a monolayer, RPE cells trigger a Ca^{2+} wave that originates from the stimulated cell and propagates to neighboring cells [23–25]. Previously, we found that, similarly to

spontaneous $[Ca^{2+}]_i$ increases, the properties of these Ca^{2+} waves strongly depend on RPE maturation stage. In immature cells, the mechanically induced Ca^{2+} waves spread far away from the site of stimulation, while in more mature RPE these waves propagate to minute number of cells surrounding the site of stimulation [22].

In wounded monolayers, the cells located in the vicinity of the denuded area are important for triggering a wound healing process [17, 18]. Furthermore, in the healed wounds, the RPE cells transiently change their morphology towards a less mature phenotype [5, 12, 13]. Thus, we hypothesize that these changes are reflected in Ca^{2+} dynamics of cells located around the wounded area and inside of healed wounds.

In this paper, we utilized image analysis tool to assess whether wounding and wound healing has effects on Ca^{2+} dynamics in hESC-RPEs cultured different periods of time. In addition, the effect of culture time on wound speed and time of hESC-RPE cells was evaluated. The knowledge of Ca^{2+} dynamics in freshly wounded and healed RPE monolayers can shed light on the mechanism of wound healing, and this possibly can be applied to understand the healing process of RPEsin the pathology of wet AMD or its treatment modalities.

Methods

Differentiation of hESC-RPE cells

Two hESC lines, Regea08/023 and Regea08/017, that were derived and characterized in our laboratory as described previously [26], were used in this study. The undifferentiated hESC lines were cultured on top of mitotically inactivated, mitomycin (10 µg/ml, Sigma-Aldrich, St. Louis, USA) treated, human foreskin fibroblasts feeder cells (CRL-2429TM, ATCC, Manassas, VA, USA) [27].

The hESCs were differentiated towards RPE in a RPEbasic medium as cell aggregates for 56–93 days. The selection of pigmented areas from floating aggregates was done manually, isolated areas were dissociated with 1× Trypsin–EDTA (Lonza, Walkersville, USA), plated with methods described previously, [28] and cultured in average for 85 days (ranging from 28 to 130) to expand amount of cells.

Cell culturing for experiments

When the amount of cells was sufficient, the hESC-RPE cells were dissociated with 1× Trypsin–EDTA again and plated on top of Ormocomp-treated (Micro Resist Technology GmbH, Germany) [29], ColIV (Sigma-Aldrich)-coated coverslips (7 mm in diameter; Thermo Fisher Scientific, Inc., Leicestershire, UK) at a density of 10^5 cells/cm^2. Cells were cultured for a period of 9 ± 1, 16 ± 1, 28 ± 1, or 35 ± 1 days in RPEbasic medium, during which the medium was replenished thrice a week.

RT-PCR analysis

The expression of RPE specific genes, the microphthalmia-associated transcription factor (*MITF*), bestrophin (*BEST*) and tyrosinase were assessed with reverse transcription–polymerase chain reaction (RT-PCR). A housekeeping gene, glyceraldehyde 3-phosphate dehydrogenase (GAPDH) was used as an internal control. The total RNA was extracted from hESC-RPE cells after 9, 16, 28, and 35 days of culture with a NucleoSpin XS-kit (Macherey–Nagel, GmbH & Co, Duren, Germany) according to the manufacturer's

instructions. The RT-PCR protocol was carried out as previously reported [28]. The primer sequences, annealing temperatures and product sizes are presented in Table 1.

Quantitative RT-PCR analysis

The expression of RPE specific genes was further analysed with quantitative RT-PCR by utilising TaqMan® Gene Expression Assays (Applied Biosystems Inc.) with FAM-labeled primers for retinal pigment epithelium specific protein 65 kDa (RPE65, hs01071462_m1) and receptor tyrosine kinase MerTK (MERTK, hs00179024_m1). The glyceraldehyde 3-phosphate dehydrogenase (GAPDH) (Hs99999905_m1) was used as an endogenous control. Samples and negative controls (no template) were run as triplicate reactions using the 7300 Real-time PCR system (Applied Biosystems Inc.) similarly as in Sorkio and others [30]. Thereafter the relative quantification of each gene was calculated with the $2^{-\Delta\Delta Ct}$ method [31] using GAPDH expression level of 9-day cultured Regea08/017 as the calibrator for both the 9- and 28-day-cultured Regea08/017, and the GAPDH expression level of 9-day Regea08/023 as the calibrator for both the 9- and 28-day-cultured Regea08/023. For both calibrators the fold change equals 1.

Immunofluorescence staining and quantification of cell area

Localization of tight junction-forming Zona Occludens Protein 1 (ZO-1), marker of proliferative cells (Ki67), extracellular matrix forming collagen I (ColI) and laminin (Lam) were assessed with indirect immunofluorescence labeling as described previously [25]. Briefly, the hESC-RPE cells on Ormocomp® coated coverslips were rinsed in PBS thrice and fixed in 4% paraformaldehyde (Sigma-Aldrich) in 1× PBS (Lonza Group Ltd) for 10 min. Then, the cells were again rinsed with PBS 3 times and permeabilized for 10 min with 0.01% Triton X (Sigma-Aldrich) in PBS at RT. Cells were washed thrice in PBS, and unspecific antibody binding sites were blocked with 3% bovine serum albumin (BSA; Sigma-Aldrich) in PBS at RT for 1 h. Next, the cells were incubated with primary antibodies (see Table 2) dissolved in 0.5% BSA-PBS for 1 h at RT, and thereafter were washed thrice with 1× PBS. Cells were then incubated with secondary antibodies (see Table 2) diluted in 0.5% BSA-PBS for 1.5 h at RT. Finally, the cells were washed thrice with PBS and mounted with Vectashield mount with 4′,6′diamidino-2-phenylidole (DAPI [Vector Laboratories Inc., Burlingame, CA, USA]). Samples were visualized under Zeiss LSM 700 confocal microscope (Zeiss, Jena, Germany) with a 63× oil immersion objective or under Olympus IX51 fluorescence microscope with a 20× air objective. Confocal images were edited with ZEN 2012 black (Zeiss).

Table 1 Reverse-transcriptase-PCR primer sequences, product lengths (bp) and used annealing temperatures

Gene	Forward	Reverse	bp	Tm
GAPDH	GTTCGACAGTCAGCCGCATC	GGAATTTGCCATGGGTGGA	229	55
MITF	AAGTCCTGAGCTTGCCATGT	GGCAGACCTTGGTTTCCATA	352	52
BEST	GAATTTGCAGGTGTCCCTGT	ATCAGGAGGACGAGGAGGAT	214	60
Tyrosinase	TGC CAA CGA TCC TAT CTT CC	GAC ACA GCA AGC TCA CAA GC	52	316

Primer sequences (5′ > 3′)

Table 2 Primary and secondary antibodies for immunofluorescence staining

Antibodies	Dilution	Manufacturer
I Ab: Mouse-anti-human ZO-1	1:250	Life Technologies, Carlsbad, USA
I Ab: Ki67	1:500	Millipore, Darmstadt, Germany
I Ab: Laminin	1:100	Abcam, Cambridge, UK
I Ab: Coll	1:250	Abcam, Cambridge, UK
II Ab: Alexa Fluor 488 donkey-anti-rabbit	1:800	Molecular Probes, Leicestershire, UK
II Ab: Alexa Fluor 568 donkey-anti-mouse	1:800	Molecular Probes, Leicestershire, UK

I Ab primary antibody, *II Ab* secondary antibody

The differences in cell shapes were estimated from cell areas from immunofluorescence images with ZO-1 labeling. In Fiji, the cell borders of 100 randomly selected cells were defined manually for 9-, 16-, 28-, and 35-day-cultured non-wounded cells and inside 7-day-healed wounds of the cells wounded on day 28 of culture. Individual cell areas were calculated with a standard Fiji measurement option. The presented data are combined from Regea08/017 and Regea08/023 hESC-RPEs.

Wounding of hESC-RPEs

The wounding of day 9- or 28-day cultured hESC-RPE monolayers were done mechanically by performing a linear scratch with a plastic 10 µl pipette tip. Although the person who did the injury was always the same and tried to perform it similarly, with same speed and pressure, there might be variation due to the manual handling. When Ca^{2+} dynamics immediately after wounding was about to be assessed, the cells were allowed to rest for 15 min after wounding, before the actual experiments were started, thus the samples are abbreviated as 9 days + 15 min or 28 days + 15 min samples. When wound healing was evaluated, the cellular monolayers were allowed to grow for 7–8 days prior to the experiments (abbreviated as 9 days + 7 days or 28 days + 7 days samples). Wound healing process was tracked with time-lapse microscopy in Nikon BioStation CT (Nikon, Nikon Instruments Europe BV, Netherlands). There, the cells were cultured at 37 °C and 5% CO_2, and phase contrast images of wounded areas were automatically recorded every 1–3 h during the healing period with a 10× objective. The medium was replenished thrice a week.

Wound healing speed and time were assessed only from the samples without visible ColIV coating damage. The speed of healing was calculated by analyzing the wound size at the beginning of the assay (in pixels) divided by full healing time in hours. Wound healing time was estimated as time in hours needed for the hESC-RPEs to completely cover the cell-free lane with the cells. The percentage of healed samples was assessed from samples with both damaged and intact ColIV coating. The presented data are combined from Regea08/017 and Regea08/023 hESC-RPEs.

Ca^{2+} imaging

The Ca^{2+} dynamics in cells around fresh wounds (9 days + 15 min and 28 days + 15 min samples) and in healed cultures (9 days + 7 days and 28 days + 7 days samples) was evaluated with live-cell Ca^{2+} imaging. Two types of measurements were performed on control and wounded hESC-RPEs: first the spontaneous Ca^{2+} activity was recorded from

unstimulated cells at least for 5 min time; second, intercellular Ca^{2+} waves spreading was recorded after mechanical stimulation again at least for 5 min time.

All Ca^{2+} imaging recordings were performed in HBSS medium, containing 5 mM glucose, 20 mM HEPES, 0.44 mM KH_2PO_4, 137 mM NaCl, 5 mM KCl, 4.2 mM $NaHCO_3$, 1.2 mM $MgCl_2$, and 2 mM $CaCl_2$. pH was adjusted to 7.37 with 3 M NaOH; osmolarity was adjusted to 335 ± 5 mOsm/kg with sucrose. All components were from Sigma-Aldrich.

For the live-cell Ca^{2+} imaging recordings hESC-RPEs were loaded with Fluo-4-acetoxymethyl ester (Fluo-4 AM; 4 μM, in 1 h incubation at room temperature (RT), Life Technologies, Carlsbad, USA). Next, the cells were washed with HBSS thrice. The coverslips with Fluo-4 AM loaded cells were then mounted on a perfusion chamber (Warner Instruments, Hamden, USA) and filled with HBSS. The recording of the fluorescence signal was done under an Olympus IX51 fluorescence microscope (Olympus, Tokyo, Japan) with ANDOR iXion 885 camera (Oxford Instruments, Oxfordshire, UK). Fluo-4 AM was excited at 490 nm (bandwidth 15 nm) with Polychrome V at 30% light intensity (TILL Photonics, Pittsburgh, USA) with an exposure time of 20 ms; the emission was collected at 510–560 nm. The recording was done at a rate of 2 frames per second with the binning of 2×2 with Live Acquisition software v. 2.4.0.13 (FEI Munich GmbH), at least for 5 min (600 frames) time. From each individual fluorescence time-series a corresponding brightfield images were taken to assess cell morphology.

The mechanical stimulation was induced by touching single hESC-RPE cell with a glass micropipette during the recording of Ca^{2+} activity, similarly as described above. The micropipette was made from a glass capillary (Biomedical Instruments, Zollnitz, Germany; 0.86 9 1.50 9 80 mm) with a Narishige pipette puller. The micropipette was mounted on a Luigs & Neumann SM 5–9 vertical microinjection system (Luigs & Neumann, Ratingen, Germany) and intermittently lowered to touch a target cell membrane [25]. In samples with fresh wounds (9 days + 15 min and 28 days + 15 min), the site for mechanical stimulation was chosen to be in the vicinity to the wound edge. In samples with healed or partially healed wounds (9 days + 7 days and 28 days + 7 days), the stimulated cell belonged to the healed area.

All experiments were performed at RT at least 4 times. For each wounded area, the non-wounded area from the same coverslip was used as a control. The presented data are combined from Regea08/017 and Regea08/023 hESC-RPEs.

Ca^{2+} imaging data analysis

The recorded time-series were analyzed with our in-house Matlab (R2013 A, Mathworks) algorithms and Fiji [32].

The cells on fluorescence time-series images were identified as described in [22]. At first cell centers were detected from averaged fluorescence images in Matlab with in-house algorithm developed for this purpose. Thereafter, cells were approximated as fixed-sized circles in Fiji [32]. The cells with immature, fusiform morphology, this fitting was done manually in Fiji. Next, average fluorescence kinetics from each detected cell at every recorded time point was extracted in Fiji and exported to Matlab for further analysis.

In Matlab, the fluorescence kinetics from single cells was corrected for background fluorescence and smoothed with a moving average algorithm with the 5 points span. Then, baselines in the beginning and in the end of a recording were automatically detected for each cell, and the fluorescence curves were corrected for bleaching and normalized to initial baseline levels. Finally, the peaks in the fluorescence curves were automatically detected. The amplitude of peak threshold was set to 1.1 (10% higher than the baseline). The cell identification and fluorescence curves analysis algorithms together with Matlab codes were similar to the ones used in Abu Khamidakh et al. [22]. The fluorescence kinetics from single cells was corrected for background fluorescence and smoothed with a moving average algorithm with the 5 points span. The fluorescence values were corrected for bleaching with the normalizing value achieved by comparing baselines in the beginning and in the end of a recording from each cell. Finally, the peaks in the fluorescence curves were automatically detected. The amplitude of peak threshold was set to 1.1 (10% higher than the baseline).

The spontaneous activity of hESC-RPEs was assessed as the percentage of cells with spontaneous $[Ca^{2+}]_i$ increases (%RC—percentage of responsive cells). In wounded samples, the cellular monolayer in the field of view was divided into several areas: 1—"Wound" area included the cells in the healed part of a monolayer (analyzed from samples that were fully or partially healed during the 7-day healing time), 2—"Area 1" included cells directly adjacent to the wound (within a distance of 40–60 μm), 3—"Area 2" consisted of cells directly adjacent to "Area 1" (40–60 μm distance), 4—"Area 3" included cells that immediately followed "Area 2" (40–60 μm distance). The cells belonging to each area were automatically detected with an in-house algorithm developed for this purpose.

The spreading of mechanically induced Ca^{2+} waves was estimated by identifying cells that were participated in the wave. Any two cells were considered to propagate a wave, if they had fluorescence peaks with a peak time difference of less than 4 s, and the distance between these cells was less than 2–3 characteristic cell sizes [22]. Only the cells that had a fluorescence peak and which were connected to the cell/site of mechanical stimulation via other cells having fluorescence peak were considered to be involved in a wave. Cell clusters with small Ca^{2+} waves that were disconnected from the site of mechanical stimulation were considered as spontaneous Ca^{2+} waves. The extent of Ca^{2+} wave spreading was assessed by calculating a total number of cells propagating a Ca^{2+} wave and by estimating the area in the field of view that was covered by the wave. The presented data are combined from Regea08/017 and Regea08/023 hESC-RPEs.

Ethical issues

University of Tampere has the approval of the National Authority for Medicolegal Affairs Finland (TEO) to study human embryos (Dnro 1426/32/300/05) and a supportive statement of the Ethical Committee of the Pirkanmaa Hospital District to derive, culture, and differentiate hESC lines from surplus human embryos (R05116). No new lines were derived for this study.

Statistics

The statistical significance between healed cell areas, and differences in wound healing time and speed was done with two-sample unpaired Student's *t* test. The number of cells involved in a mechanically induced Ca^{2+} wave, or area of Ca^{2+} wave spreading in different groups was done with Mann–Whitney test. The $p < 0.05$ was considered statistically significant. The results were expressed as mean ± standard error of mean (SEM). Number of samples is referred to as n_s in the figure legends.

Results

Morphology and differentiation status of wounded and intact hESC-RPE cells

Differentiation status of 9-, 16-, 28-, and 35-day-cultured hESC-RPE cells was evaluated with RT-PCR. The samples from both Regea08/017 and Regea08/023 cell lines expressed RPE-specific markers *MITF*, *bestrophin* and *Tyrosinase* (Fig. 1A, B). The maturation status was further assessed with quantitative RT-PCR with two RPE specific genes. The expression of both *RPE65* and *MERTK* was very low (i.e. the target gene Ct:s were approximately 30), still there was a detectable increase in *RPE65* and *MERTK* mRNA expression when the 9 day and 28 day cultured samples were compared together. The morphology and pigmentation of representative 9-, 16-, 28-, and 35-day-cultured cells from both cell lines is represented on bright field images in Fig. 1E–H (Regea08/017) and Fig. 1I–L (Regea08/023).

The cultures were labelled with the tight junction protein ZO-1 antibody to visualize the cell confluence and polarization (Fig. 2). Indirect immunofluorescence staining showed that Regea08/017 hESC-RPE cells expressed ZO-1 on cell junctions in control non-wounded samples (Fig. 2A–C), as well as in wounded and healed samples (Fig. 2D–F), although the cells surrounding the wound still had elongated i.e. fusiform shaped morphology. The Regea08/023 hESC-RPE samples (Fig. 2G–L) were similar to the Regea08/023 hESC-RPEs.

The presence of proliferating cells was evaluated by labeling cultures with Ki67 antibody. There were no Ki67 positive cells in Regea08/017 hESC-RPE the control cultures (Fig. 2A–C). In wounded Regea08/017 cultures that were partially healed on day 7 after wounding, there were only few Ki67 positive cells (Fig. 2D–F) which located close to the edge, but not on the 1st rim of cells lining the wound. In the Regea08/023 monolayer, there were no dividing, i.e. Ki67 positive cells either in control or wounded and 7 days healed samples were found (Fig. 2J–l).

Because migration and wound healing depends on the cell substrata, [33] we next assessed the localization of laminin and ColI. We saw that Regea08/017 hESC-RPEs produced laminin in control cultures (Fig. 3A–C). After wounding cells produced a thin layer of ColI (Fig. 3D–F). In the wounded and healed culture of Regea08/023 hESC-RPE cells produced a clearly marked layer of ColI (Fig. 3J–L). The deposition of COLI labelling close to the substrata (arrows on the orthopanels), and low background labelling in other areas of the cells are presented in Additional file 1: Fig S1.

Because the culture time influences the morphology of the cells, we analyzed cell sizes by measuring the cell areas in 9-, 16-, 28-, and 35-day-cultured hESC-RPEs and in cells inside healed wounds in 28 days + 7 days samples. An example of manual cell border

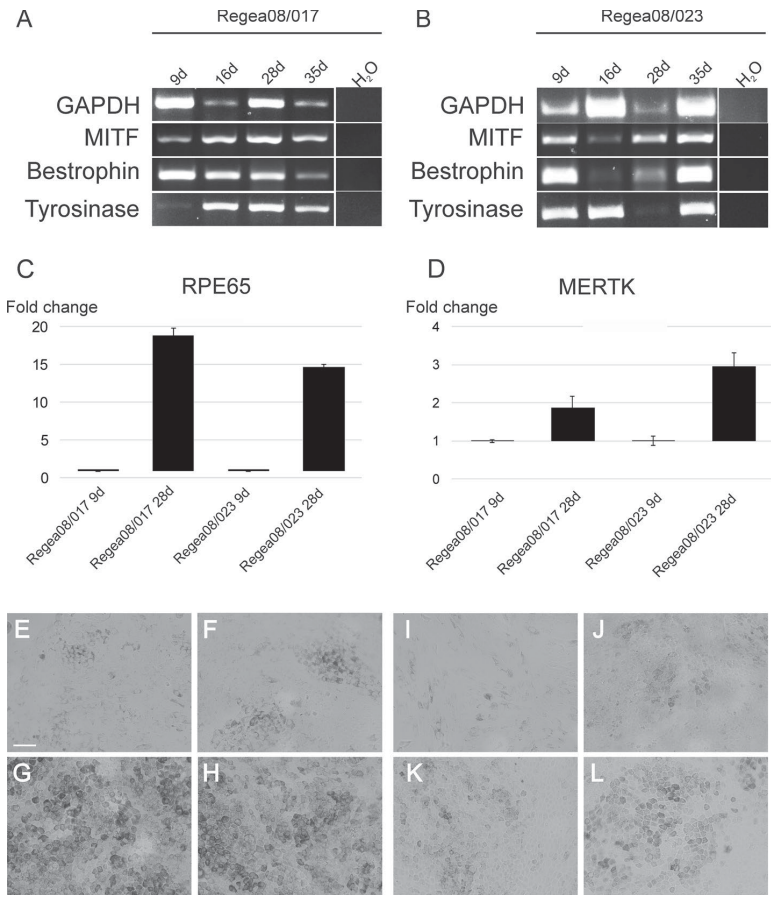

Fig. 1 Gene expression analysis and morphology of hESC-RPE cells. Gene expression of a house-keeping gene GAPDH, and RPE-specific marker genes MITF, bestrophin and tyrosinase were assessed with reverse transcription–polymerase chain reaction (RT-PCR) from Regea08/017 (**A**) and Regea08/023 (**B**) hESC-RPE cells cultured for 9, 16, 28, and 35 days. Water was used as negative control. Relative gene expression of mature RPE markers, the retinal pigment epithelium specific protein 65 kDa (RPE65) (**C**) and receptor tyrosine kinase MerTK (MERTK) (**D**) of 9-day and 28-day cultured non-wounded (i.e. control) samples. The Ct values of target genes were approximately 30. A bright filed image of Regea08/017 hESC-RPEs cultured for 9 days (**E**), 16 days (**F**), 28 days (**G**), and 35 days (**H**). Bright filed image of Regea08/023 hESC-RPEs cultured for 9 days (**I**), 16 days (**J**), 28 days (**K**), and 35 days (**L**). Scale bar 50 µm

segmentation is presented in Fig. 4a. Figure 4b indicates that cells wounded on the day 28 of culture have the same size inside the healed wounds after 7 days as 9-day-cultured cells. In the Table 3 are all *p*-values of presented datasets.

Wound healing speed of hESC-RPEs

To assess wound healing capabilities of hESC-RPE cells, the 9- and 28-day-cultured cells were followed for 7–8 days post-wounding. Both wounded 9- and 28-day-cultured hESC-RPEs were able to heal by filling denuded areas with cells (Fig. 5A–C).

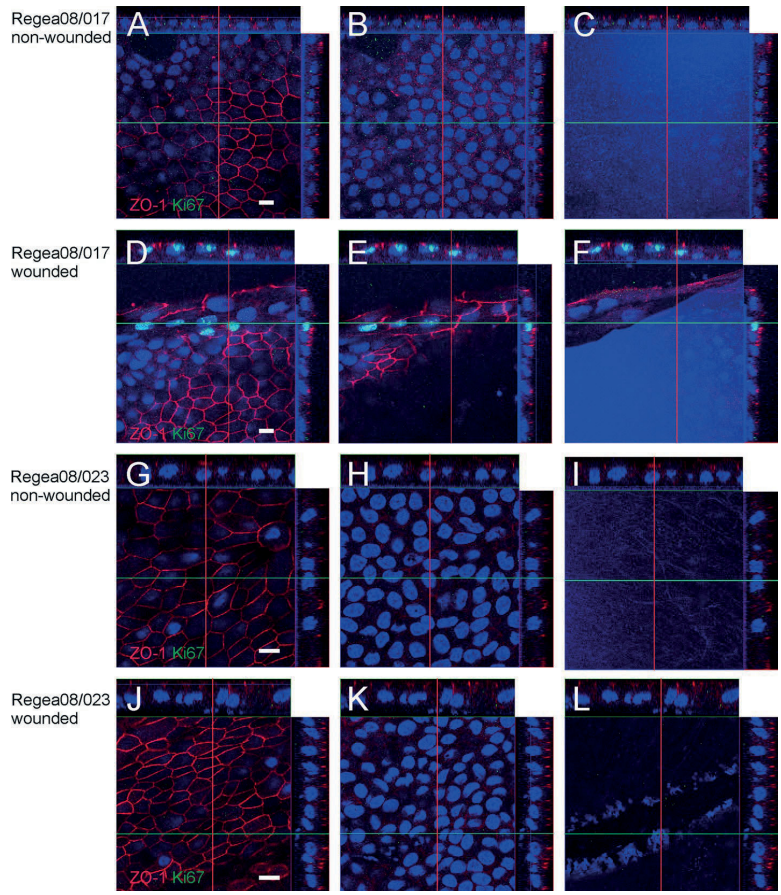

Fig. 2 Morphology and polarity of hESC-RPE cultures. Localization of tight junction protein ZO-1 (red) and Ki67-positive proliferative cells (green) in control and wounded Regea08/017 and Regea08/023 hESC-RPEs. Nuclei were counterstained with DAPI (blue). Non-wounded area of Regea08/017 hESC-RPEs cultured for 35 days (**A**–**C**). Regea08/017 hESC-RPEs wounded on day 28 of culture and allowed to heal for 7 days, 35 days of culture in total (**D**–**F**). Non-wounded area of Regea08/023 hESC-RPEs cultured for 35 days (**G**–**I**). Regea08/023 hESC-RPEs wounded on day 28 of culture and allowed to heal for 7 days, 35 days of culture in total (**J**–**L**). On the left row are the Z-stack from the apical side, in the middle from the nuclear level, and on the right row from the basal side of the culture. The cross-hairs of Z-plane indicators are intensified for clarity. Scale bar 10 µm

Samples, where ColIV coating was damaged during wounding, had significantly poorer ability to heal (Fig. 5D). When no visible ColIV damage occurred during the wounding process, 100% of samples wounded on day 9 of culture and 61% of samples wounded on day 28 were able to heal. The monolayers wounded on day 9 healed almost 3 times faster compared to those wounded on day 28 ($p = 2 \times 10^{-6}$) (Fig. 5E). The full healing time of wounded 9-day-cultured hESC-RPEs was 20 ± 3 h, while 28-day-cultured cells healed 2.5-fold slower with a healing time of 49 ± 9 h ($p = 0.002$). (Fig. 5F).

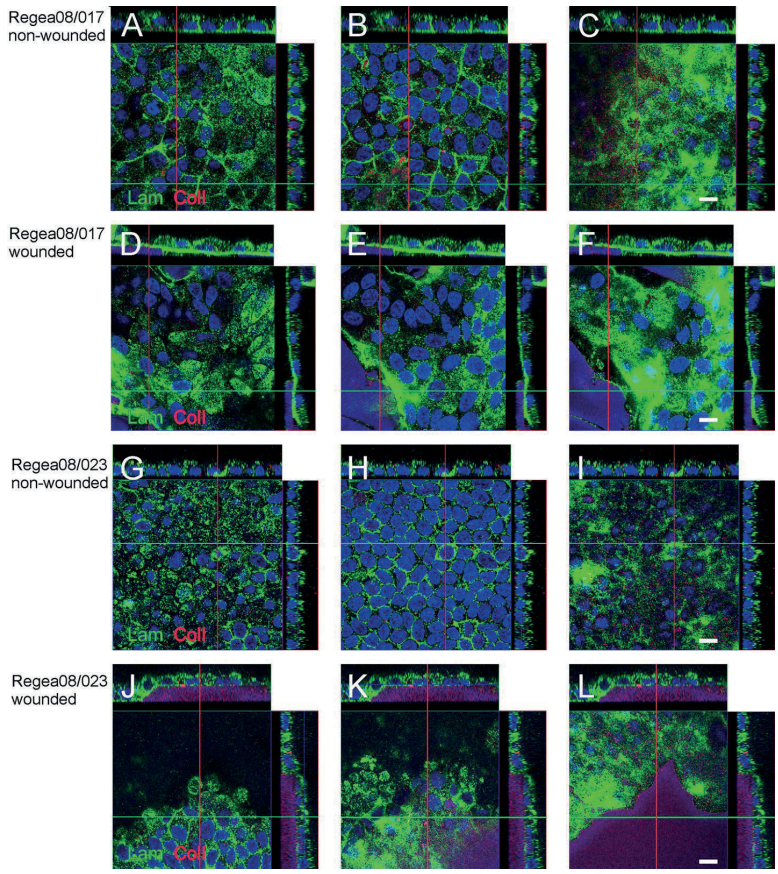

Fig. 3 Extracellular protein localization in hESC-RPE cultures. Localization of extracellular matrix protein collagen I (red) and laminin (green) in control and wounded Regea08/017 and Regea08/023 hESC-RPEs. Nuclei were counterstained with DAPI (blue). Non-wounded area of Regea08/017 hESC-RPEs cultured for 16 days (**A**–**C**). Regea08/017 hESC-RPEs cultured for 9 days, wounded and imaged 7 days after wounding, cultured for 16 days in total (**D**–**F**). Non-wounded area of Regea08/023 hESC-RPEs cultured for 16 days (**G**–**I**). Regea08/023 hESC-RPEs wounded on day 9 of culture and allowed to heal for 7 days, cultured for 16 days in total (**J**–**L**). On the left row are the Z-stack from the apical side, in the middle from the nuclear level, and on the right row from the basal side of the culture. The cross-hairs of Z-plane indicators are intencified for clarity. Scale bar: 10 µm

Spontaneous $[Ca^{2+}]_i$ increases in wounded hESC-RPEs

Then, the effect of wounding on spontaneous transient $[Ca^{2+}]_i$ increases was evaluated. The samples of 9 d + 15 min (Fig. 6A–C), 9 days + 7 days (Fig. 6D–F), 28 days + 15 min (Fig. 6G–I), and 28 days + 7 days (Fig. 6J–L) samples are in Fig. 6. On the left are the representative bright field images, in the middle are the corresponding fluorescence images of the cells in the same field of view loaded with Fluo-4 AM are shown, and on the right are the analysed areas, where the percentage of the cells with spontaneous $[Ca^{2+}]_i$ increases (%RC) were compared. In 9-day-cultured hESC-RPE cells with fresh wounds (9 days + 15 min samples), %RC in the area closest to the wound edge ("area 1") was

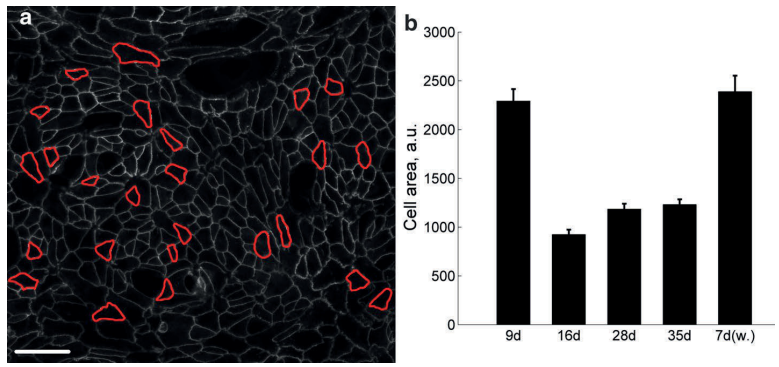

Fig. 4 Cell size differences in 9- to 35-day-cultured hESC-RPE. Cell area was analyzed by manual cell boarder segmentation indicated by red lines (**a**). Scale bar: 50 µm. Analysis of cell areas (**b**) of hESC-RPEs cultured for 9 days ($n_s = 4$), 16 days ($n_s = 6$), 28 days ($n_s = 6$) or 35 days ($n_s = 5$), and 28-day-cultured hESC-RPEs, wounded and visualized 7 days after wounding (7 days) ($n_s = 2$). The presented data are combined from Regea08/017 and Regea08/023 hESC-RPEs

Table 3 *p*-values calculated with the unpaired Student's two-sample t-test for datasets presented in Fig. 4

p	9 days	16 days	28 days	35 days	7 days w.
9 days	–				
16 days	2.33×10^{-20}	–			
28 days	2.08×10^{-14}	4.94×10^{-04}	–		
35 days	1.44×10^{-13}	3.48×10^{-05}	0.541	–	
7 days w.	0.636	3.30×10^{-15}	4.67×10^{-11}	1.94×10^{-10}	–

Samples are abbreviated as follows: "9 days"—9-day-cultured; "16 days"—16-day-cultured; "28 days"—28-day-cultured; "35 days"—35-day-cultured; "7 days w."—7-day-cultured cells within wounds made on day 28

more than twice higher compared to control (%RC in area 1 = 33.2 ± 6.4%; %RC in control = 15.3 ± 4.4%; $p = 0.028$) (Fig. 6C). The 9 days + 7 days (Fig. 6F) and 28 days + 15 min samples (Fig. 6I) did not have statistically significant changes in %RC in any of the investigated areas. Healed or partially healed hESC-RPEs that were wounded on day 28 of culture and then allowed to heal for 7 days (28 days + 7 days samples) had almost twofold decreased %RC inside the healed wound compared to the control (%RC in the healed wound area = 19.7 ± 4.6; %RC in control = 38.7 ± 2.0%; $p = 0.029$) (Fig. 6L).

Mechanically induced Ca^{2+} waves in wounded hESC-RPEs

Next, the effect of wounding on the propagation of intercellular Ca^{2+} waves induced by mechanical stimulation was assessed. Mechanical stimulation of a single cell in a hESC-RPE monolayer resulted in a $[Ca^{2+}]_i$ increase in the stimulated cell that propagated in a wave-like manner to neighboring cells in 9 days + 15 min, 9 days + 7 days, 28 days + 15 min, and 28 days + 7 days samples.

The wounded hESC-RPE monolayer (9 days + 7 days) and a shadow of a micropipette used for mechanical stimulation is represented in Fig. 7A and the fluorescence image of the same culture loaded with Ca^{2+}-sensitive dye in the same field of view is shown

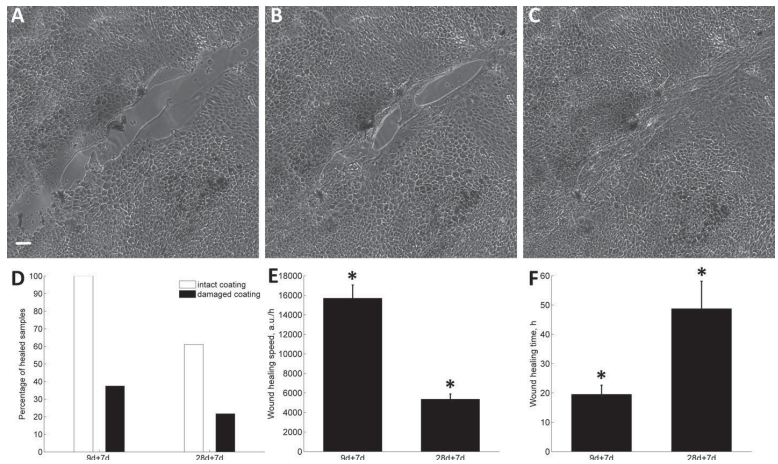

Fig. 5 Wound healing speed and time. Bright field image of Regea08/023 hESC-RPEs wounded on day 28 of culture, then healed for 7 days, visualized immediately after wounding (**A**), 58 h after wounding (**B**), and 118 h after wounding (**C**). Scale bar: 50 µm. Percentage of completely healed samples (white bar—intact coating; black bar—damaged coating) wounded on day 9 and healed for 7 days (coating intact, $n_s = 16$; coating damaged, $n_s = 8$) or wounded on day 28 and healed for 7 days (coating intact, $n_s = 18$; coating damaged, $n_s = 23$) (**D**). Wound healing speed during a 7-day follow-up of 9-($n_s = 16$) or 28-day-cultured ($n_s = 11$) hESC-RPEs (**E**). Wound healing time during a 7-day follow-up of 9-($n_s = 16$) or 28-day-cultured ($n_s = 11$) hESC-RPE cells (**F**). The presented data are combined from Regea08/017 and Regea08/023 hESC-RPEs

in Fig. 7B, see also corresponding Additional file 2: Video S1. The white polygon indicates the area of wave spreading, and cells indicated with white dots are the cells participating in the wave propagation. A representative brightfield images with a wounded hESC-RPE monolayer and a shadow of a micropipette used for mechanical stimulation is represented in Fig. 7C (the 28 days + 7 days) and the fluorescence image of the same culture loaded with Ca^{2+}-sensitive dye in the same field of view is shown in Fig. 7D, see also corresponding Additional file 3: Video S2. The latter figure also indicates the area of Ca^{2+} wave spreading (white polygon) and the cells participating in the wave propagation (white dots).

Samples that were cultured for 28 days prior to wounding and later allowed to heal for 7 days (28 days + 7 days samples) showed a 4.6-fold higher number of cells involved in Ca^{2+} wave spreading within a healed area compared to control (79 ± 19 cells in wounded area and 17 ± 6 cells in control area; $p = 0.0047$) (Fig. 7E). Furthermore, in these samples Ca^{2+} waves covered 8.9-fold larger areas compared to control ($p = 0.0023$) (Fig. 7F).

In 9 d + 15 min, 9 days + 7 days, and 28 days + 15 min samples Ca^{2+} waves inside or close to the wounded areas propagated in the same manner as in non-wounded controls (Fig. 7E, F.

Discussion

The complex RPE-derived wound healing process in AMD is weakly understood. In a recent study the healing of scratch wounded H9 hESC-RPE cells has been shown to have partial wound closure within 30 days [12]. Ca^{2+} has an important role in

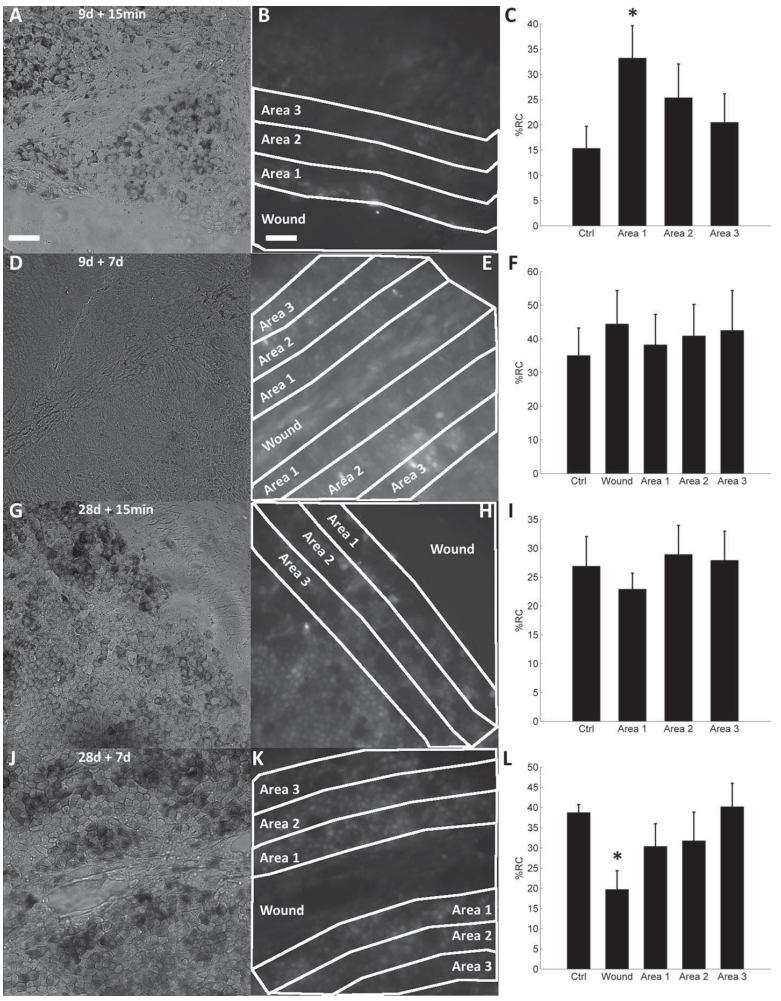

Fig. 6 Percentage of cells with spontaneous $[Ca^{2+}]_i$ increases (%RC) in wounded hESC-RPEs at different areas related to the wound location. A bright field image of 9-day-cultured, wounded hESC-RPEs, visualized immediately after wounding (**A**). A fluorescence image of the same sample as in **A** loaded with Ca^{2+}-sensitive indicator Fluo-4 AM (**B**). The wound area ("wound") and adjacent areas ("Area 1", "Area 2", "Area 3") are marked with white lines. Analyzed percentage of responsive cells (%RC) in non-wounded control ($n_s = 8$), and area 1 ($n_s = 8$), area 2 ($n_s = 8$) and area 3 ($n_s = 8$) (**C**). Statistical significance: $p < 0.05$ is marked with Asterisk. A bright field image of 9-day-cultured then wounded hESC-RPEs, visualized 7 days after wounding (**D**). A fluorescence image of the same sample as in D loaded with Ca^{2+}-sensitive indicator fluo-4 AM (**E**). The wound area and adjacent areas are marked with white lines. The %RC in non-wounded control ($n_s = 8$), wounded area ($n_s = 8$) and area 1 ($n_s = 8$), area 2 ($n_s = 8$), and area 3 ($n_s = 6$) (**F**). A bright field image of 28-day-cultured and wounded hESC-RPEs, visualized immediately after wounding (**G**). A fluorescence image of the same sample as in G loaded with Ca^{2+}-sensitive indicator Fluo-4 AM (**H**). The wound area and adjacent areas are marked with white lines. The %RC in non-wounded control ($n_s = 8$) and area 1 ($n_s = 8$), area 2 ($n_s = 8$), and area 3 ($n_s = 8$) (**I**). A bright field image of 28-day-cultured then wounded hESC-RPEs, visualized 7 days after wounding (**J**). A fluorescence image of the same sample as in J loaded with Ca^{2+}-sensitive indicator Fluo-4 AM (**K**). The wound area and adjacent areas are marked with white lines. The %RC in non-wounded control ($n_s = 4$), wounded area ($n_s = 4$) and area 1 ($n_s = 4$), area 2 ($n_s = 4$), and area 3 ($n_s = 4$) (**L**). The presented data are combined from Regea08/017 and Regea08/023 hESC-RPEs

(See figure on next page.)

Fig. 7 Ca^{2+} wave propagation in wounded hESC-RPEs after mechanical stimulation. A bright field image of a hESC-RPE monolayer (9d + 7d) (**A**). The dark shadow of micropipette lowered towards the cell to perform mechanical stimulation can be seen. Fluorescence image of the same culture as in A loaded with fluorescent Ca^{2+} sensitive dye Fluo-4 AM that reflects $[Ca^{2+}]_i$ concentration in the cytoplasm (**B**). A white line indicates the area of the monolayer that responded to single-cell mechanical stimulation. White dots indicate the cells that participate in a mechanically induced Ca^{2+} wave. Similarly a bright field image of a hESC-RPE monolayer (28 days + 7 days) (**C**). The dark shadow of micropipette lowered towards the cell to perform mechanical stimulation can be seen. Fluorescence image of the same culture as in A loaded with fluorescent Ca^{2+} sensitive dye Fluo-4 AM that reflects $[Ca^{2+}]_i$ concentration in the cytoplasm (**D**). A white line indicates the area of the monolayer that responded to single-cell mechanical stimulation. White dots indicate the cells that participate in a mechanically induced Ca^{2+} wave. Number of hESC-RPE cells participating in a mechanically induced intercellular Ca^{2+} wave in wounded 9-day-cultured cells followed for 15 min (ctrl, $n_s = 7$; wounded, $n_s = 7$), or for 7 days (ctrl, $n_s = 7$; wounded, $n_s = 7$). The mechanically induced intercellular Ca^{2+} wave in wounded 28-day-cultured cells followed for 15 min (ctrl, $n_s = 8$; wounded, $n_s = 8$), or for 7 days (ctrl, $n_s = 6$; wounded, $n_s = 7$). **E** White bar—control; black bar—wound edge or healed wound. Statistical significance: $p < 0.05$ is indicated with Asterisk. Area of a mechanically induced intercellular Ca^{2+} wave spreading in wounded 9-day-cultured cells followed for 15 min (ctrl $n_s = 7$; wounded, $n_s = 7$), or for 7 days (ctrl, $n_s = 7$; wounded, $n_s = 7$). The mechanically induced intercellular Ca^{2+} wave spreading in wounded 28-day-cultured cells followed for 15 min (ctrl, $n_s = 8$; wounded $n_s = 8$), or for 7 days (ctrl, $n_s = 6$; wounded, $n_s = 7$). **F** White bar—control; black bar—wound edge or healed wound. Statistical significance: $p < 0.05$ is indicated with Asterisk. The presented data are combined from Regea08/017 and Regea08/023 hESC-RPEs

the wound healing of epithelial cells but less is known about cellular Ca^{2+} dynamics implicated in the response to fresh wounds and wound healing of RPE. Here, we analyzed spontaneous and mechanically induced $[Ca^{2+}]_i$ increases of cells in freshly wounded and healed hESC-RPE monolayers at two different maturation stages. There are great expectations of hESC-RPE as becoming cell source for cell replacement therapy [34–36]. To understand the integration of surgical transplants, it is essential to study the wound healing mechanisms of the hESC-RPEs.

For RPE cells, the ability to heal scratch wounds has been demonstrated in different in vitro and in vivo models, e.g. in [5, 7–9, 12]. For hESC-RPE cells, Schwartz et al. showed that, in vitro, their attachment to substrata strongly depends on cell differentiation stage: the lighter pigmented cells attach and proliferate better than heavily pigmented cells. Thus, it was proposed that less mature cells may provide better results for transplantation studies [37]. In line with the latter, we found that wound healing capacity of our hESC-RPEs depended on cell culture time: cells wounded after 9-days of culture showed a higher percent of healed samples and faster healing speed compared to those wounded on 28-day of culture. Substratum is crucial for wound healing: the percentage of healed samples with damaged collagen IV coating was much lower compared to that with intact coating in hESC-RPE cells wounded on both day 9 and day 28 after plating. This is in line with the knowledge that cells in general prefer the extracellular matrix substrata and that the plain Ormocomp coating does not support hESC-RPE cell spreading [29]. In addition, with confocal orthoimages, we showed that within 7 days the cells had produced new extracellular matrix layer with laminin and collagen I to the site of the wound and had migrated on top of it. In confocal analyses this layer appeared to be thicker than the extracellular matrix prior to the wounding.

In epithelial monolayers, several rows of cells behind the wound edge participate in wound healing, pushing the monolayer towards the denuded area [38–40]. In chick

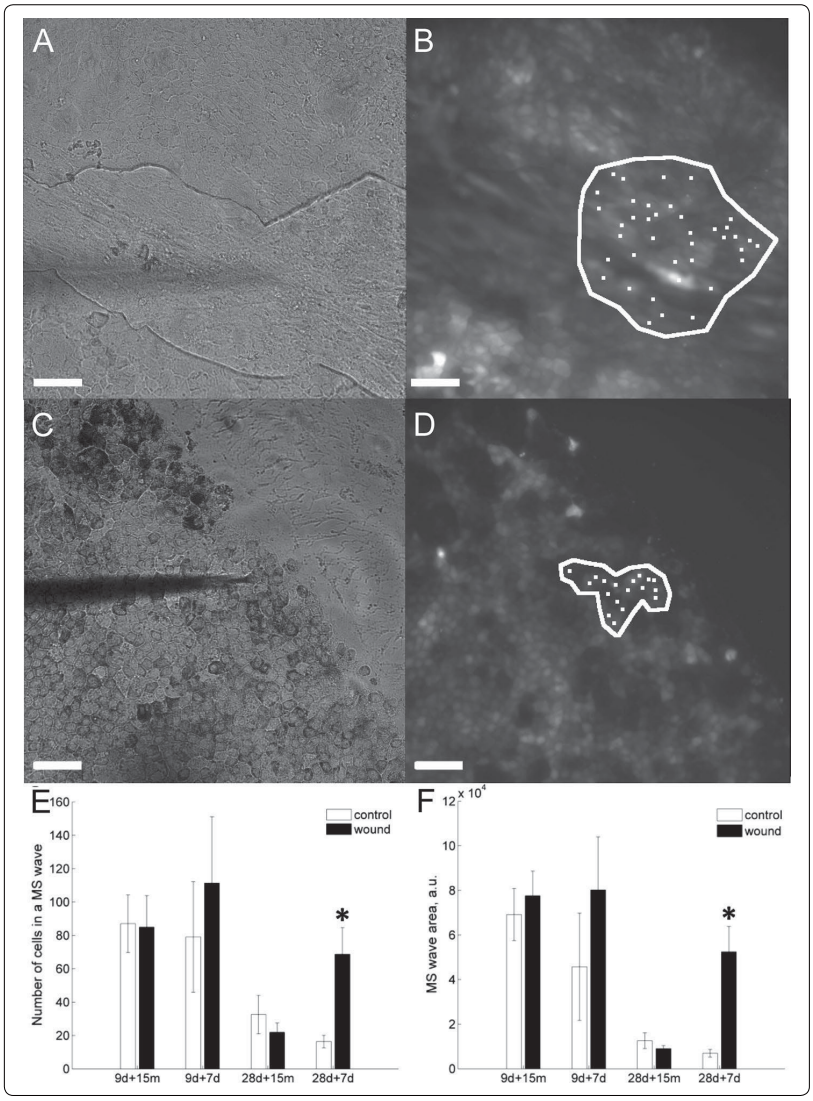

model of small wounds, the RPE cells stretch from wound edges towards each other and then fill the wound without proliferation [7]. But, if the wound is wide, RPE cells start proliferating to seal it [7]. In accordance with these data, we saw hESC-RPE cells which were proliferating during wound healing, but there were no proliferating cells after the wound closure. In cultures with proliferating cells, the Ki-67 positive cells located few cell layers away from the wound edge.

The scratch-wounding of a cellular monolayer is known to trigger an intercellular Ca^{2+} wave that spreads several rows away from the leading wound edge [18, 41–43]. For example in human corneal epithelial cells, it has been shown that ATP released

at the time of injury serves as an early signal that enables activation of wound healing processes [44]. In our 9-day cultured hESC-RPEs, after wounding we detected the elevated percentage of cells with spontaneous $[Ca^{2+}]_i$ increases close to the wound edge. Thus, in this study, we could also observe distinct behavior of the cells near the denuded area in terms of Ca^{2+} dynamics compared to the rest of the monolayer. We can hypothesize that the initial Ca^{2+} wave which occurs at the time of wounding affects the Ca^{2+} dynamics of the cells close to the wound edge to promote the healing.

In freshly wounded 28-day-cultured cells, the percentage of cells with spontaneous $[Ca^{2+}]_i$ increases was the same as in control, regardless of the distance to the wound edge. We hypothesize that 28-day-cultured hESC-RPEs are not able to make their spontaneous activity any higher, as previously we have shown that the percentage of cells with spontaneous $[Ca^{2+}]_i$ increases does not elevate further after day 28 of culture [22].

Here, the hESC-RPEs wounded on day 28 of culture and then allowed to heal for 7 days, had lower percentage of cells with spontaneous $[Ca^{2+}]_i$ increases inside the healed area. This finding is in accordance with our previously published observation that the percentage of cells with spontaneous $[Ca^{2+}]_i$ increases raises during maturation in hESC-RPE cells [22]. Thus, cells with shorter culture time within the healed wounds have lower spontaneous Ca^{2+} activity compared to surrounding cells, which have been cultured for a longer period of time.

Mechanical stimulation has been shown to induce intercellular Ca^{2+} waves in RPE [22–25]. In rat RPE, the mechanically induced intercellular Ca^{2+} waves spread to up to 3 cell tiers away from the site of mechanical stimulation [23, 24], whereas in human ARPE-19 cell line, such waves are more intense, covering up to 14 cell layers [25]. Our previous studies show that in hESC-RPE cells, the spreading of mechanically induced Ca^{2+} waves strongly depends on cell culture time. In cells cultured for a longer period of time (28 days), the Ca^{2+} waves propagate to only few cells away from the stimulation site, similarly to the waves in rat RPE. On the other hand, the cells cultured for a shorter period of time (9 days) respond with wide-spreading Ca^{2+} waves, similarly to ARPE-19 [22].

In the current study, we demonstrated that in hESC-RPEs wounded on day 28 of culture and then allowed to heal for 7 days, mechanical stimulation resulted in wide-spreading intercellular Ca^{2+} waves, when a cell inside the healed wound had been stimulated. Inside the healed wounds, the cells have less mature morphology compared to the non-wounded surroundings, and indeed, such a strong response to mechanical stimulation is typical for immature hESC-RPEs.

On the other hand, control non-wounded areas exhibited more mature morphology, and the wave spreading was restricted to only few cells that is typical for more mature hESC-RPE cells, as we have shown in our previous study [22]. In contrast, the cells wounded on day 9 of culture and then allowed to heal for 7 days, did not show significant differences in the mechanically stimulated Ca^{2+} wave spreading in the healed areas and in control. The cells within the healed areas had similar morphology as the surrounding cells, and the Ca^{2+} wave spreading pattern corresponded to immature hESC-RPE cells. In addition, when cells were wounded on day 9 of culture and then healed for 7 days, the cells inside the healed area did not show significant

difference in the percentage of cells with spontaneous $[Ca^{2+}]_i$ activity compared to the surroundings. Thus, we can speculate that if there is no big difference in maturation status of the cells within the wound and in the surroundings, the cells can adapt to share similar Ca^{2+} dynamics behavior.

Conclusions

We have shown here that the effect of wounding on Ca^{2+} dynamics of hESC-RPE monolayers depends on cell culture time: 9-day-cultured freshly wounded cells have elevated amount of cells with spontaneous $[Ca^{2+}]_i$ increases in vicinity to the wound compared to control, whereas 28-day-cultured freshly wounded cells had similar Ca^{2+} dynamics around the wound edge as in other areas. Most importantly, we have shown that 28-day-cultured, wounded and thereafter 7-day-healed areas resemble the behavior of 9-day-cultured cells both in Ca^{2+} dynamics and cell morphology. In addition, we have demonstrated that cells cultured for a shorter period of time heal faster than cells cultured for a longer period of time. This acquired knowledge about Ca^{2+} dynamics in hESC-RPE cells is important for understanding the fundamental mechanisms of RPE wound healing that can lead to new insights in AMD pathological process and therapy.

Additional files

Additional file 1: Fig S1. Confocal images of non-wounded (A) and wounded (B) Regea08/017 hESC-RPE cultures in which COLI is shown in red and nuclei in blue. As seen from the ortho-sections on the right and above, the COLI is concentrated close to the substrata. This is indicated also with white arrows. The background labeling, which would be visible is other areas of the cell, is very low. Scale bars are 10 μm.

Additional file 2: Video S1. Calcium wave in hESC-RPE monolayer (9d + 7d) followed for 300 s after mechanical stimulation. The video corresponds Fig. 7A, B. Prior the stimulation hESC-RPEs (9d + 7d) were loaded with fluorescent Ca^{2+} sensitive dye Fluo-4 AM that reflects $[Ca^{2+}]_i$ concentration in the cytoplasm. The site of mechanical stimulation is marked with white an arrow. Mechanical stimulation of a single cell in a hESC-RPE monolayer resulted in a $[Ca^{2+}]_i$ increase, seen as an increase in fluorescent signal, in the stimulated cell that propagates in a wave-like manner to neighbouring cells.

Additional file 3: Video S2. The video corresponds Fig. 7C, D. Calcium wave in hESC-RPE monolayer (28d + 7d) followed for 300 s after mechanical stimulation. Prior the stimulation hESC-RPEs were loaded with fluorescent Ca^{2+} sensitive dye Fluo-4 AM that reflects $[Ca^{2+}]_i$ concentration in the cytoplasm. The site of mechanical stimulation is marked with white an arrow. Mechanical stimulation of a single cell in a hESC-RPE monolayer resulted in a $[Ca^{2+}]_i$ increase, seen as an increase in fluorescent signal, in the stimulated cell that propagates in a wave-like manner to neighbouring cells.

Abbreviations

RPE: retinal pigment epithelium; hESCs: human embryonic stem cells.

Authors' contributions

Conceived and designed the experiments: AAK, JHy, KJ-U. Performed the experiments: AAK, KJ-U. Analyzed and interpreted the data: AAK, AR-M, Aka, JHy, KJ-U, Contributed regents/materials/analysis tools: AAK, AR-M, Aka, JHy, KJ-U. Drafted the manuscript: AAK, KKa, HSk, JHy, KJ-U. Participated in the critical revision of the manuscript and approval of the article: AAK, AR-M, KKa, Aka, HSk, JHy, KJ-U. Acquired the funding: AAK, KKa, HSk, JHy, KJ-U. All authors read and approved the final manuscript.

Author details

[1] Faculty of Biomedical Sciences and Engineering, BioMediTech, Tampere University of Technology, Arvo Ylpön Katu 34, Tampere, Finland. [2] Faculty of Medical and Life Sciences, BioMediTech, University of Tampere, Arvo Ylpön Katu 34, Tampere, Finland. [3] Department of Ophthalmology, Institute of Clinical Medicine, University of Eastern Finland, Kuopio, Finland. [4] Department of Ophthalmology, Kuopio University Hospital, Kuopio, Finland.

Acknowledgements

Outi Melin, Hanna Pekkanen and Outi Heikkilä are thanked for excellent technical assistance.

Competing interests

The authors declare that they have no competing interests.

Availability of data and materials
After publication on the https://figshare.com.

Consent for publication
All authors have approved the final version of the manuscript.

Ethics approval and consent to participate
University of Tampere has the approval of the National Authority for Medicolegal Affairs Finland (TEO) to study human embryos (Dnro 1426/32/300/05) and a supportive statement of the Ethical Committee of the Pirkanmaa Hospital District to derive, culture, and differentiate hESC lines from surplus human embryos (R05116). No new lines were derived for this study.

Funding
This work was supported by the Academy of Finland [Grant Numbers 296840 (KKa), 252225 (JHy), 218050 (HSk) and 137801 (KJ-U)], the Finnish Funding Agency for Technology and Innovation (JHy, HSk), Päivikki and Sakari Sohlberg foundation (HSk), The Finnish Eye Foundation (KKa), and Tampere University of Technology President's Doctoral Program (AAK). The funders had no role in study design, data collection and analysis, decision to publish, or preparation of the manuscript.

Publisher's Note

Received: 31 January 2018 Accepted: 24 July 2018
Published online: 31 July 2018

References

1. Sparrow JR, Hicks D, Hamel CP. The retinal pigment epithelium in health and disease. Curr Mol Med. 2010;10(9):802–23.
2. Strauss O. The retinal pigment epithelium in visual function. Physiol Rev. 2005;85(3):845–81.
3. Binder S, Stanzel BV, Krebs I, Glittenberg C. Transplantation of the RPE in AMD. Progress Ret Eye Res. 2007;26(5):516–54.
4. Klettner A, Kauppinen A, Blasiak J, Roider J, Salminen A, Kaarniranta K. Cellular and molecular mechanisms of age-related macular degeneration: from impaired autophagy to neovascularization. Int J Biochem Cell Biol. 2013;45(7):1457–67.
5. Lopez PF, Sippy BD, Lambert HM, Thach AB, Hinton DR. Transdifferentiated retinal pigment epithelial cells are immunoreactive for vascular endothelial growth factor in surgically excised age-related macular degeneration-related choroidal neovascular membranes. Invest Ophthalmol Vis Sci. 1996;37(5):855–68.
6. Oganesian A, Bueno E, Yan Q, Spee C, Black J, Rao NA, Lopez PF. Scanning and transmission electron microscopic findings during RPE wound healing in vivo. Int Ophthalmol. 1997;21(3):165–75.
7. Hergott GJ, Nagai H, Kalnins VI. Inhibition of retinal pigment epithelial cell migration and proliferation with monoclonal antibodies against the beta 1 integrin subunit during wound healing in organ culture. Invest Ophthalmol Vis Sci. 1993;34(9):2761–8.
8. Tamiya S, Liu L, Kaplan HJ. Epithelial–mesenchymal transition and proliferation of retinal pigment epithelial cells initiated upon loss of cell–cell contact. Invest Ophthalmol Vis Sci. 2010;51(5):2755–63.
9. Miura Y, Yanagihara N, Imamura H, Kaida M, Moriwaki M, Shiraki K, Miki T. Hepatocyte growth factor stimulates proliferation and migration during wound healing of retinal pigment epithelial cells in vitro. Jpn J Ophthalmol. 2003;47(3):268–75.
10. Wang H, Ninomiya Y, Sugino IK, Zarbin MA. Retinal pigment epithelium wound healing in human Bruch's membrane explants. Invest Ophthalmol Vis Sci. 2003;44(5):2199–210.
11. Guo CM, Wang YS, Hu D, Han QH, Wang JB, Hou X, Hui YN. Modulation of migration and Ca2+ signaling in retinal pigment epithelium cells by recombinant human CTGF. Curr Eye Res. 2009;34(10):852–62.
12. Croze RH, Thi WJ, Clegg DO. ROCK inhibition promotes attachment, proliferation, and wound closure in human embryonic stem cell-derived retinal pigmented epithelium. Transl Vision Sci Technol. 2016;5(6):7.
13. Gallagher-Colombo S, Maminishkis A, Tate S, Grunwald GB, Philp NJ. Modulation of MCT3 expression during wound healing of the retinal pigment epithelium. Invest Ophthalmol Vis Sci. 2010;51(10):5343–50.
14. Miyagishima KJ, Wan Q, Corneo B, Sharma R, Lotfi MR, Boles NC, Hua F, Maminishkis A, Zhang C, Blenkinsop T, et al. In pursuit of authenticity: induced pluripotent stem cell-derived retinal pigment epithelium for clinical applications. Stem Cells Transl Med. 2016;5:1562–74.
15. Singh R, Phillips MJ, Kuai D, Meyer J, Martin JM, Smith MA, Perez ET, Shen W, Wallace KA, Capowski EE, et al. Functional analysis of serially expanded human iPS cell-derived RPE cultures. Invest Ophthalmol Vis Sci. 2013;54(10):6767–78.
16. Cordeiro JV, Jacinto A. The role of transcription-independent damage signals in the initiation of epithelial wound healing. Nat Rev Mol Cell Biol. 2013;14(4):249–62.
17. Tran POT, Hinman LE, Unger GM, Sammak PJ. A wound-induced [Ca2+], increase and its transcriptional activation of immediate early genes is important in the regulation of motility. Exp Cell Res. 1999;246(2):319–26.
18. Woolley K, Martin P. Conserved mechanisms of repair: from damaged single cells to wounds in multicellular tissues. BioEssays. 2000;22(10):911–9.
19. Wimmers S, Karl MO, Strauss O. Ion channels in the RPE. Progress Retinal Eye Res. 2007;26(3):263–301.

20. Pearson RA, Catsicas M, Becker DL, Bayley P, Luneborg NL, Mobbs P. Ca(2+) signalling and gap junction coupling within and between pigment epithelium and neural retina in the developing chick. Eur J Neurosci. 2004;19(9):2435–45.
21. Pearson RA, Dale N, Llaudet E, Mobbs P. ATP released via gap junction hemichannels from the pigment epithelium regulates neural retinal progenitor proliferation. Neuron. 2005;46(5):731–44.
22. Abu Khamidakh AE, Dos Santos FC, Skottman H, Juuti-Uusitalo K, Hyttinen J. Semi-automatic method for Ca2+ imaging data analysis of maturing human embryonic stem cells-derived retinal pigment epithelium. Ann Biomed Eng. 2016;44:11.
23. Stalmans P, Himpens B. Properties of intra- and intercellular Ca(2+)-wave propagation elicited by mechanical stimulation in cultured RPE cells. Cell Calcium. 1999;25(6):391–9.
24. Himpens B, Stalmans P, Gomez P, Malfait M, Vereecke J. Intra- and intercellular Ca2+ signaling in retinal pigment epithelial cells during mechanical stimulation. FASEB J. 1999;13(Suppl):S63–8.
25. Abu Khamidakh AE, Juuti-Uusitalo K, Larsson K, Skottman H, Hyttinen J. Intercellular Ca(2+) wave propagation in human retinal pigment epithelium cells induced by mechanical stimulation. Exp Eye Res. 2013;108:129–39.
26. Skottman H. Derivation and characterization of three new human embryonic stem cell lines in Finland. In Vitro Cell Dev Biol Anim. 2010;46(3–4):206–9.
27. Sorkio A, Porter PJ, Juuti-Uusitalo K, Meenan BJ, Skottman H, Burke GA. Surface modified biodegradable electrospun membranes as a carrier for human embryonic stem cell-derived retinal pigment epithelial cells. Tissue Eng Part A. 2015;21(17–18):2301–14.
28. Vaajasaari H, Ilmarinen T, Juuti-Uusitalo K, Rajala K, Onnela N, Narkilahti S, Suuronen R, Hyttinen J, Uusitalo H, Skottman H. Toward the defined and xeno-free differentiation of functional human pluripotent stem cell-derived retinal pigment epithelial cells. Mol Vision. 2011;17:558–75.
29. Kapyla E, Sorkio A, Teymouri S, Lahtonen K, Vuori L, Valden M, Skottman H, Kellomaki M, Juuti-Uusitalo K. Ormocomp-modified glass increases collagen binding and promotes the adherence and maturation of human embryonic stem cell-derived retinal pigment epithelial cells. Langmuir. 2014;30(48):14555–65.
30. Sorkio A, Hongisto H, Kaarniranta K, Uusitalo H, Juuti-Uusitalo K, Skottman H. Structure and barrier properties of human embryonic stem cell derived retinal pigment epithelial cells are affected by extracellular matrix protein coating. Tissue Eng A. 2014;20:622–34.
31. Schmittgen TD, Livak KJ. Analyzing real-time PCR data by the comparative C(T) method. Nat Protoc. 2008;3(6):1101–8.
32. Schindelin J, Arganda-Carreras I, Frise E, Kaynig V, Longair M, Pietzsch T, Preibisch S, Rueden C, Saalfeld S, Schmid B, et al. Fiji: an open-source platform for biological-image analysis. Nat Methods. 2012;9(7):676–82.
33. Geiger B, Bershadsky A, Pankov R, Yamada KM. Transmembrane crosstalk between the extracellular matrix–cytoskeleton crosstalk. Nat Rev Mol Cell Biol. 2001;2(11):793–805.
34. Carr AJ, Smart MJ, Ramsden CM, Powner MB, da Cruz L, Coffey PJ. Development of human embryonic stem cell therapies for age-related macular degeneration. Trends Neurosci. 2013;36(7):385–95.
35. Schwartz SD, Regillo CD, Lam BL, Eliott D, Rosenfeld PJ, Gregori NZ, Hubschman JP, Davis JL, Heilwell G, Spirn M, et al. Human embryonic stem cell-derived retinal pigment epithelium in patients with age-related macular degeneration and Stargardt's macular dystrophy: follow-up of two open-label phase 1/2 studies. Lancet. 2015;385(9967):509–16.
36. da Cruz L, Fynes K, Georgiadis O, Kerby J, Luo YH, Ahmado A, Vernon A, Daniels JT, Nommiste B, Hasan SM, et al. Phase 1 clinical study of an embryonic stem cell-derived retinal pigment epithelium patch in age-related macular degeneration. Nat Biotechnol. 2018;36(4):328–37.
37. Schwartz SD, Hubschman JP, Heilwell G, Franco-Cardenas V, Pan CK, Ostrick RM, Mickunas E, Gay R, Klimanskaya I, Lanza R. Embryonic stem cell trials for macular degeneration: a preliminary report. Lancet. 2012;379:713–20.
38. Matsubayashi Y, Ebisuya M, Honjoh S, Nishida E. ERK activation propagates in epithelial cell sheets and regulates their migration during wound healing. Curr Biol. 2004;14(8):731–5.
39. Farooqui R, Fenteany G. Multiple rows of cells behind an epithelial wound edge extend cryptic lamellipodia to collectively drive cell-sheet movement. J Cell Sci. 2005;118(Pt 1):51–63.
40. Jacinto A, Martinez-Arias A, Martin P. Mechanisms of epithelial fusion and repair. Nat Cell Biol. 2001;3(5):E117–23.
41. Tran POT, Tran QHP, Hinman LE, Sammak PJ. Co-ordination between localized wound-induced Ca2+ signals and pre-wound serum signals is required for proliferation after mechanical injury. Cell Proliferat. 1998;31(3–4):155–70.
42. Shabir S, Southgate J. Calcium signalling in wound-responsive normal human urothelial cell monolayers. Cell Calcium. 2008;44(5):453–64.
43. Berra-Romani R, Raqeeb A, Torres-Jacome J, Guzman-Silva A, Guerra G, Tanzi F, Moccia F. The mechanism of injury-induced intracellular calcium concentration oscillations in the endothelium of excised rat aorta. J Vasc Res. 2012;49(1):65–76.
44. Yin J, Xu K, Zhang J, Kumar A, Yu FS. Wound-induced ATP release and EGF receptor activation in epithelial cells. J Cell Sci. 2007;120(Pt 5):815–25.